

# INAUGURAL - DISSERTATION

zur  
Erlangung der Doktorwürde  
der  
Naturwissenschaftlich-Mathematischen Gesamtfakultät  
der  
Ruprecht-Karls-Universität  
Heidelberg

vorgelegt von

Diplom-Chemikerin Hye-Ryun Cho  
aus Seoul (Korea)

Tag der mündlichen Prüfung: 10.02.2006



# THEMA

## **Chemistry of tetravalent plutonium and zirconium:** Hydrolysis, solubility, colloid formation and redox reactions

Gutachter: Prof. Dr. Thomas Fanghänel

Prof. Dr. Margot Isenbeck-Schröter



**Meiner Familie**

## **Danksagung**

Die vorliegende Arbeit wurde unter Leitung von Prof. Dr. Thomas Fanghänel am Institut für Nukleare Entsorgung (INE) des Forschungszentrums Karlsruhe in der Helmholtz-Gemeinschaft in der Zeit vom Mai 2002 bis Dezember 2005 durchgeführt.

Mein besonderer Dank gilt Herrn Prof. Dr. Jae-Il Kim für die Vorstellung des fortschrittlichen Instituts und den interessanten Forschungsbereich der Radiochemie und Herrn Prof. Dr. Thomas Fanghänel für die Bereitstellung des Arbeitsplatzes, die interessante Themenstellung und das hervorragende Arbeitsklima sowie Frau Prof. Dr. Margot Isenbeck-Schröter für die bereitwillige Übernahme des Korreferats.

Mein herzlicher Dank gilt Dr. Clemens Walther für seine wissenschaftliche Betreuung zum Gelingen der Arbeit und die sehr angenehme Zusammenarbeit und Dr. Jong-Il Yun für die Diskussionsbereitschaft bei allen Problemen.

Mein Dank gilt auch Dr. Melissa Denecke, Dr. Jörg Rothe und Dr. Kathy Dardenne für die XAFS Untersuchungen, Dr. Christian Marquardt, Dr. Alice Seibert und Dr. Marcus Altmaier für die Hilfestellung und Ratschläge im Rahmen der komplexen aquatischen Pu Chemie sowie Dr. Volker Neck für wertvolle Diskussion über die aquatische Thermodynamik von vierwertigen Elementen.

Mein Dank gilt auch Herrn Frank Geyer und Frau Cornelia Walschburger für die hervorragenden ICP-MS Analysen bei der Zr-Untersuchung sowie Frau Regina Müller für die freundliche Hilfestellung bei der Präparation von kolloidfreien Lösungen und der Einführung der coulometrischen Titration. Weiterhin sei allen Mitarbeitern des Instituts für Nukleare Entsorgung für ihre Unterstützung zur erfolgreichen Durchführung der Arbeit herzlich bedankt.

Der größte Dank gilt meiner Tochter, meinem Mann und meinen beiden Eltern für ihre lange Geduld und permanente Unterstützung. - 제가 학업을 무사히 마칠 수 있도록 기다려준 단아와 남편, 그리고 저희 가족이 한국에서 지난 일년간 잘 보낼 수 있도록 돌봐주시고 항상 버팀목이 되어주신 양가 부모님과 가족 모두에게 진심으로 감사드립니다.

## Contents

<b>Zusammenfassung</b> .....	<b>iii</b>
<b>Abstract</b> .....	<b>iv</b>
<b>1 Introduction</b> .....	<b>1</b>
<b>2 The state of knowledge in literature</b> .....	<b>4</b>
2.1 Chemistry of actinides in aquatic systems.....	4
2.1.1 Oxidation states of actinides in aquatic systems .....	5
2.1.2 Hydrolysis of tetravalent actinides .....	9
2.1.3 Solubility of An(IV) hydroxides and oxides .....	11
2.1.4 Colloid formation of actinides.....	14
2.2 Chemistry of plutonium in aquatic systems .....	15
2.2.1 Oxidation states of Pu in aquatic systems .....	15
2.2.2 Hydrolysis constants of Pu(IV) .....	16
2.2.3 Solubility of Pu(IV) hydroxide/hydrous oxide.....	19
2.2.4 Redox reactions of plutonium.....	22
2.3 Hydrolysis and solubility data of Zr(IV) .....	26
2.3.1 Hydrolysis constants of Zr(IV).....	26
2.3.2 Solubility product of Zr(IV) .....	29
<b>3 Experimental Techniques</b> .....	<b>31</b>
3.1 UV-VIS absorption spectroscopy.....	33
3.2 Capillary Electrophoresis (CE) coupled with ICP-MS.....	41
3.3 X-ray Absorption Fine Structure (XAFS) .....	45
3.4 Laser Induced Breakdown Detection (LIBD) .....	49
3.4.1 Principle of LIBD .....	50
3.4.2 Measurement of multimodal size distributions by LIBD .....	52
3.4.3 Setup of LIBD apparatus .....	54
3.5 Single particle counter (SPC) .....	56
<b>4 Experiments</b> .....	<b>58</b>
4.1 Zirconium .....	58
4.1.1 Preparation of background materials and samples .....	58
4.1.2 Coulometric pH titration.....	59
4.2 Plutonium.....	61

4.2.1	Preparation of Pu(IV) stock solution .....	61
4.2.2	Dilution with 0.5M (H/Na)Cl solution .....	63
4.2.3	pH and Eh measurements .....	65
<b>5</b>	<b>Results and Discussions I – Zirconium .....</b>	<b>67</b>
5.1	Solubility of Zr(IV) using coulometric pH titration and LIBD .....	67
5.2	Structure of various Zr(IV) species by XAFS .....	77
<b>6</b>	<b>Results and Discussion II – Chemistry of Pu .....</b>	<b>81</b>
6.1	LIBD investigation of background materials and Pu stock solutions .....	81
6.2	Solubility of Pu(IV) hydrous oxide in acidic solution.....	83
6.3	Redox reactions of plutonium in acidic solution.....	90
6.3.1	Redox reactions of plutonium in contact with air.....	93
6.3.2	The change of oxidation state distribution by acidifying .....	98
6.3.3	Redox reactions of plutonium under argon atmosphere .....	99
6.4	Determination of hydrolysis constants from Eh measurements .....	100
<b>7</b>	<b>Conclusion .....</b>	<b>106</b>
<b>8</b>	<b>Appendix.....</b>	<b>113</b>
8.1	Ionic strength corrections: Specific ion interaction theory (SIT).....	113
8.2	Tables of zirconium investigation .....	115
8.3	Coulometric titration of the Pu(IV) solution .....	118
8.4	The absorption spectrum of Pu(IV) colloids .....	119
8.5	LIBD system for the Pu investigation .....	120
8.6	Tables of Pu oxidation state distribution .....	121
8.7	List of abbreviations .....	125
8.8	List of symbols .....	126
8.9	List of Figures.....	129
8.10	List of Tables.....	131
<b>9</b>	<b>References.....</b>	<b>132</b>



## Zusammenfassung

In Rahmen der Sicherheitsforschung für nukleare Endlager sind thermodynamische Daten von Actiniden von großer Bedeutung. In dieser Arbeit werden Hydrolyse, Löslichkeit, Kolloidbildung und Festphasenumwandlung von vierwertigem Plutonium und seinem Homolog Zirkonium in 0.5 M HCl/NaCl mittels Absorptionsspektroskopie, Laser-induzierter Breakdown Detektion (LIBD) und Röntgenabsorptionsspektroskopie (XAFS) untersucht. Im Falle des Pu werden zusätzlich Redoxreaktionen im sauren Bereich betrachtet.

Die Löslichkeitsuntersuchungen am Zirkonium wurden in einem weiten Konzentrationsbereich ( $\log [\text{Zr}] = -3 \sim -7.6$ ) und pH (3 – 9) durchgeführt. Durch Erhöhung des pH gelangt man zu übersättigten Lösungen. Ein sehr sensitives Indiz für das Überschreiten der Löslichkeit ist die Bildung von Kolloiden, die mittels LIBD direkt nachgewiesen werden. Das aus diesen Messungen bestimmte Löslichkeitsprodukt  $\log K_{\text{sp}}^{\circ}(\text{Zr(IV)}) = -53.1 \pm 0.5$  wurde mit Hydrolysekonstanten für mononukleare Zr-hydroxokomplexe berechnet. Vergleicht man Löslichkeitsdaten für Zirkonium aus der Literatur, so bilden die Werte zwei verschiedene Gruppen. Mutmaßlich handelt es sich um zwei verschiedene Festphasen, eine mikrokristalline und eine amorphe. Um die Abhängigkeit der Löslichkeit von der Festphase zu verifizieren, wurden Lösungen bei verschiedenem pH mit XAFS untersucht und die Struktur der jeweils dominierenden Zirkonpezies bestimmt. Im Bereich der niedrigeren Löslichkeit dominieren mikrokristalline Partikel während im Bereich der höheren Löslichkeit die gefundenen Strukturen keiner bekannten  $\text{ZrO}_2$  Struktur ähneln. Es handelt sich dabei um Zr-oxyhydroxokolloide mit starker struktureller Unordnung. Daher bezieht sich die Löslichkeit in dieser Arbeit auf amorphes Zirkonhydroxid,  $\text{Zr(OH)}_4(\text{am})$ .

Die Löslichkeitsuntersuchungen an Pu(IV)-hydroxid wurden im pH Bereich  $< \text{pH } 2$  durchgeführt. Pu(IV) ist sogar im sauren pH Bereich redoxinstabil. Daher muß für die Untersuchungen von Pu(IV), der Anteil von Pu(IV) an der Gesamtkonzentration in Lösung vor jedem Versuch mittels Absorptionsspektroskopie bestimmt werden. Wenn man, wie beim Zr, nur mononukleare Pu-hydroxokomplexe berücksichtigt, erhält man ein Löslichkeitsprodukt von  $\log K_{\text{sp}}^{\circ}(\text{Pu(IV)}) -58.3 \pm 0.4$ .

Die Redoxreaktionen des Plutonium bei unterschiedlichem pH und Pu Konzentrationen wurden als Funktion der Zeit beobachtet. Sie folgen nicht dem nach der Disproportionierung erwarteten Verlauf sondern können durch gleichzeitige Reduktion des Pu(IV) ( $\text{Pu(IV)}_{\text{aq}} \rightleftharpoons \text{Pu(III)}_{\text{aq}}$ ) und Oxidation des Pu(IV) ( $\text{Pu(IV)}_{\text{coll}} \rightleftharpoons \text{Pu(V)}_{\text{aq}} \rightleftharpoons \text{Pu(VI)}_{\text{aq}}$ ) beschrieben werden. In allen Fällen dominiert die Reduktion des Pu(IV) über die Oxidation, das heißt, es wird mehr Pu(III) als  $\text{Pu(V)} + 2\text{Pu(VI)}$  gebildet. Hieraus ist ersichtlich, dass ein weiteres Reduktionsmittel an der Reaktion beteiligt ist. Durch sukzessiven Ausschluß bleibt die Oxidation von Wasser als einzige Möglichkeit. Die Redoxreaktionen des Pu sind abhängig vom pH. Mit zunehmendem pH nimmt  $[\text{Pu}^{4+}]$  durch die Reduktion oder die Hydrolyse und Kolloidbildung ab. Folglich nehmen  $[\text{Pu(III)}]$  und  $[\text{Pu(V)}] + [\text{Pu(VI)}]$  zu. Um die Rolle von gelöstem Sauerstoff an der Reaktion  $\text{Pu(IV)}_{\text{coll}} \rightleftharpoons \text{Pu(V)}_{\text{aq}}$  zu untersuchen, wurden die gleichen Experimente unter Argon Atmosphäre in einer Handschuhbox durchgeführt.

Um die mononuklearen Hydrolysekonstanten von Pu(IV) zu bestimmen, wurde das Redoxpotential (Eh) der Pu Lösungen gemessen. Neben der direkten Messung kann der Eh-Wert aus zwei Redoxpaaren,  $\text{PuO}_2^{2+}/\text{PuO}_2^+$  und  $\text{PuO}_2^+/\text{PuO}_2(\text{Koll.})$  gewonnen werden, die gut übereinstimmen. Um auch das dritte Redoxpaar  $\text{Pu}^{4+}/\text{Pu}^{3+}$  zur Eh-Bestimmung heranziehen zu können, muß die starke Hydrolyse des Pu(IV) berücksichtigt werden; schon bei  $\text{pH} < 1$  liegt ein großer Teil des  $\text{Pu(IV)}_{\text{aq}}$  als Hydroxokomplex vor. Die

Bestimmung von  $\text{Pu}^{4+}$  aus  $[\text{Pu(IV)}_{\text{aq}}] = [\text{Pu}^{4+}] + \sum_{y=1}^4 [\text{Pu(OH)}_y^{4-y}]$  ist sensitiv auf die Hydrolysekonstanten.

Folglich können aus dem Vergleich des aus dem  $\text{Pu}^{4+}/\text{Pu}^{3+}$  Paar bestimmten Eh-Wertes mit gemessenen Eh-Werten  $\beta_{1y}$  ( $y = 1-2$ ) gewonnen werden. Diese Messung legt eine leichte Korrektur der Literaturkonstanten zu niedrigeren Werten hin nahe.

## Abstract

The chemical properties of plutonium and zirconium are important in order to assess nuclear waste disposals with respect to isolation and immobilization of radionuclides. In this study, the hydrolysis, solubility and colloid formation of tetravalent plutonium and zirconium are investigated in 0.5 M HCl/NaCl solution using several complementary methods and the redox behavior of plutonium is investigated in acidic conditions as well.

The solubilities of Pu(IV) and Zr(IV) are determined from the onset of colloid formation as a function of pH and metal concentration using LIBD (laser-induced breakdown detection). The investigation of the solubility of Zr(IV) is carried out at different concentrations ( $\log [Zr] = -3 \sim -7.6$ ) and in a wide pH range (pH = 3 - 9) yielding  $\log K^{\circ}_{sp}(Zr(IV)) = -53.1 \pm 0.5$  based on the assumption that only mononuclear hydrolysis species exist in solution. Comparing the present results with literature data, the solubilities of Zr can be split in two groups, a crystalline phase with lower solubility and an amorphous phase ( $Zr(OH)_4(am)$ ) with higher solubility. The data obtained in the present work set an upper limit for the solubility of freshly formed  $Zr(OH)_4(am)$ . To understand this difference of solubilities, the geometrical structure of the dominant solution species is investigated as a function of pH using XAFS (X-ray absorption fine structure). The samples at pH >2, still below the solubility limit determined by LIBD, contain the polynuclear Zr(IV) species probably due to the high concentration ( $[Zr] = 1$  mM) and their structure do not resemble any reported simple  $ZrO_2$  structure. The Zr(IV) colloid species in oversaturated solution under this experimental condition resembles amorphous Zr(IV) hydroxide rather than crystalline  $ZrO_2$ .

The solubility of Pu(IV) is investigated in acidic solution below pH 2. Considering only mononuclear hydrolysis species,  $\log K^{\circ}_{sp}(Pu(IV)) = -58.3 \pm 0.4$  is obtained. Since Pu(IV) is not redox stable even in acidic condition, the concentration of each oxidation state of Pu must be determined prior to each experiment. The solubility data are determined directly after preparation and then the redox reactions between four different plutonium oxidation states are observed at different pH and Pu concentrations as a function of time. The results indicate that the redox behavior of Pu cannot be described by disproportionation of Pu alone. Under the experimental conditions, the redox reactions of Pu seem to be divided into two groups,  $Pu(IV)_{aq} \rightleftharpoons Pu(III)_{aq}$  and  $Pu(IV)_{coll} \rightleftharpoons Pu(V)_{aq} \rightleftharpoons Pu(VI)_{aq}$ . In the Pu solution containing initially only Pu(IV), the reduction of Pu(IV) to  $Pu(III)_{aq}$  dominates rather than the oxidation to  $Pu(V)_{aq}$  and  $Pu(VI)_{aq}$ . The observed two groups of reactions show the dependency of pH due to the related hydrolysis and colloid formation of Pu(IV). With increasing pH, the  $[Pu^{4+}]$  decreases either through its hydrolysis and colloid formation (increase of  $Pu(IV)_{coll}$ ) or through its reduction (increase of  $Pu(III)_{aq}$ ). The polymer species or colloids may dissolve to  $Pu(V)_{aq}$  through the second reaction group (increase  $Pu(V)_{aq} + Pu(VI)_{aq}$ ). Consequently, it is observed that with increase of pH,  $[Pu(IV)_{aq}]$  decreases,  $[Pu(III)_{aq}]$  increases, and  $[Pu(IV)_{coll}] + [Pu(V)_{aq}] + [Pu(VI)_{aq}]$  increases. This study is also performed under inert gas conditions in order to investigate the influence of dissolved oxygen on the oxidation of Pu(IV) ( $Pu(IV)_{coll} \rightleftharpoons Pu(V)_{aq}$ ).

From the relative abundance of the Pu oxidation states, namely the couples  $PuO_2^{2+}/PuO_2^+$  and  $PuO_2^+/Pu(IV)_{coll}$ , the redox potential Eh(V) can be obtained. The respective values agree well with the measured Eh values. In order to use the redox couple  $Pu^{4+}/Pu^{3+}$ , one has to take into account the strong hydrolysis of Pu(IV) which sets in below pH 1. When the abundance of  $Pu^{4+}$  is calculated from the amount

of  $[Pu(IV)_{aq}] = [Pu^{4+}] + \sum_{y=1}^4 [Pu(OH)_y^{4-y}]$  by use of hydrolysis constants from earlier solvent extraction studies,

deviations from the measured Eh arise. By use of slightly lower values for  $\log \beta_{1y}$  ( $y = 1-2$ ) a good agreement between all calculated and measured Eh values is achieved, suggesting that at least the first and second hydrolysis constants should be corrected.

## 1 Introduction

For the past several decades, large amounts of the actinide elements have been produced and accumulated predominantly from nuclear weapon production and from spent fuel of nuclear power plants. In the early days, much of the interest in actinide chemistry had been directly associated with the separation science. The primary motive in most studies of actinide solutions was the isolation and purification of these elements rather than expansion of the knowledge about their fundamental chemical properties [Chop 83a]. Along with the worldwide growing use of nuclear energy, the actinide elements which are produced from commercial nuclear technology as spent fuel are augmented. As shown in Fig. 1.1, plutonium and other actinide elements dominate the radiotoxicity of spent fuel and it takes hundreds of thousands of years for the radiotoxicity reducing to the level of the uranium which the fuel was made of.

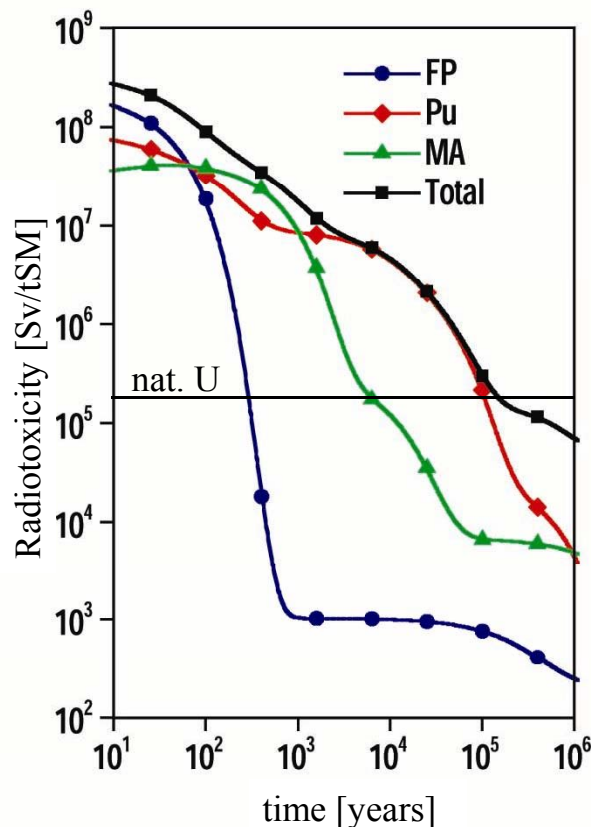


Fig. 1.1 The radiotoxicity inventory of one ton spent fuel in a pressurized water reactor (enrichment 4.2%  $^{235}\text{U}$ , burn-up 50 GW). The radiotoxicity contributions of plutonium (Pu), minor actinides (MA) and fission products (FP) [Geis 2004].

Many countries consider the disposal of the abundant radioactive waste in underground and for the success of the radioactive waste disposal, the most important factors are the isolation and the immobilization of radioactive elements. Proposed disposal of high level radioactive waste in deep geological formations is the possible source for actinides introducing into the environment.

It is a major challenge for natural and technical sciences to model the behavior of radioactive materials under environmental conditions and hence establish the basis for protecting the environment. In order to assess the safety of a waste repository, it is essential to be able to predict the eventual dispersion of its radioactive inventory in the environment. For radioactive materials stored in the ground or in geological formations, the most probable transport medium is the aqueous phase and several experimental evidences indicate that colloids can be a major factor in the rapid migration of radioactivity in groundwater. For example, Kersting *et al.* [Kers 99] reported detection of  $^{239/240}\text{Pu}$  in groundwater samples taken from aquifers at the Nevada test site. The  $^{239/240}\text{Pu}$  isotope ratio of the samples established an underground nuclear test site 1.3 km north of the sampling area as the origin of the plutonium. The plutonium was found to be associated with colloids.

To understand the role of colloids in waste disposal, it is necessary to consider their source and the mechanism of formation. Two kinds of colloids can be formed in groundwater. Intrinsic colloids are produced by condensation of actinide molecules or ions and pseudocolloid are generated by adsorption of actinide ions on aquatic colloids [Rams 88; Kim 94; Kim 2000] (for detail explanation, see Section 2.1.4). An important factor is the quantitative prediction of the reactions that are likely to occur between radioactive elements dissolved or suspended in groundwater and the surrounding rock material or natural colloids in order to estimate the quantities of waste that can be transported in the aqueous phase.

For the precise geochemical modeling, it is essential to know the relative stabilities of the compounds and complexes that may form under the relevant conditions. This information is often provided by speciation calculations using chemical thermodynamic data. The local conditions, such as ground water and rock composition or temperature, may not be constant along the migration paths of radioactive materials, and fundamental thermodynamic data are the indispensable basis for dynamic modeling of the chemical behavior of radioactive waste components. The scientific literature on thermodynamic data, mainly on equilibrium constants and redox potentials in aqueous solution, is contradictory in a number of cases, especially in plutonium chemistry [Lemi 2001].

Plutonium can exist in solution as different oxidation species: Pu(III), Pu(IV), Pu(V), and Pu(VI). Moreover, Pu(IV) can easily form polymeric species or colloids under certain conditions. An understanding of the behavior of different Pu species under environmental conditions is required for the accurate estimation

of migration rates. Plutonium migration rates are affected by the adsorptive properties of different plutonium aqueous species on geological media, by the solubility of the plutonium and by the stability of plutonium colloids [Rai 81].

Among the different Pu oxidation states, the tetravalent plutonium has the strongest tendency toward hydrolysis, polymerization and further colloid formation due to its high effective charge [Kim 91]. Accordingly, the solubility of Pu(IV) hydroxide or oxide is very low compared to other Pu oxidation states. Because of the low solubility, the possibility to investigate the aqueous speciation by spectroscopy is rather poor. Moreover, Pu(IV) is easily oxidized or reduced to other oxidation states such as Pu(V) and Pu(VI) or Pu(III). Such problems complicate the experimental investigation and thermodynamic evaluation of the hydrolysis constants and solubility product of Pu(IV). In particular, the solubility products reported for Pu(OH)<sub>4</sub>(am) show considerable discrepancy [Lemi 2001; Guil 2003].

Prior to studying the complex plutonium chemistry, the investigation of Zr(IV) is carried out as a homolog to Pu(IV) in the present work. Zr is also an important element in nuclear waste management, since it is not only a fission product (<sup>93</sup>Zr,  $t_{1/2} = 1.5 \cdot 10^6$  a) of high yield in spent fuel but is also used directly as cladding of fuel rods or even as mixed metal fuels ((Pu/Zr)O<sub>2</sub>). The chemistry of Zr shows some remarkable similarities to Pu(IV). Zr also has a strong tendency to hydrolysis and colloid formation and low solubility like Pu(IV). The first hydrolysis constant of Zr is similar to that of Pu(IV) and also the solubility of Zr hydroxide is reported to be similar in literature. However, the investigation of Zr is easier than Pu due to its redox stability and the availability of non-radioactive isotopes.

In this study, the solubility of Zr is determined by detecting the formation of Zr(IV) colloids using LIBD (laser induced breakdown detection). The results suggest the presence of at least two different colloidal species. In order to appraise the respective structures, Zr species in solution are investigated using XAFS. With an experimental approach similar to that used for Zr, the solubility of Pu(IV) hydroxide is determined using LIBD and spectroscopy in acidic solution. In addition, to understand the complex plutonium chemistry, the redox behavior of Pu is precisely observed as a function of time using spectroscopy. Formation constants for the first and second hydrolysis species are determined through the measurement of redox potentials of the solutions.

## 2 The state of knowledge in literature

In order to predict the introduction of actinides into the environment, to perform safety assessment studies to determine the ability of repositories and to design ways to retard their release and migration rates, it is essential to understand the chemical properties of actinides, such as the relative stabilities of the compounds and complexes that actinides may form under environmental conditions [Silv 95]. However, the scientific literature on thermodynamic data, mainly on equilibrium constants and redox potentials in aqueous solution, has been contradictory in a number of cases, especially in actinide chemistry [Lemi 2001].

### 2.1 Chemistry of actinides in aquatic systems

For understanding and predicting the chemical behavior and transport properties of actinides under aqueous environmental conditions, several chemical reactions should be considered, which control the amounts and species of the actinides in solution. In particular, complexation (for example, hydrolysis reactions), solubility, colloid formation, precipitation, and sorption have to be understood [Kim 86; Silv 95].

A number of inorganic and organic ligands which can form complexes with the actinide ions in solution are present in groundwater. Complexation increases the amount of the actinides in solution and thus tends to increase release and migrations rates.

The primary complexation reaction in aquatic phase is hydrolysis, which produces mononuclear and polynuclear species. Further aggregation, dehydration or crystallization processes may lead to the formation of colloids which may exhibit a considerably different migration behavior from aqueous species. Depending on colloidal size and charge relative to the surrounding porous media, colloids can move more rapidly or more slowly than the average groundwater velocity [Avog 84; Rams 88]. Precipitation can occur if the concentration of the actinides in solution exceeds the solubility with respect to the formation of a solid phase. This effect will limit the amount of the actinides in solution and thus will tend to have a retarding effect on release and migration rates. However, the solubility of actinide elements in the environment is somewhat different from that of well defined laboratory solutions due to the influence of complexation with many kinds of ligands present in groundwater.

The actinide ions may adsorb to mineral or rock surfaces in contact with the aqueous phase. Because this process removes actinide ions from solution, it tends to reduce the amount of actinide ions in solution and produce a retarding effect on the migration process.

The above reactions depend substantially on the oxidation state of each actinide element. Therefore the speciation of actinide ions is an absolutely necessary prerequisite for any investigation. The stability of individual oxidation states in the aquatic phase is different for each element and the oxidation state changes depending on the chemical properties of a given solution (pH, redox potential, etc.).

### 2.1.1 Oxidation states of actinides in aquatic systems

Characteristic for the actinide series of elements is the filling of the  $5f$  electron orbital. The chemical similarity to the  $4f$  lanthanide series was recognized more than 50 years ago [Seab 49; Seab 54]. While the trivalent oxidation state prevails throughout the lanthanide series, higher oxidation states are found to be the most stable in the early members of the actinide series [Katz 86].

Most neutral lanthanide atoms have the electronic configuration,  $4f^n 5s^2 5p^6 6s^2$ , and lose one  $4f$  and the  $6s^2$  electrons to form the trivalent oxidation state. The  $4f$  electrons are sufficiently shielded from the environment by the  $5s$  and  $5p$  orbitals that their contribution to valence forces is negligible. In a few cases, the energy difference between the  $4f$  and  $5d$  electrons is so small that changes of environment around a cation can lead to excitation of a  $4f$  electron to the valence shell ( $5d$  orbital). This results in formation of the tetravalent ions as in the case of Ce(IV). Alternately, the result may be the transfer of the  $5d$  electron to a  $4f$  orbital, leading to the formation of divalent ions (e.g.,  $\text{Sm}^{2+}$ ,  $\text{Eu}^{2+}$  and  $\text{Yb}^{2+}$ ) [Chop 94].

The light actinide elements exhibit an unusually broad range of oxidation states. The  $5f$  electrons of actinide elements are shielded to a larger extent from the nucleus of the atom than the  $4f$  electrons. This results in a smaller energy difference between the  $5f$ ,  $6d$ , and  $7s$  electrons than in the lanthanide series [Katz 86] and a wider range of oxidation states are possible, from III to VII. The oxidation states of the light actinide elements up to curium, that exist normally in solution, and their electron configurations are given in Fig. 2.1.

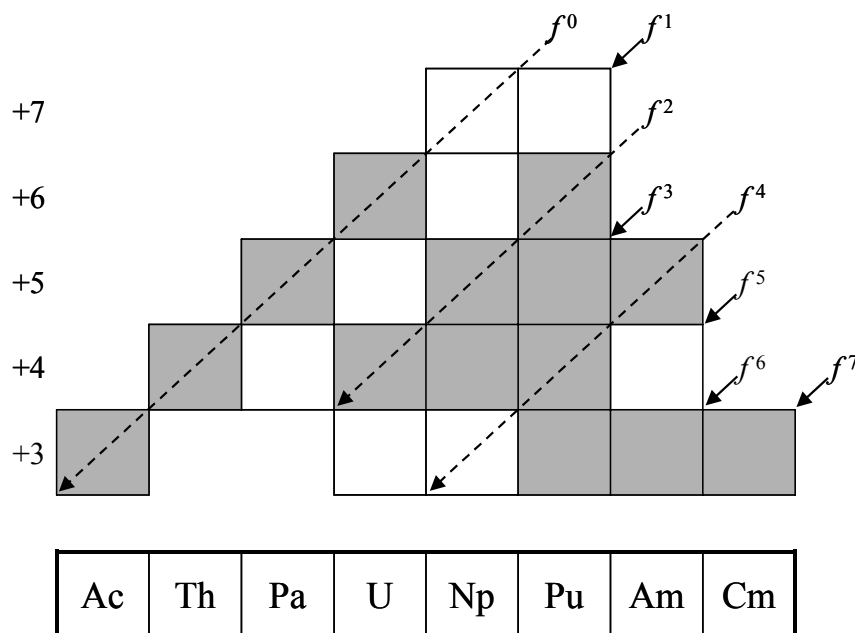


Fig. 2.1 Oxidation states of the light actinide elements and their electron configuration ( $f$  electrons).

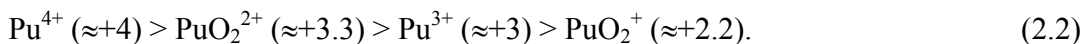
While the charge remains 3+, the ionic radii of the lanthanides decrease slightly across the series (the lanthanide contraction) [Durr 70]. Many chemical reactions of ions are correlated with the charge to volume ratio of the ions, the charge density [Lars 65]. The change of the charge density across the series is sufficiently small that the chemical properties are nearly identical. The trivalent actinides exhibit a similar decrease in ionic radii across the series (the actinide contraction) and they tend also to exhibit similar chemical properties [Katz 86]. Furthermore, trivalent actinides tend to exhibit similar chemical properties to trivalent lanthanides of the same ionic radius [Katz 86], e.g., trivalent actinides and trivalent lanthanide have similar hydrolysis constants [Baes 76]. The radii of the tetravalent actinides exhibit the same regular contraction with atomic number and tetravalent actinides might also have similar chemical properties. That has been confirmed for the solubilities of many compounds and for the formation constants for many complexes [Katz 86].

Actinide ions in the trivalent and tetravalent states in acidic solutions are in the form of the simple hydrated ions  $An^{3+}$  and  $An^{4+}$ .  $An^{5+}$  and  $An^{6+}$  form oxygenated species in solution called actinyl ions [Katz 86]. They have a symmetric and nearly linear structure. The actinyl ions  $AnO_2^+$  and  $AnO_2^{2+}$  are extremely stable and act as a unit in chemical reactions. This structure decreases the effective charge on the central actinide ion. The effective charge of the actinide ions decreases in the order of [Chop 83a]

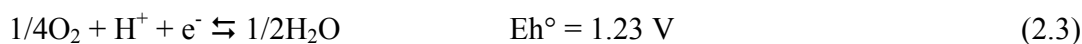




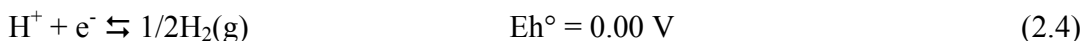
and in the case of plutonium [Chop 84; Chop 2003], the effective charges are



Redox potential, Eh [V] (the relative redox potential to the standard hydrogen electrode (SHE)) and pH are the most important parameters, which determine the redox equilibrium between different oxidation states of actinide elements in aquatic systems. The oxidizing and reducing reactions of water in acid solution [Stum 81] result in limits on the possible redox potentials and hence the oxidation state of actinides in solution, which are



and



where  $\text{H}_2(\text{g})$  is at unit fugacity (an ideal gas at unit pressure, 1 bar) and  $\text{H}^+$  is at unit activity. The standard redox potential,  $\text{Eh}^\circ$  [V], refers to a standard condition (as a hypothetical state) of an ideal 1 molar solution of ions at 25 °C and 1 bar gaseous pressure. The redox potential of water is a function of pH, because the reactions (2.3) and (2.4) by water constituent ions are directly influenced by pH. The ways in which Eh [V] varies with pH are given by the solid lines in Fig. 2.2.

The points shown in Fig. 2.2 are values obtained from Eh and pH measurements on natural waters from hundreds of different sources around the world [Baas 60] and illustrate the wide range in Eh and pH values. Any half reaction with a potential between the two lines of  $\text{H}_2\text{O}$  is stable with respect to oxidation or reduction by water. Of the many oxidation states that have been found for the actinides, only those with potentials that lie between the limits of water stability will persist in natural aquatic environments.

The redox potential for other than standard conditions (for the reaction (2.5)) is given by Nernst's equation (2.6) [Stum 81]:



$$\text{Eh} = \text{Eh}^\circ + \frac{RT}{nF} \ln \frac{[\text{ox.}]}{[\text{red.}]} \quad (2.6)$$

where  $R$  = the gas constant ( $8.314 \text{ J mol}^{-1} \text{ K}^{-1}$ ),  $T$  = temperature in Kelvin,  $n$  = number of electrons (mol) involved,  $F$  = the Faraday constant ( $96487 \text{ C mol}^{-1}$ ),  $[\text{ox.}]$  = the concentration of the oxidized species and  $[\text{red.}]$  = the concentration of the reduced species.

Redox potential follows relation (2.9) with electron activity in aqueous solutions,  $p_e = -\log a_e$ , defined in analogy with  $\text{pH} (= -\log a_{\text{H}^+})$ . Positive values of  $p_e$  represent oxidizing conditions while small or negative values correspond to reducing conditions. The relationship between  $p_e$  and  $\text{Eh}$  is induced as follows.

Reaction (2.4) and Nernst's law (2.6) can be used to introduce  $a_e$ :

$$\text{Eh} = \text{Eh}^\circ(2.4) + \frac{RT}{F} \ln \frac{\sqrt{f_{\text{H}_2}}}{a_{\text{H}^+} a_e} \quad (2.7)$$

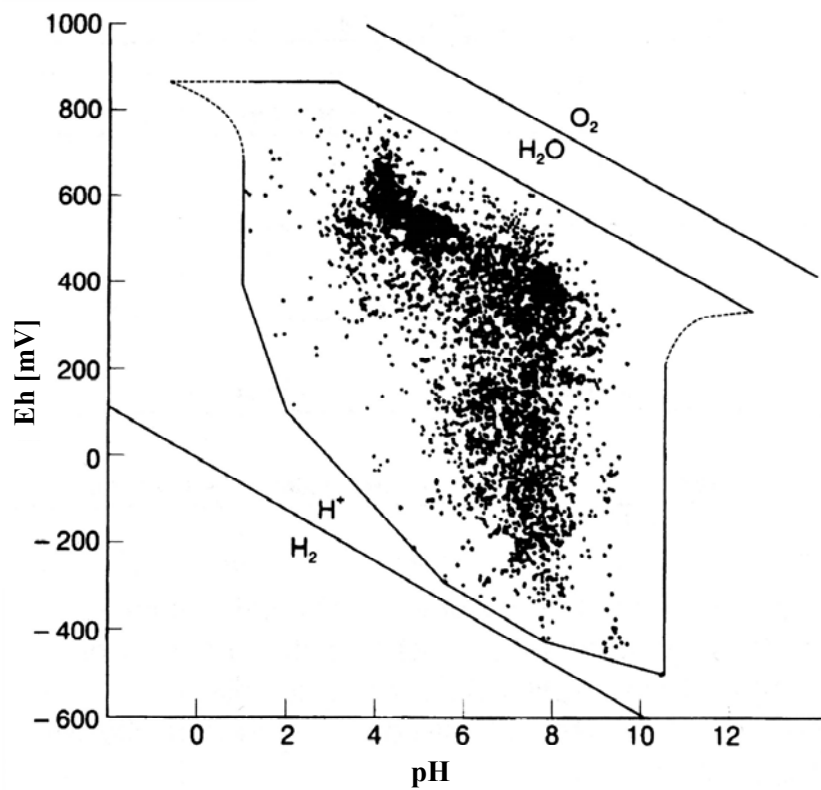


Fig. 2.2 The Eh-pH correlation found in waters in the natural environment. The oxidation of water (2.3) is the upper limit for Eh ( $\text{Eh} [\text{V}] = 1.3 + 0.0148 \times \log P_{\text{O}_2} - 0.059 \text{ pH}$ ) and the reduction of water (2.4) is the lower limit ( $\text{Eh} [\text{V}] = -0.0295 \times \log P_{\text{H}_2} - 0.059 \text{ pH}$ ). The solid lines represent the stability of water [Silv 95].

According to the SHE convention  $Eh^\circ(2.4) = 0$ ,  $f_{H_2} = 1$  (fugacity),  $a_{H^+} = 1$ , hence

$$Eh = -\frac{RT}{F} \ln a_{e^-} . \quad (2.8)$$

Eq. (2.8) is used to calculate a numerical value of  $a_{e^-}$  from measured Eh:

$$pe = -\log a_{e^-} = \frac{F}{RT \ln(10)} Eh = 16.9 Eh \text{ (at room temperature)}. \quad (2.9)$$

While the redox reactions between the An(III) and An(IV) states (2.10) as well as the An(V) and An(VI) states (2.11) are pH independent, oxidation or reduction reactions from either of the two lower oxidation states towards either of the two upper oxidation states (e.g., (2.12)) will be pH dependent because of the formation or decomposition of the actinyl ion:

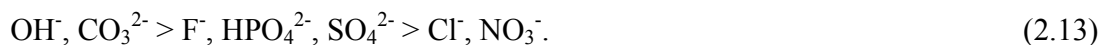


Low pH values tend to favor the lower oxidation states while the higher oxidation states become more accessible as the pH is increased.

Strong complexation (for example, with the  $OH^-$  ligand) of one member of a redox pair can significantly shift the potential in favor of its formation. Therefore, in order to calculate the exact pe value where redox reactions occur for U, Np, Pu, and Am, all of the significant reactions of the actinide ions would be included.

### 2.1.2 Hydrolysis of tetravalent actinides

The inorganic ligands in ground water responsible for the complexation of the actinides are hydroxide, carbonate, sulfate, phosphate, chloride, fluoride, nitrate and silicate. Complexation can occur with more than one ligand or actinide ion, so several species may be associated with a given ligand. The tendency of complexation for actinides in different oxidation states with a given ligand follows the effective charge of the actinide ions (2.1) and the trend in strengths of complexation of the various ligands are [Silv 95]:



Among the most important chemical reactions of all actinides in groundwater, hydrolysis has to be considered.

The formation constant of hydrolysis species is known to correlate with the electrostatic interaction energy,  ${}^{\text{el}}E_{\text{An-OH}}$  between the actinide ion and the  $\text{OH}^-$  ligand [Baes 76; Chop 83a; Gren 97]:

$$\log \beta_{\text{An}}^{\circ} \propto {}^{\text{el}}E_{\text{An-OH}} \propto (z_{\text{An}}/d_{\text{An-OH}})$$
 (2.14)

where  $z_{\text{An}}$  is the effective charge of the actinide ion and  $d_{\text{An-OH}}$  is the distance between the centers of actinide ion and  $\text{OH}^-$  ligand ion. This empirical linear correlation is usually applied to the first complexation constants, as used by Choppin [Chop 83a; Chop 94] to derive effective charges of  $z(\text{AnO}_2^+) = 2.3 \pm 0.1$  and  $z(\text{AnO}_2^{2+}) = 3.3 \pm 0.1$ . Fig. 2.3 shows the application of this correlation to the known hydrolysis constants summarized in [Neck 2001a].

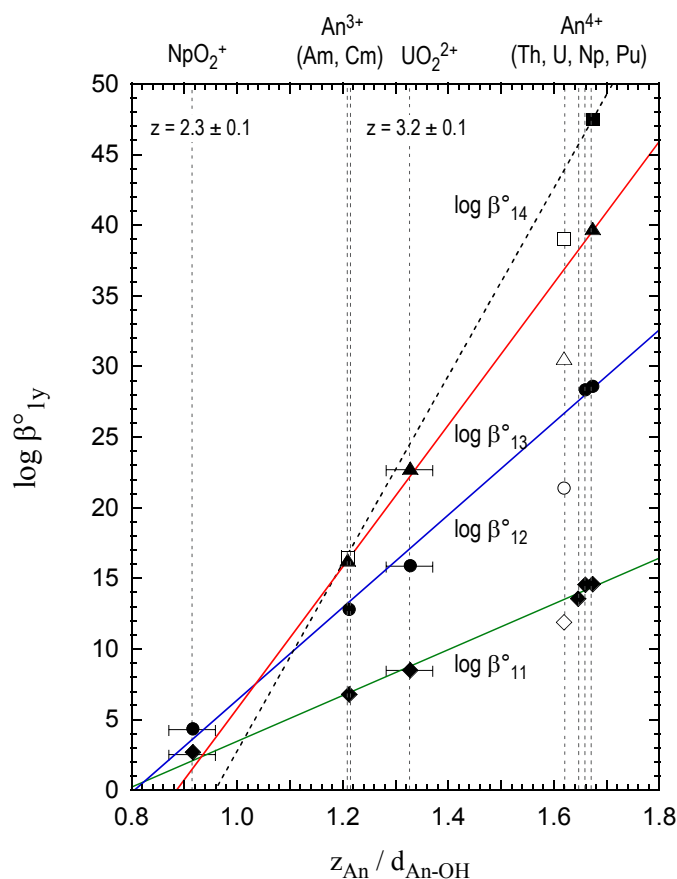
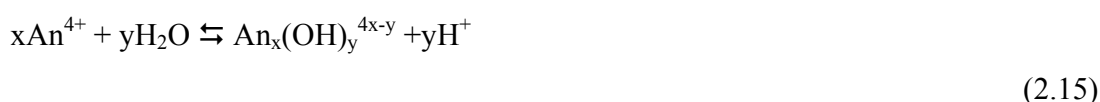


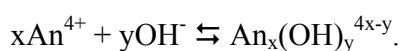
Fig. 2.3. The correlation of the formation constants  $\log \beta_{1y}^{\circ}$  of actinide hydrolysis species with the electrostatic interaction energy  ${}^{\text{el}}E_{\text{An-OH}}$  between the actinide ions and  $\text{OH}^-$  ions [Neck 2001a].

The tendency toward hydrolysis is strongest for tetravalent actinides as compared to other oxidation states. Within the series of An(IV), the distance  $d_{\text{An-OH}}$  decreases in the order of Th(IV) > U(IV) > Np(IV) > Pu(IV) and accordingly, the hydrolysis constants increase respectively. The relatively large differences of the hydrolysis constants of Th<sup>4+</sup> and those of other An<sup>4+</sup> ions cannot be explained by the differences in the ionic size [Neck 2001a].

The hydrolysis reactions of the An<sup>4+</sup> ions are usually written as



or



The hydrolysis constant  $K'_{xy}$  (in a given medium) and  $K^\circ_{xy}$  (at infinite dilution) are defined by

$$K'_{xy} = \frac{[\text{An}_x(\text{OH})_y^{4x-y}][\text{H}^+]^y}{[\text{An}^{4+}]^x} = \frac{K^\circ_{xy}(\gamma_{\text{An}^{4+}})^x(a_w)^y}{(\gamma_{\text{An}_x(\text{OH})_y})(\gamma_{\text{H}})^y} \quad (2.16)$$

and the corresponding formation constants  $\beta'_{xy}$  and  $\beta^\circ_{xy}$  are given by

$$\beta'_{xy} = \frac{[\text{An}_x(\text{OH})_y^{4x-y}]}{[\text{An}^{4+}]^x[\text{OH}^-]^y} = \frac{\beta^\circ_{xy}(\gamma_{\text{An}^{4+}})^x(\gamma_{\text{OH}^-})^y}{(\gamma_{\text{An}_x(\text{OH})_y})}. \quad (2.17)$$

[i] denotes the concentration of species i,  $\gamma_i$  its activity coefficient and  $a_w$  the activity of water. The hydrolysis constants  $\log K^\circ_{xy}$  are related to  $\log \beta^\circ_{xy}$  by the ion product of water ( $\log K^\circ_w = -14.00 \pm 0.01$ ). In the present work the specific ion interaction theory (SIT) (explained in detail in appendix 8.1) is applied for the calculation of activity coefficients.

### 2.1.3 Solubility of An(IV) hydroxides and oxides

As mentioned above, probably the most important chemical property of An(IV) for the assessment of transport in environmental conditions is the solubility. In addition to the strong tendency to hydrolysis, An(IV) rapidly undergoes colloid formation and its solubility is then low. It depends on the solid phase which is in equilibrium with aqueous species and the solubility products reported for amorphous hydroxide, microcrystalline or oxide show considerable differences [Neck 2001a]. However, the chemical form of freshly precipitated or aged An(IV) solid phases is not always clear. In the literature, they are called either amorphous hydroxides An(OH)<sub>4</sub>(am) or amorphous, partly microcrystalline hydrous oxides

$\text{AnO}_2 \cdot x\text{H}_2\text{O}(\text{am})$ . They may not have a unique composition but consist of a hydrated oxyhydroxide  $\text{AnO}_{(2-y)}(\text{OH})_{2y}(\text{am})$  with  $0 < y < 2$ , where  $y$  decreases with aging or increasing temperature. The preparation of water free crystalline dioxide  $\text{AnO}_2(\text{cr})$  requires heating above  $700^\circ\text{C}$  [Kim 89a; Moon 89]. However, even in the case of initially crystalline solids, a less crystalline solid or an amorphous surface layer can be formed by  $\alpha$  radiation damage or by dissolution-precipitation reactions. Therefore, solubilities calculated from thermodynamic data of well crystallized (thermodynamic stable) solids are often many orders of magnitude lower than those derived from experimental solubility data [Kim 89a]. The solubility products  $K'_{\text{sp}}$  of amorphous An(IV) solid phase,  $\text{An}(\text{OH})_4(\text{am})$  or  $\text{AnO}_2 \cdot x\text{H}_2\text{O}(\text{am})$  refers to the following equilibrium



or



with

$$K'_{\text{sp}} = [\text{An}^{4+}][\text{OH}^-]^4 \quad (2.20)$$

The corresponding  $K^\circ_{\text{sp}}$  at infinite dilution:

$$K^\circ_{\text{sp}} = K'_{\text{sp}} (\gamma_{\text{An}})(\gamma_{\text{OH}})^4 \quad (\text{for } \text{An}(\text{OH})_4(\text{am})) \quad (2.21)$$

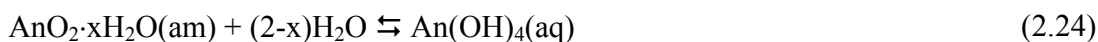
or

$$K^\circ_{\text{sp}} = K'_{\text{sp}} (\gamma_{\text{An}})(\gamma_{\text{OH}})^4 (a_w)^{(x-2)} \quad (\text{for } \text{AnO}_2 \cdot x\text{H}_2\text{O}(\text{am})). \quad (2.22)$$

If there are no complexes with other inorganic ligands or colloidal species present in solution, the total An(IV) equilibrium concentration is given by

$$\begin{aligned} [\text{An}(\text{IV})]_{\text{tot}} &= [\text{An}^{4+}] + \sum_{y=1}^4 [\text{An}(\text{OH})_y^{4-y}] \\ &= (K'_{\text{sp}} [\text{OH}^-]^{-4}) \left( 1 + \sum_{y=1}^4 \beta'_{1y} [\text{OH}^-]^y \right) \end{aligned} \quad (2.23)$$

In neutral and alkaline solutions which are of interest for natural groundwater systems,  $\text{An}(\text{OH})_4(\text{aq})$  is the predominant aqueous species if the tetravalent species is stable at all. The equilibrium between solid phase and aqueous species can be written as



and the solubility in this range is independent on pH.

The solubility products of the amorphous An(IV) hydroxide decrease by orders of magnitude in the series  $\text{Th}(\text{IV}) > \text{U}(\text{IV}) > \text{Np}(\text{IV}) > \text{Pu}(\text{IV})$ , which correlates with the decreasing distance  $d_{\text{An-O}}$  in the lattice [Shan 76]. The same trend is shown for the solubility product of the crystalline An(IV) dioxide calculated from thermodynamic data [Neck 2003] (Fig. 2.4).

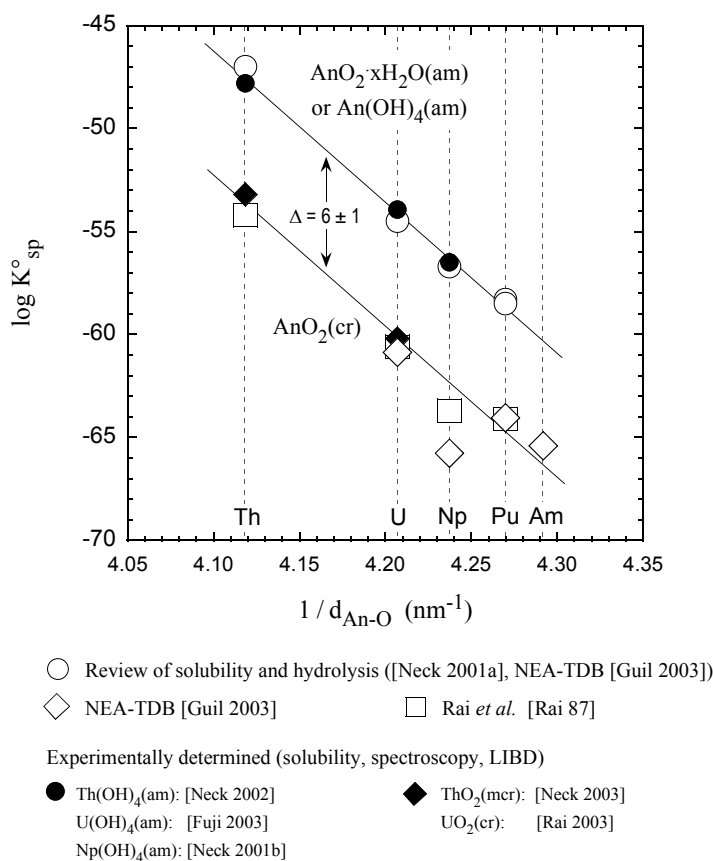


Fig. 2.4. Solubility products of  $\text{An}(\text{OH})_4(\text{am})$  and  $\text{AnO}_2(\text{cr})$  as a function of the distance  $d_{\text{An-O}}$  (sum of crystal radii of  $\text{An}^{4+}$  and  $\text{O}^{2-}$  in the fluorite structure [Shan 76]). Filled symbols represent  $\log K_{\text{sp}}^{\circ}$  values derived from experimental solubility studies, open symbols represent calculated values from thermodynamic data (summarized in [Neck 2003]).

#### 2.1.4 Colloid formation of actinides

The “*colloid*” was named by Thomas Graham in 1860 to represent substances which do not diffuse through a semipermeable membrane. Nowadays, normally the term colloid is used to refer to a particle of small size dispersed in solution. Although there are no precise boundaries of size between suspended particles and colloids, the size range for colloids is usually defined by convention between 1 nm and 1  $\mu\text{m}$ .

For many years, there is experimental evidence that colloids may enhance the migration of radioactive elements in given aquifer systems. Some studies reported that plutonium and americium migrated up to 30 m, though a model which ignored the influence of colloids predicted that migration was limited to a few millimeters [Nyha 85; Nutt 93]. Kersting *et al.* reported that plutonium residue from one of several underground nuclear weapon tests in Nevada had migrated more than a km from the test site by colloid mediated transport [Kers 99]. When the influence of colloids for migration is not considered then radionuclide transport out of a repository might be strongly underestimated. Therefore, recently, some classical models were extended for groundwater contaminant transport to account for the presence of colloids in the system [Mars 2001a; Mars 2001b].

To understand the role of colloids for enhancing migration, it is necessary to understand the source of colloids and the mechanism of their formation. “Aquatic colloids” are ubiquitous in natural aquifer systems. The amount and nature of these colloids depend on the surrounding geologic structure. Colloids are commonly composed of materials produced by the disintegration and weathering of rocks and minerals (e.g., clays, silica, aluminum oxide minerals) as well as hydroxide or hydrated oxides of metals (e.g., iron). Various natural organic colloids (humic or fulvic substances) are also present.

When actinide ions are introduced into groundwater, then two types of actinide colloids can be formed [Kim 89a; Kim 94; Silv 95].

- (1) “Real” (pure, eigen, true, or intrinsic) colloids are produced by condensation of actinide molecules or ions by a hydrolytic or precipitation process. These colloids might have similar chemical properties to those of the assumed compound in macroamounts. Actinide hydroxides and oxides usually have very small solubilities in natural water, making them the common source of real colloids. Because the formation of real colloids is related to their hydrolysis, thermodynamic studies are primary references to colloid studies. The tendency of actinides to form real colloids is the same as their tendency of hydrolysis and controlled by the effective charge of each ion,  $\text{An}^{4+} > \text{AnO}_2^{2+} \geq \text{An}^{3+} > \text{AnO}_2^+$  (2.1).



(2) “Pseudo” (fremd or associative) colloids are generated by adsorption of trace amounts of actinide ions on aquatic colloids. The chemical properties of these colloids might not be altered by the adsorbed metal ion. Various reaction mechanisms are conceivable for the generation of actinide pseudocolloids in natural aquifer systems. Since actinide ions are present either as hydrolyzed or complexed species, the hydrolyzed species may interact with aquatic colloids through ion exchange, complexation, or isomorphous substitution reactions [Kim 91]. In case of organometallic colloids of humic acid composition, the actinide ions are adsorbed by ion exchange or chelate complexation, particularly with carboxylic and phenolic groups [Kim 92]. The formation of actinide pseudocolloids stabilizes actinide ions in natural water and could increase amounts of dissolved actinide species by many orders of magnitude [Kim 89b].

## 2.2 Chemistry of plutonium in aquatic systems

Plutonium was first synthesized and identified (atomic number 94) at the University of California Berkeley in spring 1941, by Glenn T. Seaborg and his colleagues. In spite of the one half century of research on plutonium metal, alloys and compounds in solution, there are still many unanswered questions. Recent works on plutonium transport in groundwater [Nyha 85; Kers 99] indicate that the migration of plutonium is quite different from expectations by modeling. The chemistry of plutonium in near neutral solutions is poorly understood. That complicates the prediction of its behavior in groundwater present at proposed nuclear waste disposals. Plutonium can migrate in the environment via aqueous media such as ground-, surface-, river-, lake-, and sea-water. There are four important processes that can control the amounts and forms of the plutonium in solution: complexation, colloid formation, precipitation, and sorption. Because these processes strongly depend on the plutonium species, detailed knowledge on oxidation state and overall charge of the respective stable species at given conditions is necessary [Hoff 2002].

### 2.2.1 Oxidation states of Pu in aquatic systems

The chemical behavior of plutonium is controlled by its electronic structure. The lowest energy configuration of the valence electrons is nominally  $5f^6 7s^2$ , but the energy levels of the 6 *d* and 5 *f* orbitals are similar, and the  $5f^6 7s^2$  and  $5f^5 6d^1 7s^2$  electronic configurations compete. In fact, as one moves from

thorium to plutonium in the periodic table, the order of orbital energies is inverted, i.e. the 5 *f* orbitals become lower in energy than the 6 *d* orbitals [Heck 2001].

A plutonium atom in aqueous solution will lose between three and seven of its outer electrons to form cations in five formal oxidation states ranging from Pu(III) to Pu(VII). This diversity of oxidation states makes Pu solution chemistry very complex because each of them forms different compounds or complexes. Moreover, the formal potentials of each oxidation are very similar (approximately 1 V, see below Fig. 2.5) and thus the oxidation and reduction of one oxidation state toward the others can undergo easily. As a consequence, Pu can exist in several oxidation states within the same solution and can, at low pH, even exhibit four oxidation states simultaneously [Heck 2001].

The instabilities of Pu oxidation states in conjunction with the generation of free radicals through its radioactive decay for the short lived isotopes, yield solution chemistry that is constantly changing and affecting chemical processing operations, nuclear waste storage and treatment, and the reactivity and mobility of plutonium in the environment [Heck 2001].

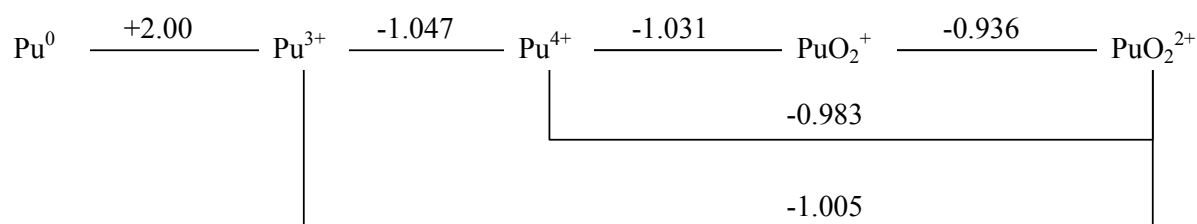


Fig. 2.5 Formal potentials at  $I = 0$  (extrapolated to zero ionic strength) reviewed in [Lemi 2001] for plutonium at 25°C, in units of V vs. SHE.

## 2.2.2 Hydrolysis constants of Pu(IV)

At low concentration, the hydrolysis reactions (2.15) of the tetravalent plutonium ion,  $\text{Pu}^{4+}$ , lead to the formation of mononuclear complexes  $\text{Pu}(\text{OH})_y^{4-y}$  ( $y = 1 - 4$ ). It is not yet confirmed whether or not the anionic species  $\text{Pu}(\text{OH})_5^-$  is formed in strongly alkaline solutions. At higher Pu(IV) concentrations, polynuclear species ( $\text{Pu}_x(\text{OH})_y^{4x-y}$ ) are probably formed. The hydrolysis constants  $K'_{xy}$  (in a given medium) and  $K^\circ_{xy}$  (at infinite dilution) are given by (2.16) and the corresponding formation constants  $\beta'_{xy}$  and  $\beta^\circ_{xy}$  for the species  $\text{Pu}_x(\text{OH})_y^{4x-y}$  are given by (2.17) in Section 2.1.2

A number of studies of the hydrolysis constants for mononuclear species,  $\text{Pu}(\text{OH})_y^{4-y}$  ( $y = 1 - 4$ ), are well summarized in [Lemi 2001]. Most data are obtained by spectroscopy [Krau 50; Rabi 60; Clev 68; Nits 96;

Yuso 2004] and complemented by potentiometry [Rabi 51; Rabi 57] at high and extraction [Meti 72] at low Pu concentration. In some studies the thermodynamic equilibrium might not have been reached due to slow oxidation, disproportionation, radiolysis, or polymerization reactions. Especially due to the pronounced redox sensitivity of Pu (see 2.2.1), reliable values for the hydrolysis constant can be found only from studies in which the electrochemical potential was carefully controlled, or in which the measurements were carried out rapidly enough to exclude the influence from those slow reactions. An overview of the reported hydrolysis constants is given in Table 2.1.

Table 2.1 Pu(IV) hydrolysis constants at 20 - 25°C and the values converted to  $I = 0$  with the specific ion interaction theory (SIT)<sup>1)</sup> approach.

Medium/Species	$\log K'_{1y}$	$\log K^{\circ}_{1y}$	$\log \beta^{\circ}_{1y}$	Method	Ref.
1.0 M (H/Na)ClO <sub>4</sub> , room temp., 10 <sup>-8</sup> M Pu(IV)				extr.	[Meti 72]
Pu(OH) <sup>3+</sup>	-0.45	0.60	14.6 ± 0.2		
Pu(OH) <sub>2</sub> <sup>2+</sup>	-1.2	0.63	28.6 ± 0.3		
Pu(OH) <sub>3</sub> <sup>+</sup>	-4.5	-2.25	39.7 ± 0.4		
Pu(OH) <sub>4</sub> (aq)	-10.8	-8.54	47.5 ± 0.5		
Pu(OH) <sup>3+</sup>					
0.5 M (H/Na)Cl, 25°C, 7.2·10 <sup>-4</sup> M Pu(IV)	-1.65	-0.63	13.37	spec.	[Krau 50]
0.5 M (H/Na)ClO <sub>4</sub> , 25°C, 7.2·10 <sup>-4</sup> M Pu(IV)	-1.60	-0.64	13.36	spec.	[Krau 50]
2.0 M (H/Na)ClO <sub>4</sub> , 25°C, 10 <sup>-3</sup> M Pu(IV)	-1.73	-0.70	13.30	spec.	[Rabi 60]
0.19 M HClO <sub>4</sub> , 23°C, 1.8·10 <sup>-3</sup> M Pu(IV)	-1.96	-1.19	12.81	spec.	[Clev 68]
0.06 M HClO <sub>4</sub> , 23°C, 1.6·10 <sup>-3</sup> M Pu(IV)	-1.48	-0.94	13.06	spec.	[Clev 68]
0.5 M (H/Na)ClO <sub>4</sub> , room temp., 1.3·10 <sup>-4</sup> M Pu(IV) (pH 0.3 - 1.5)	-1.57	-0.61	13.39	spec.	[Nits 96]
0.5 M (H/Na)ClO <sub>4</sub> , room temp., 1.2·10 <sup>-4</sup> M Pu(IV)	-1.57	-0.61	13.39	spec.	[Yuso 2004]
0.1 M (H/Na)ClO <sub>4</sub> , room temp., 1.2·10 <sup>-4</sup> M Pu(IV)	-1.20	-0.57	13.43	spec.	[Yuso 2004]
1.0 M (H/Na)ClO <sub>4</sub> , 25°C, 10 <sup>-3</sup> M Pu(IV)	-1.51	-0.45	13.55	redox.	[Rabi 51]
2.0 M (H/Li)ClO <sub>4</sub> , 25°C, 8·10 <sup>-3</sup> M Pu(IV)	-1.27	-0.24	13.76	redox.	[Rabi 57]

1) SIT (See appendix 8.1).

One favorite method to investigate the first hydrolysis constant is the spectrophotometric measurement, probably because of its ease of use. In these studies, the decrease of the characteristic Pu(IV) absorption bands (mostly at 470 nm) is ascribed to the initial mononuclear hydrolysis step (reaction (2.15),  $x = 1$  and  $y = 1$ ). However, neither are there characteristic absorption bands which differ considerably for  $\text{Pu}^{4+}$  and  $\text{Pu}(\text{OH})^{3+}$  nor is there a shift of the peak position and these studies might suffer from similar misinterpretation as was the case for Np and clarified only recently [Neck 2001a]. Most Pu studies are performed in the range pH 0 - 2 at relative high concentrations, which exceed the operational range of conventional spectrophotometers and actually, in all of these spectroscopic studies, the total Pu(IV) concentrations considerably exceed the solubility limit of amorphous Pu(IV) solid at pH 1 - 2 (See Fig. 2.6), thus polymer species or colloids could be present in solutions and account for the decreasing absorption.

Especially in the recent work [Yuso 2004], the influence of colloid formation is well observed. This work is carried out in the pH range from 1.00 to 1.34 at Pu concentration  $1.20 \cdot 10^{-4}$  M in 0.5 M (H/Na)ClO<sub>4</sub> matrix. In these results, absorption at 470 nm decreases with increasing pH whereas at about 620 nm the absorption increases. The authors conclude that the colloid formation didn't occur in this area using only an indirect method to detect colloids by acidifying of solutions. However, the concentration already exceeds the solubility limit at pH 1 (See Fig. 2.6). Moreover, the increasing absorption at 620 nm with pH actually indicates the formation of colloidal plutonium which has a specific absorption band at 620 nm [Clev 79] (see Appendix 8.4). This leads to the conclusion that the absorption decrease at 470 nm with increasing pH is due to the formation of colloids which have no absorption bands in the considered wavelength range. Therefore the hydrolysis constants obtained by spectroscopy may be systematically in error.

Some potentiometric studies were carried out to determine the hydrolysis constant [Rabi 51; Rabi 57] but these had also some shortcomings. In these studies, the redox potential was measured as a function of the pH at relative high Pu concentration (over  $10^{-3}$  M) and two equilibria, redox equilibrium of the Pu(III) and Pu(IV) couple and first hydrolysis reaction of Pu(IV), were considered. From the measured redox potential, the first hydrolysis constant was determined. However, the authors didn't always allow reactions such as disproportionation of Pu(IV) and precipitation to reach equilibrium state, though these reactions need some reaction times to reach equilibrium.

The stepwise hydrolysis equilibria for  $\text{Pu}^{4+}$  are determined in undersaturated solutions by the solvent extraction technique using  $^{238}\text{Pu}$  in trace concentration ( $[\text{Pu}]_{\text{tot.}} = 10^{-7}$  M  $\sim$   $10^{-8}$  M) [Meti 72]. The value is an order of magnitude larger than the value found potentiometrically in a similar medium [Rabi 51]. This difference could be due to decrease of  $\text{Pu}^{4+}$  through disproportionation or polymerization and colloid formation at higher pH in spite of the low concentration. Actually, Pu(IV) disproportionation cannot be neglected in solutions with pH values at which  $\text{Pu}^{4+}$  is expected to be hydrolyzed to  $\text{PuOH}^{3+}$ . Thus, to stabi-

lize Pu(IV) in this study, the distribution experiments were carried out with different redox agents in different pH regions. However, the data were not corrected for effects on counting rate due to variations in scintillation quenching caused by varying concentrations of TTA (thenoyl trifluoroacetone) in the organic phase. The experimental uncertainties are estimated to be about 0.2 logarithmic units for the first hydrolysis step [Knop 99].

There are no experimental data other than those of [Meti 72] to check the values of  $\log \beta^{\circ}_{12}$  and  $\log \beta^{\circ}_{13}$ , but the value of  $\log \beta^{\circ}_{14}$  was confirmed from solubility experiments. Neck and Kim [Neck 2001a] pointed out that at least the formation constant of the first hydrolysis species,  $\beta^{\circ}_{11}$  should be known from an experiment where the presence of colloids is excluded in order to reliably calculate  $\beta^{\circ}_{1y}$  ( $y = 2 - 4$ ) by an electrostatic approach [Neck 2000]. Therefore, the value,  $\log \beta^{\circ}_{11} = 14.6$ , derived from experiments at trace levels [Meti 72] is taken for the estimation of other formation constants. These values from the model calculation in [Neck 2001a] are in close agreement with the experimental values of [Meti 72].

### 2.2.3 Solubility of Pu(IV) hydroxide/hydrous oxide

The solubility product of  $\text{Pu}(\text{OH})_4(\text{am})$  or  $\text{PuO}_2 \cdot x\text{H}_2\text{O}(\text{am})$  is defined according to ((2.20) - (2.22)) in Section 2.1.3. If the Pu(IV) concentration of polynuclear and colloidal species is quite lower than that of mononuclear hydrolysis species, the solubility is given by (2.23) in Section 2.1.3. For the calculation of the solubility product using Eq. (2.23), the total concentration of all tetravalent plutonium aqueous species ( $[\text{Pu}(\text{IV})]_{\text{aq}} = \sum [\text{Pu}(\text{OH})_y^{4-y}] (y=0-4)$ ) and the hydrolysis constants ( $y = 1 - 4$ ) must be known.

There are a number of reports on the solubility of solids resulting from hydrolysis of Pu(IV) [Kash 49; Pere 65; Rai 84; Lier 86; Kim 89a; Knop 99; Rai 99; Bite 2005] as shown in Fig. 2.6. The values reported scatter considerably with an uncertainty of several orders of magnitude. There are various reasons to explain the discrepancy of solubility data.

- (1) For the experiments from undersaturation (the prepared solid phase is contacted with a solution and then the concentration of dissolved Pu is determined in the supernatant), the important question is when the dissolution reaction reaches the equilibrium state. Too short reaction time causes the underestimation of solubility.
- (2) It is very important to consider the distribution of the oxidation states of the dissolved species in the solution. As mentioned in Section 2.2, Pu can exist in several oxidation states simultaneously.

So, if some fraction of Pu is present in an oxidation state other than Pu(IV), but not subtracted from the total solute amount, then the solubility is overestimated.

- (3) Colloids must be separated from the solution, before the concentration of soluble Pu is determined. When this is not done, the colloids can be mistaken for the dissolved species and the solubility appears to be too high.
- (4) Since the solubility product refers to  $\text{Pu}^{4+}$  and not to  $\text{Pu(IV)}_{\text{aq}}$ , for the calculation of solubility product, hydrolysis constants must be known. However, the first hydrolysis constant is still not consistently known though many studies have been carried out and for the other hydrolysis constants there is only one set of experimental data.
- (5) The solid phase has to be well defined. The aging of  $\text{Pu(OH)}_4(\text{am})$  or  $\text{PuO}_2 \cdot x\text{H}_2\text{O}(\text{am})$  might form  $\text{PuO}_2$  [Lloy 78] (analogous to the case of thorium [Pras 67]), or conversely, the crystalline dioxide, when contacted with water over a period of time, is slowly converted to (or coated with a small amount of) a less crystalline form (see [Rai 82] for  $^{238}\text{PuO}_2$ ). Therefore an ill defined solid phase can lead to such discrepancy in the literature.
- (6) When an isotope which has a relative short life time is applied for experiments, the radiolysis effects must be considered. The autoradiolysis leads not only to the conversion of the solid phases but also causes reduction of Pu oxidation states due to formation of radicals.

The solubility data of  $\text{Pu(OH)}_4(\text{am})$  or  $\text{PuO}_2 \cdot x\text{H}_2\text{O}(\text{am})$  were reviewed in literature [Neck 2001a]. In this literature, authors considered the average of experimental data to represent the best value for solubility product resulting in  $\log K_{\text{sp}}^{\circ} = -58.5 \pm 0.7$ . The solubility curves in Fig. 2.6 (b) are calculated at 1 M ionic strength (solid line) and 0.1 M (dashed line) on the basis of the hydrolysis constants from [Meti 72]. In a recent review [Guil 2003], based on the solubility constants determined by [Capd 98; Knop 99; Fuji 2001; Rai 2002] who used three different, independent methods,  $\log K_{\text{sp}}^{\circ} = -58.33 \pm 0.52$  is selected as un-weighted mean value. All the values recently reported agree relative well with this selected value and the uncertainty has been decreased but still remains relatively large.

The solubility data of  $\text{PuO}_2(\text{cr})$  were summarized in [Lemi 2001] as  $\log K_{\text{sp}}^{\circ} = -64.0 \pm 0.5$  and this value is about 6 orders of magnitude lower than of  $\text{Pu(OH)}_4(\text{am})$  solid phase.

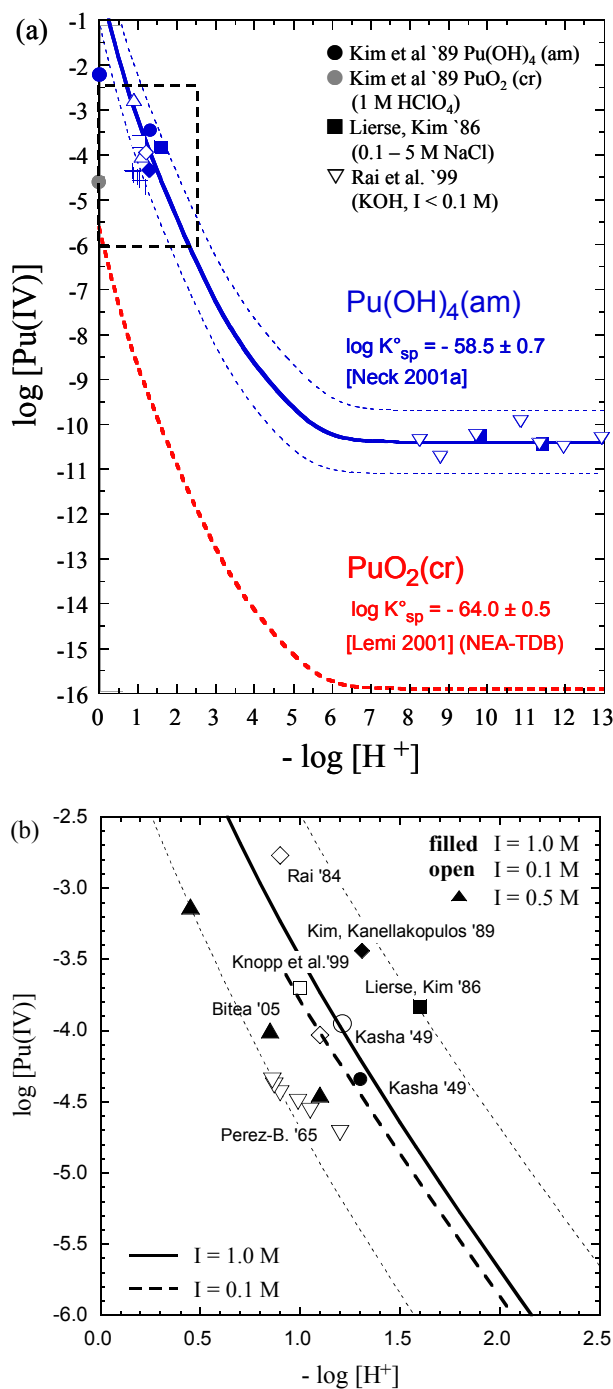


Fig. 2.6 (a) Solubility data of  $\text{Pu}(\text{OH})_4(\text{am})$  and  $\text{PuO}_2(\text{cr})$  for acidic and basic media ( $\text{pH} = 0 - 12$ ). The solubility curve for  $\text{Pu}(\text{OH})_4(\text{am})$  is calculated at 1 M  $\text{NaClO}_4$  with  $\log K_{\text{sp}}^{\circ} = -58.5 \pm 0.7$  [Neck 2001a] and hydrolysis constants from [Meti 72] and for  $\text{PuO}_2(\text{cr})$  with  $\log K_{\text{sp}}^{\circ} = -64.0 \pm 0.5$  [Lemi 2001]. (b) Magnification of the dashed region in (a). The dashed solubility curve of  $\text{Pu}(\text{OH})_4(\text{am})$  is calculated at 0.1  $\text{NaClO}_4$ . Solubility data summarized in [Neck 2001a] and of a LIBD study ( $\blacktriangle$ ) [Bitea 2005] are depicted.

## 2.2.4 Redox reactions of plutonium

In Section 2.2.1, it is already mentioned that the plutonium can have five different oxidation states and, depending on pH, up to four oxidation states can be present simultaneously. In this section, the most important reactions contributing to the redox behavior of plutonium in solution are discussed.

Even in solutions which are carefully prepared to contain only one well defined oxidation state, the equilibrium of two or more oxidation states may form over time. This phenomenon is explained by disproportionation of Pu(IV) or Pu(V) in literature.

If, for instance, a solution which contains only Pu(IV) is considered, the Pu(IV) is assumed to disproportionate to Pu(III) and Pu(V) by the following reaction (2.25) via collision of two Pu(IV) atoms



If the Pu(V) is not stable due to pH and Eh in solution, then the Pu(V) undergoes further disproportionation to Pu(IV) and Pu(VI) by the following reaction,

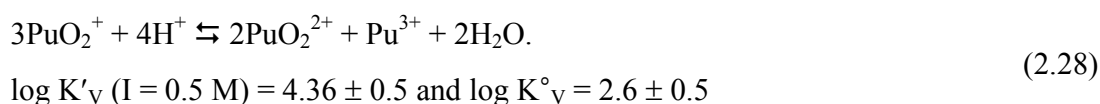


Combining reactions (2.25) and (2.26) leads to the reaction (2.27), if Pu(V) is not stable:



In some studies the equilibrium constants of this reaction (2.27) were investigated in different media and converted to zero ionic strength. The obtained equilibrium constants of reaction (2.27),  $\log K'_{\text{IV}}$ , are -2.05 in perchlorate medium at  $I = 1 \text{ M}$  [Rabi 53], -0.42 in  $\text{HNO}_3$  medium at  $I = 0.16$  [Cost 73], and  $-2.09 \pm 0.5$  in  $1.3 \text{ M HClO}_4$  [Capd 92] with the respective  $\log K^\circ_{\text{IV}}$  values (at zero ionic strength) of 2.43, 2.38 and 2.39 which agree well each others.

Capdevila *et al.* [Capd 92] studied the Pu(V) disproportionation at pH 1,  $I = 0.5 \text{ M}$  ( $(\text{H}/\text{Na})\text{ClO}_4$ ) and a total Pu concentration of  $1.6 \text{ mM}$  where 95% of plutonium was Pu(V). In this solution, two Pu(V) form Pu(IV) and Pu(VI) (reaction (2.26)) and subsequently two Pu(IV) disproportionate to Pu(V) and Pu(VI) (reaction (2.25)), resulting in the total reaction (2.28):



In [Capd 92], these reactions did not reach the equilibrium state because of radiolysis that caused additional reduction of Pu(IV) and Pu(VI), and lead to an increase in  $\text{PuO}_2^{2+}$  and  $\text{Pu}^{3+}$  concentration. Conse-



quently,  $K_{IV}$  was then overestimated and  $K_V$  underestimated. Nevertheless,  $\log K^\circ_{IV}$  by Capdevila *et al.* was nearly the same as the two previous values. Capdevila *et al.* themselves explained it as follows. The measurements and the data treatment of these experiments were quite different, but the chemical reaction studies were the same and it might suffer from the same systematic error (the poor achievement of the equilibrium).

All the reactions above can alternatively be represented by the summation or subtraction of the following half reactions. Firstly, there are the redox equilibria between  $\text{Pu}^{3+}$  and  $\text{Pu}^{4+}$  and between  $\text{PuO}_2^+$  and  $\text{PuO}_2^{2+}$ . Normally it is assumed that these reactions are fast because the electron transfer between two species of the same structure is rapid and reversible.



$$\log K^\circ = -17.74 \pm 0.051 \text{ [Lemi 2001]}$$

and



$$\log K^\circ = -15.86 \pm 0.085 \text{ [Lemi 2001]}$$

These reactions do not depend on the pH of the solution. Secondly, there are the oxidation or reduction reactions between either of the two lower oxidation states (Pu(III) or Pu(IV)) and either of the two upper oxidation states (Pu(V) or Pu(VI)). These reactions are slow since they require the formation or decomposition of Pu-O bonds and the reorganization of the solvent shell [Katz 86], for example, is the oxidation of Pu(IV) to Pu(V),



$$\log K^\circ = -17.47 \pm 0.17 \text{ [Lemi 2001]}.$$

This reaction (2.31) also reflects the fourth power dependence on the hydrogen ion concentration for the oxidation to plutonyl ions and explains the increasing stability of the Pu(V) state with decreasing  $\text{H}^+$  concentration [Fuge 76]. Finally, if Pu(IV) colloids or precipitates are present, then these Pu(IV) solid phases are in equilibrium with  $\text{Pu(V)}_{\text{aq}}$  according to,



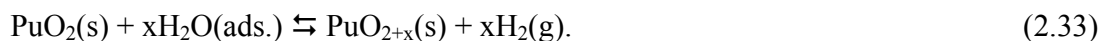
$$\log K^\circ = -19.8 \pm 0.9 \text{ [Guil 2003]}$$

To precisely understand the reaction (2.32), the reactions of Pu(IV) solid are inspected closer in the following.

For more than fifty years, many researchers investigated the structure, properties, and reactivity of plutonium oxides and the existence of hyperstoichiometric solids ( $\text{PuO}_{2+x}$ ). These studies were carried out to predict the behavior of plutonium oxides in nuclear waste disposals, likewise corrosion and other chemical reactions affected by changes in molecular structure of these solids. For example, the solubility of  $\text{PuO}_{2+x}$  is larger than that of  $\text{PuO}_2$  because of the simultaneous presence of Pu(IV) and Pu(V) in this compound. In early works,  $\text{PuO}_2$  was considered to be the most valent bulk oxide [Clev 79; Katz 86] and no evidence for the existence of  $\text{PuO}_{2+x}$  was found. In addition, the thermodynamic calculations suggested that higher oxides than  $\text{PuO}_2$  were unstable [Brew 53]. Brewer concluded that the hyperstoichiometric solid ( $\text{PuO}_{2+x}$ ) could not be present.

However, recently by help of some sensitive methods like as X-ray absorption fine structure spectroscopy (XAFS) and X-ray photoelectron spectroscopy (XPS),  $\text{PuO}_{2+x}$  was observed to be a mixed valent oxyhydroxide  $\text{Pu(V)}_{2x}\text{Pu(IV)}_{1-2x}\text{O}_{2+x-y}(\text{OH})_{2y}$  [Conr 2004]. The position of the X-ray absorption near edge demonstrated that the oxidation state of the  $\text{PuO}_{2+x}$  was a mixture of Pu(IV) and Pu(V), not Pu(VI). The Fourier transforms (FT) of extended X-ray absorption fine structure (EXAFS) data of the  $\text{PuO}_{2+x}$  indicated the splitting of the first oxygen shell (distance of 2.34 Å,  $x = 0$ ) and the appearance of a short Pu-O bond distance of 1.84 Å with increasing  $x$  from  $\text{PuO}_2$  to  $\text{PuO}_{2.26}$  [Conr 2004]. The XPS results of the same samples indicated the presence of Pu in an oxidation state higher than 4+ in the  $\text{PuO}_{2+x}$  structure from the shift of the binding energy of the Pu 4  $f_{7/2}$  electrons to higher energy. However, the XPS measurements of  $\text{PuO}_{2+x}$  at different temperatures showed that the hyperstoichiometric solid was not stable. The binding energy of the Pu 4  $f_{7/2}$  electrons shifted to lower values with increasing temperature and reached the characteristics of  $\text{PuO}_2$  at the highest temperature 600 °C. This could be due to the effect of surface de-hydroxylation. The gradual shift to lower binding energies for the Pu 4  $f$  peaks indicates a change from a more electron-withdrawing hydroxide environment (the presence of Pu(V)) to one that has the spectral features expected for the dioxide (only Pu(IV)) [Farr 2004].

At the same time, the formation mechanisms of  $\text{PuO}_{2+x}$  were investigated. One of them was the water catalyzed reaction suggested by Haschke *et al.* (summarized in [Hasc 2000a]). In these studies, the oxidation of  $\text{PuO}_2$  to  $\text{PuO}_{2+x}$  was observed and the authors suggested the formation of  $\text{PuO}_{2+x}$  ( $x \leq 0.27$ ) by a water catalyzed reaction at the gas-solid interface according to,

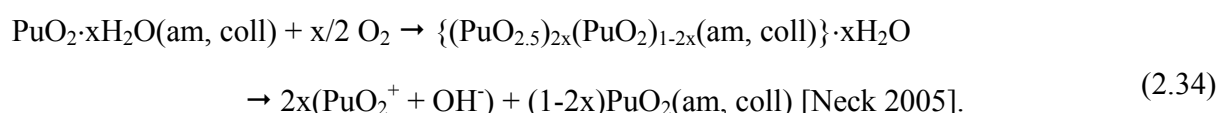


The reactivity of  $\text{PuO}_2(\text{s})$  with water was examined at temperatures ranging from 25°C to 350°C, and the rate of reaction at 25°C was obtained from three independent kinetic measurements. Haschke *et al.*

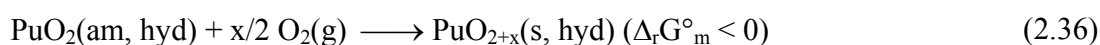
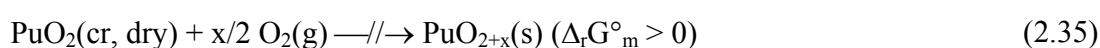
claimed that these kinetic results showed the dependence on temperature and accordingly, the reaction was not the result of radiolysis of water.

Actually it is very surprising that water is a more efficient oxidizing agent than oxygen itself for the conversion of  $\text{PuO}_2$  into  $\text{PuO}_{2+x}$ . Moreover, in recent experiments using X-ray absorption spectroscopy,  $\text{PuO}_{2+x}(\text{s})$  was not produced through the reaction (2.33) under absence of oxygen at relative high temperature [Mart 2003]. Accordingly, the water catalysis reaction of  $\text{PuO}_2$  is still in discussion.

Neck *et al.* [Neck 2005] suggested the oxidation of  $\text{PuO}_2$  by oxygen as the mechanism in aquatic system, on the basis of solubility studies of  $\text{PuO}_2 \cdot x\text{H}_2\text{O}(\text{am, hyd})$  by conventional undersaturation experiments containing different amounts of oxygen. In these experiments,  $\text{PuO}_2 \cdot x\text{H}_2\text{O}(\text{am})$  was in equilibrium with the  $\text{PuO}_2^+$  aqueous species at pH 4 - 9 and the results indicated that the amount of dissolved Pu species ( $\text{PuO}_2^+$  and  $\text{PuO}_2^{2+}$ ) at relative low pH 1 - 3 is limited by the total amount of oxygen being present in solution. Accordingly, they suggested the oxidation of  $\text{PuO}_2$  by oxygen as first step and then the dissolution of the oxidized fractions of  $\text{PuO}_{2+x} \cdot x\text{H}_2\text{O}$  as second step, which are below the solubility of  $\text{PuO}_{2.5} \cdot x\text{H}_2\text{O}(\text{s})$ :



They derived the molar standard Gibbs energies for formation of  $\text{PuO}_{2+x}(\text{s})$  from solubility data,  $\Delta_f G_m^\circ(\text{PuO}_{2.5}(\text{s})) = -971.2 \pm 6.7 \text{ kJ/mol}$  and  $\Delta_f G_m^\circ(\text{PuO}_{2.25}(\text{s})) = -968.4 \pm 5.4 \text{ kJ/mol}$ . Experimental attempts to oxidize dry  $\text{PuO}_2(\text{cr})$  by  $\text{O}_2(\text{g})$  in absence of water failed, whereas oxidation occurs in the presence of liquid water  $\text{H}_2\text{O}(\text{l})$  or water vapor  $\text{H}_2\text{O}(\text{g})$  [Hasc 2002b]:



Combined with  $\Delta_f G_m^\circ(\text{O}_2(\text{g})) = 0$ ,  $\Delta_f G_m^\circ(\text{PuO}_2(\text{cr})) = -998.1 \pm 10 \text{ kJ/mol}$ , and  $\Delta_f G_m^\circ(\text{PuO}_2(\text{am, hyd})) = -965.5 \pm 4.0 \text{ kJ/mol}$  [Lemi 2001; Guil 2003], these observations set lower and upper limits for the standard Gibbs energies of formation of  $\text{PuO}_{2+x}(\text{s})$ :

$$-(998.1 \pm 10) \text{ kJ/mol} < \Delta_f G_m^\circ(\text{PuO}_{2+x}(\text{s})) < -(965.5 \pm 4.0) \text{ kJ/mol} \quad (2.37)$$

These molar standard Gibbs energies for formation of  $\text{PuO}_{2+x}(\text{s})$  derived from solubility data are exactly within this narrow range [Neck 2005].

### 2.3 Hydrolysis and solubility data of Zr(IV)

Zirconium is a fission product (long lived isotope is  $^{93}\text{Zr}$ ,  $t_{1/2} = 1.5 \cdot 10^6$  a) of high yield and abundant in spent fuel. In addition, Zr was used to a large extent in nuclear power reactors due to its low neutron capture cross-section and high resistance to corrosion. The interest in the solution chemistry of Zr arises from several perspectives including the problem of radioactive waste management. For example, Zr is alloyed with uranium to produce nuclear fuels which are processed using hydrofluoric acid (HF). Given that HF is corrosive to stainless steel, corrosion can only be minimized by maintaining a low level of free HF concentration by complexation with metals such as Zr and aluminum [Aja 95].

In addition, Zr(IV) has been widely considered as an analog of tetravalent actinide elements, especially Pu(IV). Actually, experiments for the investigation of Pu(IV) chemistry are not easy because of not only the complex redox behavior of plutonium but also its high radiotoxicity. However, Zr (valence electron configuration  $4d^2 5s^2$ ) is dominated by tetravalent oxidation state in solution. Moreover, the experiments using non-radioactive Zr isotopes can be carried out without need for hot laboratories. According to literature data, the first hydrolysis constant of Zr(IV) which is one of the most important factors in solution chemistry equals that of Pu(IV). Some studies [Kova 61; Adai 87; Ekbe 2004] suggest that also the solubilities of both are equal within one order of magnitude. However, there are also other studies that show many orders of magnitude higher solubility [Bili 66].

#### 2.3.1 Hydrolysis constants of Zr(IV)

Baes and Mesmer reviewed the early results about Zr hydrolysis [Baes 76], which indicated that the mononuclear species of Zr ( $\text{Zr}(\text{OH})_y^{4-y}$ ,  $y = 1 - 5$ ) were dominant only at low Zr concentration ( $< 10^{-4}$  M). They concluded that only the formation constant of the first hydrolysis species was determined with reasonable accuracy by Noren, who measured potentiometrically the effect of hydrolysis on the stability of the  $\text{ZrF}^{3+}$  complexes and its value was  $\log \beta_{11}^{\circ} = 14.3 \pm 0.05$  [Nore 73]. However, the other formation constants of  $\text{Zr}(\text{OH})_y^{4-y}$  ( $y = 2 - 5$ ) were only roughly estimated.

Veyland *et al.* studied the hydrolysis of Zr using the potentiometric method [Veyl 98]. In this study,  $\text{Zr}(\text{OH})_3^+$  was assumed to be the dominant species at the beginning of the titration based on the exchange of pH when  $\text{ZrOCl}_2$  dissolved in water. However, the dominant species could vary with both Zr concentration (from  $8 \cdot 10^{-5}$  to  $8 \cdot 10^{-3}$  M) and pH (1.5 - 3.5) at which the dissolution takes place (in  $\text{HNO}_3$  media).

The most recent study of Zr hydrolysis was carried out by Ekberg *et al.* [Ekbe 2001; Ekbe 2004] and these hydrolysis constants extrapolated to zero ionic strength are listed in Table 2.2. The first hydrolysis constant was determined by potentiometric measurements at low pH in 1 M (H/Na)ClO<sub>4</sub>,  $\log K'_{11} = -0.87 \pm 0.05$ . The authors calculated the formation constant at zero ionic strength,  $\log \beta^{\circ}_{11} = 14.29 \pm 0.06$ , using the SIT. This value is well consistent with the reliable results referred to above [Nore 73]. For the calculation, they used the ion interaction coefficients estimated from literature data [Para 58; Nore 73; Davy 87] determined at different ionic strengths of the same media. The formation constants of the remaining mononuclear Zr species (Zr(OH)<sub>y</sub><sup>4-y</sup>, n = 2 - 4) were determined from solvent extraction experiments. However, the solvent extraction curves are fairly insensitive to the higher order formation constants, and the derived formation constants are highly uncertain.

Table 2.2 also shows the formation constants of mononuclear Zr hydrolysis species (Zr(OH)<sub>y</sub><sup>4-y</sup>, y = 2 - 4) estimated by using the semi-empirical ligand repulsion model of Neck and Kim [Neck 2000], which correlates the mononuclear formation constants  $\log \beta^{\circ}_{1y}$  for a given metal ion with a ligand electrostatic repulsion energy term:

$$\log \beta^{\circ}_{1n} = n \log \beta^{\circ}_{11} - {}^{\text{rep}}E_L / RT \ln 10 \quad (2.38)$$

The parameters necessary to calculate the Coulomb repulsion energy terms  ${}^{\text{rep}}E_L$  from the charge and inter-distance of the ligands involved are known. The empirical shielding coefficients for OH<sup>-</sup> ligands (independent of the metal ion) have been adjusted to the known mononuclear hydrolysis constants of trivalent and tetravalent actinides [Neck 2001a] and the distance  $d_{\text{Zr-OH}}$  is taken as sum of the ionic radii ( $r(\text{OH}^-) = 1.38 \text{ \AA}$  and  $r(\text{Zr}^{4+}) = 0.84 \text{ \AA}$  at coordination number of 8 [Shan 76]).

Table 2.2 Formation constants for mononuclear Zr(IV) hydroxide complexes.

	Zr(IV) [Ekbe 2004]	Zr(IV) present work
$\log \beta^{\circ}_{11}$	$14.29 \pm 0.06$	14.3 <sup>1)</sup>
$\log \beta^{\circ}_{12}$	$27.71 \pm 0.24$	27.6 <sup>2)</sup>
$\log \beta^{\circ}_{13}$	$40.12 \pm 0.26$	38.1 <sup>2)</sup>
$\log \beta^{\circ}_{14}$	$52.11 \pm 0.33$	45.4 <sup>2)</sup>

1) experiment value in [Baes 76]

2) Estimated by applying the legend repulsion model of [Neck 2000]

The ligand repulsion approach leads to accurate formation constants of mononuclear hydrolysis species of tetravalent actinide ions ( $M(OH)_y^{4-y}$ ,  $y = 2 - 4$ ,  $M = Th, U, Np$  and  $Pu$ ) [Neck 2001a], but the estimated formation constants of  $Zr(OH)_y^{4-y}$  ( $y = 3$  and  $4$ ) show relative large different from data by Ekberg *et al.*. The  $\log \beta_{1y}^0$  proposed by Ekberg *et al.* for  $Zr(OH)_3^+$  and  $Zr(OH)_4(aq)$  are expected to be overestimated by 2 and 6 orders of magnitude, respectively.

The first formation constant and the estimated formation constants for mononuclear Zr(IV) hydrolysis species are compared with the formation constants of mononuclear Pu(IV) hydrolysis species determined by Metivier *et al.* in Fig 2.7. Although  $\log \beta_{11}^0$  of Zr(IV) is expected to be a slightly larger than that of Pu(IV) since it scales linearly with the ionic index<sup>1</sup> ( $z^2 / r$ ,  $r(Pu^{4+}) = 0.96 \text{ \AA}$  and  $r(Zr^{4+}) = 0.84 \text{ \AA}$  at coordination number of 8 [Shan 76] ) [Humm 2002], the first two formation constants are very close.

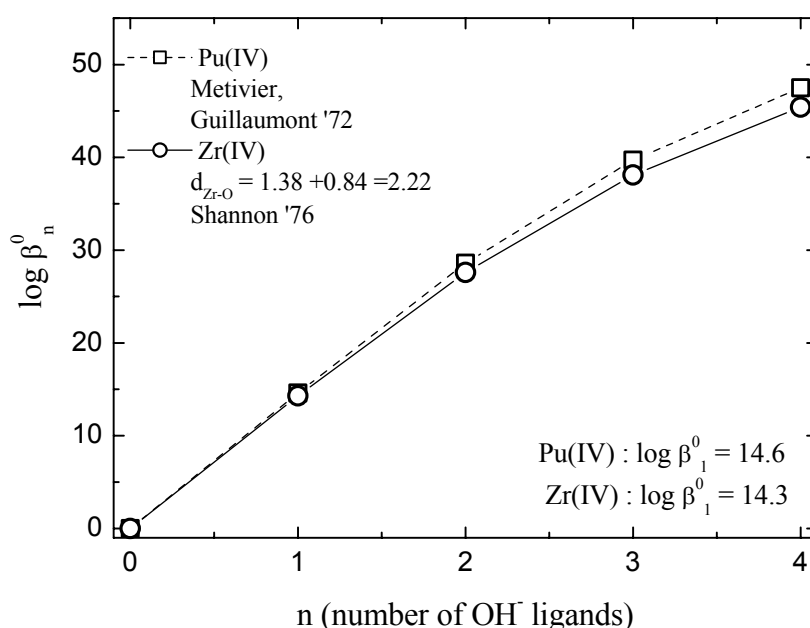


Fig. 2.7 Comparison between the formation constants for mononuclear hydrolysis species of Pu(IV) ( $\square$ : [Meti 72]) and Zr(IV) ( $\circ$ : the estimated values by applying the ligand repulsion model of [Neck 2000] in Table 2.2).

<sup>1</sup> square of formal charge divided by ionic radius

### 2.3.2 Solubility product of Zr(IV)

The solubility product of  $\text{Zr}(\text{OH})_4(\text{am})$  or  $\text{ZrO}_2 \cdot x\text{H}_2\text{O}(\text{am})$  is defined accordingly to that of  $\text{An}(\text{IV})$  in Section 2.1.3. Similar to Pu, the hydrolysis starts at  $\text{pH} > 0.3$  and cannot be neglected in solution with pH values at which the solubility limit is expected to be exceeded. If only mononuclear species are present in solution, which should be the case for low Zr concentration ( $[\text{Zr}] < 10^{-4} \text{ M}$ ), the solubility is given by (2.23) in Section 2.1.3. For the calculation of the solubility product using Eq. (2.23), the concentrations of zirconium and the hydrolysis constants ( $y = 1 - 4$ ) must be known.

A number of results on the solubility of Zr(IV) which show large discrepancies are summarized in Fig. 2.8. We can distinguish between two different types of data in Fig. 2.8. Data obtained from undersaturation experiments [Kova 61; Adai 87; Pouc 2001] yielded solubility products several orders of magnitude lower than data obtained from oversaturation [Bili 66]. Possible reasons for the scattered literature data are too short equilibrate time, the effect of colloids, uncertainties of hydrolysis constants, and differences of the solid phases as was discussed already in Section 2.2.3 for the case of Pu.

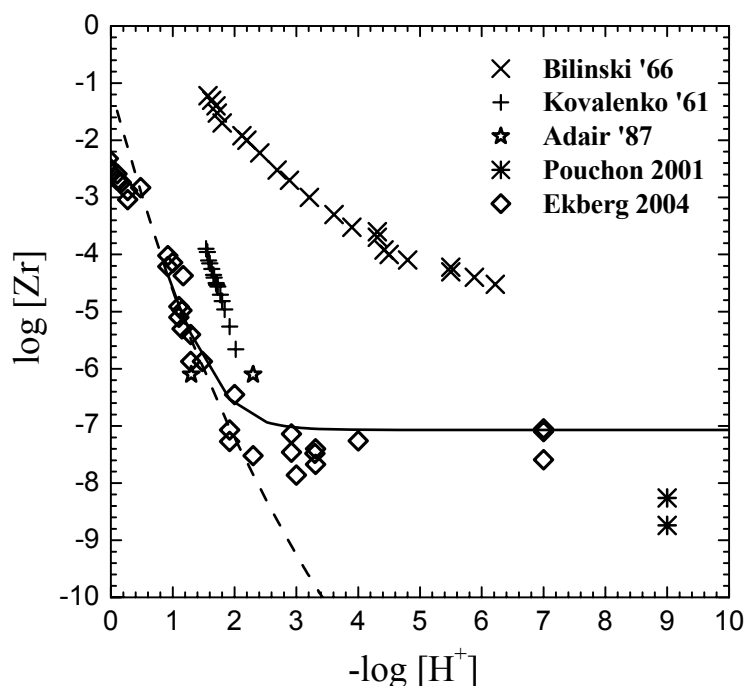


Fig. 2.8 The Solubility data of zirconium in acidic and neutral media from literature [Kova 61; Bili 66; Adai 87]. The solubility curve (solid line) is calculated by Ekberg *et al.* with mononuclear hydrolysis constants and  $\log K'_{\text{sp}} = -56.1$  in 1 M  $(\text{H}/\text{Na})\text{ClO}_4$  [Ekbe 2004]. The dashed line is calculated with mononuclear hydrolysis constants estimated by applying the ligand repulsion approach [Neck 2000] and the same solubility product from Ekberg *et al.*

The three sets of data from undersaturation experiments yield similar solubilities, even though these were carried out with different solid phases,  $\text{ZrO}_2(\text{cr})$  or  $\text{Zr}(\text{OH})_4(\text{am})$ . The most recent study by Ekberg *et al.* was carried out with a claimed  $\text{Zr}(\text{OH})_4$  solid<sup>2</sup> in different acidic solutions using 1 M (H/Na)ClO<sub>4</sub> in a glove box [Ekbe 2004]. After centrifugation, the Zr concentrations were determined by ICP-MS at different times to make sure that chemical equilibrium was established. They calculated the solubility product as  $\log K'_{\text{sp}} = -56.1$  in 1 M (H/Na)ClO<sub>4</sub> and  $\log K^{\circ}_{\text{sp}} = -59.2$  (at zero ionic strength). Kovalenko *et al.* who also investigated the dissolution of  $\text{Zr}(\text{OH})_4$  solid, obtained only a little higher solubility [Kova 61]. This discrepancy is probably due to unsuccessful separation of colloids using filtration or centrifugation. In contrast, the data from Adair *et al.* referred to experiments with pure monoclinic  $\text{ZrO}_2$  [Adai 87]. After filtration with pore size 100 nm, the concentration and pH of filtrate were determined. In spite of their poor reproducibility, these results are roughly consistent with the results above. Recently, Pouchon *et al.* investigated the influence of carbonate complexation on the Zr solubility with two different solid phases, amorphous hydroxide (upper point in Fig. 2.8) and monoclinic  $\text{ZrO}_2$  (lower point in Fig. 2.8), at the same pH 9 [Pouc 2001]. These data points were results from solutions containing 0.005 M carbonate ion concentration which was low enough to form no significant carbonate complexes, thus it is reasonable to compare these with the data points in carbonate free systems.

In contrast, the experiments from strongly oversaturated solutions done by Bilinski *et al.* yielded much higher solubility [Bili 66]. They measured the turbidity of the solution using tindallometry in a large range of pH at constant Zr concentration. These experiments were carried out for many different Zr concentrations and at different ionic strengths and different temperatures. Among these data, the lowest pH at which one could still observe, after 24 hours, some turbidity or precipitate at 1 M (H/Na)ClO<sub>4</sub> and 20°C are depicted in Fig. 2.8. The calculated solubility product was  $\log K'_{\text{sp}} = -50.3$  (using  $a_{\text{H}_2\text{O}} = 0.966$  at 1M NaClO<sub>4</sub> in [Lemi 2001]) in 1 M (H/Na)ClO<sub>4</sub> or  $\log K^{\circ}_{\text{sp}} = -53.4$  at zero ionic strength respectively and it was about 6 orders of magnitude larger than the value calculated by Ekberg *et al.*.

The classical solubility data for not well characterized Zr(IV) oxide/hydroxide solids [Kova 61; Ekbe 2004] and for mononuclear  $\text{ZrO}_2$  [Adai 87; Pouc 2001] are scattered due to the variability of the solubility of Zr(IV) oxides/hydroxides, depending on preparation, particle size, etc.

---

<sup>2</sup> see discussion in Section 5.1



### 3 Experimental Techniques

As discussed in Section 2.1.1, up to four oxidation states of plutonium can coexist. The chemical properties of each oxidation state vary widely, thus for the precise investigation of plutonium, a reliable method for the quantification of the oxidation states is needed. The methods to be used for the quantitative determination of oxidation states depend on the concentration range of plutonium. For concentrations of Pu below  $\sim 1 \mu\text{M}$ , the chemical separation technique is a unique method and above this concentration, spectroscopic techniques can be used [Hoff 2002].

As for the chemical separation techniques, there are coprecipitation, selective sorption, liquid chromatography and solvent extraction [Koba 88; Chop 97]. Of these, the solvent extraction technique has been used most frequently, especially for trace concentrations of Pu, because this technique allows a rapid and nearly complete separation of oxidation states at trace levels. Many other extractants have been developed but were tailored to very specific applications. Thus they have to be carefully selected whether they are suited for the respective solution under investigation.

Absorption spectroscopy methods are considered to be among the most reliable and versatile techniques for the detection and characterization of solution species [Ross 61; Baum 62] and have been widely used for the characterization of actinides in solution [Kell 71; Katz 86]. Unfortunately, conventional absorption spectrometers have detection limits between 0.01 mM and 1 mM for plutonium. With the advent of high powered pulsed lasers, new laser based techniques have been developed for measuring very weak sample absorbance, photoacoustic spectroscopy (PAS) [Stum 84; Tam 86], photothermal deflection spectroscopy (PDS) [Jack 81], and thermal lensing spectroscopy (TLS) [Fang 83]. These are potentially about two orders of magnitude more sensitive than absorption spectroscopy using conventional spectrometers [Torr 90]. For example, recent studies about the hydrolysis and solubility of Pu(IV) [Walt 2003b] and Np(IV) [Neck 2001b] at low concentrations were carried out using sensitive laser induced photoacoustic spectroscopy (LPAS) [Kita84; Kim90].

Another sensitive method, which recently was applied by Kuczewski *et al.* for a plutonium speciation at low ion concentration, is the capillary electrophoresis (CE) combined with inductively coupled plasma mass spectrometry (ICP-MS). The main advantages are the short separation time and high separating efficiency of CE combined with the elemental and isotopic selectivity and the sensitivity of the ICP-MS detection [Kucz 2003].

In the following subsections, two techniques which were applied to determine the distribution of plutonium oxidation states in the present work, the absorption spectroscopy and the CE coupled ICP-MS, are described in detail in Section 3.1 and 3.2.

In order to investigate the solubility and colloid formation of Pu(IV) and Zr(IV), sensitive characterization methods for colloids are needed. These methods are used for the investigation of particle size distribution (PSD), element composition and the structure of colloids. Very often the PSD extends over several orders of magnitude and many methods are needed to separate these different size fractions. Filtration and centrifugation have been used most frequently and several chromatographic methods are also applicable. Recently, CE [Kral 97] and field flow fractionation (FFF) [Cölf 2000] were applied for colloid fractionation. For the determination of PSD of colloids, there are useful methods based on light scattering, e.g. photon correlation spectroscopy (PCS) and the single particle counter (SPC) [Degu 89] and others based on light matter interaction using lasers such as LIBD [Kita 88]. For the investigation of element composition and the structure of colloids, different types of microscopes are applicable, e.g., transmission electron microscopy (TEM), scanning electron microscopy (SEM), and atomic force microscopy (AFM). By these versatile techniques, morphology, size distributions and element composition can be appraised simultaneously, however the sample must be specifically prepared prior to the investigation, and samples could be changed during these treatments. For the more precise structure investigation, in recent years, X-ray spectroscopy based on the interaction of atoms with X-rays, e.g. X-ray photoemission spectroscopy (XPS) which is a surface sensitive technique, detecting the outer layers of sample and X-ray absorption fine structure spectroscopy (XAFS) which can be applied to samples covered by a water layer were applied (overview in [Tonn 99]). For the appropriate characterization of colloids, it is important to use some complementary methods in conjunction.

In the present work, in order to make a speciation and analysis of Zr(IV) species in solution, XAFS is applied. For detection of the colloids of Zr(IV) and Pu(IV) present in oversaturated solution, LIBD is applied. LIBD is a very sensitive detection method especially for small particles ( $< 50$  nm) in solution [Kita 89; Sche 96; Walt 2003a], and is used for the determination of the onset of colloid formation which indicates that the metal concentration in a solution exceeds the solubility limit. In addition the size distribution of colloids can be appraised by use of a multi-modal evaluation fit program [Walt 2004]. As a supplementary method for determination of the PSD, single particle counting (SPC) is applied, especially, to detect colloids which are relative large of size ( $> 1\mu\text{m}$ ) and low of particle number density ( $<$  detection limit of LIBD). These methods are mentioned below in Section 3.3 (XAFS), Section 3.4 (LIBD) and Section 3.5 (SPC).

### 3.1 UV-VIS absorption spectroscopy

UV-Vis absorption spectroscopy is considered to be one of the most reliable techniques for the detection and characterization of actinides in solutions. The optical absorption spectra of actinides show bands due to the excitation of electronic intraband ( $f-f$ ) transitions. These bands are quite narrow, usually a few nanometers wide (full width at half maximum height (FWHM)), and the wavelength ( $\lambda$ ) of the absorption peaks are uniquely characteristic of the actinide element and its oxidation states. The concentrations of the solution species are obtained from specific absorption bands for each oxidation state through the use of Lambert-Beer's law,

$$A = \varepsilon c l \quad (3.1)$$

where  $A$  is absorption,  $\varepsilon$  molar extinction coefficient [ $M^{-1}cm^{-1}$ ],  $c$  concentration [ $M$ ] and  $l$  beam path length [ $cm$ ]. In the case of plutonium, this allows speciation because the absorption spectra of the oxidation states of plutonium are sufficiently different. For quantifying a certain oxidation state by a specific band, the other states must have a small absorption at the same wavelength. By measuring a spectrum in a wide range of wavelengths, a rapid determination of the distribution of the various oxidation states in a given solution is possible. The analytically useful absorption bands of plutonium are listed in Table 3.1 [Katz 86].

Table 3.1 The molar extinction coefficients ( $\varepsilon$  [ $M^{-1}cm^{-1}$ ]) for different oxidation states of plutonium (summarized in [Katz 86]).

Wavelength [nm]	Molar extinction coefficients $\varepsilon$ [ $M^{-1}cm^{-1}$ ]			
	$\varepsilon$ Pu(III) <sub>aq</sub>	$\varepsilon$ Pu(IV) <sub>aq</sub>	$\varepsilon$ Pu(V) <sub>aq</sub>	$\varepsilon$ Pu(VI) <sub>aq</sub>
600	<b>35.3</b>	0.91	0.5	1.35
470	3.46	<b>49.6</b>	1.82	11.25
653	3.1	34.4	1.15	0.9
		37.8 <sup>1)</sup>		
		<b>36.7<sup>2)</sup></b>		
569	34.3	5.6	<b>17.1</b>	1.75
831	5.25	15.5	4	<b>550</b>

1) 0.5M (H/Na)ClO<sub>4</sub>, 25°C,  $7.2 \cdot 10^{-4}$  M Pu(IV) from [Krau 50]

2) 2 M HClO<sub>4</sub>,  $1.2 \cdot 10^{-4}$  M Pu(IV) from [Yuso 2004]

The spectral analysis for the Pu ionic species is a very convenient method because all oxidation states can be analyzed at the same time with only one spectrum. However, the low molar absorption coefficients of the plutonium absorption bands (especially  $\text{Pu(III)}_{\text{aq}} - \text{Pu(V)}_{\text{aq}} < 50 \text{ M}^{-1}\text{cm}^{-1}$ ) make this spectroscopic method with a conventional 1 cm absorption path length inadequate for studies at dilute concentrations.

When all of four different oxidation states exist simultaneously in solution, which is the case for most of present experiments, the classical analysis gets to be more complex and uncertain. Especially the quantification of Pu(V) is difficult, which has a characteristic band at 569 nm where the absorption of Pu(III) and Pu(IV) cannot be neglected. Therefore, in this study, the precise quantification of Pu aqueous species is done by spectral deconvolution. We carry out the analysis of spectra in a wide wavelength range (normally from 465 nm to 833 nm) by least squares fit with 4 variables (concentrations of four Pu oxidation states) based on the calibrated  $\epsilon$  [ $\text{M}^{-1}\text{cm}^{-1}$ ] in the UV-Vis range for reference solutions (See Fig. 3.1). Some details of the spectral fitting procedure are discussed in further course.

Reference solutions for each Pu oxidation state are prepared at different concentrations and media, respectively, (the preparation processes of Pu solutions are described in Section 4) and measured by a Cary 5E spectrometer (VARIAN) applying a quartz cell of 1 cm beam path length. The reference solutions are prepared in  $\text{HClO}_4$  because normally the perchloric ligand is a very weak complex with regard to Pu ionic species [Katz 86].

The reference solution of tetravalent plutonium contains only small amounts of  $\text{Pu(III)}_{\text{aq}}$  and  $\text{Pu(VI)}_{\text{aq}}$ . Their concentrations calculated with the extinction coefficients of Table 3.1 are about  $1.30 \cdot 10^{-4}$  M of  $\text{Pu(III)}_{\text{aq}}$  (3.0 % of  $[\text{Pu}]_{\text{tot.}}$ ) and  $2.18 \cdot 10^{-5}$  M of  $\text{Pu(VI)}_{\text{aq}}$  (0.51 % of  $[\text{Pu}]_{\text{tot.}}$ ), respectively. LIBD results of this solution indicate that it contains no colloids being large enough to be detected by LIBD ( $< 5$  nm). When  $\epsilon = 36.7 \text{ M}^{-1}\text{cm}^{-1}$  at 653 nm [Yuso 2004] is used, the  $\text{Pu(IV)}_{\text{aq}}$  concentration is obtained to be  $4.14 \cdot 10^{-3}$  M. The sum of all oxidation states of Pu agrees well with the total Pu concentration measured by LSC (liquid scintillation counter),  $4.3 \cdot 10^{-3}$  M. Therefore it can be assumed that there are no additional Pu species in the  $\text{Pu(IV)}_{\text{aq}}$  reference solution, such as Pu(IV) polymeric species or small colloids.

As already mentioned in Section 2.2.2, the  $\text{Pu}^{4+}$  ion forms strongly complexes with  $\text{OH}^-$  even at low pH. The distributions of Pu(IV) hydrolysis products at certain pH are shown in Table 3.2, which are calculated using the hydrolysis constants by Metivier *et al* [Meti 72]. According to these hydrolysis constants, at pH 0, about 30% and at pH 1, over 90% of Pu(IV) is already hydrolyzed.

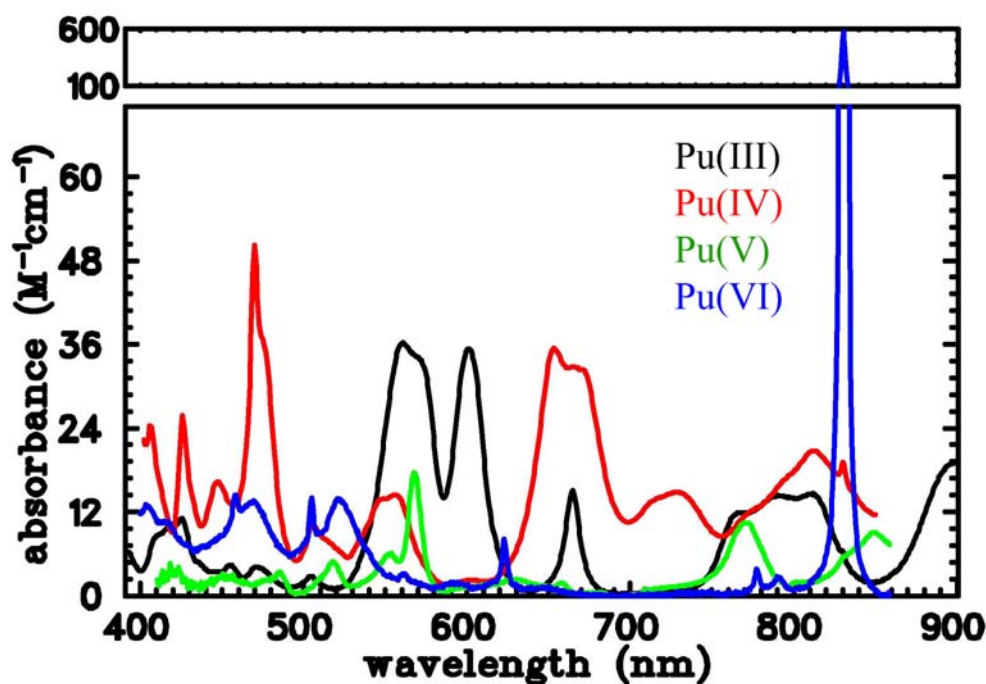


Fig. 3.1 The absorption spectra of four reference solutions scaled to 1 M concentration. The solutions were prepared at different concentrations and in different media: Pu(III) at  $3.8 \cdot 10^{-3}$  M in 1 M HClO<sub>4</sub>, Pu(IV) at  $4.3 \cdot 10^{-3}$  M in 0.75 M H(ClO<sub>4</sub>/Cl), Pu(V) at  $3 \cdot 10^{-4}$  M in 0.001 M HClO<sub>4</sub> and Pu(VI) at  $5.3 \cdot 10^{-4}$  M in 0.1 M HClO<sub>4</sub>, respectively.

Table 3.2 The distributions of Pu(IV) hydrolysis species ( $I = 0.5$  M NaCl) at different pH estimated with the hydrolysis constants by Metivier *et al* [Meti 72].

pH	Pu <sup>4+</sup> [%]	Pu(OH) <sup>3+</sup> [%]	Pu(OH) <sub>2</sub> <sup>2+</sup> [%]
0	69	26	5
0.5	35	41	24
0.8	16	38	46
1.0	9	32	59
1.2	4	24	71

In all previous studies where spectroscopic methods have been used to determine the hydrolysis constants, they assumed that the molar absorption coefficients for the Pu hydrolysis species are different from that of the Pu<sup>4+</sup> ion, and thus it was assumed that the decrease of the characteristic Pu(IV) absorption bands was due to the initial formation of mononuclear hydrolysis species. However, inspecting the solutions which are carefully prepared to have no colloids or polymer species, this could not be confirmed. In the present work, five different Pu solutions are prepared, whose total plutonium concentrations are about  $3 \cdot 10^{-4}$

M (measured using LSC) and the distribution of oxidation states at each pH, which are obtained through fitting, is listed in Table 3.3. LIBD measurements indicate that they have no colloids larger than 5 nm (for details see Section 3.4). Furthermore, the sums of all Pu aquatic species obtained by fitting are close to 100 % (100 % corresponds to the  $[\text{Pu}]_{\text{tot}}$  measured by LSC). This means that there are no polymeric species or colloids in solutions, because otherwise, the sum of the spectroscopic detectable species  $\text{Pu(III)}_{\text{aq}}$ ,  $\text{Pu(IV)}_{\text{aq}}$ ,  $\text{Pu(V)}_{\text{aq}}$  and  $\text{Pu(VI)}_{\text{aq}}$  should be considerably lower than the total concentration detected by LSC which includes colloids and polynuclear species.

The deconvoluted spectra due to the  $\text{Pu(IV)}$  fraction at different pH (from 0.5 to 1.2) are shown in Fig. 3.2 and the  $\epsilon$  values at the peak maximum (470 nm and 653 nm) are listed in Table 3.3. To obtain the  $\epsilon$  [ $\text{M}^{-1}\text{cm}^{-1}$ ] for  $\text{Pu(IV)}$  at each pH, the reference spectra for the other oxidation states are subtracted from the measured spectra. The poor quality of the spectrum at pH 1.21 is due to the low fraction of  $\text{Pu(IV)}_{\text{aq}}$  in the samples (cf. Section 6.3.1 for the equilibrium distribution of Pu oxidation states as a function of pH). The spectra in Fig. 3.2 indicate neither peak shifts nor a significant difference of the extinction coefficients which should be caused by decrease of  $\text{Pu}^{4+}$  ion concentration with increasing pH, e.g.,  $[\text{Pu}^{4+}] < 5\%$  at pH 1.2 (see Table 3.2). In conclusion, when no colloids and polymer species are present in solution, then the absorption of  $\text{Pu(IV)}$  does not depend on pH even if the “free ion”  $\text{Pu}^{4+}$  ion is a minor species. From these results, it is concluded that the Pu hydrolysis species,  $\text{Pu(OH)}_y^{4-y}$  ( $y = 0 - 2$ ), have similar molar extinction coefficients.

Table 3.3 The distribution of Pu oxidation states (%) at a steady state as a function of pH from the analysis of the absorption spectrum. The total Pu concentration is about  $3 \cdot 10^{-4}$  M. The extinction coefficients are obtained from deconvoluted spectra of  $\text{Pu(IV)}$  fraction at specific wavelengths.

pH	$\text{Pu(III)}_{\text{aq}}$ [%]	$\text{Pu(IV)}_{\text{aq}}$ [%]	$\text{Pu(V)}_{\text{aq}}$ [%]	$\text{Pu(VI)}_{\text{aq}}$ [%]	Sum [%]	$\epsilon$ at 470 nm [ $\text{M}^{-1}\text{cm}^{-1}$ ]	$\epsilon$ at 653 nm [ $\text{M}^{-1}\text{cm}^{-1}$ ]
0.48	38.88	54.07	0	7.07	100.03	51.1	35.2
0.66	46.45	39.87	0	10.92	97.24	48.9	36.1
0.83	50.03	28.5	3.48	15.57	97.57	47.8	35.1
1.01	58.54	17.42	6.98	16.83	99.77	48.1	35.9
1.21	60.83	11.32	13.72	15.06	100.93	47.2	36.9 <sup>1)</sup>

1) The value is taken after the smoothing of the spectrum at pH 1.21 by averaging adjacent 5 points.

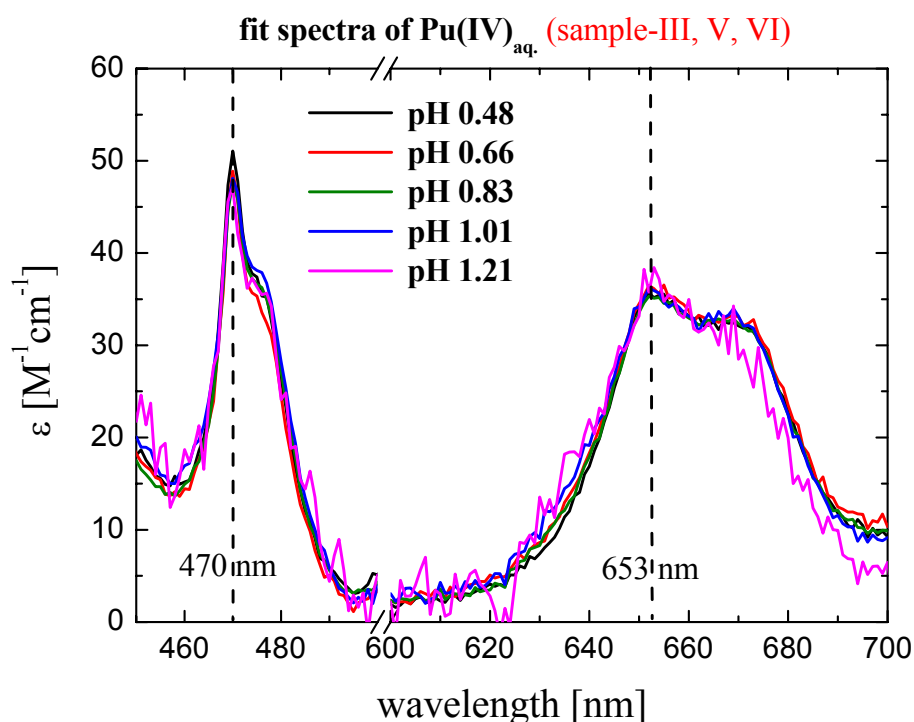


Fig. 3.2 The absorption spectra of Pu(IV) as a function of pH in the range from 0.5 to 1.2. The solutions have no colloidal fraction (checked by LIBD – see Section 3.4) and no significant polymer species (from analysis of spectrum – see the text). The concentration of Pu(IV) in each solution is listed in Table 3.3.

Secondly, the influence of colloids in the blue and UV range must be considered. When colloids are present in solution, the maximal absorption of Pu(IV)<sub>aq</sub> at 470 nm can be apparently increased due to the Rayleigh scattering by small colloids. Because the light scattering scales with  $\lambda^{-4}$ , at shorter wavelength light transmission decreases thus the light scattering is more prominent to the close UV range. This can be a reason for the somewhat larger  $\epsilon$  value at 470 nm ( $56 \text{ M}^{-1}\text{cm}^{-1}$ ) in [Yuso 2004], although the  $\epsilon$  value at 653 nm ( $36.7 \text{ M}^{-1}\text{cm}^{-1}$ ) is very close to our result. In our study, some solutions have a sufficiently high amount of colloids to interfere which the spectra in the blue and UV range. For the analysis of these solutions the fitting is carried out by excluding the 470 nm band for Pu(VI)<sub>aq</sub> and using only the spectral range from about 500 to 835 nm.

When a plutonium solution contains specific ligands whose concentration is high enough to form complexes with Pu ion species, the absorption bands can be shifted significantly and thus it can affect the quantification. All reference spectra are taken in HClO<sub>4</sub> media but our experiments are carried out in 0.5 M (Na/H)Cl media. If Pu aqueous species form complexes with Cl<sup>-</sup> which causes deviations in the spectra, then the influence of the Pu chloro complex must be considered for precise analysis. Among the ions of

plutonium, the  $\text{PuO}_2^{2+}$  ion is expected to have the least tendency to form complex ions and little effect of chloride ion is noted on the spectra of  $\text{Pu(III)}_{\text{aq}}$  and  $\text{Pu(IV)}_{\text{aq}}$  in 0.5 M  $\text{Cl}^-$  ion concentration. However, in the case of  $\text{PuO}_2^{2+}$ , optical studies indicated the formation of at least three chloride complexes with increasing hydrochloric acid concentration [Katz 86]. In 0.5 M (Na/H)Cl media, we can see only the first chloride complex and its spectrum is shown in Fig. 3.3. The maximum of the bands are 830.7 nm (FWHM: 2.6 nm) for  $\text{PuO}_2^{2+}$  and 837.3 nm (FWHM: 6.0 nm) for  $\text{PuO}_2\text{Cl}^+$ . The amount of the secondary complex does not suffice to alter the spectra. It is in good agreement with the spectral parameters about the Pu(VI)-chloride complexes reported recently by Runde *et al.* [Rund 99] (See Table 3.4). The monochloro complex contributes 15% of the total  $\text{Pu(VI)}_{\text{aq}}$  concentration in 0.5 M (Na/H)Cl media, thus this factor is considered.

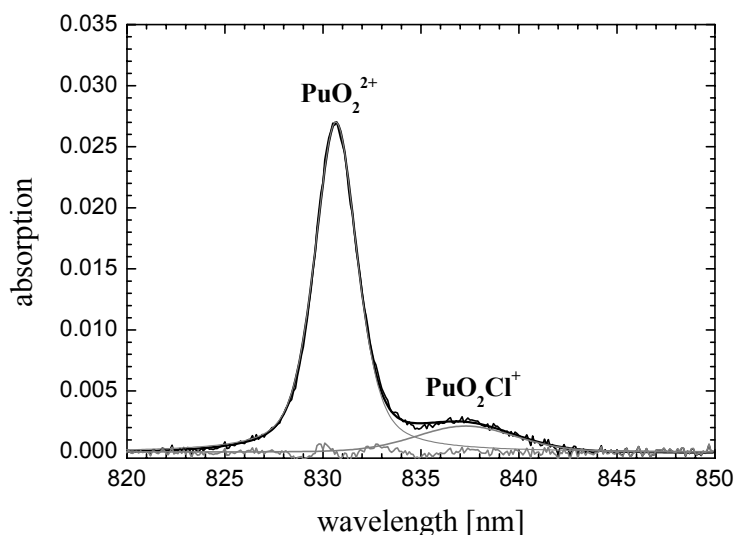


Fig. 3.3 The spectrum of  $\text{Pu(VI)}_{\text{aq}}$  in 0.5 M (H/Na)Cl.  $[\text{PuO}_2^{2+}] = 4.86 \cdot 10^{-5}$  M (85%) and  $[\text{PuO}_2\text{Cl}^+] = 0.734 \cdot 10^{-5}$  M (15%) calculated with the molar extinction coefficients in Table 3.4.

Table 3.4 The spectroscopic parameters of the predominant  $\text{Pu(VI)}_{\text{aq}}$  species in NaCl [Rund 99].

species	Peak maximum	FWHM height	$\epsilon$ [ $\text{M}^{-1}\text{cm}^{-1}$ ]
$\text{PuO}_2^{2+}$	$830.6 \pm 0.1$ nm	$2.5 \pm 0.2$ nm	$555 \pm 12$
$\text{PuO}_2\text{Cl}^+$	$837.6 \pm 0.2$ nm	$5.6 \pm 0.3$ nm	$290 \pm 23$
$\text{PuO}_2\text{Cl}_2$	$843.0 \pm 0.4$ nm	$7.6 \pm 0.4$ nm	$140 \pm 80$



The sensitivity of absorption spectroscopy can be simply improved by extending the optical path length. Making use of total reflection, the sample is probed in a liquid core waveguide (LCW) which enables the light propagation within a liquid medium which has a higher refractive index than the surrounding solid tubing [Wei 83]. The coating material outside of the fused silica capillary is Teflon AF whose RI is about 1.29 and the length is 100 cm and the diameter of capillary 550  $\mu\text{m}$ , respectively. A 100 cm capillary enhances the sensitivity by two orders of magnitude as compared to a 1 cm cell. In this work, LCW (WPI, World Precision Instruments, see Fig. 3.4) coupled with a diode array spectrometer (Zeiss) is used for analysis of Pu aqueous species at relative low concentration ( $10^{-5}$  M).

The absorption spectra of a plutonium solution (total concentration of plutonium is  $1.9 \cdot 10^{-4}$  M in 0.5 M  $\text{HClO}_4$ ) is measured twice: with a 1 cm quartz cell (Fig. 3.5 bottom) and the 100 cm LCW (Fig. 3.5 top) using the diode array spectrometer. The two spectra are almost identical and the setup using the capillary shows almost 100 times larger sensitivity. The concentration of the oxidation states is  $3.11 \cdot 10^{-5}$  M,  $1.53 \cdot 10^{-4}$  M and  $0.69 \cdot 10^{-5}$  M for  $\text{Pu(III)}_{\text{aq}}$ ,  $\text{Pu(IV)}_{\text{aq}}$  and  $\text{Pu(VI)}_{\text{aq}}$ , respectively. No  $\text{Pu(V)}_{\text{aq}}$  is detected.

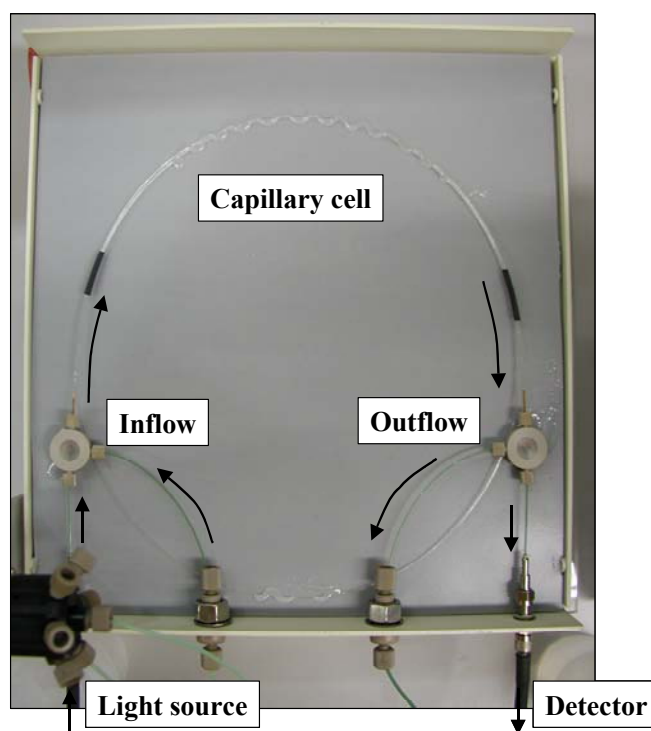


Fig. 3.4 LCW: 100 cm fused silica capillary (diameter 550  $\mu\text{m}$  and volume 240  $\mu\text{l}$ ) coated by Teflon AF ( $\text{RI} \approx 1.29$ ) coupled with diode array spectrometer.

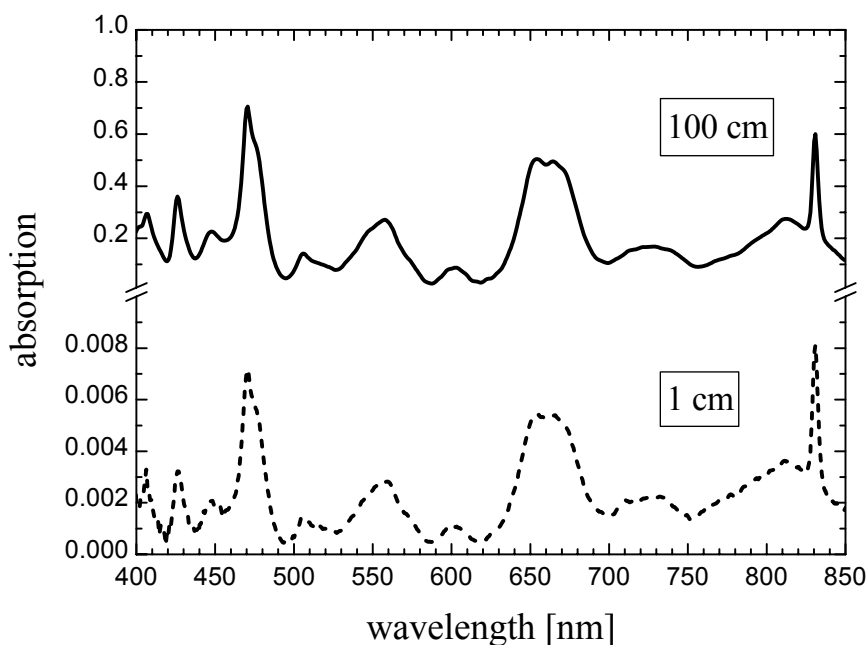


Fig. 3.5 The absorption spectra of plutonium solution  $[\text{Pu}]_{\text{tot.}} = 1.9 \cdot 10^{-4} \text{ M}$  in  $0.5 \text{ M HClO}_4$ . The dashed line shows the spectrum obtained with a 1 cm quartz cell and the solid line shows the one measured with the LCW using the diode array spectrometer.

When plutonium solution is investigated with LCW-DAS, an error of spectra deconvolution based on reference spectra measured using CARY 5E spectrometer can be caused from the resolution of the diode array spectrometer. While the broad spectral features used for the quantification of  $\text{Pu(III)}_{\text{aq}}$ ,  $\text{Pu(IV)}_{\text{aq}}$  and  $\text{Pu(V)}_{\text{aq}}$  are uncritical, the reproduction of the narrow peak of  $\text{Pu(VI)}_{\text{aq}}$  at 831 nm depends strongly on the resolving power of the spectrometer. Recently, Wilson *et al.* reported molar extinction coefficients and detection limits for each plutonium oxidation state using a 100 cm LCW [Wils 2005]. In this study, the authors obtained  $288 \text{ M}^{-1}\text{cm}^{-1}$  as molar extinction coefficient for  $\text{Pu(VI)}_{\text{aq}}$  at 831 nm, which is only an “operative”  $\epsilon$  due to the limited spectral bandwidth of spectrometer. In our system, the “operative”  $\epsilon$  is about  $302 \text{ M}^{-1}\text{cm}^{-1}$  and this value is largely different from the reference spectra using the CARY spectrometer (See Fig. 3.6). It is a shortcoming of the molar absorbance convention to depend on resolution. The physically more meaningful quantity is the differential cross section  $d\epsilon/dnm$ . The peak absorptivity

$$A = \int \frac{d\epsilon}{dnm} dnm \text{ is independent of resolution.}$$

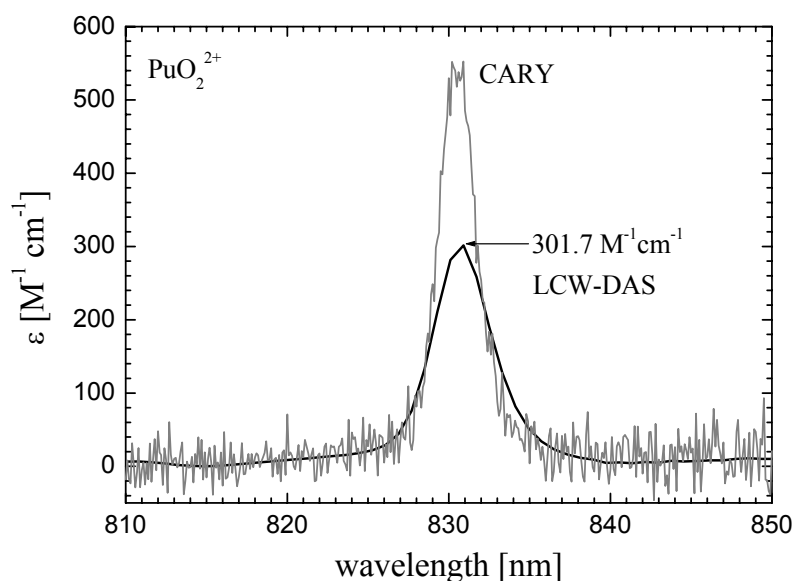


Fig. 3.6 The concentration of  $\text{PuO}_2^{2+}$  is  $8.13 \cdot 10^{-5}$  M (calculated with  $550 \text{ M}^{-1} \text{ cm}^{-1}$ ) in 1 M  $\text{HClO}_4$ . The peak area and FWHM are  $2000 \text{ nmM}^{-1} \text{ cm}^{-1}$  (between 820 – 840 nm) and 2.7 nm, respectively, for the spectrum measured by Cary 5E and  $1600 \text{ nmM}^{-1} \text{ cm}^{-1}$  and 4.0 nm for the LCW coupled with the diode array spectrometer. The areas are similar but using the diode array spectrometer, the band width is wider and therefore the band maximum is lower.

### 3.2 Capillary Electrophoresis (CE) coupled with ICP-MS

In this work, as a supplementary method to determine the concentration of plutonium oxidation states below the detection limit of UV-Vis spectrometry, the capillary electrophoresis (CE) coupled with ICP-MS is applied. CE is a simple method for the separation of different oxidation states. The basic components of the CE system are a fused silica capillary as the separation channel, electrolyte vials with electrodes, a regulated high voltage power supply, and a detector (here ICP-MS). The principle of CE is mentioned shortly as follows [Jand 93].

At the beginning of an analytical run, a very small volume (typically 10 to 100 nanoliters) of sample is injected at the injection side of the capillary by means of differential pressure or electromigration. A desirable outcome of CE separations is the migration of separated zones of all analytes toward the detector. The time interval between the beginning of the separation and the passage of an analyte zone through the point of detection (migration time) is used for identification of sample components. In order to be able to com-

pare data of different instrumentations, the migration times ( $t_m$ ) which depend on capillary length  $L_d$ , between sample introduction and detection, is converted to a migration rate or velocity of migration ( $v_{obs}$ ), as following

$$v_{obs} = \frac{L_d}{t_m} . \quad (3.2)$$

Since the velocity is due not only to electrophoretic migration, but sensitive to other contributions as well, the term “observed” is included. The  $L_d$  dimension should thus be included in all descriptions of CE conditions along with  $L_t$ , the total capillary length. To compare migration data not only for varying  $L_d$ , but also at different separation potentials  $U$  [V] applied to different  $L_t$ , it is necessary to calculate the observed electrophoretic mobilities ( $\mu_{obs}$ ):

$$\mu_{obs} = \frac{v_{obs} L_t}{U} = \frac{L_d L_t}{U t_m} . \quad (3.3)$$

There are two main contributions to the observed electrophoretic mobility, the mobility of electroosmotic flow (EOF),  $\mu_{EOF}$ , and the inherent ionic mobility of the ionic analyte,  $\mu_{ion}$ . As shown in Fig. 3.7, the observed or apparent mobility,  $\mu_{obs}$  is usually a sum of two contributions. The mobility contributions have not only a magnitude, but also a direction, and so it is correct to treat them as vectors.

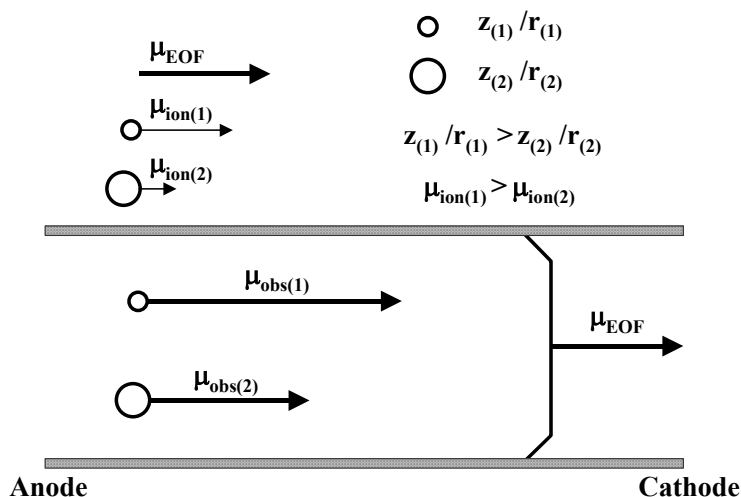


Fig. 3.7 The contributions to the directions and magnitude of the resulting apparent or observed mobility  $\mu_{obs}$  in the applied electric field inside a capillary:  $\mu_{EOF}$  is the mobility of EOF;  $\mu_{ion}$  describes the inherent ionic mobility of the ionic analyte.

The contribution depicted in Fig. 3.7 describes the most frequently reported types of CE. The analyte of interest is transported toward a detector mainly by the electroosmotic flow. EOF is a consequence of the surface charge on the capillary wall. The fused silica capillaries which are typically used for separations have ionizable silanol groups in contact with the buffer contained within the capillary. The degree of ionization is controlled mainly by the pH of the buffer. The negatively charged wall attracts positively charged ions from the buffer, creating an electric double layer. The potential at the surface of shear between electric double layer is called the zeta potential ( $\zeta$  [V]) which is related to the concentration of ions in the fluid, the thickness of the electric double layer, pH of the solution and the surface properties of the capillary [Tava 95; Thor 98]. The EOF mobility is related to the dielectric constant of the electrolyte ( $\epsilon_{rel}$ ), the zeta potential and the viscosity of electrolyte medium ( $\eta$ ) and is represented as:

$$\mu_{EOF} = -\frac{\epsilon\zeta}{\eta} \quad (3.4)$$

The flow profile in EOF is uniform as shown in Fig. 3.7. For separating sample mixtures, EOF is preferred over pressure driven flow because the flat flow gives better resolution. Another advantage of EOF is that no moving parts like valves and pumps are required. The electric field acts as a pump and a valve, controlling the direction and magnitude of the flow velocity.

The inherent ionic mobility ( $\mu_{ion}$ ), i.e. the second main contribution of  $\mu_{obs}$ , provides a selectivity by changing the observed mobility of other ionic species to a different degree. A possible calculation for ionic mobilities from hydrated ionic radii,  $r_i$  is

$$\mu_{ion} = \frac{10^7 z_i e}{6\pi\eta r_i} \quad (3.5)$$

where  $z_i$  is the valence number of an ion, determining by its sign one of the two possible directions of the ionic mobility vector,  $e$  is the charge of an electron ( $1.602 \cdot 10^{-19}$  C), and  $\eta$  is the dynamic viscosity of the electrolyte medium. As shown in Fig. 3.7, considering two different cations ( $z_{(1)}/r_{(1)} > z_{(2)}/r_{(2)}$ ), the ionic mobility of ion number 1 is larger than that of ion number 2, because  $\mu_{ion}$  depends on  $z_{(i)}/r_{(i)}$  of each ion  $i$ . Thus the difference of ionic mobilities causes the different apparent mobilities of each ionic species and continuously separation of the ionic species.

The homemade CE system used in this work is described in detail in [Kucz 2003] and depicted in Fig. 3.8. The equipment was designed in a flexible way allowing tests of different components such as nebulizers, spray chambers, and ICP-MS apparatus. Hydrodynamic injection was applied to introduce the solution

into the capillary with a pressure continuously adjustable from 20 to 1000 mbar. About 44 nL ( $\pm 5\%$ ) sample was injected within 10 sec with 100 mbar. A fused silica capillary (inner diameter 50  $\mu\text{m}$  and outer diameter 363  $\mu\text{m}$ , PolyMicro Technologies, Phoenix, AZ) was applied. Before the use, the fused silica capillary was purged for 10 min with 0.1 M HCl, 0.1 M NaOH, and again 0.1 M HCl and then for 20 min with water and the electrolyte solution. As a CE electrolyte buffer, 1 M AcOH, pH 2.47 was used and + 30 kV was applied for separation. An Elan 5000 ICP-MS (Perkin Elmer) combined with a glove box to allow the analysis of  $\alpha$  emitting radionuclides was used. The interface between CE and ICP-MS was made of PEEK as a four way fitting with special dimensions adapted to the CE system. As microcentric nebulizer, the MicroMist nebulizer AR 30-I-FM02 (Glass Expansion, West Melbourne, Australia) was used and as spray chambers, a Cinnabar small volume cyclonic spray chamber (Glass Expansion), respectively. A polyvinyl chloride tubing of 7 m length was necessary to connect the spray chambers inside the CE ventilation hood with the inlet of the plasma torch inside the glove box of the ICP-MS. The aerosol was transferred within 15 s from the nebulizer to the ICP. The waste solution from the spray chamber was removed by a peristaltic pump. For the CE separations, the plutonium solutions were diluted with 1 M AcOH to metal concentrations between  $10^{-7}$  and  $10^{-5}$  M. The separation of four oxidation states of plutonium took about 10 min.

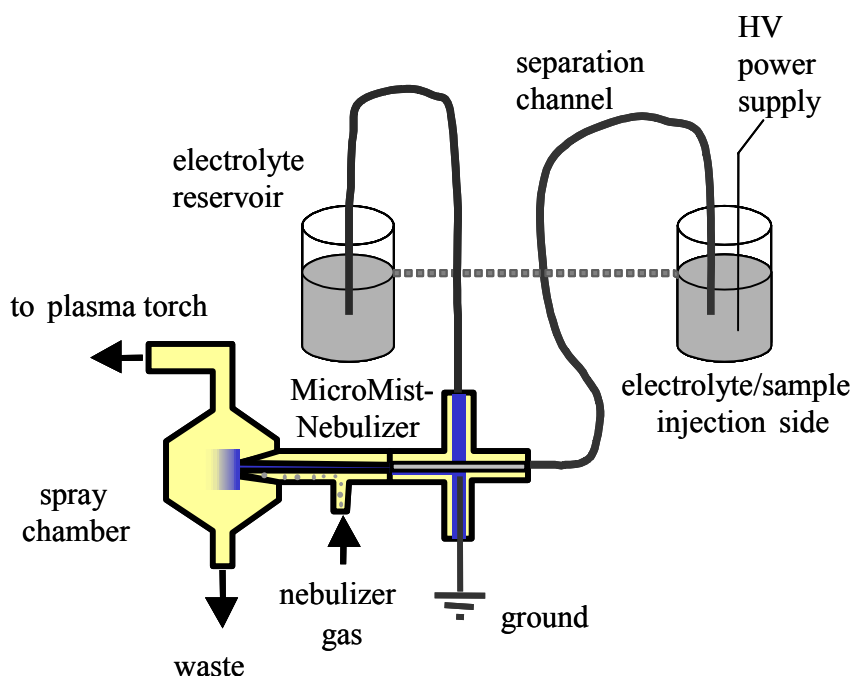


Fig. 3.8 The set up of the homemade CE with the interface and nebulizer unit for coupling to the ICP-MS [Kucz 2003].

As mentioned above, the order of the migration times depends on the charge, size and shape of the ionic species. The charge in this case is determined by the degree of complexation with acetate. Kuczewski *et al.* calculated the species distribution with known complex constants and estimated the order of mobilities for the plutonium ions according to the degree of complexation as follows



and they also showed that this order is very similar to the experimental data.

### 3.3 X-ray Absorption Fine Structure (XAFS)

X-rays are electromagnetic radiation with energies between ultraviolet light and gamma rays in the electromagnetic spectrum. X-ray wavelengths lie in the range of 0.01 Å and 100 Å, with hard X-rays on one end and soft X-rays on the other, respectively. Throughout the history of modern physical and chemical science, X-rays have been used as powerful tools in analytical, physical, chemical, biological, and structural characterization of matter [Teo 86].

X-rays absorption fine structure (XAFS) spectroscopy is one of the most powerful tools for mapping the short range atomic order and is used to investigate the molecular structure of chemical species in - besides others - solution or in amorphous solids such as glasses. When X-rays are absorbed by the atoms in a sample, a steep increase of absorption in the amount of absorbed intensity being specific to each element is observed at certain energy values. This phenomenon is known as absorption edges (see Fig. 3.9).

The absorption edge occurs when the energy of the incident X-rays is equal to the threshold energy necessary to eject an electron (XANES region [Behr 92b]). The electron excited from a core orbital level to a bound or continuum state can be considered as a wave traveling outwards from the central absorbing atom. Simple models of X-ray absorption predict a gradual monotonic decrease in the absorption coefficient with increasing energy after the absorption edge. Such behavior is observed in spectra of isolated atoms, *e.g.*, noble gases (Xe, Kr *etc.*). However, the presence of other atoms either in a molecule or a condensed phase around the absorber causes oscillations in the absorption coefficient up to 1000 eV above the edge (EXAFS region [Fay 88]) as shown in Fig. 3.9.

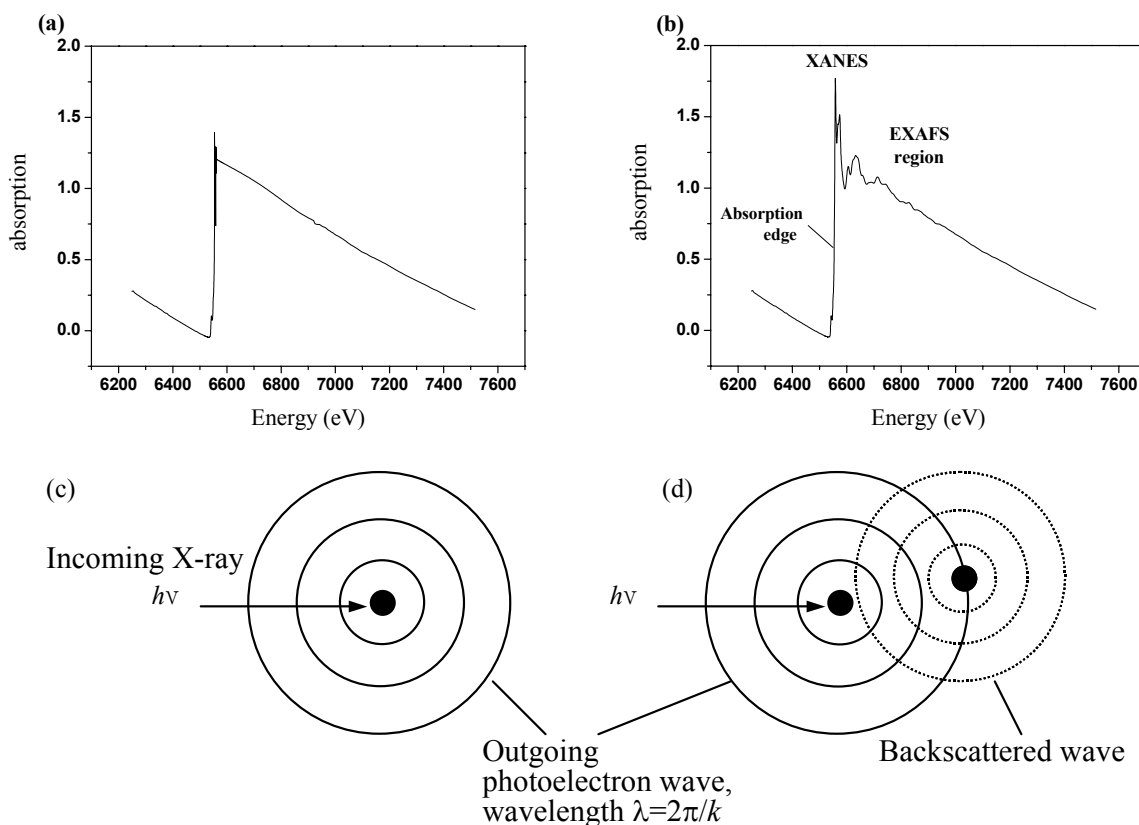


Fig. 3.9 Schematic representation and XAFS spectra of two different atoms: the absence and presence of a neighboring atom. A monatomic gas such as Kr (a and c) and a diatomic gas such as Br<sub>2</sub> (b and d), respectively [Teo 86].

XANES refers to the prominent peaks and shoulders that modify the appearance of the absorption edge and the 20 - 30 eV regions beyond it. It is a technique of exciting core level electrons into the unoccupied molecular orbital states and the continuum by varying the energy of the incident X-rays. The XANES can reveal the oxidation state of an element in the sample, as well as serve as a “fingerprint” to identify certain structural modes of a chemical species like its site symmetry.

The oscillations in the post edge region (EXAFS region in Fig. 3.9 (b)) arise from the back scattering of the emitted electron wave from neighboring atoms and thus the structure of the post edge region of the X-ray absorption spectrum is related to the radial distribution of atoms in the sample. The frequency and amplitude of the oscillations carry information about the local environment of the absorbing element and can be derived by analyzing this structure.

If the core ( $1s$ ,  $2s$ ,  $2p$ ) electron of the absorbing atom is excited by the X-ray beam, then the electron can be represented as an outgoing spherical wave. The outgoing photoelectron wave is backscattered by the neighboring atom. The final state will be the sum of the outgoing wave and the backscattered waves from shells of neighboring atoms.



It is the interference between the outgoing and incoming waves that gives rise to the sinusoidal variation of  $\mu$  (X-ray absorption coefficient) vs.  $E$  [eV] as EXAFS. Codes like FEFF [Anku 96; Anku 97] can be used to simulate the EXAFS based on assumptions on the local structure around the absorbing atom.

The general equation for EXAFS is

$$\chi(k) = S_0^2 \sum_i N_i F_i(k) \exp(-2\sigma_i^2 k^2) \exp(-2R_i/\lambda_i(k)) \frac{\sin(2kR_i + \Phi_i(k))}{kR_i^2} \quad (3.7)$$

where  $k$  is the wave vector;  $R_i$ : the distance from absorbing atom;  $N_i$ :  $i$ -th coordination number;  $S_0^2$ : amplitude reduction factor due to many body effects such as shake up/off process at the absorbing atom;  $F_i(k)$ : backscattering amplitude from neighboring atom type  $i$ ;  $\sigma_i$ : Debye-Waller factor due to thermal vibration and static disorder;  $\lambda_i$ : electron mean free path, and  $\Phi_i(k)$ : total phase shift experienced by the photoelectron.

Since the experimental X-ray absorption data can be simulated based on equation (3.7), the local information such as bond-lengths, coordination numbers and Debye-Waller factors are obtained. In general, the data can be fitted with small error range obtaining reliable local structural information.

In this study, XAFS measurements are performed at the Angströmquelle Karlsruhe (ANKA), Forschungszentrum Karlsruhe, Germany. Zr K edge spectra of samples are recorded at the INE-Beamline (see Fig. 3.10) for actinide research [Dene 2005] using a pair of Ge (422) crystal ( $2d = 3.412 \text{ \AA}$ ) in the Lemonnier-type double crystal monochromator (DCM). The INE-Beamline is equipped with a collimating first and a focusing second mirror and the beam spot used is  $4 \times 2 \text{ mm}^2$ . Fluorescence spectra are recorded by registering the normalized Zr  $K_{\alpha 1,2}$  fluorescence radiation ( $\sim 15.7 \text{ keV}$ ) as a function of the incident photon energy using a 5-pixel energy dispersive solid state Ge detector (Canberra LEGe). Argon filled ionization chambers are used. Three to six scans are collected and averaged for each sample.

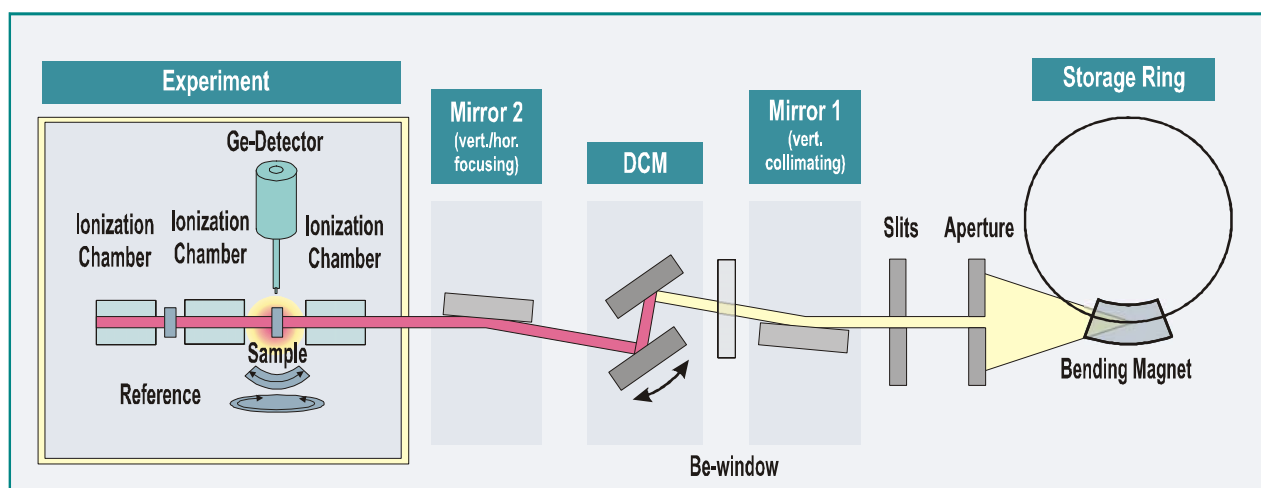


Fig. 3.10 INE-Beamline at the ANKA, Forschungszentrum Karlsruhe, Germany. Optics used for INE-Beamline are a pair of Ge (422) crystal ( $2d = 3.412 \text{ \AA}$ ) in the Lemonnier-type DCM and a collimating first and a focusing second mirror. The left box indicates the experimental area where work with radioactive samples is allowed. Fluorescence spectra are recorded by a Ge detector (Canberra LEGe). Argon filled ionization chambers are used.

XANES spectra are isolated from XAFS scans following subtraction of the pre-edge background absorption, approximated as a linear function, and normalization of the edge jump (average between 18.100 and 18.300 keV) to unity.

EXAFS data analysis is based on standard least squares fit techniques [Saye 88] using the WinXAS [Ress 97] (v 3.0) and the UWXAFS (University of Washington XAFS analysis program) [Ster 95] program packages and the matrix parameters ( $R_i$ ,  $\sigma_i$ , and  $N_i$ ) are determined using the *feffit* code (v2.98). Backscattering amplitude and phase shift functions for single scattering paths in a 60-atom cluster in Cartesian coordinates of monoclinic  $\text{ZrO}_2$  (crystallographic data taken from [Gual 96]) are obtained from FEFF8.2 [Anku 96; Anku 97] calculations. Prior to analysis, the  $k^3$ -weighted Zr K EXAFS spectra are Fourier-transformed over a  $k$ -space range of  $\sim 2.5 - 14.5 \text{ \AA}^{-1}$ , using symmetric square windows with  $\Delta k = 0.2 \text{ \AA}^{-1}$  ‘Hanning sills’. The amplitude reduction factor  $S_0^2$  is fixed at 1.

### 3.4 Laser Induced Breakdown Detection (LIBD)

The laser induced breakdown detection (LIBD) for characterizing aquatic colloids was developed to detect trace contaminations in liquids for semiconductor industry by Kitamori *et al.* [Kita 88; Kita 89]. The method is now applied in many research fields: size determination of aerosols *in situ* [Poul 95; Hahn 98], microbubble formation in an aqueous solution of a silver/dendrimer nanocomposite [Mila 2003], drinking water characterization [Sait 99], and *in situ* groundwater colloid characterization, e.g. in Grimsel (Switzerland) and Äspö (Sweden) [Haus 2002]. Colloids of tetravalent actinides formed in oversaturated solutions are investigated in order to determine thermodynamic solubility data [Bund 2000; Neck 2002] and predict their long term stability [Bite 2003; Roth 2004]. LIBD is a very sensitive detection method especially for small particles in comparison to the conventional light scattering method (see Fig. 3.11). LIBD can cover three orders of magnitude in size (5 – 1000 nm) and many orders of magnitude in particle concentration (several ppt – several ppm). [Bund 2001a].

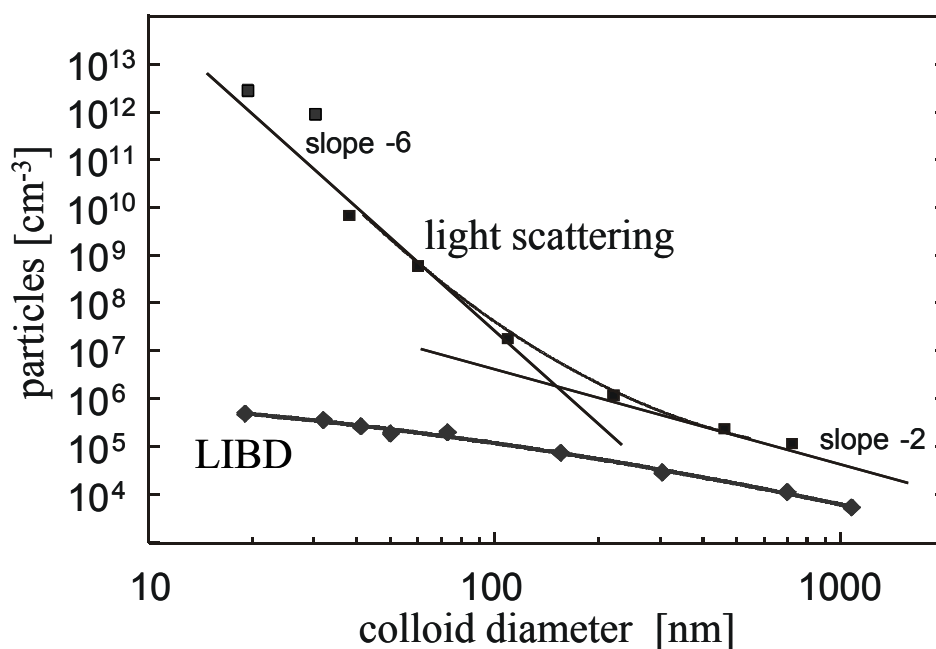


Fig. 3.11 The detection limit of LIBD in comparison to the conventional light scattering [Bund 2001a].

### 3.4.1 Principle of LIBD

The breakdown process has been described in detail [Radz 89; Sche 96] and will be mentioned here briefly. When a pulsed laser is focused tightly into a medium exceeding certain threshold irradiance, a so called breakdown occurs. In the beginning at least one atom is ionized by multi-photon ionization early during the laser pulse, and the resulting seed electron is accelerated due to inverse bremsstrahlung in the high electric field of the laser focus. After gaining sufficient energy, additional atoms are ionized by collisions, multiplying the number of electrons. The density of free charge carriers increases in an avalanche after a few consecutive iterations and plasma is created. However, the energy density to initiate the above process (threshold) depends on the phase of the matter in the focal region. It is highest for the gas phase, lower for liquids and lowest for bulk matter. Therefore, when the pulse energy is adjusted such that no breakdown occurs in pure water, the selective particle detection is possible. When a colloid enters the focal region and the threshold for the solid phase applies (which is exceeded) then a plasma is created, which can be detected by a CCD camera recording its optical emission [Bund 2001b] or by a piezoelectric detector coupled to the sample cell, recording the acoustic signal of the plasma expansion [Haus 98; Haus 99] (See Fig. 3.12).

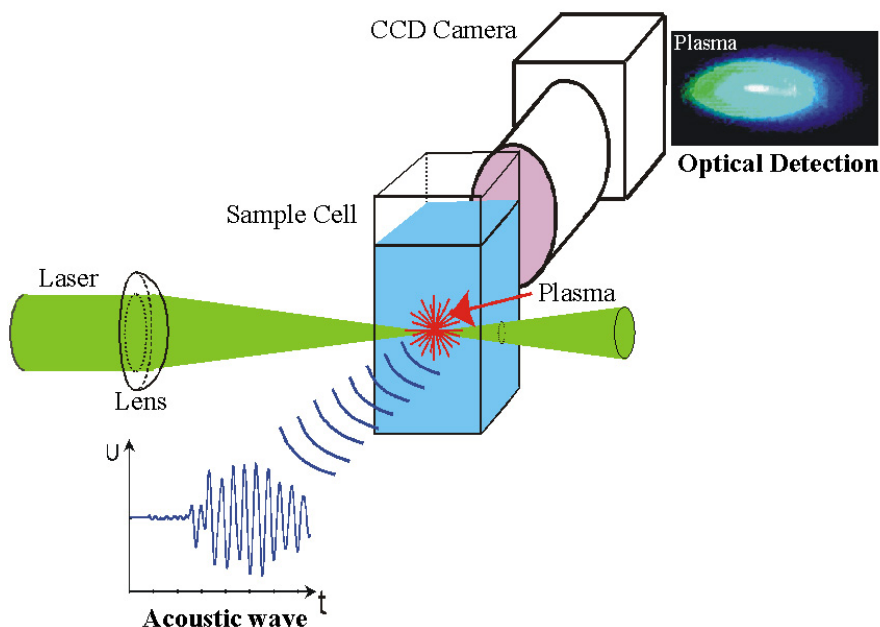


Fig. 3.12 LIBD, principle of operation: plasma is ignited selectively on colloids in solution by a tightly focused pulsed laser. Its expansion causes an acoustic wave which can be detected by a piezoelectric receiver. In addition, the emitted light is observed spatially resolved by a CCD camera [Walt 2003a].

By counting the number of breakdown events relative to the total number of laser shots (breakdown probability (BDP)<sup>3</sup>), the particle number density in the solution can be determined [Sche 96; Bund 2001]. Size and concentration information is obtained by measuring the BDP as a function of pulse energy, the so called ‘s-curve’ [Walt 2002]. The ionization rate of a particle is proportional to the MPI cross section multiplied by an appropriate power of the photon flux density. The cross section increases proportionally to the particle volume (proportional to the number of valence electrons in the particle), so the breakdown threshold energy ( $E_T$  [mJ]) decreases with increasing particle size (Fig. 3.13 (a)) [Izum98; Walt 2002]. The slope of the s-curve scales with the particle concentration (Fig. 3.13 (b)).

The use of reference colloids of well defined diameters provides a calibration for relating breakdown thresholds to particle size. For an unknown sample, the threshold is determined by recording the s-curve and subsequently converted to a mean particle diameter.

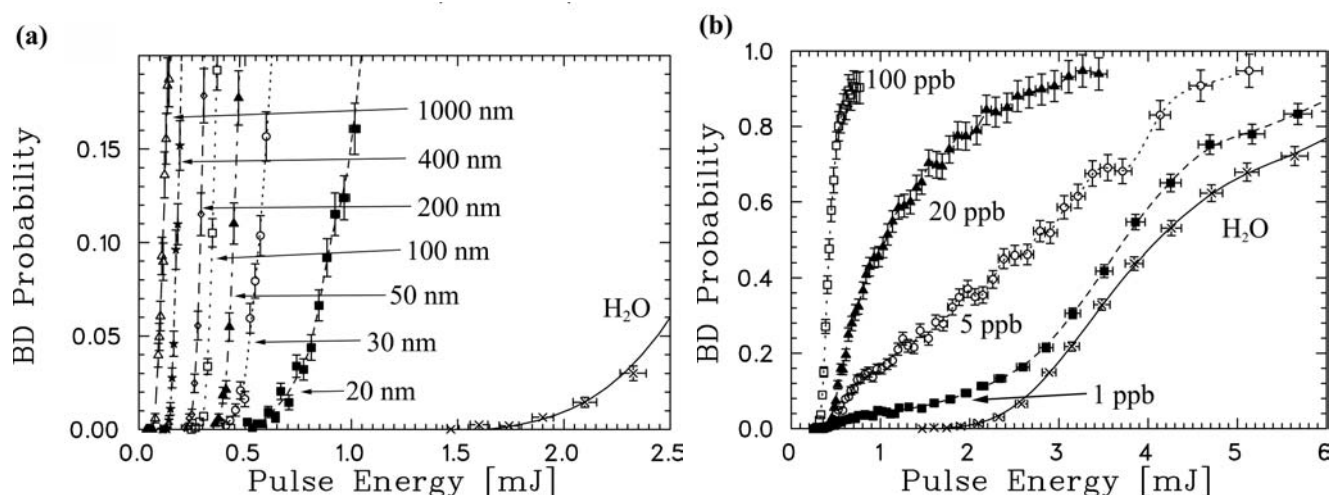


Fig. 3.13 The BDP is plotted as a function of laser pulse energy,  $E$  [mJ]. (a) The threshold  $E_T$  [mJ] of the s-curve increases with decreasing particle size (polystyrene reference colloids). (b) While the threshold remains constant, the slope changes with colloid concentration (polystyrene 100 nm).

<sup>3</sup> 1 % BDP means 10 breakdown events occur during 1000 laser shots

### 3.4.2 Measurement of multimodal size distributions by LIBD

For multimodal disperse samples, an evaluation scheme based on s-curve detection has been developed recently [Walt 2004]. The s-curves can be described by a semi-empirical model with only two free parameters.

$$\text{BDP}_{\text{mono}} = 1 - \left\{ 1 + C(E - E_T) - \frac{1}{2}(C(E - E_T))^2 + \frac{1}{6}(C(E - E_T))^3 \right\} \cdot \exp(-C(E - E_T)) \quad (3.8)$$

where the breakdown threshold  $E_T$  [mJ] is a measure of the particle size and the concentration determines the constant  $C$ . Since the ‘first electron’ is generated by four-photon-ionization in this case of polystyrene ( $h\nu=2.3$  eV, ionization potential of polystyrene = 8.9 eV) and in case of most inorganic colloids, at low pulse energy, a  $\text{BDP}_{\text{mono}} \propto E^4$  dependence is required [Chyl 86]. If Eq. (3.8) is expanded in a Taylor’s series, the first three terms up to  $(E - E_T)^3$  are canceled that results in the  $\propto E^4$  dependence. The negative sign of the quadratic term causes a weak second order ( $E^2$ ) dependency which describes the increase of the effective focal volume  $V_{\text{eff}} \propto E^2$  with increase of the pulse energy [Cerv 75]. Since the BDP is linearly dependent on the focal volume, the BDP also increases with increasing energy. BDP approaches unity asymptotically as  $E[\text{mJ}] \rightarrow \infty$ .

Eq. (3.8) describes only narrow size distributions (monomodal), which can be prepared synthetically, but it is little relevant for natural suspensions. For a bimodal suspension containing particles of sizes  $D_1$  and  $D_2$  ( $D_2 < D_1$ ), with thresholds  $E_T^{(2)} > E_T^{(1)}$ , the s-curve will be identical to that of a monomodal suspension (particle size  $D_1$ ) at energy below the threshold ( $E_T^{(2)}$ ) of the second fraction. At energy exceeding  $E_T^{(2)}$ , the s-curve is the sum of the s-curves for two monomodal suspensions (size  $D_1$  and  $D_2$ ). Since the s-curve represents probability, the sum of two s-curves means the probability that either the first fraction of colloids with size  $D_1$  or the second fraction of colloids with size  $D_2$  generates a breakdown event (logical OR). Such a probability is defined as one minus the product of the probabilities that each monomodal suspension causes no breakdown event:

$$\text{BDP}_{\text{Bi}} = 1 - (1 - \text{BDP}_1) \cdot (1 - \text{BDP}_2). \quad (3.9)$$

Combining Eqs. (3.8) and (3.9), we get

$$\text{BDP}_{\text{Bi}} = 1 - \prod_{i=1}^2 \left\{ 1 + C^{(i)}(E - E_T^{(i)}) - \frac{1}{2}(C^{(i)}(E - E_T^{(i)}))^2 + \frac{1}{6}(C^{(i)}(E - E_T^{(i)}))^3 \right\} \cdot \exp[-C^{(i)}(E - E_T^{(i)})] \quad (3.10)$$

where  $E_T^{(i)}$  and  $C^{(i)}$  are the threshold and the parameter of colloid number density, respectively. Eq. (3.10) is easily extended for any number of size classes.

In practice, it is necessary to limit the number of free fitting parameters. In the following example, the thresholds,  $E_T^{(i)}$ , are obtained by calibration with monodisperse polystyrene reference spheres whose sizes are 20, 30, 40, 50, 70 and 100 nm and remain as fixed values thereafter. Monomodal suspensions of several concentrations are measured in order to obtain the slope parameter  $C^{(i)}$  versus colloid number density  $N^{(i)}$  according to the following semi-empirical equation,

$$\log C^{(i)} = a^{(i)} \log(b^{(i)} N^{(i)}) \quad (3.11)$$

To obtain the size distribution, the s-curve of a sample is measured with optimal statistics, especially in the low energy region, i.e. the region that contains the size information. The increase of the particle size from 20 nm to 100 nm causes the decrease of threshold by a factor of 2 (from 0.5 mJ to 0.28 mJ, see Fig. 3.13), which is small compared to the typical energy interval of a complete s-curve (as depicted in Fig. 3.14(a)). Equation (3.10) is then fit to the data. The thresholds  $E_T^{(i)}$  remain fixed and only the concentration parameters  $C^{(i)}$  are varied. In spite of six parameters being fit simultaneously, the fit turns out to be quite robust. The parameters hardly affect one another, but rather each parameter is sensitive at a unique region of the s-curve.  $C^{(1)}$  is determined only in the energy region below  $E_T^{(2)}$  which is the threshold of the second size class  $C^{(2)}$  is most sensitive at energies  $E_T^{(2)} < E < E_T^{(3)}$  and so forth. Several data points (BDP) should be measured between  $E_T^{(i)}$  and  $E_T^{(i+1)}$  in order to exactly estimate the amount of size class  $i$ ,  $C^{(i)}$ .

Fig. 3.14 illustrates the case of a trimodal sample prepared by mixing of three polystyrene reference particles,  $1.5 \cdot 10^8$  particles  $\text{cm}^{-3}$  of 20 nm diameter,  $2.0 \cdot 10^7$  particles  $\text{cm}^{-3}$  of 50 nm and  $2.7 \cdot 10^6$  particles  $\text{cm}^{-3}$  of 100 nm. They are combined in order to simulate a Pareto-like PSD found in natural waters [Buff 95; Degu 2000; Evan 2000]. The differential number density of different sizes scales as a power law of the particle diameter  $D$ :

$$\frac{dN_{\text{coll}}}{dD} \propto D^{-\beta} \quad ; \quad 3 < \beta < 5 \quad (3.12)$$

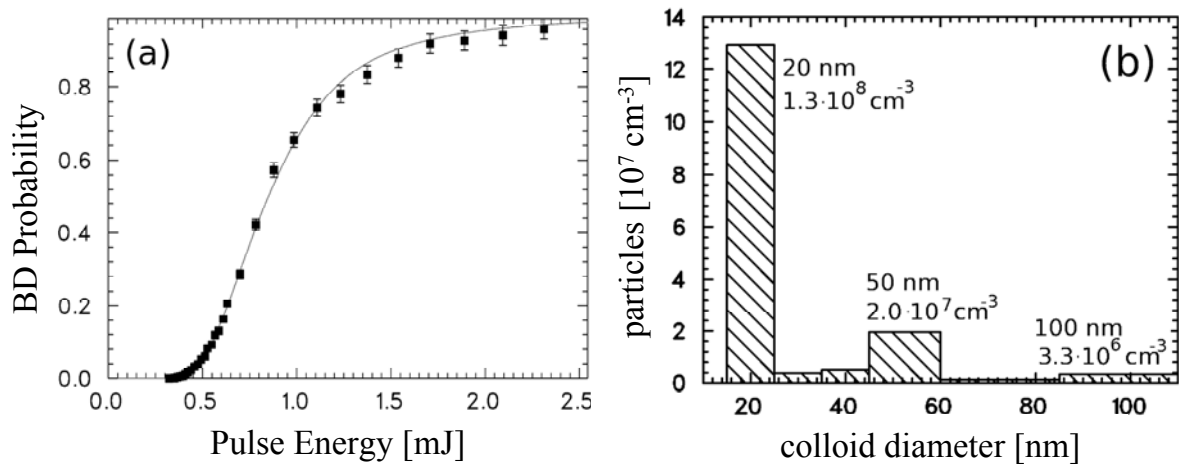


Fig. 3.14 The PSD of a three modal colloid sample prepared by mixing with polystyrene reference particles is reproduced within 20 % error (see text). (a) The BDP as a function of the laser pulse energy (s-curve) and (b) PSD determined from the fit curve [Walt 2004].

In Fig. 3.14 (a), the raw data, i.e., the BDP as a function of the laser pulse energy are plotted. Note the high quality of the data at low pulse energies which is crucial to achieve meaningful results. All six concentration parameters  $C^{(i)}$  are varied and the result is displayed in the histogram in Fig. 3.14 (b).  $C^{(1)}$ ,  $C^{(4)}$  and  $C^{(6)}$  yield finite values, whereas  $C^{(2)}$ ,  $C^{(3)}$  and  $C^{(5)}$  remain close to zero. The particle number densities are reproduced with an approximately 20 % error. If, however, a sample contains a predominant fraction of large colloids, some size screening effects may occur. Colloids do not contribute to the sum curve below their specific threshold  $E_T^{(i)}$ . In order for the contribution of small colloids (at comparatively high energy) to be of measurable relevance, the signal caused by the large colloids must remain sufficiently low. As the s-curve, BDP ( $E$ ), approaches unity, an additional increase due to a fraction of very small sizes can no longer be resolved.

### 3.4.3 Setup of LIBD apparatus

The optical system used for this experiment is described in detail in literature [Walt 2002] (Fig. 3.15). Here some important points are only mentioned again. A diode pumped Nd:YAG laser (BMI-Soliton DIVA II) is used as a light source, which provides a laser beam of 1 mm diameter and 0.5 mrad divergence. Pulses of 7 ns (FWHM) and up to 10 mJ at 532 nm are emitted at a repetition rate of 20 Hz. Besides the small dimension ( $35 \times 17 \times 8$  cm) and low maintenance requirement (no flash lamp change, air cooled), the single transversal mode profile (TEM 00) is an important criterion to choose this kind of laser.



The following two elements serve as pulse energy control. The initial horizontal polarization of the laser beam is transformed to circular polarization by a  $\lambda/4$  plate (QWP1, quarter wave plate). By a second  $\lambda/4$  plate (QWP2) which can be rotated by a stepper motor along its c-axis, a new polarization plane is selected. The resulting vertical component is separated by a Glan-Thompson polarizer (P) and guided into a beam dump, while only the remaining horizontal component is transmitted. By varying the angle of the second quarter wave plate, the power passing through the polarizer is then controlled. The pulse energy is monitored by a pyroelectrical detector (Pyro 1).

A mirror (B1) deflects the main beam by  $90^\circ$  through two diaphragms (D3 and D4) which define the principal axis of the experiment. In the center between these diaphragms, quartz cell (QC) containing the sample is located. Beam focusing is achieved by a Galilean telescope of spherical lenses: by a  $f = -50\text{mm}$  planoconcave lens the beam is expanded by a factor of three and 100 mm behind collimated by a  $f = +50\text{mm}$  planoconvex lens, resulting in an effective focal length of some 80 mm.

Along the principal axis the counter propagating light of a HeNe laser is superimposed on the Nd:YAG beam, guided by four aluminum coated mirrors (A1) and monitored by CCD3 before and after passing the quartz cell in analogy to the Nd:YAG beam. Its good spatial coherence is used to align the lenses exactly on axis and parallel to each other by observing interference fringes, which is not possible with the Nd:YAG. In addition misalignments of the lenses can be detected on line during operation, due to the distortions of the far field laser profile they cause.

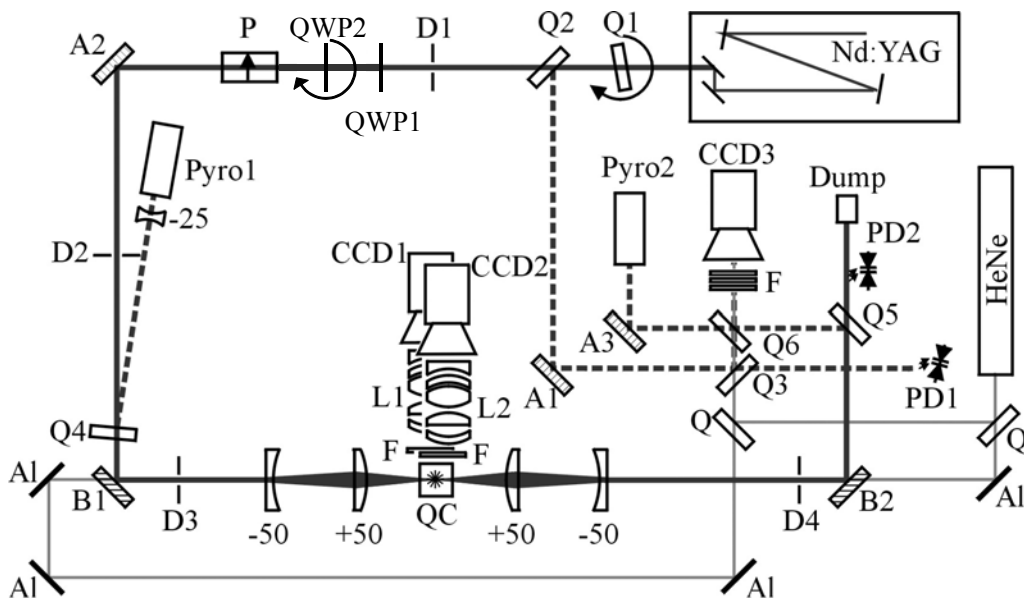


Fig. 3.15 Setup of the LIBD apparatus. The plasma is created inside the quartz cell (QC) containing the sample and the acoustic wave and the emitted light are observed by piezoelectric detector and cameras CCD1 and CCD2, respectively [Walt 2002].

### 3.5 Single particle counter (SPC)

In 1989, Degueldre *et al.* applied a single particle counter (SPC) system to characterize groundwater colloids and showed that the results were in good agreement with other conventional techniques [Degu 89]. The advantages of the SPC which is designed to determine sub-micron PSD, are to give an absolute colloid number concentration, to measure without bias highly polydispersed samples and to avoid preconcentration artifacts (i.e., aggregation) even with dilute samples.

SPC is based on the light scattering by single particles. When a colloid in solution passes through a light beam, then the light is scattered. The intensity of the scattered light depends on the scattering angle, the wavelength of incident light, the refractive indices and the shape and size of the colloid. The amplitude of the scattered light shows a monotonic relation with the colloid size [Köpf 79], allowing size determination. For small particles, the intensity depends on  $D^6$  (Rayleigh scattering) and for large particle on  $D^2$  (Mie scattering,  $D$ : particle diameter). For precise counting of single particles, colloids must pass the light beam one after the other. For that the sample volume must be very small or the sample has to be highly diluted prior to the measurement.

The SPC system used in this work is similar to that in literature [Ross 2003] (see Fig. 3.16). A high sensitivity liquid *in-situ* monitor (HSLIS) and a Volumetric Spectrometer LiQuilaz S02 (Particle measuring Systems, Boulder, CO) are used. The former is designed for small colloids (50 - 200 nm) by which the intensity of light scattering is very low. The latter counter covers relative large colloids in range from 200 – 2000 nm. Additionally, the system comprise supplementary equipments: (1) the filtration system is needed to produce ultra-filtered water used for sample dilution, (2) the sample injection system is used for precisely controlling the injected sample volume rate, (3) the flow controller system maintains constant water flow rate, and (4) the data processing system is based on a PC.

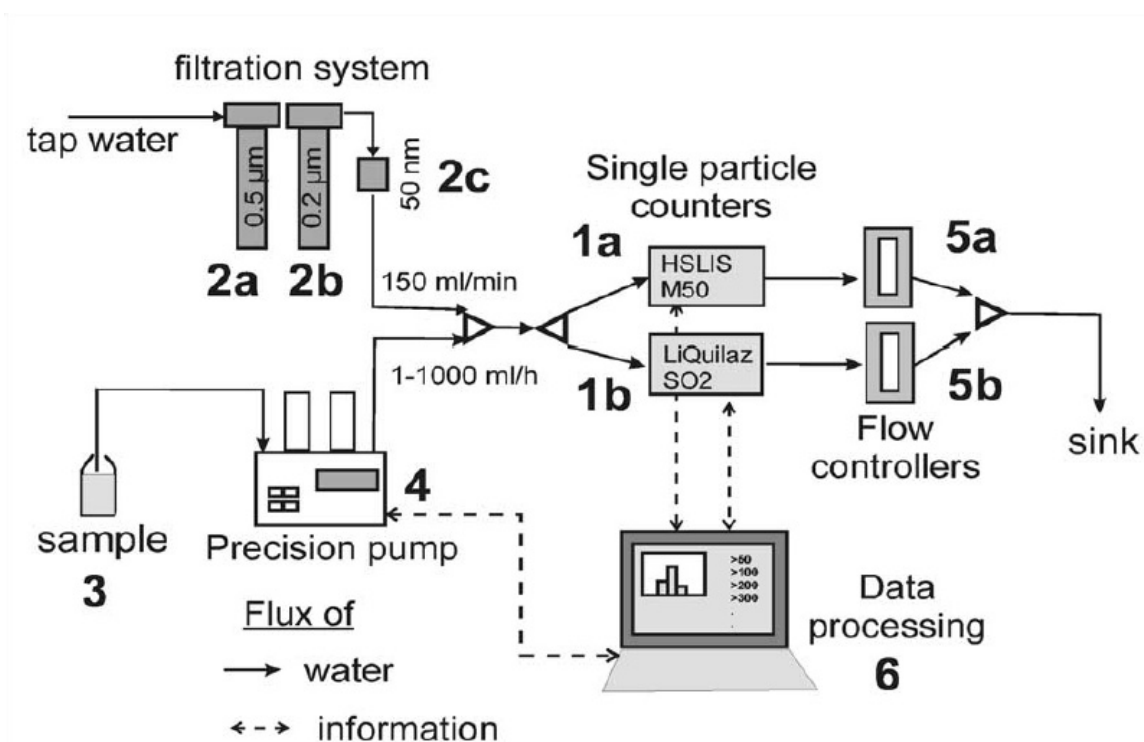


Fig. 3.16 The system set-up. (1) SPC (Particles measuring System): (1a) HSLIS-M50, (1b) LiQuilaz SO<sub>2</sub>. (2) Filter cartridges (Millipore): (2a) Polygard-CR 0.5 µm, (2b) Durapore 0.2 µm, (2c) Optimizer DI 0.05 µm. (3) Sample. (4) Precision Volumetric Pump KP2000 (Desaga GmbH), flow 1 - 1000 ml per hour. (5) Water Flow Controllers FS-100 (PMS): (5a) 100 ml min<sup>-1</sup>, (5b) 50 ml min<sup>-1</sup>. (6) Laptop PC: data processing with 'Facility Net' software (PMS Inc.) [Ross 2003].

## 4 Experiments

### 4.1 Zirconium

#### 4.1.1 Preparation of background materials and samples

The background medium of all solutions is 0.5 M (H/Na)Cl. The ultrapure NaCl (99.99%, optical grade) is purchased from Sigma Aldrich. It contains potassium (35 ppm) and iron (2 ppm) as main metal contaminations and all other contaminated metals are less than 0.2 ppm (information from manufacturer). To obtain colloid free 0.5M NaCl solution, ultracentrifugation for 1 hour at 40 000 rpm (corresponding to a max. relative centrifugal force of about  $5 \cdot 10^5$  g) is used. The colloidal free 0.5M HCl solution (Merck) is obtained by filtration through an Amicon 1 kD ultrafilter (pore size ca. 1 nm). All solutions are prepared with ultrapure water from a water purification apparatus (Milli-Q-academic, Millipore) and checked using LIBD whether the solution contains colloids or not.

A concentrated zirconium stock solution is prepared from ultrapure  $\text{ZrOCl}_2 \cdot x\text{H}_2\text{O}$  (Sigma Aldrich, 99.99%) in 0.5M HCl and then two times ultrafiltrated through Amicon 10 kD and 1 kD filters (pore size about 1 nm). Its concentration is  $5.2 \cdot 10^{-3}$  M as determined by ICP-MS. For the coulometric titration series (explained in detail in Section 4.1.2), the starting solutions (volume 40 ml) are prepared at constant ionic strength ( $I = 0.5$  M) by dilution of the stock solution with a mixed solution of 0.5 M NaCl and 0.5 M HCl. The Zr concentrations are determined by ICP-MS. The 13 starting solutions for the coulometric titrations are depicted in Fig. 4.1 ( $\Delta$ ) and listed in Table 8.2 (in Appendix 8.2) and the concentration ranges over 4 orders of magnitude (from  $2 \cdot 10^{-8}$  to  $1 \cdot 10^{-3}$  M). In addition, six samples of the coulometric titration series 2 with increasing pH are measured by XAFS (Fig. 4.1 ( $\circ$ ), **d - i**).

For the XAFS measurement, the sample **a** ( $\otimes$ , in Fig. 4.1) containing a concentrated solution at  $[\text{Zr}] = 0.1$  M and pH 0.21 is prepared by dilution of about 1.6 g  $\text{ZrOCl}_2 \cdot x\text{H}_2\text{O}$  (Sigma Aldrich, 99.99%) in 40 ml of 0.5 M HCl and then addition of 1 ml of 4 M NaOH. After over 2 months, the sample is measured with LIBD and XAFS. The reference colloids (sample **b**) are obtained from Postnova ( $100 \text{ nm} \pm 2.5 \%$ , 2.5 g/l) and the monoclinic  $\text{ZrO}_2$  (sample **c**) is a commercially available sample (Fluka, p.a.). The information of samples examined by XAFS is summarized in Table 8.3.

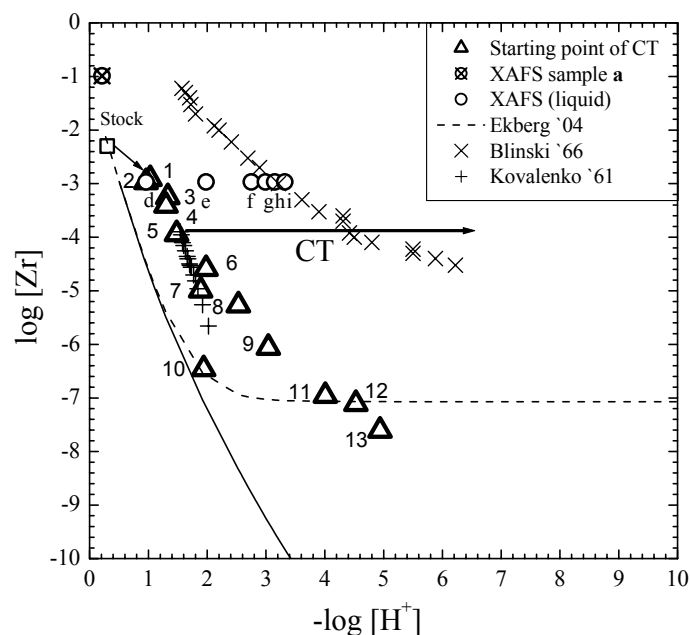


Fig. 4.1 From the stock solution ( $\square$ , pH 0.3,  $[\text{Zr}] = 5.2 \cdot 10^{-3}$  M in 0.5 M HCl), 13 starting solutions ( $\triangle$ ) for the coulometric titrations (CT) are obtained by dilution with 0.5 M (H/Na)Cl. pH is increased by coulometric pH titration (CT) as indicated exemplarily for series 5 (arrow) until colloids are formed. Six samples from series 2 are measured by XAFS **d - i** ( $\circ$ ). In addition, a concentrated solution (sample **a** at pH 0.2,  $[\text{Zr}] = 0.1$  M) is investigated ( $\otimes$ ).

XAFS measurements for all samples are carried out at INE-Beamline (see Section 3.3) except for the reference sample **c** (monoclinic  $\text{ZrO}_2$ ) which is measured at the ANKA-XAS endstation. The standard beam spot size is  $8 \times 1 \text{ mm}^2$ . Higher harmonic radiation in the incident beam is suppressed by detuning the parallel alignment of the double crystal monochromator (DCM) to 60 % of photon flux peak intensity. The spectra are calibrated against the first derivative XANES spectrum of a Zr foil (17.998 keV).

#### 4.1.2 Coulometric pH titration

Conventionally, the solubility data is obtained by measuring the equilibrium amount of solvated species in the presence of a precipitate starting from undersaturation. In this study, a different approach is applied, similar to the previous study with thorium [Bund 2000; Neck 2003]. When pH is increased slowly at constant Zr concentration, the point at which colloids form is detected by LIBD. The colloids formed in the

solution and detected with LIBD remain suspended by Brownian motion due to their small size (10 –100 nm) and serve as a very sensitive indicator of exceeding the solubility limit. Solubility data obtained by this method [Neck 2001b] is of high quality and consistent with solubility data of well characterized solubility limiting phases, provided pH is increased very slowly. A well suited method for this is coulometric titration [Bund 2000; Neck 2003], where  $H^+$  is reduced in the solution by an electric current from Hg half cell electrode to a Pt working electrode:



Typical currents of 50  $\mu A$  reduce about  $5 \cdot 10^{-10}$  mol  $H^+$  per second. A pH increase from 3.0 to 3.1 in a 50 ml solution, for instance, takes 320 minutes and an increase from pH 1.0 to 1.1 takes 540 hours. Addition of a base (e.g., NaOH) to increase pH leads to strong local gradients, i.e. regions of oversaturation, in which colloids may form and might be metastable for weeks [Bite 2003] even in undersaturated solution.

The coulometric titration set-up is described in Fig. 4.2. Current control (constant current source, Digistant 6706, Burster), pH detection and LIBD measurements are fully automated and operated via a remote control up to several weeks continuously for a single titration-LIBD series. pH is initially increased by predefined 0.1 units using an appropriate current (20  $\mu A$  – 1 mA). After each incremental increase, the current is turned off to equilibrate the solution for 10 minutes, prior to the measurement of the colloid size distribution with LIBD. S-curves (BDP as a function of laser pulse energy) are measured for each solution and 1000 laser shots are applied at same energy. Once the LIBD measurement (for about 30 min.) has finished, the current is switched on again and the pH is increased further and the procedure is repeated. Close to the expected solubility limit, the pH is increased more slowly by reducing the electric current down to 20  $\mu A$ . In this work, in order to avoid sorption of formed colloids on equipments, the reaction vessel and the end of the salt bridge made from quartz are used. For flow-through experiments PFA (perfluoroalkoxy) tubing and a quartz flow-through cell (volume 450  $\mu l$ ) are used as well. Since the internal fill solution of pH electrodes (e.g., Ross electrode with liquid junction) tend to leak out into the sample solution, it may cause colloidal contamination of the sample. To prevent this kinds of contamination, two half cells ( $H^+$ -glass electrode and Ag/AgCl-electrode, Merck) are used. For the pH electrode calibration, standard solutions ( $I = 0.5M$ ) covering the range of pH values in the experiments (pH 0.3 – pH 10, namely 0.5 M HCl –  $10^{-4}$  M NaOH in 0.5 M NaCl) are applied.

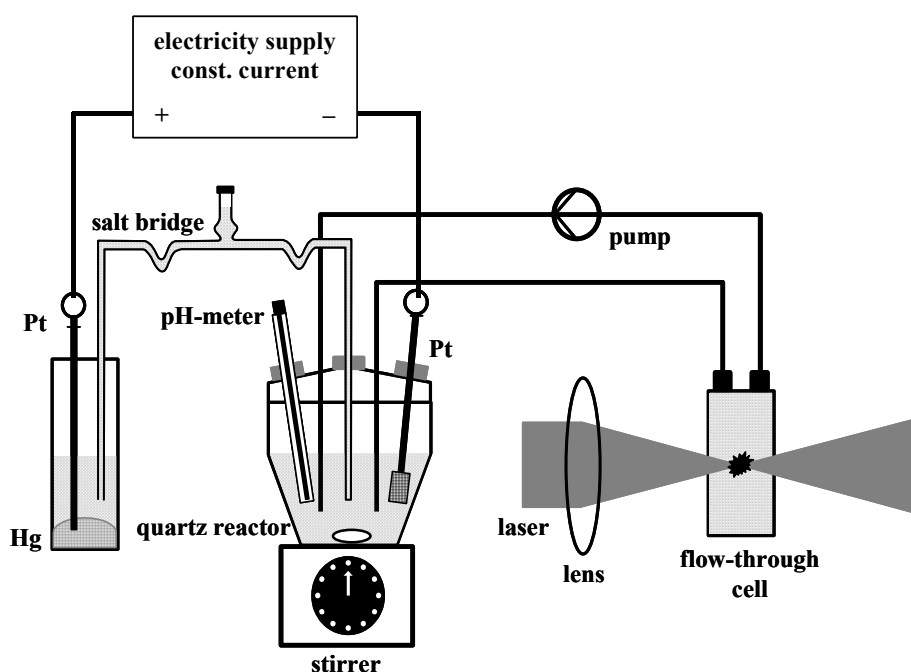


Fig. 4.2 Experimental setup of the coulometric pH titration combined with LIBD.

## 4.2 Plutonium

### 4.2.1 Preparation of Pu(IV) stock solution

87 mg  $\text{PuO}_2$  (brown powder) is diluted in 20 ml of 14 M  $\text{HNO}_3$  / 0.1 M  $\text{HF}$  and then heated a few hours until all powder is dissolved. In order to remove hydrofluoric acid, the solution is evaporated several times in 8 M  $\text{HNO}_3$  and subsequently is dissolved in 8 M  $\text{HNO}_3$ . The solution is investigated using  $\alpha$ - and  $\gamma$ -spectroscopy as well as ICP-MS. The result from  $\alpha$ -spectrometry indicates that the plutonium contains three different isotopes,  $^{242}\text{Pu}$ ,  $^{239/240}\text{Pu}$  and  $^{238}\text{Pu}$ . Since the energy of  $\alpha$ -radiation for  $^{238}\text{Pu}$  (5.499 and 5.456 MeV) is similar to that for  $^{241}\text{Am}$  (5.486 and 5.443 MeV), the two isotopes are not distinguishable using  $\alpha$ -spectrometry. Therefore  $\gamma$ -spectrometry is applied to determine the amount of  $^{241}\text{Am}$  (9 Bq) with  $\gamma$ -rays at 13.9, 26.4, 33.2 and 59.5 keV and about 67 % of  $\alpha$ -radiation is emitted from  $^{241}\text{Am}$ , namely  $\alpha$ -emission from  $^{238}\text{Pu}$  is only 33 %.

From the  $\beta$ -counts by LSC,  $^{241}\text{Pu}$  is found. The ICP-MS results indicate the contribution of  $^{242}\text{Pu}$  (11 Bq) which is slightly smaller than the amount (13.6 Bq) determined by  $\alpha$ -spectrometry. This is probably be-

cause of matrix effect during the ICP-MS measurement of plutonium. In addition, the Pu solution contains a small amount of iron. The metal contaminations (for example, americium and iron) are removed from the plutonium solution using an anion exchange column with Dowex 1 × 4 (50 – 100 mesh). In 8 M HNO<sub>3</sub> solution, most of plutonium is tetravalent with only a small quantity of Pu(VI). The contamination (Am and Fe) as well as Pu(VI) are eluted through the column with 8 M HNO<sub>3</sub> and only Pu(IV) is retained in the column. After the washing with 8 M HNO<sub>3</sub>, Pu(IV) is reduced and eluted with 0.35 M HNO<sub>3</sub> / 0.02 M HN<sub>2</sub>OH-HCl solutions. At the beginning of purification, Pu(IV) is observed as a green band at the top of the column. After reducing to Pu(III) and giving eluant, the movement of a blue band can be observed. For the removal of organic contamination, the Pu(III) solution is evaporated in concentrated HClO<sub>4</sub> solution until the volume is reduced to one third of the original volume and subsequently is diluted in 5 ml of 1 M HClO<sub>4</sub>. The aliquot of the obtained pink solution is analytically investigated using  $\alpha$ - and  $\gamma$ -spectrometry. The results are listed in Table 4.1. After the purification, the amount of americium is considerably reduced, therefore <sup>242</sup>Pu is about 99.4% by mass balance and the amount of americium can be neglected. The activity of <sup>242</sup>Pu is about 75.6% of the total activity, and this factor is taken into account for the determination of the total plutonium concentration with the LSC measurements.

The prepared Pu solution can contain four different oxidation states of plutonium as well as colloids, which can be Pu(IV) colloids or contaminant colloids. Pu(IV) stock solutions are prepared by electrolysis at constant potential as described by Cohen [Cohé 61]. The schematic diagram of the electrolysis is shown in Fig 4.3. The electrolysis cell is separated into three parts with glass diaphragms, and the Pu solution is oxidized or reduced in the right cell which contains a working electrode (Pt). The other separated cells contain the counter electrode (Pt wire) and the reference electrode (Ag/AgCl), in 1 M HClO<sub>4</sub> or 0.5 M HCl, respectively. The constant potential is given from the coupled potentiostat. During electrolysis, the current is varied.

Table 4.1 Isotope distribution after the purification of Pu solution using  $\alpha$ - and  $\gamma$ -spectrometry.

Nuclide	Half life time, $t_{1/2}$ [year]	Activity [%]	Concentration [M]	Concentration [%]
<sup>242</sup> Pu	$3.75 \cdot 10^5$ a	75.6	$8.61 \cdot 10^{-4}$	99.39
<sup>239/240</sup> Pu	$2.411 \cdot 10^4 / 6563$ a	7.0	$5.22 \cdot 10^{-6}$	0.604
<sup>238</sup> Pu	87.74 a	17.2	$4.59 \cdot 10^{-8}$	$5.3 \cdot 10^{-3}$
<sup>241</sup> Am	432.2 a	0.2	$2.61 \cdot 10^{-9}$	$3.0 \cdot 10^{-4}$



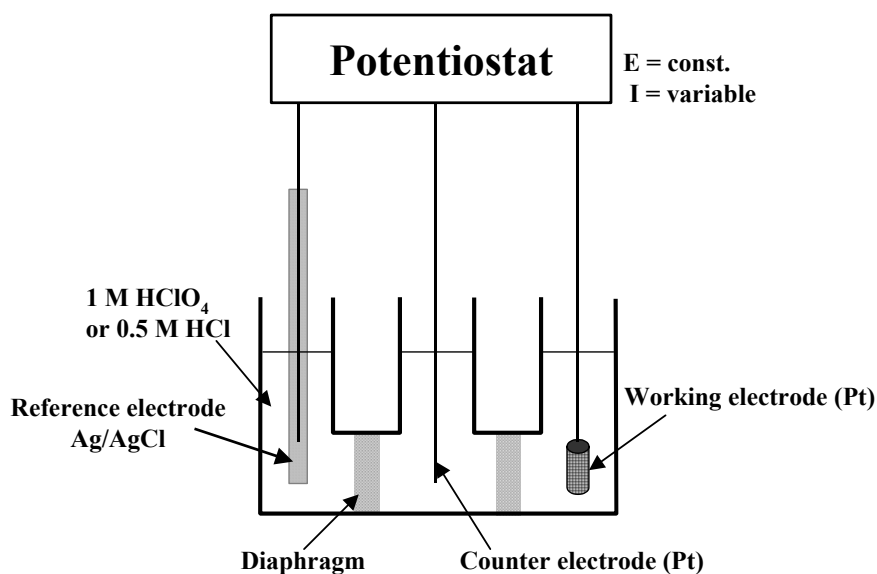


Fig. 4.3 The set-up of electrolysis for the preparation of Pu(IV) stock solutions.

The Pu(IV) solution is prepared through the oxidation of Pu(III). Therefore, at first, the mixture of different Pu oxidation states in 1M HClO<sub>4</sub> or 0.5M HCl is reduced to Pu(III) ( $E_{\text{cathode}} = \text{ca. } -0.2 \text{ V}$ ) and subsequently oxidized to Pu(IV) ( $E_{\text{anode}} = \text{ca. } 0.8$ ). For better reaction condition by mixing the Pu solution in the working cell, the Pu solution is bubbled with argon gas during the electrolysis. The oxidation states of the Pu solution are measured before and after electrolysis using a diode-array spectrometer to ascertain the process of redox reactions.

After the electrolysis, the Pu(IV) stock solution is filtered through a cellulose membrane microfilter (Amicon, 10 kDalton: pore size about 1.5 nm) to remove latent colloids. After filtration, the filtrate is tested using LIBD, whether the colloids are separated from solution or not, and is measured by UV-Vis absorption spectrometry to determine the distribution of oxidation states.

#### 4.2.2 Dilution with 0.5M (H/Na)Cl solution

For the investigation of Pu solubility, the same approach is applied as in the case of Zr. LIBD is used to detect colloids with increasing pH at constant Pu concentration. Due to its redox sensitivity, however, the coulometric titration cannot be applied for pH titration. The coulometric pH titration causes the reduction of Pu(IV) to Pu(III) (See Appendix 8.3). Therefore, batch samples are prepared by slow dilution with colloidal free 0.5M (H/Na)Cl. The colloid free 0.5 M HCl and NaCl solutions are prepared by the same methods as for Zr experiments. Dilution of an acidic plutonium solution with neutral solution (e.g. water)

will frequently cause polymerization in localized areas of low acidity, even when the final acidity of the solution is too high for polymerization to occur. Moreover, when Pu(IV) colloids are once formed, they might be stable for days or weeks [Clev 79]. For this reason, 0.5M (H/Na)Cl solution for the dilution is added very slowly in 10  $\mu$ l per minute under stirring to prevent the localized oversaturation. All samples depicted in Fig. 4.4 are prepared in quartz cells (Hellma) except series 4 (in Teflon PFA vials).

Most experiments are carried out in air except for series 2 which is carefully carried out under argon atmosphere (see below). The total Pu concentrations are determined by LSC. The Pu concentrations of stock solutions are in the range from  $1 \cdot 10^{-3}$  to  $4 \cdot 10^{-3}$  M in 1 M HClO<sub>4</sub> or 0.5 M HCl. These stock solutions are diluted to concentration ranges between  $1 \cdot 10^{-5}$  and  $3 \cdot 10^{-4}$  M at acidities between pH 0.3 and 2.1. To determine the concentration of each oxidation state, spectra of the concentrated solutions (series 1 to 3) are measured by Cary 5E with 1 or 2 cm quartz cell (Hellma) and the others (series 4 and 5) are measured using the LCW coupled with a diode-array spectrometer. To determine the concentration below the detection limit of absorption spectroscopy, especially for Pu(V) having low molar absorption coefficients, the CE coupled with ICP-MS is applied.

For the experiments without oxygen (series 2 in Fig. 4.4), all processes are carefully carried out in an Ar-glove box ( $O_2 < 20$  ppm). The electrolysis of the Pu(IV) stock solution is carried out in a glove box bubbling with Ar gas. The filter is washed several times with oxygen free 0.5 M HCl before the filtration to remove colloid contaminations. Then filtration is performed also under argon atmosphere. For the dilution of the stock solution, the two solutions 0.5 M NaCl and HCl are bubbled with argon gas for several hours in a glove box and then measured using LIBD to confirm that external colloids are not introduced during Ar-bubbling. All samples are diluted in closed quartz cells (Hellma) and taken out of the glove box only for short periods of time to measure the UV-Vis absorption and LIBD.

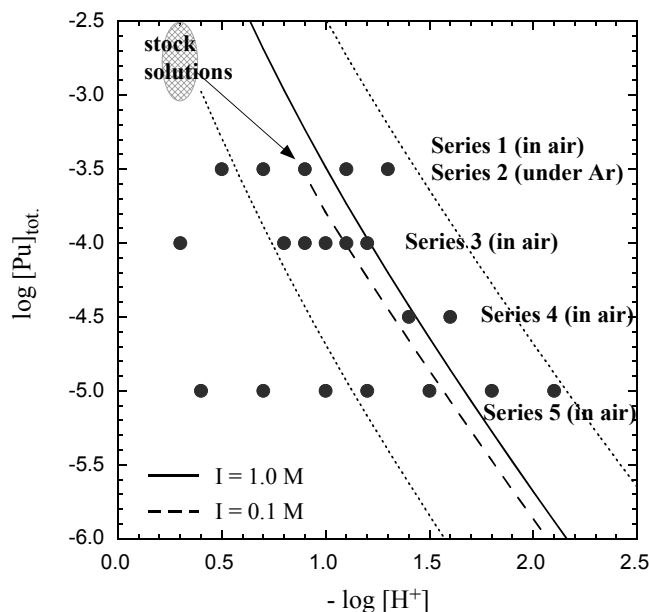


Fig. 4.4 From stock solutions (in 0.5 M HCl or 1 M HClO<sub>4</sub>), plutonium samples are very slowly prepared by dilution with 0.5 M (H/Na)Cl solution. Most experiments are carried out in air condition except for series 2 which is carefully carried out under argon atmosphere (see text).

### 4.2.3 pH and Eh measurements

The pH values in 0.5 M NaCl solution are measured in small aliquots of the samples (250  $\mu$ l) with a combination glass electrode (Ross electrode, Orion Co.) calibrated against pH buffers (pH 1 - 3, Merck) and standard solutions 0.5M HCl/NaCl covering the range of pH values in the experiments (pH 0.3 – pH 2, namely 0.5M HCl – 0.01M HCl/0.49 M NaCl). The relation between  $[H^+]$  and measured  $pH_{exp}$  is given by

$$-\log [H^+] = pH_{exp} + A, \quad (4.2)$$

where  $A = \log \gamma_{H^+} + \Delta pH = 0.00 \pm 0.02$ .  $\gamma_{H^+}$  is the activity coefficient of the  $H^+$  ion and the term  $\Delta pH$  results from the variation of the liquid junction potential when measuring diluted pH buffer solutions for calibration and 0.5M NaCl test solutions [Neck 2002].

Redox potentials are measured with the combined electrodes of two half-cells, which are a micro-Ag/AgCl electrode (Kurt-Schwabe-Institut für Meß- u. Sensortechnik, Germany) and a home-made micro-Pt electrode (Pt wire covered with glass). The micro-electrode is 1.5 mm in diameter and has a ceramic dia-

phragm. The micro-Ag/AgCl electrode is filled with saturated KCl solution. The combined electrodes are calibrated with a redox-buffer (640mV).

The measured redox potentials are subsequently converted to electron activity in order to represent both chemical and electrochemical reactions by equilibrium constants. The negative logarithm of electron activity ( $-\log a_e = pe$ ) at 25°C is related to the redox potential (Eh (V)) by  $pe = 16.9 Eh$  (Eq. (2.9)).

To protect samples against external colloidal contamination by leaching from the pH or Eh electrodes during measurements, each measurement is not carried out directly in the sample cell but separately in a small vial (about 0.5ml volume) with a sample volume of only 250  $\mu$ l.

## 5 Results and Discussions I – Zirconium

### 5.1 Solubility of Zr(IV) using coulometric pH titration and LIBD

The pure solutions (background) are investigated using LIBD prior to preparing zirconium samples. In Fig. 5.1, LIBD results of 0.5 M HCl and 0.5 M NaCl solutions are compared to MQ water (18 M $\Omega$  cm) whose threshold energy  $E_T$  [mJ] is relatively high (2.0 mJ) and which is assumed to contain no colloids or at least only small colloids below 5 nm, the detection limit of LIBD. The s-curve of 0.5 M HCl is similar to that of MQ water. That means the colloidal contaminations are relative well separated from the HCl solution by ultrafiltration. The s-curve of 0.5 M NaCl solution shows a little steeper slope than that of MQ water, but the threshold energies,  $E_T$  [mJ], are about 1.7 mJ which is still much higher than the  $E_T$  of 20 nm polystyrene particles (about 0.5 mJ, see Fig. 3.13) and similar to that of MQ water. As a consequence, 0.5 M NaCl contains more colloids than MQ water, but their size can be negligible small.

The LIBD measurement for the concentrated Zr stock solution is also shown in Fig. 5.1. The concentration of Zr stock solution is  $5.2 \cdot 10^{-3}$  M in 0.5 M HCl after ultrafiltration (with about 1 nm pore size). The s-curve is similar to those of MQ water and 0.5 M HCl, thus the stock solution contains almost no colloids as is the case for the pure chemicals. From this Zr stock solution, 13 diluted starting solutions for coulometric titration are prepared in the range of the solubility data by Kovalenko (see Fig. 4.1). These 13 starting solutions are also investigated using LIBD and they have no colloids to be detected by LIBD.

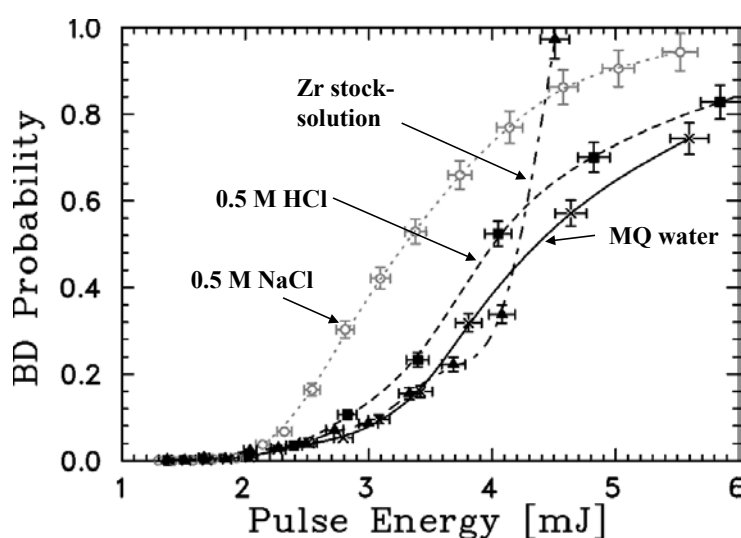


Fig. 5.1 LIBD measurements of Zr stock solution ( $[Zr] = 5 \cdot 10^{-3}$  M in 0.5 M HCl) and 0.5 M HCl and NaCl used for preparing each starting solution.

In Fig. 5.2, the LIBD measurements of the series 2 are shown exemplarily. The starting solution for coulometric titration is prepared by diluting five times with 0.5 M NaCl from stock solution (concentration  $1.07 \cdot 10^{-3}$  M, pH 1.0) and its *s*-curve resembles one of the 0.5 M NaCl solution (see sample **d** in Fig. 5.2). Continuously, the pH is increased using coulometric titration and the LIBD measurement is conducted at each 0.1 pH unit. All *s*-curves from pH 1.0 to pH 2.9 are similar to 0.5 M NaCl solution or show a little lower BDP than the NaCl solution. It means that these Zr solutions contain no larger and no more colloids than colloidal contaminations already present in the NaCl solution. Only three of them (at pH 1.0, pH 2.0 and pH 2.8) are shown in Fig. 5.2, which are also investigated by XAFS (see Section 5.2).

At pH 3.0, many breakdown events occur at low energy and the  $E_T$  of the *s*-curve is shifted to below 0.4 mJ and at pH 3.1, the *s*-curve becomes steeper, which means that colloids are formed at pH 3.0 and grow up with increasing pH. The formation of colloids indicates that the metal concentration in solution exceeds its solubility limit. Therefore, we can determine the solubility limit for  $1.07 \cdot 10^{-3}$  M zirconium at pH 3.0 (with regard to amorphous  $Zr(OH)_4$ , see below). By the same procedure as above, the solubility limits for 13 different concentrations of Zr are determined (see Fig. 5.6) and the lowest pH of solution at which colloids form, “onset of colloid formation” are listed in Table 8.2 (Appendix 8.2).

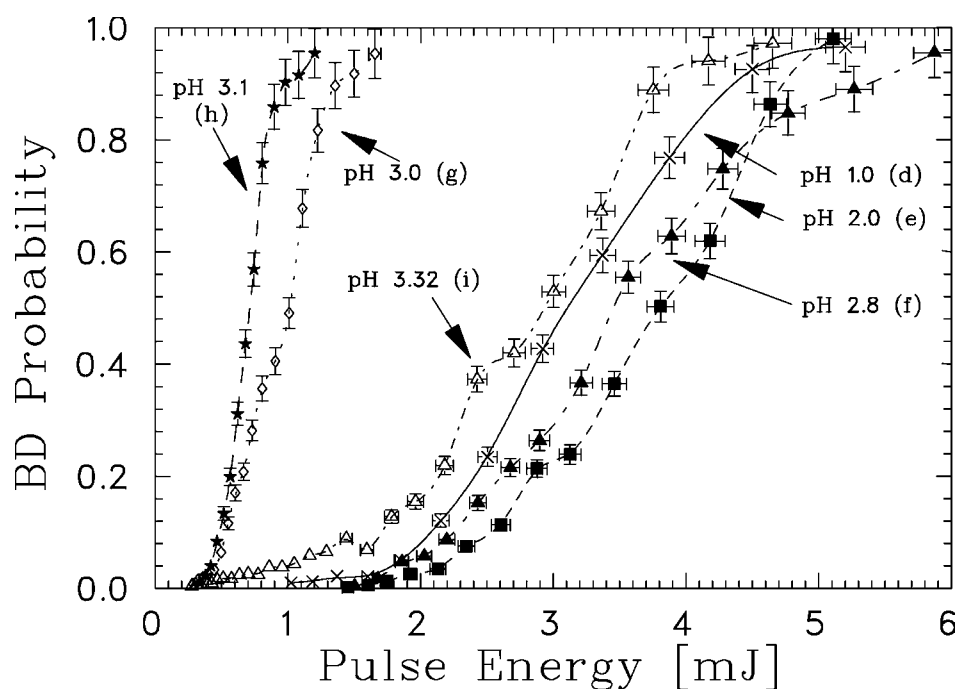


Fig. 5.2 LIBD measurements of titration series 2 ( $[Zr]=1.07 \cdot 10^{-3}$  M). Samples **d**, **e**, and **f** below pH 3 are colloid free (high threshold of the *s*-curves), whereas the breakdown thresholds of samples **g**, **h**, and **i** are shifted toward lower pulse energy, due to the presence of colloids (for size distributions see Fig. 5.4).

When the pH is continuously increased after the onset of colloid formation, we observe a decrease of BDP at a certain pH (e.g. sample **i** at pH 3.3 in Fig. 5.2). This could be interpreted as disappearance of colloids in solution due to precipitation which results from the instability of Zr intrinsic colloids or alternatively due to the dissolution of colloids which formed prematurely due to local oversaturation. To clarify this phenomenon, the s-curve investigation is applied.

The s-curve investigation has a great advantage compared to the measurements of BDP at one laser energy. The latter is a simple LIBD method to determine the onset of colloid formation as a function of pH and it requires very short time for measurement. This method was successfully applied to investigate the solubility of Th(IV) combining with 2-D distribution of breakdown events measured by CCD camera system [Bund 2000; Neck 2003].

However, the measurements of BDP at only one laser energy without the investigation of spectral distribution of breakdown events are problematic due to the agglomeration of formed Zr(IV)-colloids. Fig. 5.3 shows the BDP (as examples, series 2 and 10) at certain laser energy (1.5 mJ, 75 % of  $E_T$  for MQ water) as a function of pH. This results show that the BDP suddenly increases up to almost 1 at a certain pH and then the BDP decreases after the onset of colloid formation although the pH is further increased.

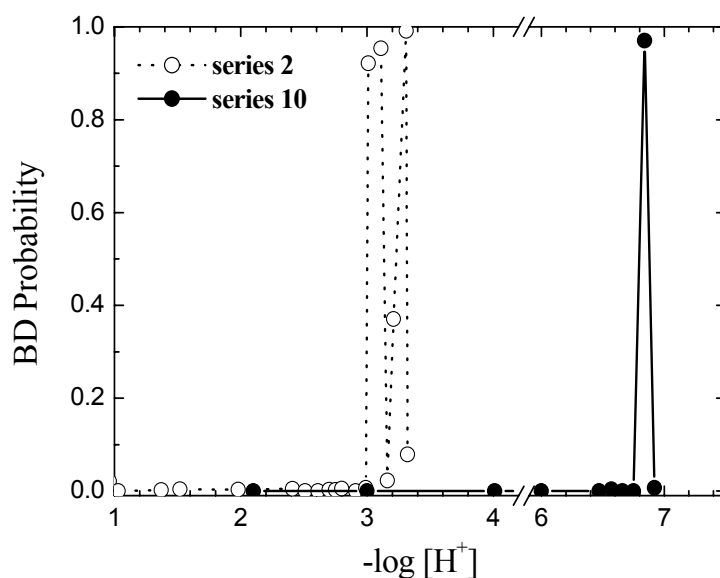


Fig. 5.3 The BDP at the same energy, 1.5mJ which is 75 % of  $E_T$  for MQ water, as a function of pH for two different titration series. One is a concentrated solution ( $\circ$ : series 2,  $[Zr] = 1.07 \cdot 10^{-3}$  M) and the other is a diluted solution ( $\bullet$ : series 10,  $[Zr] = 3.5 \cdot 10^{-7}$  M)

All experimental series show the same phenomenon except only the most diluted sample, series 13,  $[\text{Zr}] = 2.45 \cdot 10^{-8} \text{ M}$ . If the BDP is measured only at one laser energy, then it is difficult to determine whether the first sudden increase of the BDP is due to really exceeding the limit of solubility or only due to instant formation of colloids in the local oversaturation and subsequent dissolving. However, using s-curve investigation we can decide that the decreasing of BDP (the drop of s-curve) is due to growth of Zr(IV)-colloids resulting in precipitation at the end of experiment.

In the present work, the s-curves (BDP as a function of laser pulse energy) at each pH are measured for all series like in Fig. 5.2. As mentioned in Section 3.4.2, we can obtain more detailed information from multimodal evaluation [Walt 2004] of the s-curves, from which the PSD between 20 nm – 1000 nm can be obtained. The fitting results of series 2 (s-curves in Fig. 5.2) are shown in Fig. 5.4. In this figure, the differential particle number density (number of particles in  $\text{cm}^{-3} \text{nm}^{-1}$ ) is plotted against particle size in a log-log plot. Fig. 5.4 shows the sample before the beginning of coulometric titration ((a), sample **d** at pH 1.0), the two samples slightly above the solubility limit ((b), sample **g** and (c), **h**) and the titration end point of series 2 ((d), sample **i**). The colloid content of the starting solution (sample **d**) does not exceed the detection limit (shown as solid line) throughout the size range 20 – 1000 nm and the other two samples at lower pH < 3 (sample **e** and **f**), which have similar s-curves to the first one (sample **d**), have also no significant colloid content (not shown in Fig. 5.4). Fig. 5.4 (b) shows that colloids form spontaneously when the solubility is exceeded (sample **g**). The PSD is of near Pareto-like shape ( $dN_{\text{coll}}/dD [\text{nm}^{-1} \text{cm}^{-3}] \propto D^{-\beta}$ ,  $\beta = 4$ ,  $D$ : colloid diameter), typical for natural colloidal systems. The missing size fraction around 300 nm is an artefact due to poor statistical quality of the LIBD data, which shifts the fraction of colloids that should have been counted in this channel to 100 – 200 nm. When the pH is continuously increased, then more and larger colloids are formed (Fig. 5.4 (c) sample **h** at pH 3.1). The formed Zr-colloids seem to be agglomerated and precipitated with increasing pH. Sample **i** which has an even higher degree of oversaturation than sample **h** should contain more and larger colloids, however, the result shows an apparent lower number of colloids and the colloids smaller than 100 nm are not detected at all probably due to size-screening effects from the larger fraction of particles > 1  $\mu\text{m}$ . These large colloids cause the shoulder in the LIBD s-curve (Fig. 5.2) extending down to low laser pulse energies but as a principle limitation no size information > 1  $\mu\text{m}$  can be obtained. LIBD is well suited to detect colloids down to 5 nm in size and the detection limit in particle number density is only weakly size dependent. However, due to the small detection volume of the laser focal region in LIBD (about 100 pl), particles cannot be detected at concentrations below  $\sim 10^4 \text{ cm}^{-3}$  even if they are very large and easily detected with light scattering.



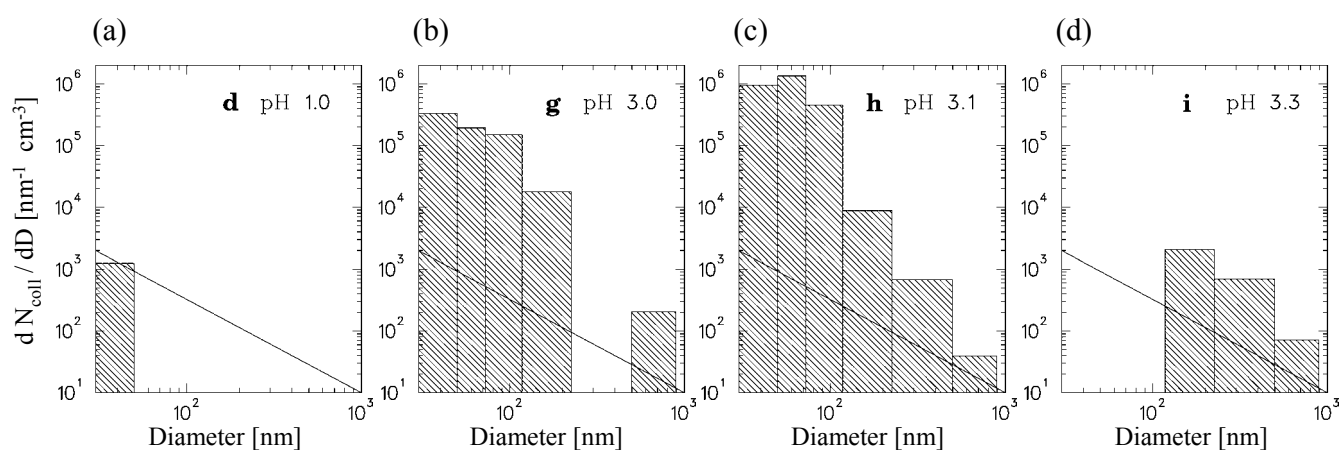


Fig. 5.4 PSD (number density as function of size) of titration series 2 ( $[Zr]=1.07 \cdot 10^{-3}$  M) obtained from the s-curves of Fig. 5.2. The line depicts the detection limit of LIBD. (a) No colloids are detected in sample **d**. (b) Colloids form spontaneously when the solubility is exceeded (sample **g**). (c) The number of colloids increases in sample **h**. (d) The sample **i** should contain more and larger colloids than sample **h**. However, the large fraction of particles  $> 1 \mu\text{m}$  prevents the simultaneous detection of colloids  $< 100$  nm (size screening).

SPC can detect colloids larger than 50 nm at very low concentrations ( $< 10^4 \text{ cm}^{-3}$ ) [Degu 95; Degu 96a]. In this work, SPC is applied to investigate relatively large particles at such low concentration ( $< 10^4 \text{ cm}^{-3}$ ). Fig. 5.5 shows the PSD obtained from the analysis of LIBD and SPC measurements after the end of pH titration for series 10 at  $[Zr] = 3.5 \cdot 10^{-7}$  M. The coulometric titration experiment for series 10 is carried out until pH 6.9 and then after about 1 week from the end of pH titration, the solution becomes slightly more acidic (to pH 6.5) probably due to the formation of colloids (Eq. (2.18)). As shown in Fig. 5.5, the PSD obtained from two different detection methods complement one another very well. The small colloids are detected using LIBD and the large colloids at low concentrations are successfully investigated using SPC. Combining LIBD and SPC, the characterization of colloids in a wide size range could be well accomplished.

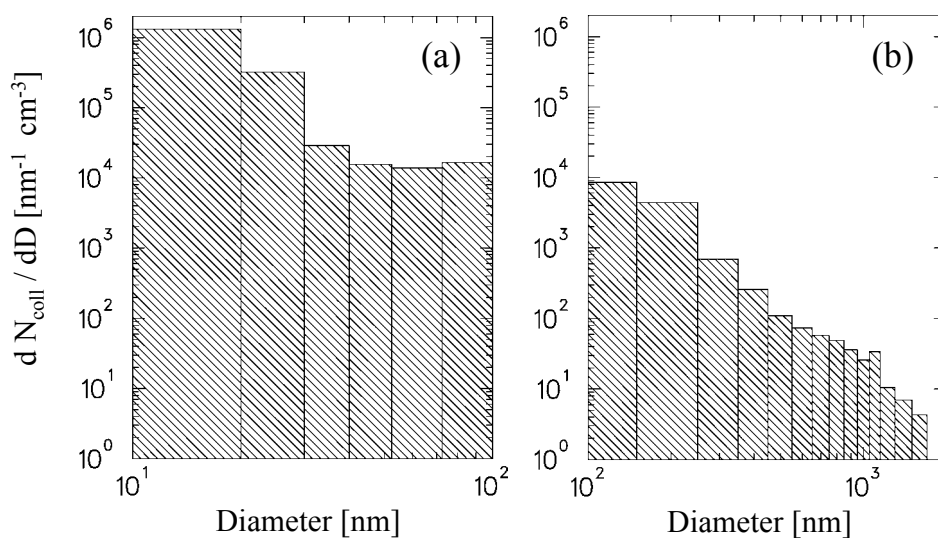


Fig. 5.5 The PSD from (a) LIBD measurement and (b) SPC measurement for series 10, at  $[Zr] = 3.5 \cdot 10^{-7}$  M and pH 6.5.

All measured onsets are illustrated in Fig. 5.6, compared with solubility data from literature (see Section 2.3.2). The present LIBD solubility data ( $\blacktriangle$ ) show a similar result to early data obtained from oversaturation by Bilinski [Bili 66]. The difference of the results can be explained as follows. Titration with NaOH in [Bili 66] probably leads to local oversaturation. Large colloids or even precipitate of Zr were formed before the solubility of Zr was exceeded. This causes the lower solubility than the present results at high Zr concentrations. On the other hand, at low Zr concentrations, the higher solubility results from the sensitivity of the detection method. The tyndallometer used in [Bili 66] (based on the light scattering) is much less sensitive to detect colloids than LIBD. Accordingly, the initial observation of colloid formation / precipitation by light scattering becomes more and more shifted to higher pH values than the present results. Colloids which are large enough to be detected by the tyndallometer are formed not until the solution is strongly oversaturated (at higher pH).

As mentioned in Section 2.3.2, the solubility data can be divided into two groups which differ by several orders of magnitude in Fig. 5.6. A similar effect was observed for solubility studies of Th(IV). The solubility of crystalline or microcrystalline Th(IV) oxide is reported to be  $\log K_{sp}^{\circ} = -52.8$  [Bund 2000] and  $\log K_{sp}^{\circ} = -53.2$  [Neck 2003]. The solubility of the amorphous phase  $Th(OH)_4(am)$  is  $\log K_{sp}^{\circ} = -47.8$  [Neck 2002]. These two solubilities differ by about 5 orders of magnitude. The coulometric titration–LIBD investigation for Th(IV) [Neck 2002] shows that colloid formation occurs immediately and reproducibly when the solubility of  $Th(OH)_4(am)$  is exceeded. In addition, colloid free solutions can be prepared even at Th(IV) and  $H^+$  concentrations above the solubility limit of microcrystalline Th(IV) oxide but below the solubility of  $Th(OH)_4(am)$ .

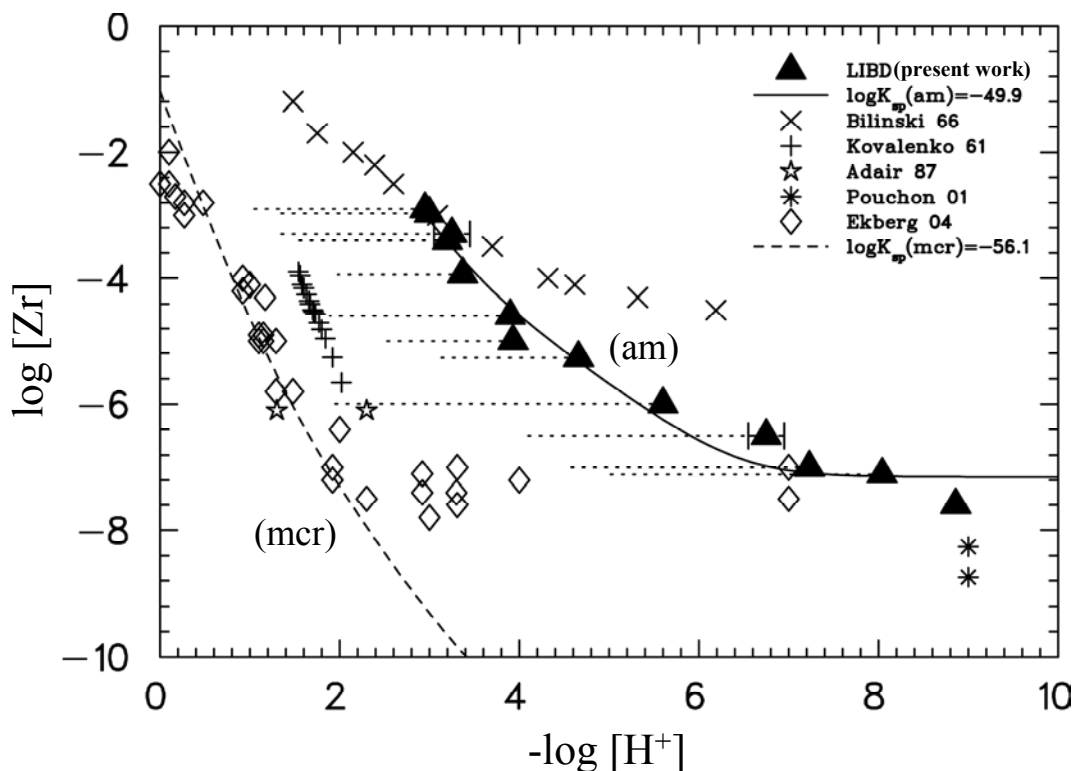


Fig. 5.6 LIBD results for solubility of Zr(IV) and literature data (see Section 2.3.2). Triangles ( $\blacktriangle$ ) depict the onsets of colloid formation determined by LIBD in the present work. The solubility product is obtained to be  $\log K'_{sp} = -49.9 \pm 0.5$  at 0.5 M (H/Na)Cl (see text).

The data at relatively low pH [Kova 61; Ekbe 2004] are obtained by experiments from undersaturation with “Zr(OH)<sub>4</sub>” solid. The authors ascribed their solubility data to Zr(OH)<sub>4</sub>(am) as a solubility limiting solid phase. However, if it is assumed that Zr(IV) exhibits a similar behavior as does Th(IV), the lower solubility data by [Kova 61; Ekbe 2004] do not seem to be related to Zr(OH)<sub>4</sub>(am) (see Fig. 5.6). In the present work, colloid free Zr(IV) solutions can be prepared above the solubility limit reported by [Kova 61; Ekbe 2004]. Therefore the lower solubility data of Zr in Fig. 5.6 might refer to microcrystalline Zr(IV) oxide. The particle size of ZrO<sub>2</sub>(mcr) might be so small that the solid is insensitive to X-ray diffraction (XRD) in [Ekbe 2004]. This Zr(IV) solid can be compared to the microcrystalline ThO<sub>2</sub>(mcr) described in [Neck 2003], showing weak and broad XRD bands and a solubility product which is about 5 orders of magnitude lower than that of “Th(OH)<sub>4</sub>(am)”. These data are in good agreement with the data for monoclinic ZrO<sub>2</sub> by Adair *et al.* [Adai 87].

The other set of solubility data at relatively high pH (the present work and [Bili 66]) can be assigned as the solubility of Zr(OH)<sub>4</sub>(am). The solubility curve (solid line in Fig. 5.6) is obtained with the onset of colloid

formation determined by LIBD and the solubility product of  $\text{Zr}(\text{OH})_4(\text{am})$  is calculated as follows. Under the assumption that the sample contains only mononuclear hydrolysis species, then the solubility product is calculated using Eq. (2.23). The solubility product,  $\log K'_{\text{sp}}$ , is obtained from a least squares fit (Gauss-Newton algorithm) to the LIBD data where the formation constants,  $\log \beta'_{1y}$  ( $y = 1, 2$ ) for  $I = 0.5 \text{ M}$  (listed in Table 2.2) are used as fixed values and  $\log \beta'_{1y}$  ( $y = 3, 4$ ) as fitting parameters in Eq. (2.23):

$$\log K'_{\text{sp}} = -49.9 \pm 0.5 \quad (I = 0.5 \text{ M (H/Na)Cl}). \quad (5.1)$$

$$\log \beta'_{13} = 35.4 \pm 0.36 \text{ and } \log \beta'_{14} = 42.7 \pm 0.27$$

The extrapolation to zero ionic strength using Eq. (2.21) (SIT, see Appendix 8.1) yields

$$\log K^{\circ}_{\text{sp}} = -53.1 \pm 0.5. \quad (5.2)$$

$$\log \beta^{\circ}_{13} = 38.3 \pm 0.36 \text{ and } \log \beta^{\circ}_{14} = 45.9 \pm 0.27$$

The LIBD data ( $\blacktriangle$  in Fig. 5.6) are well reproduced by considering only mononuclear hydrolysis products. However, the formation of polynuclear species commences at the Zr concentration of about  $10^{-4} \text{ M}$  even at high acidity, pH 0 [Conn 51; Ziel 56]. The polynuclear species are most likely present for the concentrations  $[\text{Zr}] > 10^{-5} \text{ M}$  in the pH region of the present experiments and, especially, at certain pH being close to the solubility limit, the polynuclear species can be dominant even at low Zr concentration. Therefore, the description using mononuclear hydrolysis species alone might not be a realistic model over a wide pH range.

In the present work, some series are carried out up to neutral pH and the highest pH value is 9 for series 13. In neutral or basic region, carbonate ions are introduced into solutions from air, and then the solubility can be increased due to the carbonate complexation of Zr. Some studies indicate the formation of strong Zr carbonate complexes [Veyl 2000; Pouc 2001]. Pouchon *et al.* indicates that if the carbonate concentration is lower than 0.01 M, its influence on the hydroxo complex is negligible [Pouc 2001]. Therefore, in the neutral pH region ( $5 < \text{pH} < 9$ ), where the total concentration of dissolved carbonate in solution is still low ( $< 0.01 \text{ M}$ ), the speciation of  $\text{Zr}^{4+}$  is governed not by the formation of carbonate complexes but the formation of hydroxo complexes [Veyl 2000].

The solubility data of  $\text{ZrO}_2(\text{mcr})$  by Ekberg *et al.* ( $\blacklozenge$  in Fig. 5.6) approaches the solubility data of  $\text{Zr}(\text{OH})_4(\text{am})$  ( $\blacktriangle$  in Fig. 5.6) at near neutral pH. This phenomenon is also observed in the solubility investigation for Th(IV) [Moon 89; Neck 2003]. The solubility data of  $\text{ThO}_2(\text{cr})$  do not follow the calculated

solubility curve but approach the values for amorphous precipitates. The solubility data for  $\text{ThO}_2(\text{mcr})$  are obtained at  $\text{pH} < 2.5$ , where the  $\text{Th}^{4+}$  ion is the predominant aqueous species, suggesting that there is no reversible equilibrium between  $\text{ThO}_2(\text{mcr})$  and Th(IV) hydrolysis species. In addition, the precipitation of  $\text{ThO}_2(\text{mcr})$  does not occur in solutions above  $\text{pH} 3$ , where the aqueous speciation of Th(IV) is dominated by hydroxide complexes. For instance, in an aliquot containing small amounts of  $\text{ThO}_2(\text{mcr})$ , the solid particles re-dissolve when  $\text{pH}$  is increased from  $\text{pH} 2.5$  to  $3.0$  by dilution with  $0.5 \text{ M NaCl}$  [Neck 2003]. The final thorium concentration of  $\log [\text{Th}] = -4.24$  considerably exceeds the calculated solubility of  $\text{ThO}_2(\text{cr})$  but remains below that of  $\text{Th}(\text{OH})_4(\text{am})$ .

At low  $\text{pH}$ , the dissolution of  $\text{AnO}_2(\text{cr})$  may lead to an equilibrium with  $\text{An}^{4+}(\text{aq})$ . However, at  $\text{pH}$  above the onset of hydrolysis, the dissolution of  $\text{AnO}_2(\text{cr})$  followed by the very fast hydrolysis reactions of the  $\text{An}^{4+}$  ions might result in an irreversible dissolution reaction until the concentration of the hydroxide complexes  $\text{An}_x(\text{OH})_y^{4x-y}(\text{aq})$  reach the solubility limit of  $\text{An}(\text{OH})_4(\text{am})$  [Neck 2003].

In the case of Zr(IV), however, the onset of hydrolysis is lower  $\text{pH}$  ( $< 1$ ) than that of Th(IV) ( $\approx \text{pH} 3$ ) but nevertheless, the solubility data for  $\text{ZrO}_2(\text{mcr})$  remain on the calculated curve of  $\text{ZrO}_2$  up to  $\text{pH} 3$  which resembles the case of thorium. For example at  $\text{pH} 2$ , the first and second hydroxide complexes are dominant and the free ion  $\text{Zr}^{4+}$  is only a minor species in solution. However, the crystalline Zr oxide is in equilibrium with the Zr hydroxide complexes in solution as the solubility data of Ekberg *et al.* at  $\text{pH} 2$  remains several orders of magnitude lower than solubility data for  $\text{Zr}(\text{OH})_4(\text{am})$ . The solubility data of U(IV) [Park 85; Yaji 95] show a similar phenomenon [Neck 2001a]. The solubility data of  $\text{UO}_2(\text{cr})$  approach the solubility of uranium hydroxide above  $\text{pH} 2$ , though the onset of hydrolysis is lower than  $\text{pH} 1$ . The above explanation for the case of thorium [Neck 2003] seems not to be applicable to other tetravalent metals e.g. Zr(IV) or U(IV).

Most recently, solubility data similar to the present LIBD results were obtained by Sasaki *et al.* [Sasa 2005]<sup>4</sup>. These experiments from oversaturation are carried out with Zr stock solution obtained from two different substances,  $\text{ZrCl}_4$  and  $\text{ZrOCl}_2 \cdot 8\text{H}_2\text{O}$ . The  $\text{pH}$  of solution is increased by addition of  $\text{NaOH}$  solution. The data shown in Fig. 5.7 are taken after 3 weeks equilibration in  $0.5 \text{ M (H/Na)ClO}_4$ . The samples are measured again after 6 months and the concentrations of dissolved Zr do not change. The solubility data do not vary with different sources of Zr and the results are slightly lower than the present LIBD results. A possible reason for the discrepancies is the particle size effect which is successfully applied for the interpretation of the solubility data of  $\text{ThO}_2$  colloids [Bund 2000]. The solubility product of particles  $< 300$

<sup>4</sup> The concentration of zirconium is obtained by ICP-MS. The detection limit is  $10^{-8} \text{ M}$  of  $[\text{Zr}]$  after excluding  $\text{Na}^+$  by extraction chromatography.

nm depends noticeably on the particle size. According to Schindler [Schi 65], smaller particle size results in larger solubility. Thus it can be estimated that the solutions on the solubility limit determined by LIBD contain only very small colloids formed freshly by stacking polynuclear species whereas the precipitated samples contain some large particles by aging and growing of small colloids. This assumption is supported by an ongoing study where the freshly precipitated samples are measured repeatedly as a function of time. Altmaier *et al.* [Altm 2005] determined the solubility from oversaturation: the Zr stock solution at ca. 0.02 M was diluted with NaCl-NaOH ( $I = 0.5$  M) until precipitation occurred and ultrafiltration (10 kD, Amicon) of an aliquot of the liquid phase was repeatedly performed as a function of time. The Zr concentration and pH of the filtrate were measured. The solubility data of samples aged for 7 days (○, in Fig. 5.7) are comparable to the present LIBD results. With aging time, the Zr concentration decreased,  $H^+$  concentration increased and the solubility data (●, in Fig. 5.7) moved towards the data obtained by Sasaki *et al.* From this interpretation, we conclude that the solubility data determined by LIBD relate probably to the upper limit of solubility for  $Zr(OH)_4(am)$ .

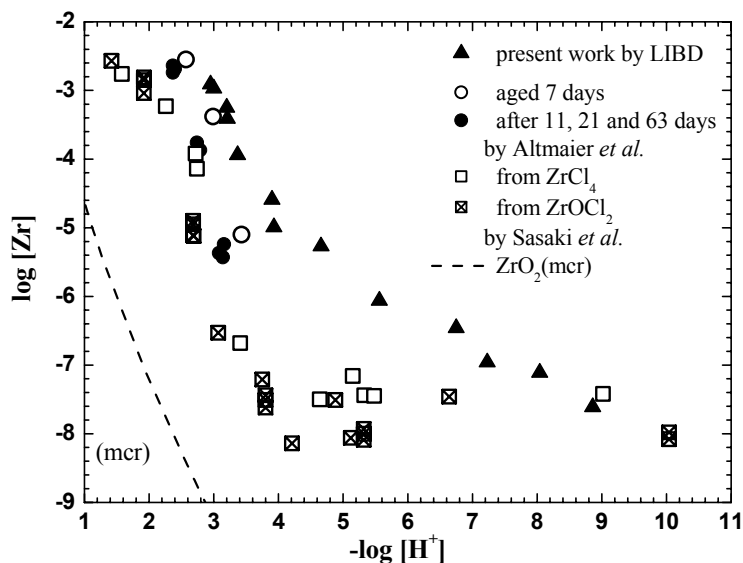


Fig. 5.7 The solubility of  $Zr(OH)_4(am)$ . The symbols indicate the three independent experiments from oversaturation. The present results by LIBD (▲), the solubility data after 3 weeks equilibration with different Zr sources (□ for  $ZrCl_4$  and ⊠ for  $ZrOCl_2 \cdot 8H_2O$ ) by Sasaki *et al.* [Sasa 2005] and the solubility data after 7 days equilibration (○) and 11, 21 and 63 days (●) by Altmaier *et al.* [Altm 2005] are depicted. The dashed line is calculated with  $\log K_{sp}^{\circ} = -59.2$  [Ekbe 2004] and mononuclear hydrolysis constants estimated by applying the ligand repulsion approach [Neck 2000].

## 5.2 Structure of various Zr(IV) species by XAFS

To understand the Zr species at different pH in solution or the mechanism of Zr(IV) colloid formation, the XAFS investigation is in parallel carried out for coulometric titration series 2 ( $[\text{Zr}] = 1.07 \cdot 10^{-3} \text{ M}$ , from pH 1.0 to pH 3.3) [Cho 2005]. The six samples (**d** - **i**) and a more concentrated sample (**a**) examined by XAFS are depicted in Fig. 4.1 and listed in Table 8.3 along with two reference samples **b** (100 nm  $\text{ZrO}_2$  colloids) and **c** (monoclinic  $\text{ZrO}_2$ ).

Comparison of the XANES features in Fig. 5.8 shows that there are slight but significant differences between the various samples. The starting solution **d** exhibits almost structureless absorption feature - the white line (WL). Samples **e** - **i** show a split absorption feature, which broadens with increasing pH (see gray bars in Fig. 5.8). *Li et al.* attributed the splitting and broadening of WL to degenerated energy levels in the valence band, which increase with decreasing Zr absorber site symmetry [Li 93]. The reference colloid sample (**b**) exhibits a similar WL appearance to that of samples **e** - **i**. Note that XANES feature of the concentrated solution at low pH (**a**) does not resemble those of the solution samples **e** - **i** and its appearance is intermediate between monoclinic  $\text{ZrO}_2$  and the starting solution **d**. This is the first indication that the Zr species in this sample **a** is significantly different to the hydrolysis species formed during the coulometric titration. The spectrum for sample **c** is the same as that reported in [Li 93] for monoclinic  $\text{ZrO}_2$ . None of the remaining XANES samples resemble any of the Zr K XANES for the polymorphs of  $\text{ZrO}_2$  shown in [Li 93].

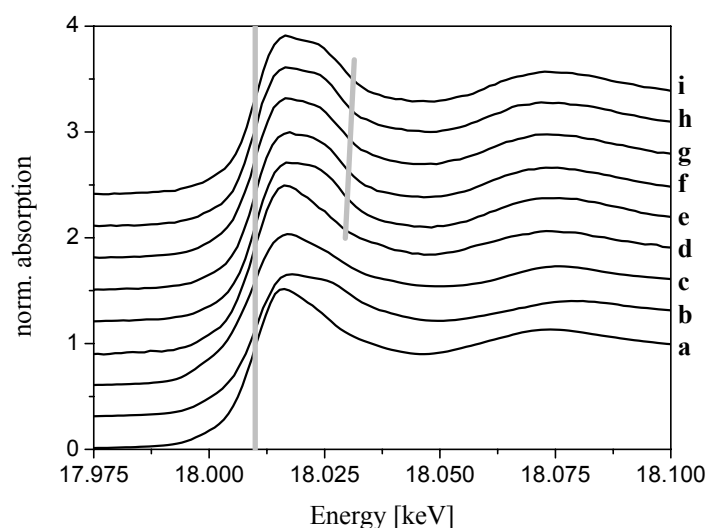


Fig. 5.8 Normalized Zr K-XANES spectra of samples **a** - **i**. See Table 8.3 for sample descriptions. The gray lines connect curve inflection points as a guide for the eye to demonstrate the peak broadening in titration samples **d** - **i**. Spectra have been shifted along the y-axis for clarity.

The Zr K EXAFS and their corresponding FT (Fourier transform) spectra for samples **a** through **c** are shown in Fig. 5.9, those for solutions **d** - **i** in Fig. 5.10. The spectrum of the titration-LIBD starting solution (**d**) exhibits a single sinusoidal EXAFS oscillation whereas those of other samples **e** - **i** show interference patterns resulting from backscattering on two shells. The interference pattern is strong in the spectrum of sample **a**, the concentrated solution at low pH. It indicates that this sample indeed contains a major fraction of the Zr in the form of a “crystalline” component. This supports our hypothesis that Zr(IV) colloids exist as microcrystalline phase of small size at low pH. The FT of the solution at pH 1 (spectrum **d**) is appropriate to be modelled with only two separate oxygen shells. No indication of any Zr–Zr interatomic distance is found. These results indicate that the sample **d** at pH 1 has significant amounts of hydrolyzed, likely monomeric, Zr(IV) species.

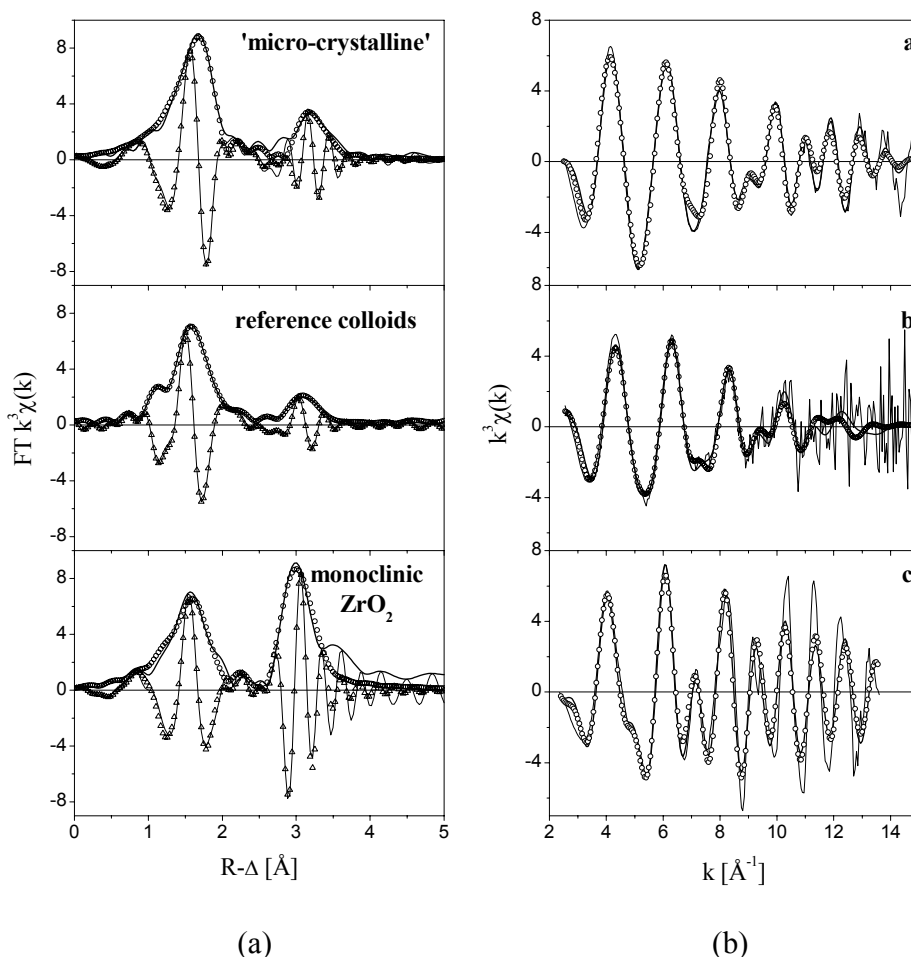


Fig. 5.9 Zr K EXAFS and R-space fit results for reference samples (**a**, **b** and **c**). (a): FT magnitude of EXAFS data (solid line), fit magnitude (open circles), FT imaginary part (thin solid line) and fit imaginary part (open triangles). (b):  $k^3$ -weighted raw data (thin solid line), back-transformed fit (open circles), and corresponding Fourier-filtered data (solid line, ranges given in Table 8.4).



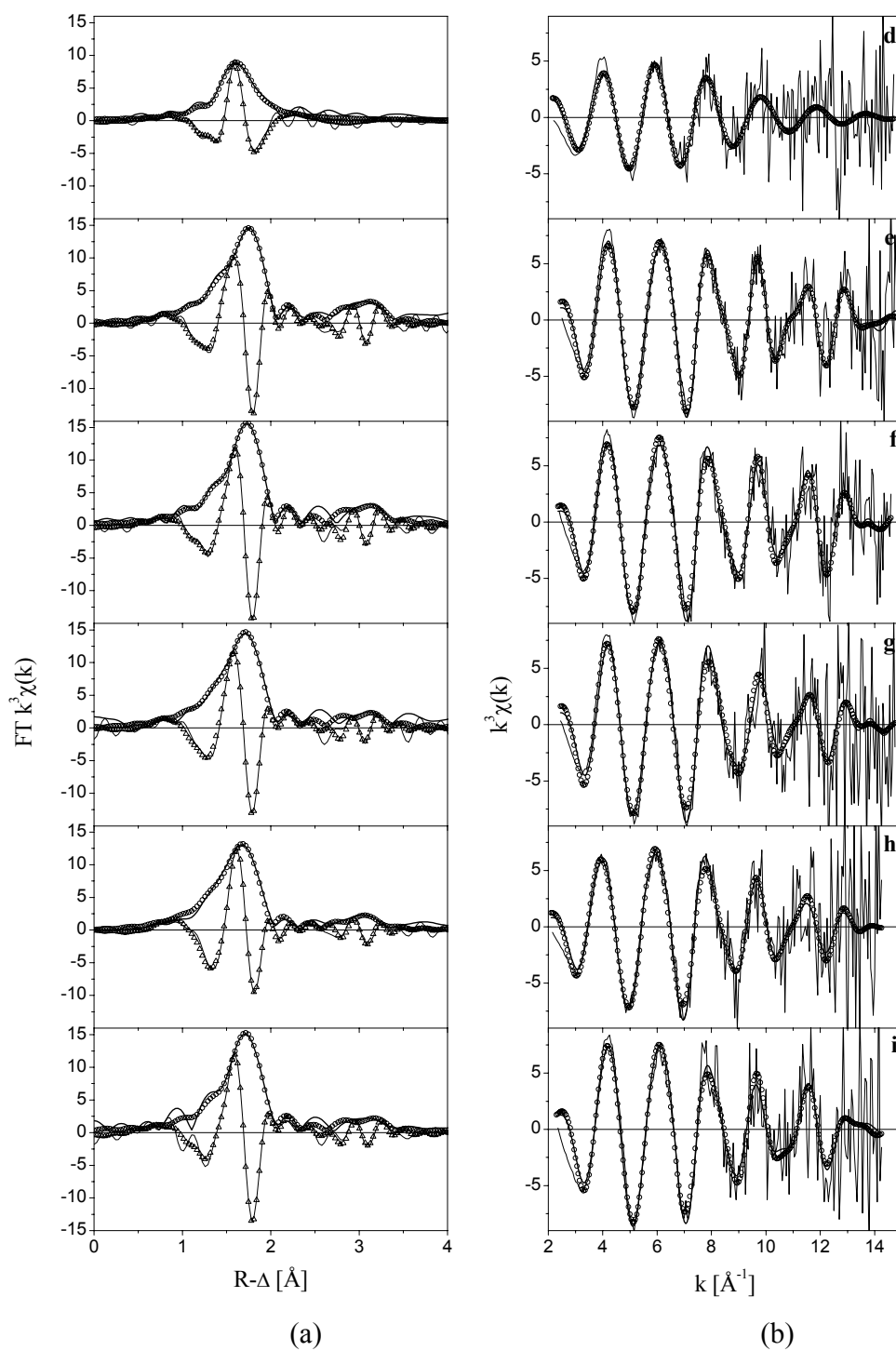


Fig. 5.10 Zr K EXAFS and R-space fit results for coulometric titration samples (**d - i**). (a): FT magnitude of EXAFS data (solid line), fit magnitude (open circles), FT imaginary part (thin solid line) and fit imaginary part (open triangles). (b):  $k^3$ -weighted raw data (thin solid line), back-transformed fit (open circles), and corresponding Fourier-filtered data (solid line, ranges given in Table 8.4).

None of the spectra for samples **e - i** resemble the spectra of other samples (**a - d**). The Zr species in the titration samples **e - i** seem to have a different structure from those in other samples. The XANES spectra discussed above suggest the same. The parameters obtained from fits to the data for samples **e - i** using a two shell (O and Zr) model are listed in Table 8.4. The fit results indicate that the values of N(O) for these samples are large. The R(O) values are invariant of pH (all  $\sim 2.21$  Å). The R(Zr) exhibits more scatter than R(O) values but remains about 3.41 Å.

The R(O) value of 2.21 Å nearly corresponds to the sum of ionic radii for octa-coordinated Zr(IV) [Shan 76], suggesting that N(O) should be eight. However, the values for N appear to be unexpectedly large (see Table 8.4). From the 2.21 Å bond distance and through comparison of amplitudes observed for monoclinic ZrO<sub>2</sub> (**c**), whose N(O) is also greater than the expected value of 7. It is concluded that the N(O) values in Table 8.4 are overestimated. The observed R(Zr) of 3.41 Å for the titration samples (**e - i**) is shorter than that for samples **a - c**, ZrOCl<sub>2</sub>·8H<sub>2</sub>O [Mak 67], orthorhombic ZrO<sub>2</sub> [Ohta 90] and for the cubic<sup>5</sup> and tetragonal forms of ZrO<sub>2</sub> [Teuf 62], and does not match with mean distances in known ZrO<sub>2</sub> polymorphs.

In addition, a mechanism of simply joining tetrameric [Zr<sub>4</sub>(OH)<sub>8</sub>(H<sub>2</sub>O)<sub>16</sub>]<sup>8+</sup> units to form sheet or stacked octamers, which may grow further to form colloids as suggested in the literature for concentrated, acidic Zr(IV) solutions [Muha 60; Sing 96; Sout 2002; Hagf 2004], appears unlikely. If tetrameric units condense to form the colloids, we would observe both an increase in N(Zr) and a longer R(Zr) than obtained in the fits. However, the amplitude of the Zr–Zr interaction does not increase, as would be expected for simple growth of octamers. The observed increase in coordination number over that of monoclinic ZrO<sub>2</sub>, and the value obtained for R(Zr) of 3.41 Å in the titration solutions is in accord with XRD results reported by Zyusin *et al.* for amorphous Zr(IV) precipitates obtained by adding ammonia to zirconium nitrate solutions [Zyuz 2004]. These authors report a comparable Zr–Zr distance of 3.40 Å, but a Zr–O bond length of 2.14 Å (with a coordination number of eight), which is shorter than that observed for the titration samples.

Furthermore, the EXAFS oscillatory pattern for samples **e - i** does not match with published data characteristic of these various individual phases [Li 93] and the Zr species in samples **e - i** seem to be also different from thin films of amorphous ZrO<sub>2</sub> reported in [Wint 2000]. In the present work, the samples **e - i** are not well modeled with just two coordination shells (O and Zr). The metrical parameters obtained in the fits have large uncertainties in the parameters associated with the EXAFS amplitude. In particular, the Zr shell for samples **e - i** does not appear to be modeled well with one distance. The large uncertainties suggest that there may be more than one distance near 3.41 Å in these samples. However, the signal-to-noise ratio in the spectra is not adequate to attempt to model this shell with more than one distance.

---

<sup>5</sup> calculated for the Fm-3m space group; a=5.09 Å

In conclusion, the observed Zr–Zr distance is an evidence that polymeric, oligomeric species, or more condensed colloid species exist in titration samples **e - i**. The structure of these solution species is neither monoclinic, cubic, orthorhombic, nor tetragonal ZrO<sub>2</sub> structure. Its structure also cannot be derived from simple stacking of tetrameric [Zr<sub>4</sub>(OH)<sub>8</sub>(H<sub>8</sub>O)<sub>16</sub>]<sup>8+</sup> units. The Zr–O coordination number of the polynuclear species in the samples **e - i** is likely near eight, and its distance shows little variation. At the same time, the Zr–Zr interaction is relatively small, and this coordination shell is possibly comprised of more than one distance. It can be assumed from these results that the species are built up of primarily ZrO<sub>8</sub> building blocks, but the associated Zr sublattice is highly disordered. The ZrO<sub>8</sub> building blocks can be related polyhedra (idealized polyhedra being cube, square antiprism, dodecahedron and hendecahedron). Zirconium exhibits a great variety of geometric variations in its primary coordination sphere. There is apparently a low energy difference between one geometry over another [Macd 73]. The order in the first O shell and the simultaneous variation in the Zr–Zr interaction may result from the polymerization of ZrO<sub>8</sub> building blocks with different geometries. Their polymerization and packing into a more condensed system would necessarily lead to a disordered and defect-rich Zr sublattice.

## 6 Results and Discussion II – Chemistry of Pu

### 6.1 LIBD investigation of background materials and Pu stock solutions

For the Pu investigation, a laser system different from that for Zr measurements is used (Section 3.4.3). The same kind of laser is applied and the optical setup is also similar to Fig. 3.15. However, different focusing conditions yield a deviation of the power density in the Gaussian focus and hence different threshold energies  $E_T$  [mJ]. The threshold energy for MQ water (18 MΩ cm) is about 1.0 mJ (see Fig. 6.1), which is only half the energy  $E_T$  [mJ] (MQ water) = 2.0 mJ in Fig. 5.1. The calibration curves with polystyrene reference colloids are depicted in Fig. 8.3 (in Appendix 8.5) and can be compared with Fig. 3.13 (for Zr experiment).

Fig. 6.1 shows the s-curves of 0.5 M HCl and 0.5 M NaCl solutions compared to that of MQ water (18 MΩ cm). The two solutions can be assumed to be “colloid free”. For the experiments under exclusion of oxygen, solutions are bubbled with argon gas for several hours. The corresponding s-curves are also shown in Fig. 6.1. There is no introduction of external colloidal contaminations through argon bubbling. The s-curves of the plutonium stock solutions for titration series 1 and 2 (see Fig. 4.4) are shown in Fig. 6.2. The most concentrated solution ( $[Pu] = 4.3 \cdot 10^{-3}$  M) is prepared in 1 M HClO<sub>4</sub> and then 2-fold diluted

with 0.5 M HCl (thus, background materials are 0.5 M HClO<sub>4</sub> and 0.25 M HCl). After electrolysis to Pu(IV), the solution contains only small colloids, therefore the solution is applied for titration series 2 (experiments under argon atmosphere) without further treatment. Other stock solutions in 0.5 M HCl are filtered (10 kDalton, Amicon) and measured by LIBD. After filtration, the solutions contain only small colloids similar to 0.5 M HCl solution.

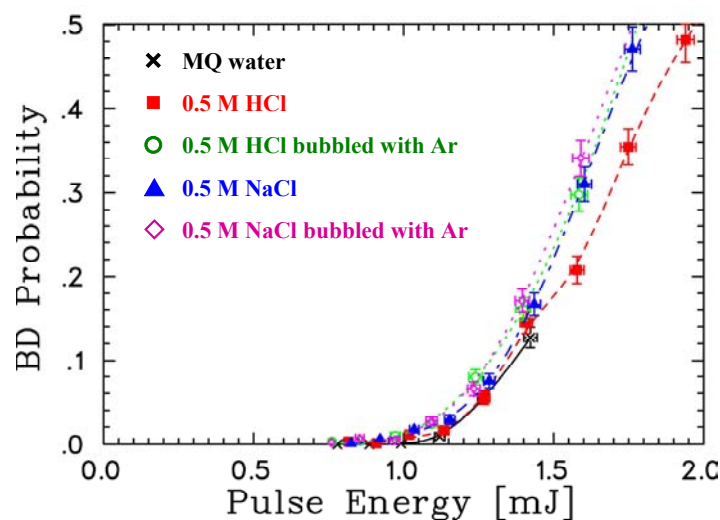


Fig. 6.1 LIBD measurements of background solutions. The threshold energy of MQ water is about 1.0 mJ. 0.5M HCl and 0.5M NaCl solutions are bubbled with argon gas for several hours. Before and after argon bubbling, all solutions are colloid free like as MQ water.

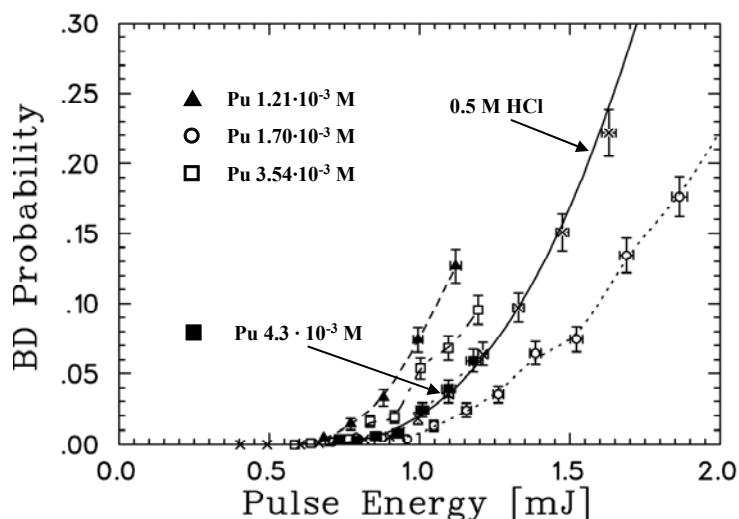


Fig. 6.2 LIBD measurements of Pu(IV) stock solutions are compared to the s-curve of 0.5 M HCl ( $\times$ ). The stock solution of  $4.3 \cdot 10^{-3}$  M in 0.5M HClO<sub>4</sub> + 0.25M HCl ( $\blacksquare$ ) is not filtered. Other stock solutions in 0.5M HCl are investigated with LIBD after filtration (10kD, Amicon).

## 6.2 Solubility of Pu(IV) hydrous oxide in acidic solution

### Formation of Pu(IV) colloids detected by LIBD - Series 3 and 5

At two different Pu(IV) concentrations (series 3 and 5), the onset of colloid formation is determined by LIBD. The s-curves of each series are presented in Fig. 6.3 (a) for series 3 ( $[\text{Pu(IV)}]_{\text{tot.}} = 7.0 \cdot 10^{-5} \text{ M}$ ) and (b) for series 5 ( $[\text{Pu(IV)}]_{\text{tot.}} = 1.0 \cdot 10^{-5} \text{ M}$ ).

#### Series 3, $[\text{Pu(IV)}]_{\text{tot.}} = 7.0 \cdot 10^{-5} \text{ M}$ , $\text{pH} = 0.3 \sim 1.2$

For the series 3 in Fig. 6.3 (a), the blank solution at pH 1.1 ( $\times$ ) and the Pu solution at pH 1.04 ( $\blacksquare$ ) do not deviate significantly from background solutions (compared with Fig. 6.1). The threshold energies of these two solutions,  $E_T$  [mJ] are comparable to that of MQ water ( $E_T = 1 \text{ mJ}$ ). At pH 1.13 ( $\circ$ ),  $E_T$  [mJ] is shifted to lower energy about 0.5 mJ and at the next pH 1.23 ( $\blacktriangle$ ), a similar s-curve is observed. Therefore, the onset of colloid formation is determined at pH 1.13 for a Pu(IV) concentration of  $7.0 \cdot 10^{-5} \text{ M}$ .

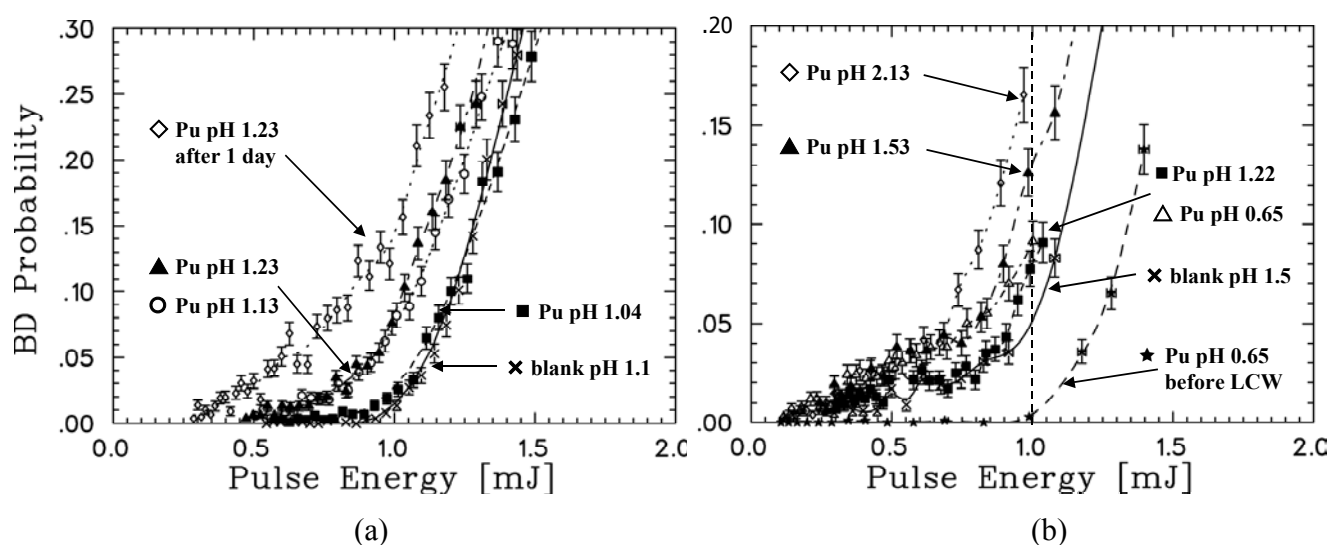


Fig. 6.3 Determination of the onset of colloid formation as function of pH. (a) Series 3,  $[\text{Pu(IV)}]_{\text{tot.}} = 7.0 \cdot 10^{-5} \text{ M}$ . Onset of colloid formation is pH 1.13 ( $[\text{Pu(IV)}]_{\text{coll.}} = 7.05 \cdot 10^{-6} \text{ M}$ , corresponding to 1.7 ppm). After 1 day : larger and more colloids. (b) Series 5,  $[\text{Pu(IV)}]_{\text{tot.}} = 1.0 \cdot 10^{-5} \text{ M}$ . Onset of colloid formation is pH 1.53 ( $[\text{Pu(IV)}]_{\text{coll.}} = 5.45 \cdot 10^{-6} \text{ M}$ ,  $\approx 1.3 \text{ ppm}$ )

In the present work, the colloid concentration at pH 1.13 is determined to  $7.05 \cdot 10^{-6}$  M (about 1.7 ppm) from the balance of the UV-VIS absorption spectrum ( $[\text{Pu(IV)}_{\text{coll}}] = [\text{Pu}]_{\text{tot.(LSC)}} - [\text{Pu(III)}_{\text{aq}}] - [\text{Pu(IV)}_{\text{aq}}] - [\text{Pu(V)}_{\text{aq}}] - [\text{Pu(VI)}_{\text{aq}}]$ ). From the comparison with the s-curve of polystyrene reference particles (cf. Fig. 8.3) a small size of the plutonium colloids ( $\sim 5$  nm) is deduced. Under this assumption, the particle number concentration exceeds  $10^{11} \text{ cm}^{-3}$  (estimated density of Pu colloid  $< 10 \text{ g/cm}^3$ ). While this number density does not suffice for conventional light scattering, detection by LIBD is very well possible. This is in line with result of Triay *et al.* who prepared Pu(IV) colloids with several different processes and determined the size of colloids using autocorrelation photon spectroscopy [Tria 91]. All solutions strongly exceeded the  $\text{Pu(OH)}_4(\text{am})$  solubility limit (cf. Fig. 6.5) ( $[\text{Pu}]_{\text{tot.}} = 3 \text{ mM} \sim 50 \text{ mM}$  at pH 1.3  $\sim$  2.8). They reported that the colloid sizes were mostly small (2 - 6 nm) and the small colloids were stable over 200 days.

### **Series 5, $[\text{Pu(IV)}]_{\text{tot.}} = 1.0 \cdot 10^{-5} \text{ M}$ , pH = 0.3 $\sim$ 2.1**

The LIBD measurements of the series 5 at low Pu concentration ( $[\text{Pu(IV)}]_{\text{tot.}} = 1.0 \cdot 10^{-5} \text{ M}$ ) as a function of pH are shown in Fig. 6.3 (b). The concentrations of Pu oxidation states are determined by absorption spectroscopy by the 100 cm capillary cell coupled with the diode-array spectrometer (LCW-DAS). The threshold energies  $E_T$  [mJ] of all Pu solutions between pH 0.3 and pH 2.1 are shifted to low energy, which means that all samples contain colloids even the undersaturated solutions at low pH. Since intrinsic Pu-colloids should not be stable under these conditions, a colloid contamination might have taken place in the capillary cell.

In order to check the influence of the capillary, a colloid free blank solution is prepared with 0.5 M HCl and NaCl solutions without plutonium. After application of the LCW-DAS, the s-curve of a blank solution at pH 1.5 (✕) is measured. The  $E_T$  [mJ] of the blank solution is shifted to below 0.5 mJ, which proves the presence of colloids. This finding is confirmed by the investigation of the Pu sample at pH 0.65 by LIBD (★, Fig. 6.3 (b)) and after (△, Fig. 6.3 (b)) before applying the LCW-DAS. The former s-curve is similar to the s-curve of MQ water ( $E_T = 1.0$  mJ in Fig. 6.1), but after the UV-Vis absorption measurement by LCW-DAS, the solution contains colloids. Thus it is concluded that some external colloids are introduced into the solution during the absorption measurement using LCW-DAS and cause the shift of the  $E_T$ .

The LIBD results in Fig. 6.3 (b) are compared with the Pu(IV) colloid fraction in Fig. 6.4,  $[\text{Pu(IV)}_{\text{coll}}] = [\text{Pu}]_{\text{tot.(LSC)}} - [\text{Pu(III)}_{\text{aq}}] - [\text{Pu(IV)}_{\text{aq}}] - [\text{Pu(V)}_{\text{aq}}] - [\text{Pu(VI)}_{\text{aq}}]$  obtained from absorption spectra as a function of pH. Fig. 6.4 shows a two step increase of formed Pu colloids. About 20 % of the Pu is present as colloidal species already between pH 0.65 and pH 1.22 increasing to about 45 % at pH  $> 1.53$ . The s-curves in Fig. 6.3 (b) remain similar from pH 0.65 to pH 1.22 (not shown at pH 1.07) and show a low BDP ( $< 0.1$ )

at  $E_T$  of MQ water (see vertical dashed line at 1.0 mJ, Fig. 6.3 (b)). From pH 1.53, the BDP increases with increasing pH at 1.0 mJ. Therefore it is concluded that small amounts of non-absorbing pseudocolloids, oligomers or polymer species form at low pH (between pH 0.65 and pH 1.22), but the solubility of plutonium is not exceeded until pH 1.53 in case of the series 5 ( $[\text{Pu(IV)}]_{\text{tot.}} = 1.0 \cdot 10^{-5} \text{ M}$ ).

The possible presence of polymers below the detection limit of LIBD is well in line with earlier studies. Most studies on the Pu(IV) colloids reported that the size of intrinsic Pu colloids is small. Lloyd *et al.* [Lloy 78] reported that Pu(IV) colloids consist of very small discrete particles, which are less than 2 nm in diameter using electron micrographs. In addition, they also demonstrated that Pu colloids could exist as either amorphous or crystalline particles and amorphous particles invariably convert to crystalline particles with aging. A similar phenomenon was observed for thorium [Rai 2000]. At 90°C and pH 1.5 – 3 in 0.1 M NaCl, an initially amorphous solid was converted into a crystalline phase. Their XRD pattern showed broad bands at diffraction angles expected for bulk  $\text{ThO}_2(\text{cr})$ . Triay *et al.* [Tria 91] reported also the Pu(IV) colloids being small (2 - 6 nm) and stable over 200 days under conditions strongly exceeding the  $\text{Pu(OH)}_4(\text{am})$  solubility limit.

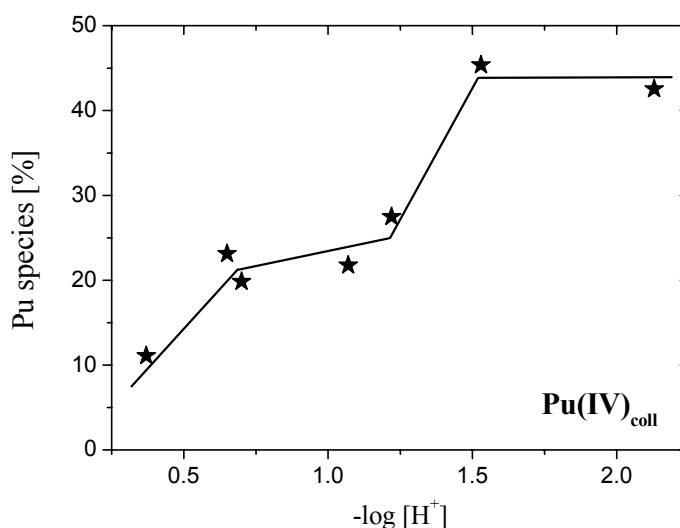


Fig. 6.4 The Pu(IV) colloid/polymer concentration (%) obtained from absorption spectra as a function of pH at  $[\text{Pu(IV)}]_{\text{tot.}} = 1.0 \cdot 10^{-5} \text{ M}$ .

### Spectroscopic study of solubility of Pu(IV) - Series 1 and 4

No sample of the series 1 ( $[\text{Pu}]_{\text{tot.}} = 3 \cdot 10^{-4} \text{ M}$ ) and 4 ( $[\text{Pu}]_{\text{tot.}} = 3 \cdot 10^{-5} \text{ M}$ ) contains colloids large enough to be detected by LIBD ( $> 5 \text{ nm}$ ). The reason might be the competition between the redox reactions of Pu(IV) (for example, reduction to Pu(III)) and the colloid formation of Pu(IV). 10 ml solutions are prepared for each sample of these series, which exceeds the volume used in the remaining series by a factor of 5. In case of the series 1 and 4, for a given concentration the sample contains a higher absolute mass of Pu and hence the ratio of Pu and titrated NaCl per unit time is higher (constant titration rate  $10 \mu\text{l}/\text{min.}$  for all samples of all series). In consequence, the pH changes 5 times more slowly than for series 2, 3 and 5. For example, compare the preparation processes for two samples of 2 ml and 10 ml at the same concentration ( $3 \cdot 10^{-4} \text{ M}$ ) and at the same pH 1.3. 200  $\mu\text{l}$  of Pu stock solution ( $[\text{Pu}]_{\text{tot.}} = 3 \cdot 10^{-3} \text{ M}$  in 0.5 M HCl) is diluted 10 folds in the first case, whereas 1 ml of Pu stock solution is needed in the second. When 0.5 M NaCl solution is added with equal rate ( $10 \mu\text{l}/\text{min.}$ ), the pH increases faster in the 200  $\mu\text{l}$  stock solution than in the 1 ml stock solution. Thus the hydrolysis and the subsequent colloid formation are faster in the 200  $\mu\text{l}$  stock solution. However, the redox reaction is of equal rate in both samples. Therefore, the longer titration time in the 10 ml sample causes a larger fraction of  $\text{Pu}^{4+}$  being reduced to  $\text{Pu}^{3+}$  rather than forming Pu(IV) hydrolysis species and Pu(IV) colloids later on.

The concentrations of Pu(IV) aquatic species and Pu(IV) colloids determined by spectroscopy are summarized in Table 6.1. The samples of the series 4 ( $[\text{Pu}]_{\text{tot.}} = 3 \cdot 10^{-5} \text{ M}$ ) have large fractions of polymeric or small colloidal species. The absorption spectra for the series 4 are measured by LCW-DAS. The Pu colloid formation due to the use of the capillary is prevented by measuring only an aliquot of the sample which is disposed thereafter. Hence, the colloid contamination by the LCW-DAS does not affect the LIBD measurements and no shift of the s-curves is observed as was the case for the series 5 (Fig. 6.3 (b)).

When pH is increased at constant Pu concentration, the amount of Pu(IV) aquatic species has to decrease by colloid formation or redox reaction. The Pu(IV) aquatic species cannot exceed the solubility of Pu(IV) hydrous oxide. In the present investigation, the concentrations of  $\text{Pu(IV)}_{\text{aq}}$  (● blue circles, Fig. 6.5) directly after dilution (fresh sample, not yet equilibrium) decrease as a function of pH until they reach the solubility curve obtained from onsets of colloid formation for the series 3 and 5 determined by LIBD (■ red squares, Fig. 6.5). This behavior agrees with the spectroscopic study of the hydrolysis, colloid formation and solubility of Np(IV) combining LPAS with LIBD carried out by Neck *et al.* [Neck 2001b]. In this investigation, a steep decrease of  $[\text{Np(IV)}_{\text{aq}}]$  as a function of pH is observed along the solubility curve due to Np(IV) colloid formation.



Table 6.1 The concentration of Pu(IV) aquatic species and the Pu(IV) colloids determined by spectroscopy.

	pH	[Pu(IV) <sub>aq</sub> ]	[Pu(IV) <sub>coll</sub> ]
Series 1 log [Pu] <sub>tot.</sub> : ca. -3.5	pH 0.48	$2.79 \cdot 10^{-4}$ M	-
	pH 0.68	$2.58 \cdot 10^{-4}$ M	2.8%
	pH 0.83	$2.16 \cdot 10^{-4}$ M	4.7%
	pH 1.01	$9.55 \cdot 10^{-5}$ M	3.2%
	pH 1.21	$6.49 \cdot 10^{-5}$ M	4.0%
Series 4 log [Pu] <sub>tot.</sub> : ca. -4.5	pH 1.38	$1.96 \cdot 10^{-5}$ M	10.6%
	pH 1.58	$9.96 \cdot 10^{-6}$ M	10.4%
	pH 1.59	$7.43 \cdot 10^{-6}$ M	13.2%

$[\text{Pu(IV)}_{\text{coll}}] = [\text{Pu}]_{\text{tot.}} (\text{measured values by LSC}) - [\text{Pu(III)}_{\text{aq}}] - [\text{Pu(IV)}_{\text{aq}}] - [\text{Pu(V)}_{\text{aq}}] - [\text{Pu(VI)}_{\text{aq}}]$   
 The plutonium species, which have no significant absorption at wavelengths in the UV-Vis region, are considered Pu-polymer or colloids.

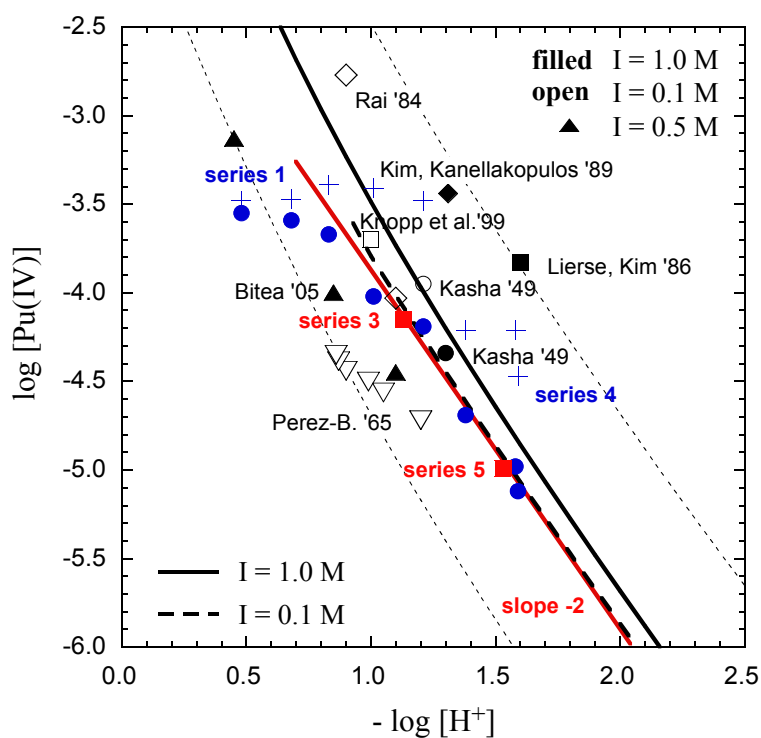


Fig. 6.5 The solubility of Pu(IV) hydroxide obtained in the present work and literature data (see Section 2.3.2). The onset of colloid formation (■) determined by LIBD investigations (series 3 and 5); the concentrations of Pu(IV)<sub>aq</sub> measured using spectroscopy directly after the dilution (●) and corresponding total concentrations (+, [Pu]<sub>tot.</sub>). All data points lie on the red solid line (—, slope -2). The solubility product obtained is  $\log K'_{\text{sp}} = -55.1 \pm 0.4$  (I = 0.5 M (H/Na)Cl) considering only mononuclear hydrolysis species.

The solubility product is calculated from the data under the assumption that there are only mononuclear species present in solution (like in the case of Zirconium)<sup>6</sup>. For the formation of mononuclear hydrolysis species, the corrected formation constants are used for first and second hydrolysis species ( $\text{Pu}(\text{OH})_y^{4-y}$  at  $y = 1$  and  $2$ , listed in Table 6.2) and the formation constants determined from solvent extraction [Meti 72] for third and fourth (listed in Table 2.1). The correction of the first and second hydrolysis constant considering measured Eh(V) values will be explained in detail in Section 6.4.

The solubility product of  $\text{Pu}(\text{OH})_4(\text{am})$  is obtained using Eq. (2.23):

$$\log K'_{\text{sp}} = -55.1 \pm 0.4 \quad (\text{I} = 0.5 \text{ M NaCl/HCl}). \quad (6.1)$$

The extrapolation to zero ionic strength using Eq. (2.21) (SIT, see Appendix 8.1) yields

$$\log K^{\circ}_{\text{sp}} = -58.3 \pm 0.4, \quad (6.2)$$

where the uncertainty originates from errors of the hydrolysis constants.

In literature [Neck 2001a], solubility data of  $\text{Pu}(\text{OH})_4(\text{am})$  or  $\text{PuO}_2 \cdot x\text{H}_2\text{O}(\text{am})$  were reviewed and the authors considered the average of experimental data [Kash 49; Pere 65; Rai 84; Lier 86; Kim 89a; Knop 99; Rai 99] to represent the best value for the solubility product resulting in  $\log K^{\circ}_{\text{sp}} = -58.5 \pm 0.7$ . The solubility curves in Fig. 6.5 are calculated at 1 M ionic strength (black solid line) and 0.1 M (black dashed line) on the basis of the hydrolysis constants from [Meti 72]. The discrepancy between the present result and literature data [Kash 49; Pere 65; Rai 84; Lier 86; Kim 89a; Knop 99] is discussed.

The experiments from undersaturation by Perez-Bustamante [Pere 65] ( $\nabla$ , Fig. 6.5) show lower solubility in acidic solution (in perchlorate medium) probably due to insufficient equilibration time (60 hours). Since the reactions of Pu are faster at higher pH (see Section 6.3), the lack of equilibration time is most pronounced at low pH and results in the strongest deviations. In addition, the author assumed that all dissolved Pu was Pu(IV) and he determined the solubility product without the exact knowledge of the Pu oxidation state distribution in solution. Accordingly, the apparent solubility increased from pH 1.5 to 3.5 due to the increasing fraction of the other oxidation states of Pu in solutions (not shown in Fig. 6.5). For the same reason, the solubility data obtained by Lierse *et al.* was also relatively high ( $\blacksquare$ , Fig. 6.5) [Lier 86].

Rai *et al.* [Rai 84] carried out undersaturation experiments (Fig. 6.5 ( $\diamond$ )) with solid hydroxide precipitate,  $\text{Pu}(\text{OH})_4$ , dissolved in  $\text{HNO}_3$  and continuously shaken for 83 days to reach a steady state and assumed that Pu(IV) hydrous oxide stayed amorphous during the experimental period based on their early investigation

<sup>6</sup> for the validity of this assumption see Chapter 7

of Pu(IV) hydrous oxide solid [Rai 80]. Redox potential, pH, total Pu concentration, and the Pu oxidation state distributions of the filtered solution were measured by solvent extraction and, where applicable, spectroscopy. The small overestimation of the solubility could be due to the assumption that only the first hydrolysis species of  $\text{Pu}^{4+}$  was dominant under the experimental conditions (pH 1.0 and pH 1.2) and the hydrolysis constant at high ionic strengths was applied to solutions of  $I < 0.1$  M [Rai 84]. The data of Kasha (in perchlorate medium) [Kash 49] is comparable to those of [Rai 84], even though Kasha reported some colloid formation prior to the end of the experiment and assumed (incorrectly) that no hydrolysis of Pu(IV) had occurred.

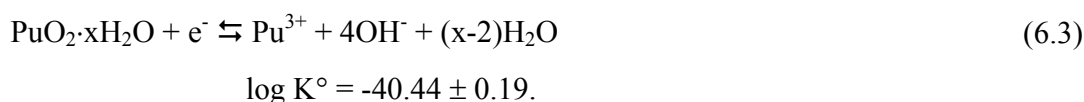
Kim and Kanellakopulos [Kim 89a] reported solubility of  $\text{Pu}(\text{OH})_4(\text{am})$  in 1 M (H/Na)ClO<sub>4</sub> from undersaturation (◆ in Fig. 6.5). The  $\text{Pu}(\text{IV})_{\text{aq}}$  concentration was measured directly by spectrophotometry in equilibrium with a solid phase  $\text{Pu}(\text{OH})_4(\text{am})$  but the measurement was not precise because of the interference with the Pu(IV) polymer and the very high fraction of colloidal Pu(IV) (80%) between pH 1.09 and pH 3.68. The  $\text{Pu}(\text{IV})_{\text{aq}}$  concentrations were not high enough to be detected by spectroscopy. The authors concluded that only the measurement obtained at 1 M acidity could be used to calculate the solubility product and only an upper limit of the solubility product at pH= 1.09 could be estimated.

According to the filtration and LIBD experiments of Knopp *et al.* [Knop 99], the greatest part of colloidal Pu(IV) is removed by filtration at filter pore sizes of about 1 nm. The error in evaluating  $\log K_{\text{sp}}$  from solubility data possibly results from a certain amount of colloids but does not exceed the range of other uncertainties (e.g. different crystallinities of solids). Knopp *et al.* calculated a mean value of  $K_{\text{sp}}^{\circ} = -58.7 \pm 0.9$  from the available solubility data at  $I = 0.06 - 1$  M and pH 0- 12 based on the hydrolysis constants of Metivier and Guillaumont [Meti 72].

The solubility data determined in the present work is in good agreement with the selected value  $\log K_{\text{sp}}^{\circ} = -58.33 \pm 0.52$  in a recent review [Guil 2003]. The solubility product is an unweighted mean value based on the experimental data by [Capd 98; Knop 99; Fuji 2001; Rai 2002] who used three different, independent methods.

Capdevila and Vitorge [Capd 98] used a non-conventional method for the investigation of solubility. They started with 95% Pu(V) solutions at  $[\text{Pu}]_{\text{tot.}} = 1.6$  mM and different ionic strengths (0.1, 0.5, 1, 2 and 3 M) in (H/Na)ClO<sub>4</sub> whose pH<sub>c</sub> were about 1. Concentrations of  $\text{Pu}(\text{III})_{\text{aq}}$ ,  $\text{Pu}(\text{V})_{\text{aq}}$  and  $\text{Pu}(\text{VI})_{\text{aq}}$  as a function of time were determined by spectroscopy. The concentration of the  $\text{Pu}^{4+}$  ion was calculated using the concentrations of other oxidation states and the known redox potential, which is independent of the hydrolysis of that ion. They obtained the solubility product as  $\log K_{\text{sp}}^{\circ} = -58.3 \pm 0.5$ , which is in qualitative agreement with the present work. Fujiwara *et al.* [Fuji 2001; Fuji 2002] measured the solubility of Pu(IV) hydrous

oxide under reducing conditions ( $\text{Na}_2\text{S}_2\text{O}_4$  as reductant) in perchlorate medium under Ar atmosphere (below 0.5 ppm of  $\text{O}_2$ ). The pH value was adjusted with  $\text{HClO}_4$  or  $\text{NaOH}$  in the range pH 4 – 9 for oversaturation experiments and in the range pH 3.4 – 4 for undersaturation experiments. At a steady state, pH and Eh were measured, the concentration of Pu ( $^{239}\text{Pu} > 99\%$ ) in the filtrate was obtained by  $\alpha$ -spectrometry and speciation was performed by use of an UV-Vis spectrophotometer. Only the  $\text{Pu}^{3+}$  species was observed in the sample solutions below pH 6, while above pH 6, no meaningful absorption bands were observed because of the low solubility of Pu(IV). The data refer to the reaction:



Combining this result with the redox potentials selected in [Lemi 2001] for the couple  $\text{Pu}^{4+}/\text{Pu}^{3+}$  ( $\log K^\circ = -17.74 \pm 0.051$ , for oxidation of  $\text{Pu}^{3+}$ ) leads to a solubility product of  $\log K^\circ_{\text{sp}} = -58.18 \pm 0.25$ .

Rai *et al.* [Rai 2002] carried out similar experiments under controlled reducing conditions ( $\text{FeCl}_2$  or hydroquinone as reductant) in NaCl solutions at low ionic strength ( $< 0.025$  M). They obtained the equilibrium constant of reaction (6.3) of  $\log K^\circ = -40.5 \pm 0.7$ . The calculated  $\log K^\circ_{\text{sp}} = -58.24 \pm 0.97$  for  $\text{Pu}(\text{OH})_4(\text{am})$  is nearly the same as that given by Fujiwara *et al.* [Fuji 2001; Fuji 2002].

Bitea reported the solubility product of  $\log K^\circ_{\text{sp}} = -59.26 \pm 0.30$  [Bite 2005]. This study is similar to the present work, as Pu solutions at five different total Pu concentrations in 0.5M NaCl were investigated by LIBD and UV-Vis absorption spectroscopy. However, only the three data points at high concentration ( $\blacktriangle$ , in Fig. 6.5) are reliable because  $[\text{Pu}(\text{IV})]_{\text{tot}}$  in solution could not be determined for the lower concentrations by conventional spectroscopic methods. The solubility data are slightly lower than the present results, probably because of the pre-existence of small colloids in the used stock solutions. These small colloids could act as seeds to form colloids even though the solution is still undersaturated.

### 6.3 Redox reactions of plutonium in acidic solution

For many decades, the redox behavior of plutonium in acidic solution has been explained using the disproportionation reactions (2.27) or (2.28) discussed in Section 2.2.4 [Rabi 53; Cost 73; Capd 92]. However, when the oxidation state distribution is measured as a function of time [Cost 73; Toth 90], deviations from the stepwise disproportionation according to (2.25) and (2.26) are observed.

In the present work, the oxidation state distributions at different Pu concentrations and pH are investigated as a function of time using spectroscopy.  $^{242}\text{Pu}$  (> 99 % weight concentration) is used to minimize the influence of radiolysis on the establishment of a steady state. All samples contain mainly Pu(IV) (> 95%) at the beginning of the measurement. The concentration of  $\text{Pu(IV)}_{\text{aq}}$  decreases whereas the amount of other oxidation states increases with time. All samples reach a steady state after several days or months. If the concentration of  $\text{Pu(IV)}_{\text{aq}}$  decreased through only disproportionation (2.25) and (2.26), then the following charge balance should be valid for  $\text{Pu(III)}_{\text{aq}}$ ,  $\text{Pu(V)}_{\text{aq}}$ , and  $\text{Pu(VI)}_{\text{aq}}$ :

$$[\text{Pu(III)}] = [\text{Pu(V)}] + 2[\text{Pu(VI)}], \quad (6.4)$$

assuming the starting solution contains no other oxidation states ( $\text{Pu(III)}_{\text{aq}}$ ,  $\text{Pu(V)}_{\text{aq}}$ , and  $\text{Pu(VI)}_{\text{aq}}$ ). However, none of the solutions investigated in the present work fulfils this balance. Fig. 6.6 shows an example at  $[\text{Pu}]_{\text{tot.}}$  of  $3.3 \cdot 10^{-4}$  M and pH 0.48 (the series 1). All samples which will be discussed in the following subsections (see Fig. 6.7, Fig. 6.8 Fig. 6.10 and Fig. 6.11 and tables in Appendix 8.6) show similar behavior.

The experimental results indicate that rather than conservation of charge (6.4), the sum  $[\text{Pu(III)}_{\text{aq}}] + [\text{Pu(IV)}_{\text{aq}}]$  (★ in Fig. 6.6) remains constant as a function of time. The formation of  $\text{Pu(III)}_{\text{aq}}$  always equals the simultaneous decrease of  $\text{Pu(IV)}_{\text{aq}}$ :

$$\frac{d[\text{Pu(III)}]}{dt} = - \frac{d[\text{Pu(IV)}]}{dt}, \quad (6.5)$$

i.e.  $[\text{Pu(III)}_{\text{aq}}] + [\text{Pu(IV)}_{\text{aq}}]$  is constant and consequently  $[\text{Pu(V)}_{\text{aq}}] + [\text{Pu(VI)}_{\text{aq}}] + [\text{Pu(IV)}_{\text{coll}}]$  is constant. This behavior suggests that plutonium does not follow disproportionation (2.25) and (2.26) under the conditions of the present work. The different plutonium species in solution seem to be in equilibrium based on two reaction groups,  $\text{Pu(IV)}_{\text{aq}} \rightleftharpoons \text{Pu(III)}_{\text{aq}}$  (reduction of Pu(IV)) and  $\text{Pu(IV)}_{\text{coll}} \rightleftharpoons \text{Pu(V)}_{\text{aq}} \rightleftharpoons \text{Pu(VI)}_{\text{aq}}$  (oxidation of Pu(IV)).

In addition, the total amount of the reduction of Pu(IV) ( $\Delta[\text{Pu(III)}_{\text{aq}}]$ ) exceeds the total amount of oxidation of Pu(IV) ( $[\text{Pu(V)}_{\text{aq}}] + 2[\text{Pu(VI)}_{\text{aq}}]$ ), i.e.

$$\Delta[\text{Pu(III)}_{\text{aq}}] > \Delta([\text{Pu(V)}_{\text{aq}}] + 2[\text{Pu(VI)}_{\text{aq}}]). \quad (6.6)$$

This indicates the existence of other reductants in addition to plutonium to drive the reduction of  $\text{Pu(IV)}_{\text{aq}}$  to  $\text{Pu(III)}_{\text{aq}}$  in solution.

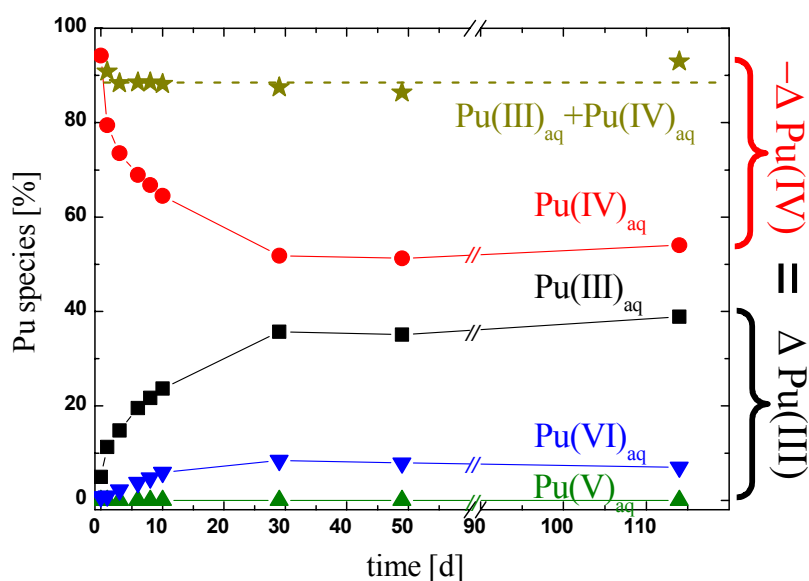


Fig. 6.6 The distribution of oxidation states versus time (days).  $[\text{Pu}]_{\text{tot.}}$  is  $3.3 \cdot 10^{-4}$  M at pH 0.48.

The excess reduction from  $\text{Pu(IV)}_{\text{aq}}$  to  $\text{Pu(III)}_{\text{aq}}$  amounts to 20% ~ 30 % of the total Pu concentration ( $[\text{Pu}]_{\text{tot.}} = \text{ca. } 3.5 \cdot 10^{-4}$  M) in the case of series 1 and 2. About 20 ppm of Pu is reduced by a reductant other than Pu. This amount is too large to be explained with the redox reaction of possible contaminants (for example, Fe) which can be oxidized in solution. In the present work, all solutions are prepared with deionized water (18 M $\Omega$  cm, Millipore) and contain relatively low concentration of redox sensitive metals. The Pu stock solution in 0.5 M HCl contains only sub-ppm amounts of redox sensitive metals (major: Fe) measured by ICP-MS. The purchased NaCl solid contains only 2 ppm Fe contamination which leads to < 100 ppb in the 0.5 M NaCl solution. Even if upper limits of all metal contaminants are considered, the great excess of reduction of plutonium cannot be explained by the oxidation of other redox sensitive metals. The remaining possible oxidation in aquatic condition is the oxidation of water (2.3),  $1/2\text{H}_2\text{O} \rightleftharpoons 1/4\text{O}_2 + \text{H}^+ + \text{e}^-$ .

The reduction and oxidation of Pu(IV) are connected with the formation of hydrolysis species ( $\text{Pu(OH)}_y^{4-y}$ ,  $y = 1-4$ ), polynuclear species and colloids ( $\text{Pu(OH)}_4(\text{am})$  or  $\text{PuO}_2 \cdot x\text{H}_2\text{O}(\text{am})$ ) of Pu(IV). In the following subsection, the dependence of these reactions on pH, Pu concentration and  $\text{O}_2$  concentration are discussed in detail.

### 6.3.1 Redox reactions of plutonium in contact with air

Fig. 6.7 shows the oxidation state distribution of the titration series 1 as a function of time (■: Pu(III)<sub>aq</sub>, ●: Pu(IV)<sub>aq</sub>, ▲: Pu(V)<sub>aq</sub> and ▼: Pu(VI)<sub>aq</sub>). The total Pu concentration of these solutions is about  $3.5 \cdot 10^{-4}$  M measured by LSC. All samples are prepared in contact with air and the pH of the samples is between pH 0.48 and 1.21. Each sample is investigated as a function of time by LIBD and spectroscopy using CARY 5E in 10 ml quartz cell (beam path length,  $l = 2$  cm) for several months until a steady state is reached. None of the samples of series 1 contains colloids being detectable by LIBD. The spectrum analysis by deconvolution (see Section 3.1) shows a difference between  $[\text{Pu}]_{\text{tot}}$  by LSC and the sum of all plutonium aquatic species by spectroscopy. This difference is considered to be the concentration of Pu polynuclear species or colloids which are too small to be detected by LIBD (for the exact information, see Table 8.5 in Appendix 8.6).

The redox kinetics shown in Fig. 6.7 exhibits some characteristic phenomena depending on pH (at constant Pu concentration).

- (1) At higher pH,  $[\text{Pu(IV)}_{\text{aq}}]$  decreases faster and a steady state is reached more rapidly. The fractions of Pu(IV)<sub>aq</sub> in the respective stock solutions are similar, about 90 % of  $[\text{Pu}]_{\text{tot}}$ . At pH 0.48, it takes almost one month to reach a steady state, whereas at pH 1.21 no further change of oxidation state distribution is observed after 1 day. The same pH dependence was observed in a study of Pu solubility by Perez-Bustamante [Pere 65].
- (2) The distribution of the aquatic species at a steady state depends on pH.  $[\text{Pu(III)}_{\text{aq}}]$  increases,  $[\text{Pu(IV)}_{\text{aq}}]$  decreases and  $[\text{Pu(V)}_{\text{aq}}]$  increases with increasing pH.  $[\text{Pu(VI)}_{\text{aq}}]$  remains constant. In addition,  $[\text{Pu(III)}_{\text{aq}}] + [\text{Pu(IV)}_{\text{aq}}]$  decrease and  $[\text{Pu(IV)}_{\text{coll}}] + [\text{Pu(V)}_{\text{aq}}] + [\text{Pu(VI)}_{\text{aq}}]$  increase with increasing pH.
- (3) Especially the fraction of Pu(V)<sub>aq</sub> increases with increasing pH. At pH 0.48,  $[\text{Pu(V)}_{\text{aq}}]$  is below the detection limit of a conventional absorption spectrometer. However, at higher pH, the increase of  $[\text{Pu(V)}_{\text{aq}}]$  is observed and Pu(V)<sub>aq</sub> contributes almost 20 % at pH 1.21. This agrees well with findings that the stability of the Pu(V)<sub>aq</sub> ion increases with increasing pH [Fuge 76; Katz 86].

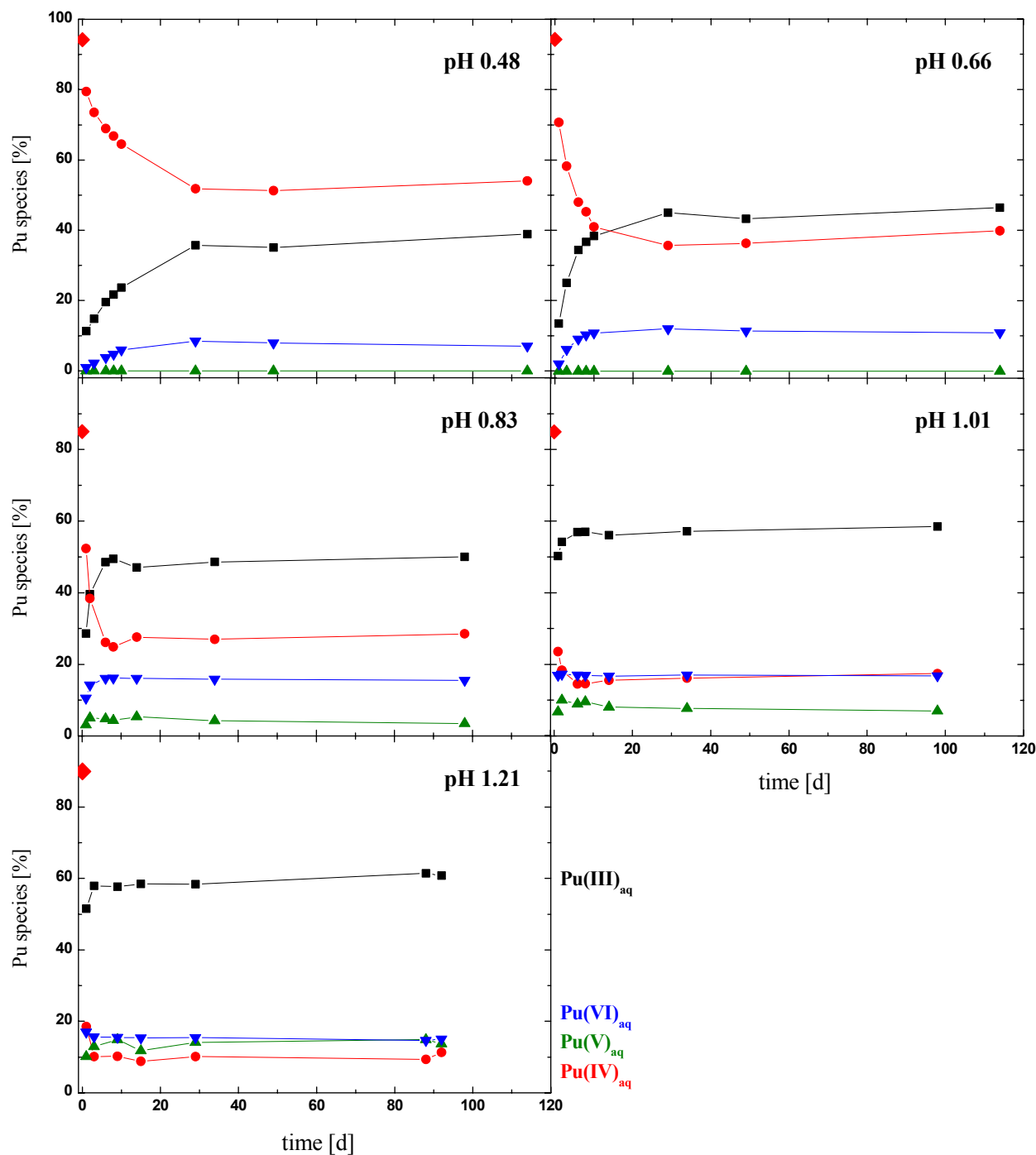


Fig. 6.7 The distribution of oxidation states versus time (days) for titration series 1. The symbol  $\blacksquare$ :  $\text{Pu(III)}_{\text{aq}}$ ,  $\bullet$ :  $\text{Pu(IV)}_{\text{aq}}$ ,  $\blacktriangle$ :  $\text{Pu(V)}_{\text{aq}}$  and  $\blacktriangledown$ :  $\text{Pu(VI)}_{\text{aq}}$ . The total Pu concentrations measured by LSC,  $[\text{Pu}]_{\text{tot}}$ , are about  $3.5 \cdot 10^{-4}$  M and pH varies in the range pH 0.48 – 1.21. All samples are prepared in air and observed for several months until a steady state is reached.  $\blacklozenge$  indicates the percentage of  $\text{Pu(IV)}_{\text{aq}}$  in stock solutions. Absorption spectra are measured using CARY 5E in 10 ml quartz cell ( $l = 2$  cm). Data in Table 8.5.



These observations indicate that  $\text{Pu(IV)}_{\text{aq}}$  is less stable at higher pH. With increasing pH, firstly, more  $\text{Pu(IV)}$  is reduced to  $\text{Pu(III)}_{\text{aq}}$  and secondly, more  $\text{Pu(IV)}$  is converted to plutonyl species ( $\text{Pu(V)}_{\text{aq}}$  and  $\text{Pu(VI)}_{\text{aq}}$ ). The increase of  $[\text{Pu(IV)}_{\text{coll}}] + [\text{Pu(V)}_{\text{aq}}] + [\text{Pu(VI)}_{\text{aq}}]$  with increasing pH is likely due to the pH dependence of the reaction between  $\text{Pu(IV)}_{\text{aq}}$  and  $\text{Pu(IV)}_{\text{coll}}$ . At higher pH, the fraction of hydroxide complexes increases and more polynuclear species can form. Consequently more plutonyl species are formed via oxidation (2.34). The same reason holds for the increase of reduction ( $\text{Pu}^{4+} + \text{e}^- \rightleftharpoons \text{Pu}^{3+}$ ) which seems to be independent of pH. The reduction of  $\text{Pu(IV)}_{\text{aq}}$  is increased as much as the increase of oxidation.

The present experiments cover only a narrow range of pH (0.5 – 1.2). However, the basic findings discussed above are useful to understand results in literature even at higher pH. Perez-Bustamante [Pere 65] did not consider the existence of other oxidation states than  $\text{Pu(IV)}$  but assumed all aqueous species in solution to be  $\text{Pu(IV)}_{\text{aq}}$ . The solubility curve of  $\text{Pu(IV)}$  showed a gradual decrease with pH and the solubility of Pu at  $1.5 < \text{pH} < 3.5$  is much higher than the solubility of the present work. This is due to the presence of other oxidation states whose relative abundance increases with increasing pH.

Fig. 6.8 shows the oxidation state distributions of four samples in the series 5.  $[\text{Pu}]_{\text{tot.}}$  (LSC) is  $1.2 \cdot 10^{-5}$  M and  $1.07 < \text{pH} < 2.13$ . Each sample is investigated as a function of time by LIBD and spectroscopy using the 100 cm capillary cell (Section 3.1). The premature formation of colloids at low pH could be induced by contaminations from the capillary as discussed in Section 6.2 and affect the redox reactions. The redox reactions follow the systematic trends observed for the series 1 and 5. However, the overall reaction rates are reduced due to the lower Pu concentration. The two samples at pH 1.07 and 1.22 do not reach the steady state even after 2 months, whereas the samples of the series 1 ( $[\text{Pu}]_{\text{tot.}} = 3 \cdot 10^{-4}$  M) at the same pH reach a steady state within a week.

At lower  $[\text{Pu}]_{\text{tot.}}$ , smaller fractions of  $\text{Pu(III)}_{\text{aq}}$  and  $\text{Pu(V)}_{\text{aq}}$  are formed at steady state and the fraction of remaining  $\text{Pu(IV)}_{\text{aq}}$  is higher than for the series 1. For example, at pH 1.2, the higher concentrated sample ( $[\text{Pu}]_{\text{tot.}} = 3.5 \cdot 10^{-4}$  M) contains 60 % of  $\text{Pu(III)}_{\text{aq}}$ , 15 % of  $\text{Pu(V)}_{\text{aq}}$  and 10 % of  $\text{Pu(IV)}_{\text{aq}}$ , whereas the diluted sample ( $[\text{Pu}]_{\text{tot.}} = 1.2 \cdot 10^{-5}$  M) contains only 40 % of  $\text{Pu(III)}_{\text{aq}}$ , below 5 % of  $\text{Pu(V)}_{\text{aq}}$  but 30 %  $\text{Pu(IV)}_{\text{aq}}$ .

The oversaturated samples at pH 1.52 and 2.13 contain a large fraction of colloids and show a tendency which differs from other samples. For example, the sample at pH 1.5 contains a smaller fraction of  $\text{Pu(III)}_{\text{aq}}$  than at pH 1.2 in contrast to the general trend of increasing  $\text{Pu(III)}_{\text{aq}}$  fractions with increasing pH. The sample at pH 2.1 exhibits remarkably slow kinetics (1 month to reach a steady state) as compared with that at pH 1.5 (in 1 day) in contradiction to the finding that the redox reactions are faster at high pH.

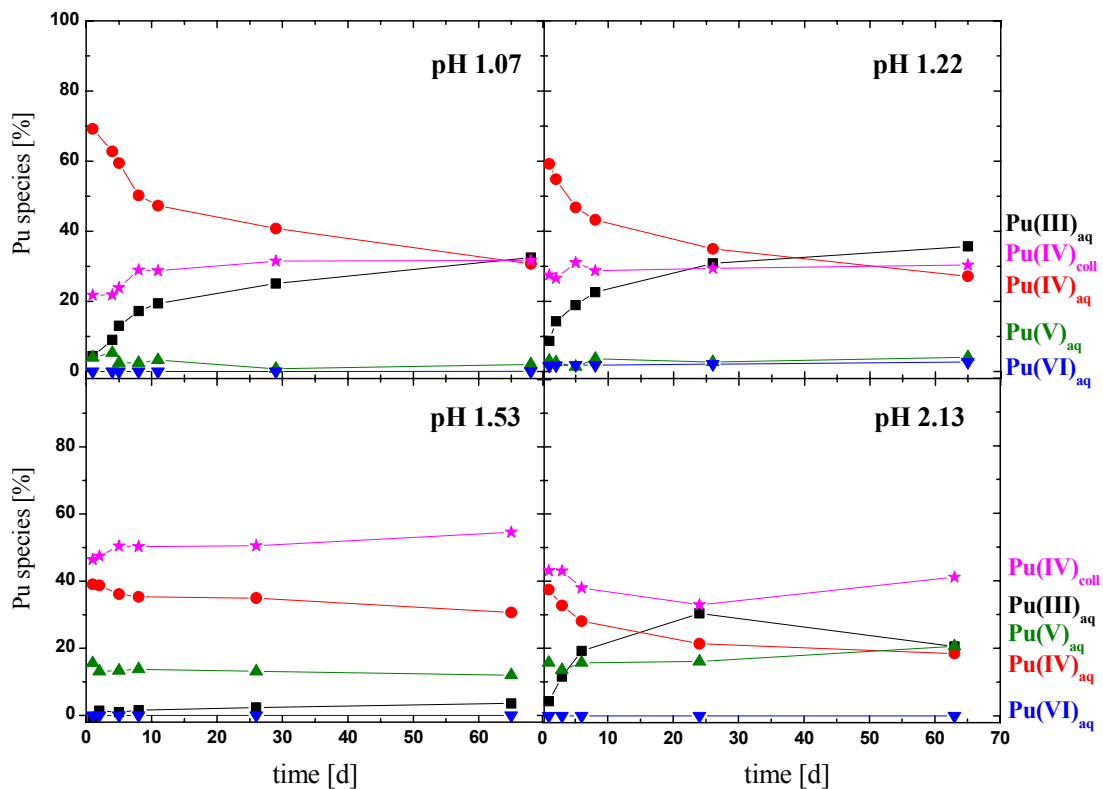


Fig. 6.8 The distribution of oxidation states versus time (days) for titration series 5. The symbol ■: Pu(III)<sub>aq</sub>, ●: Pu(IV)<sub>aq</sub>, ▲: Pu(V)<sub>aq</sub>, ▼: Pu(VI)<sub>aq</sub>, and ★: Pu(IV)<sub>coll</sub>. The total plutonium concentrations measured by LSC are about  $1.2 \cdot 10^{-5}$  M. pH varies from 1.07 to 2.13. Absorption spectra are measured using the 100 cm capillary.

The influence of the capillary on the formation of colloids is not clear. The concentration of colloids is determined by subtracting the sum of other aqueous species from the total Pu concentration measured by LSC. If, for any reason, the concentration of Pu aquatic species is underestimated, the concentration of colloids apparently increases. Aquatic Pu species adsorbed on the capillary wall might have different optical properties from aquatic species or might not be detected at all by spectroscopy, which in turn would lead to an overestimation of the concentration of colloids. However, sorption is excluded by measuring the total Pu concentration again by LSC after several spectroscopic measurements using the capillary. The total concentration of Pu does not change before and after the absorption measurement.

As mentioned in Section 6.2, the formation of Pu colloids could be induced by contamination with small colloids of the capillary acting as seed crystals. Hence, an independent method, the capillary electrophoresis (CE) coupled with ICP-MS is applied for speciation of the same sample. Fig. 6.9 shows the result of CE-ICP-MS for the sample at pH 2.13 after 60 days. The mobilities of different Pu oxidation states are in the order of Pu(III)<sub>aq</sub> > Pu(VI)<sub>aq</sub> > Pu(V)<sub>aq</sub> > Pu(IV)<sub>aq</sub> in 1M AcOH (Section 3.2) and the mobilities of

Pu(V)<sub>aq</sub> and Pu(VI)<sub>aq</sub> are very similar. In order to distinguish between the two species, the electropherogram of the sample (— solid line in Fig. 6.9) is compared to that of a standard solution of Pu(V)<sub>aq</sub> and Pu(VI)<sub>aq</sub> (- - - dashed line, in Fig. 6.9). From the peak area analysis, the relative concentration (%) of different oxidation states is determined as 19 % of Pu(III)<sub>aq</sub>, 37 % of Pu(IV)<sub>aq</sub>, 20 % of Pu(V)<sub>aq</sub> and 24 % of Pu(IV)<sub>coll</sub>, if the broad pattern after the sharp peak of Pu(IV)<sub>aq</sub> is assumed to be due to colloidal or polymeric Pu(IV) (cf. [Kucz 2003]). The concentration of Pu(VI)<sub>aq</sub> is below the detection limit of ICP-MS. The amounts of Pu(III)<sub>aq</sub> (20.5%), of Pu(V)<sub>aq</sub> (20.6 %) and of Pu(VI)<sub>aq</sub> (0 %) determined by spectroscopy agree well with the results by CE-ICP-MS. However, the relative concentration of Pu(IV)<sub>aq</sub> according to spectroscopy is only 18.5 % and Pu(IV)<sub>coll</sub> over 40 %. The total amounts of Pu(IV) species ([Pu(IV)]<sub>aq</sub> + [Pu(IV)]<sub>coll</sub>) determined by both speciation methods are consistent, but the [Pu(IV)]<sub>coll</sub> determined by CE-ICP-MS is only half of that determined by spectroscopy. CE measurement is carried out directly after the measurement of the UV-Vis absorption spectrum and it is very unlikely, that the species distribution changed in the mean time. The difference in the distribution of Pu(IV) species can be considered to be a result of the dissolution of formed (pseudo) Pu(IV)-colloids due to complexation with acetate ligand in 1 M AcOH.

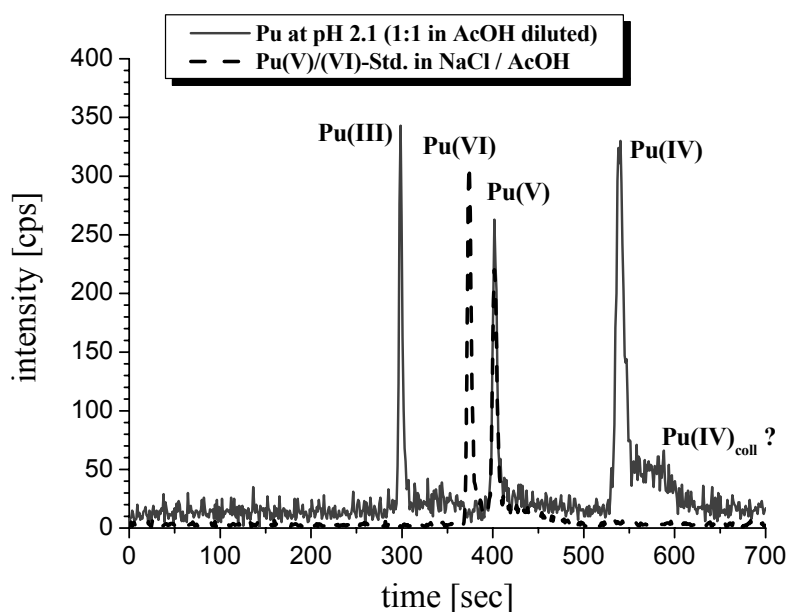


Fig. 6.9 CE-ICP-MS measurement for sample  $[Pu]_{tot.} = 1.2 \cdot 10^{-5}$  M at pH 2.13 after 60 days (series 5). The electropherogram of the sample (— solid line) is compared to standard solution with Pu(V)<sub>aq</sub> and Pu(VI)<sub>aq</sub> (- - - dashed line). The fraction of different oxidation states are 19 % of Pu(III)<sub>aq</sub>, 37 % of Pu(IV)<sub>aq</sub>, 20 % of Pu(V)<sub>aq</sub> and 24 % of Pu(IV)<sub>coll</sub>. There is no Pu(VI)<sub>aq</sub>. The broad peak eluted after the sharp peak of Pu(IV)<sub>aq</sub> is assumed to be Pu(IV)<sub>coll</sub>.

### 6.3.2 The change of oxidation state distribution by acidifying

When a steady state is reached after 92 days, the sample at  $\text{Pu } 3.32 \cdot 10^{-4} \text{ M}$  and pH 1.21 (of the series 1) is acidified by adding  $40 \mu\text{l}$  of 6 M HCl into the 3 ml sample. The pH is 0.82 after acidification and the acidified solution reaches a new steady state after about 10 days (see Fig. 6.10 and Table 8.5). Upon the pH change,  $[\text{Pu(III)}_{\text{aq}}]$  decreases about 5 %,  $[\text{Pu(IV)}_{\text{aq}}]$  increases about 15 % resulting in a net increase of the sum of both ( $[\text{Pu(III)}_{\text{aq}}] + [\text{Pu(IV)}_{\text{aq}}]$ ).  $\text{Pu(V)}_{\text{aq}}$  decreases about 10 % after acidifying and the amount of  $[\text{Pu(VI)}_{\text{aq}}]$  remains constant so that the amount of plutonyl species  $[\text{Pu(V)}_{\text{aq}}] + [\text{Pu(VI)}_{\text{aq}}]$  decreases. This behavior resembles the pH dependence of Pu solutions already discussed in Section 6.3.1. The oxidation state distribution at the end of the measurement equals the sample at pH 0.83 of series 1 (in Fig. 6.7). 5 % of  $\text{Pu(III)}_{\text{aq}}$  is oxidized to  $\text{Pu(IV)}_{\text{aq}}$  and 10 % of  $\text{Pu(V)}_{\text{aq}}$  is reduced to  $\text{Pu(IV)}_{\text{aq}}$  by acidifying. The amount of reduction exceeds that of oxidation in this experiment.

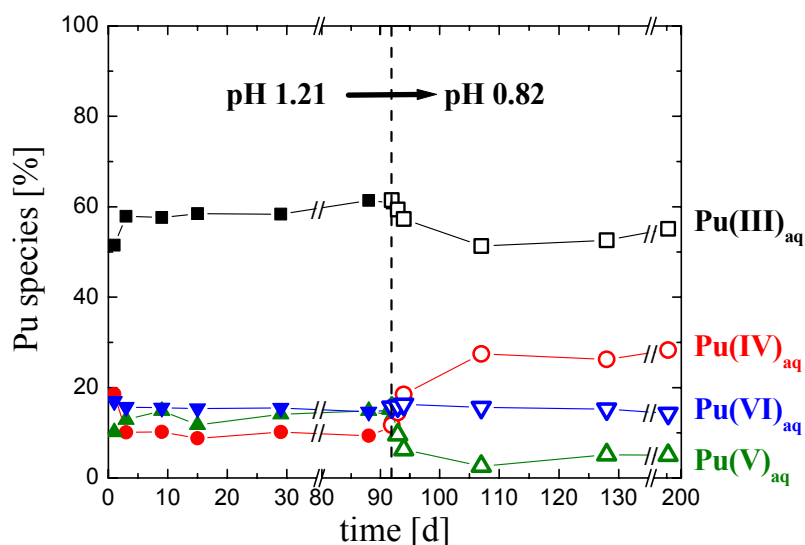


Fig. 6.10 The distribution of oxidation states for the sample,  $[\text{Pu}]_{\text{tot.}} = 3.32 \cdot 10^{-4} \text{ M}$  at pH 1.21 of series 1. The solution is acidified to pH 0.82 after 92 days (dashed vertical line) by adding  $40 \mu\text{l}$  of 6 M HCl. (■:  $\text{Pu(III)}_{\text{aq}}$ , ●:  $\text{Pu(IV)}_{\text{aq}}$ , ▲:  $\text{Pu(V)}_{\text{aq}}$  and ▼:  $\text{Pu(VI)}_{\text{aq}}$  before acidifying) The corresponding open symbols depict each species after acidifying.

### 6.3.3 Redox reactions of plutonium under argon atmosphere

As mentioned above, in the present work where the samples contain only Pu(IV) in the beginning, the reactions of plutonium can be divided into two reaction groups. The major reaction is the reduction of Pu(IV) which is well known ((2.29)  $\text{Pu}^{4+} + \text{e}^- \rightleftharpoons \text{Pu}^{3+}$ ). The other is the oxidation of Pu(IV) to plutonyl species  $\text{PuO}_2^+$  and  $\text{PuO}_2^{2+}$  ( $\text{Pu(IV)}_{\text{coll}} \rightleftharpoons \text{Pu(V)}_{\text{aq}} \rightleftharpoons \text{Pu(VI)}_{\text{aq}}$ ). In this Section, the reaction of  $\text{Pu(IV)}_{\text{coll}} \rightleftharpoons \text{Pu(V)}_{\text{aq}}$  is discussed in detail, especially, its dependence on  $\text{O}_2$  concentration.

Many studies on the solubility of  $\text{PuO}_2(\text{am})$  were carried out at neutral pH from undersaturation. In these studies,  $\text{PuO}_2^+$  is the dominant species in solution. It was concluded that  $\text{PuO}_2(\text{am})$  precipitates are in equilibrium with the  $\text{PuO}_2^+$  aquatic species (2.32) [Rai 84; Silv 89]. As a possible mechanism for the reaction (2.32), Neck *et al.* proposed that  $\text{PuO}_2(\text{am})$  is oxidized to  $\text{PuO}_{2+x}(\text{am})$  by dissolved oxygen in solution and the Pu(V) in  $\text{PuO}_{2+x}(\text{am})$  dissolves as  $\text{PuO}_2^+$  (2.34) in solution [Neck 2005] (see Section 2.2.4).

In order to investigate the role of dissolved oxygen in Pu redox reactions, the experiments of series 2 are carried out in a glove box ( $\text{O}_2 < 20$  ppm). The samples are prepared at the same Pu concentration and pH as the series 1. Two samples at pH 0.43 and pH 1.18 are shown in Fig. 6.11 with open symbols ( $\square$ :  $\text{Pu(III)}_{\text{aq}}$ ,  $\circ$ :  $\text{Pu(IV)}_{\text{aq}}$ ,  $\triangle$ :  $\text{Pu(V)}_{\text{aq}}$  and  $\nabla$ :  $\text{Pu(VI)}_{\text{aq}}$ ) together with the results of the series 1 (filled symbols,  $\blacksquare$ :  $\text{Pu(III)}_{\text{aq}}$ ,  $\bullet$ :  $\text{Pu(IV)}_{\text{aq}}$ ,  $\blacktriangle$ :  $\text{Pu(V)}_{\text{aq}}$  and  $\blacktriangledown$ :  $\text{Pu(VI)}_{\text{aq}}$ ) (for complete summarization of the series 2, see Table 8.6). The amounts of  $\text{O}_2$  in solution differ by four orders of magnitude between the series 1 and 2. The concentration of dissolved  $\text{O}_2$  in case of the series 1 is about  $[\text{O}_2]_{\text{aq}} = 2.5 \cdot 10^{-4}$  M at  $P_{\text{O}_2}(\text{g}) = 0.2$  bar at room temperature and in case of the series 2  $[\text{O}_2]_{\text{aq}}$  is about  $2.5 \cdot 10^{-8}$  M due to the low partial pressure of  $\text{O}_2$  ( $P_{\text{O}_2}(\text{g}) = 2 \cdot 10^{-5}$  bar) in the glove box. Even if the exclusion of oxygen from the sample (Pu stock solution, HCl and NaCl solution) is not complete, at least differences in the reaction rates are expected.

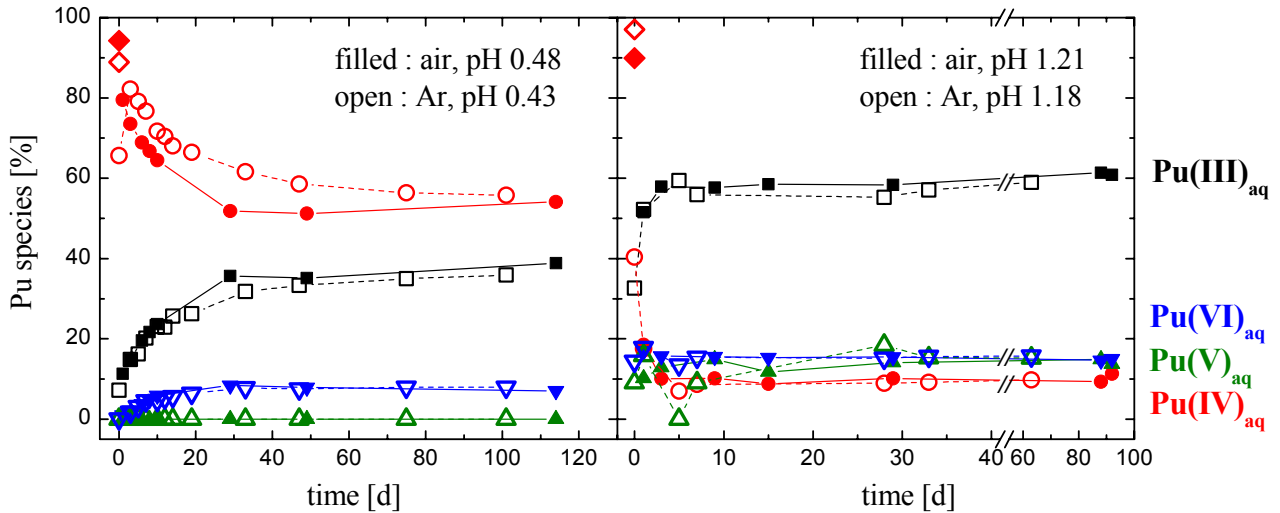


Fig. 6.11  $[\text{Pu}]_{\text{tot.}} = \text{ca. } 3.3 \cdot 10^{-4} \text{ M}$ , open symbols indicate the oxidation state distributions under argon atmosphere (series 2),  $\square$ :  $\text{Pu(III)}_{\text{aq}}$ ,  $\circ$ :  $\text{Pu(IV)}_{\text{aq}}$ ,  $\triangle$ :  $\text{Pu(V)}_{\text{aq}}$  and  $\nabla$ :  $\text{Pu(VI)}_{\text{aq}}$ . Corresponding solid points,  $\blacksquare$ :  $\text{Pu(III)}_{\text{aq}}$ ,  $\bullet$ :  $\text{Pu(IV)}_{\text{aq}}$ ,  $\blacktriangle$ :  $\text{Pu(V)}_{\text{aq}}$  and  $\blacktriangledown$ :  $\text{Pu(VI)}_{\text{aq}}$ , for samples at similar pH in air condition (series 1 in Fig. 6.9).  $\diamond$  and  $\blacklozenge$  indicate the percentage of  $\text{Pu(IV)}_{\text{aq}}$  in stock solutions.

However, the results of both experimental series are identical (see Fig. 6.11). The dissolved oxygen plays no important role for the oxidation of  $\text{Pu(IV)}_{\text{coll}}$  to  $\text{PuO}_{2+x}(\text{s})$  in contradiction to the observation of solubility investigation from undersaturation with  $\text{PuO}_2(\text{am, hyd})$  [Neck 2005]. Also for the experiments under Ar atmosphere, the amount of reduction ( $\text{Pu(IV)}_{\text{aq}} \rightarrow \text{Pu(III)}_{\text{aq}}$ ) exceeds the oxidation in the present work. The excessive oxidant ( $\text{Pu(IV)}_{\text{aq}}$ ) in solution can sustain the oxidation  $\text{Pu(IV)}_{\text{coll}} \rightleftharpoons \text{Pu(V)}_{\text{aq}}$  without need for additional oxidants such as dissolved  $\text{O}_2$ . On the other hand, the solutions in the experiment from undersaturation contain no other oxidant (no reduction of Pu observed) making dissolved  $\text{O}_2$  the only oxidant for the oxidation of  $\text{PuO}_2(\text{am})$ .

#### 6.4 Determination of hydrolysis constants from Eh measurements

The redox reactions between different Pu oxidation states are controlled by the redox potential of the solutions. Three redox couples are well known  $\text{Pu}^{4+}/\text{Pu}^{3+}$  (2.29),  $\text{PuO}_2^{2+}/\text{PuO}_2^+$  (2.30) and  $\text{PuO}_2^+/\text{Pu(IV)}_{\text{coll}}$  (2.32). The redox potential of solution can be calculated from redox equilibrium. For example, the redox reaction of the  $\text{PuO}_2^{2+}/\text{PuO}_2^+$  couple and its equilibrium constant are



$$\log K^\circ = -15.86 \pm 0.085 \text{ [Lemi 2001]}.$$

If the concentrations of both aquatic species of plutonium are known, the pe values can be calculated by Eq. (6.7),

$$K' = \frac{[\text{PuO}_2^{2+}][e^-]}{[\text{PuO}_2^+]} \quad (6.7)$$

$$\log K' = \log [\text{PuO}_2^{2+}] - \log [\text{PuO}_2^+] - pe.$$

using the equilibrium constant (2.30).

The redox potential of each sample is determined after the oxidation state distribution reached a steady state. The respective measurements are highlighted in the tables of Appendix 8.6. The measured redox potential Eh(V) can be converted to a pe value with the relationship (2.9) ( $pe = 16.9 \text{ Eh(V)}$ ). Simultaneously the pe is calculated from each redox couple by use of the oxidation state distribution. However, a meaningful determination of pe is only possible if the abundance of each oxidation state of redox couples exceeds 5 %. When the solution is at steady state, the calculated redox potentials from all redox couples should be consistent with each other as well as with the measured redox potential.

Fig. 6.12 shows the measured pe and the calculated pe values from all redox couples as a function of pH. The measured pe (+) values are in good agreement with the calculated pe from the  $\text{PuO}_2^{2+}/\text{PuO}_2^+$  couple (2.30) (○) and the  $\text{PuO}_2^+/\text{Pu(IV)}_{\text{coll}}$  couple (2.32) (△). From the least squares fit of these values, a linear relationship (solid line) is obtained as

$$pe = (17.08 \pm 0.16) - (1.44 \pm 0.14) \text{ pH}. \quad (6.8)$$

On the other hand, the pe values (□ gray square, in Fig. 6.12) calculated from the  $\text{Pu}^{4+}/\text{Pu}^{3+}$  couple (2.29) deviate from the others. The deviation may result from incorrect hydrolysis constants.

In order to calculate the pe from the  $\text{Pu}^{4+}/\text{Pu}^{3+}$  couple based on the reaction (2.29), the analogue equation to Eq. (6.7)

$$\log K' = \log [\text{Pu}^{4+}] - \log [\text{Pu}^{3+}] - pe \quad (6.9)$$

is used and the concentration of “free ion”  $\text{Pu}^{4+}$  and  $[\text{Pu}^{3+}]$  have to be known.

According to the hydrolysis constants of [Meti 72], a large amount of  $\text{Pu}^{4+}$  is readily hydrolyzed even at the low pH in the present work (see Fig. 3.2). However, the absorption spectrum of Pu(IV) does not change with the degree of hydrolysis (see Section 3.1). Thus, the concentration of  $\text{Pu(IV)}_{\text{aq}}$  obtained by spectroscopy is not  $[\text{Pu}^{4+}]$  but the sum of all Pu(IV) hydrolysis species,

$$[\text{Pu(IV)}_{\text{aq}}] = [\text{Pu}^{4+}] + \sum_{y=1}^4 [\text{Pu(OH)}_y^{4-y}] = [\text{Pu}^{4+}] \left( 1 + \sum_{y=1}^4 \beta'_{1y} [\text{OH}^-]^y \right) \quad (6.10)$$

where  $\beta'_{1y}$  indicates the formation constant of mononuclear hydrolysis species.

The pe values from the  $\text{Pu}^{4+}/\text{Pu}^{3+}$  couple in Fig. 6.12 ( $\square$ ) are calculated with the  $[\text{Pu}^{4+}]$  obtained from Eq. (6.10) with the formation constants of [Meti 72] and  $[\text{Pu(IV)}_{\text{aq}}]$  measured by spectroscopy. The deviation of the calculated pe from the  $\text{Pu}^{4+}/\text{Pu}^{3+}$  couple ( $\square$  in Fig. 6.12) from the others ( $+$ ,  $\circ$  and  $\triangle$  in Fig. 6.12) is most likely due to erroneous formation constants of [Meti 72].

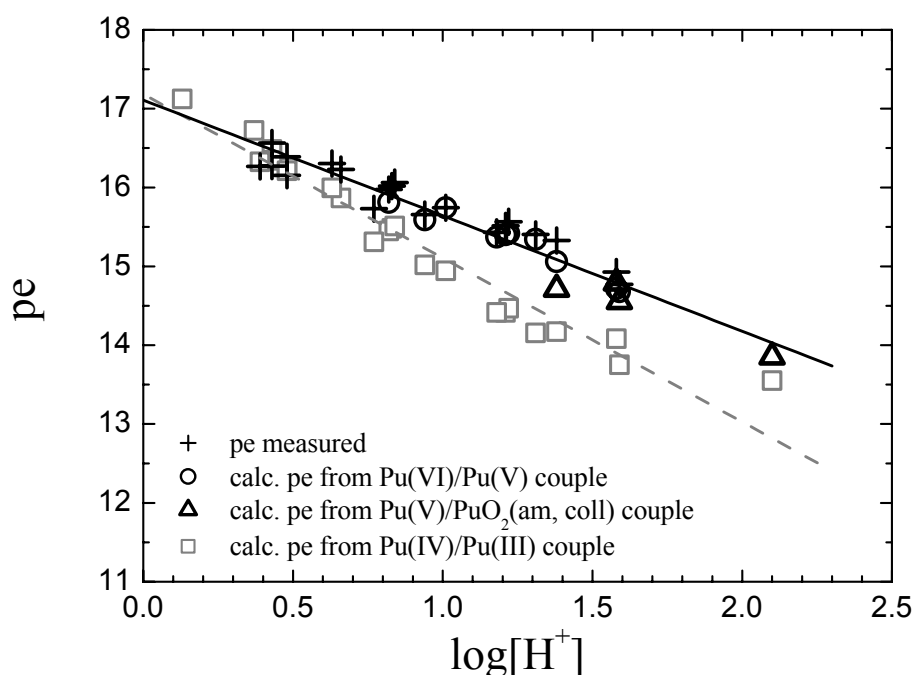


Fig. 6.12 The measured pe values and the calculated pe from three different redox couples are compared. The measured pe by redox electrodes ( $+$ ), calculated pe from the  $\text{PuO}_2^{2+}/\text{PuO}_2^+$  couple (2.30) ( $\circ$ ) and the  $\text{PuO}_2^+/\text{Pu(IV)}_{\text{coll}}$  couple (2.32) ( $\triangle$ ) and the least squares fit of these values (solid line) are depicted. These pe values are consistent with each other. The pe values from the  $\text{Pu}^{4+}/\text{Pu}^{3+}$  couple (2.29) ( $\square$ , gray square) are calculated by use of the hydrolysis constants of [Meti 72] (in order to determine  $[\text{Pu}^{4+}]$ ). These pe values deviate from the others.



The present data are used to calculate  $\beta_{11}$  and  $\beta_{12}$  in the following way. The formation constants of hydrolysis species can be estimated using Eq. (6.10), when the  $[\text{Pu}^{4+}]$  and the  $[\text{Pu(IV)}_{\text{aq}}]$  at certain pH are known. The  $[\text{Pu}^{4+}]$  of the sample at certain pH is obtained from the measured Eh value and the spectroscopically measured  $[\text{Pu}^{3+}]$  using Eq. (6.9). The  $[\text{Pu(IV)}_{\text{aq}}]$  is measured by spectroscopy. By combining Eq. (6.10) and Eq. (6.9), the measured quantities are related to the formation constants  $\beta_{1y}$  ( $y = 1-4$ ) as following equation

$$\text{pe} + \log[\text{Pu}^{3+}]/[\text{Pu(IV)}_{\text{aq}}] = -\log K' - \log\left(1 + \sum_{y=1}^4 \beta'_{1y} [\text{OH}^-]^y\right). \quad (6.11)$$

The pe are obtained from the Eh measurement or from the concentration of oxidation states ( $[\text{PuO}_2(\text{am, coll})]$ ,  $[\text{PuO}_2^+]$  and  $[\text{PuO}_2^{2+}]$ ) measured by spectroscopy.  $[\text{Pu}^{3+}]$  and  $[\text{Pu(IV)}_{\text{aq}}]$  are also directly measured by spectroscopy. The equilibrium constant at the present experiment condition ( $\log K' = 16.55$  at 0.5 M NaCl) is calculated with specific ion interaction theory (SIT) from the known equilibrium constant of the  $\text{Pu}^{4+}/\text{Pu}^{3+}$  couple (2.29) [Lemi 2001].

In Fig. 6.13, the measured quantity ( $\text{pe} + \log([\text{Pu}^{3+}]/[\text{Pu(IV)}]_{\text{aq}})$ ) is shown as a function of pH. The symbol  $\oplus$  indicates the sum of the pe obtained by Eh measurements and the  $\log([\text{Pu}^{3+}]/[\text{Pu(IV)}]_{\text{aq}})$  determined by spectroscopy. The other symbols ( $\circ$  and  $\triangle$ ) in Fig. 6.13 indicate the sum of the “calculated” pe values (shown in Fig. 6.12) and the  $\log([\text{Pu}^{3+}]/[\text{Pu(IV)}]_{\text{aq}})$ . The case of  $\text{PuO}_2^{2+}/\text{PuO}_2^+$  couple is depicted with  $\circ$  and the  $\text{PuO}_2^+/\text{Pu(IV)}_{\text{coll}}$  couple is depicted with  $\triangle$ , respectively.

The dotted line indicates the calculation (the right term of Eq. (6.11)) with the mononuclear hydrolysis constants of Metivier *et al.* [Meti 72]. If the mononuclear hydrolysis constants of Metivier *et al.* [Meti 72] were correct, the experimental data and the calculated line should agree. However, the experimental data at  $\text{pH} > 0.4$  are much higher than the calculated line, which indicates that the  $\log \beta_{1y}$  ( $y = 1-4$ ) of [Meti 72] are overestimated.

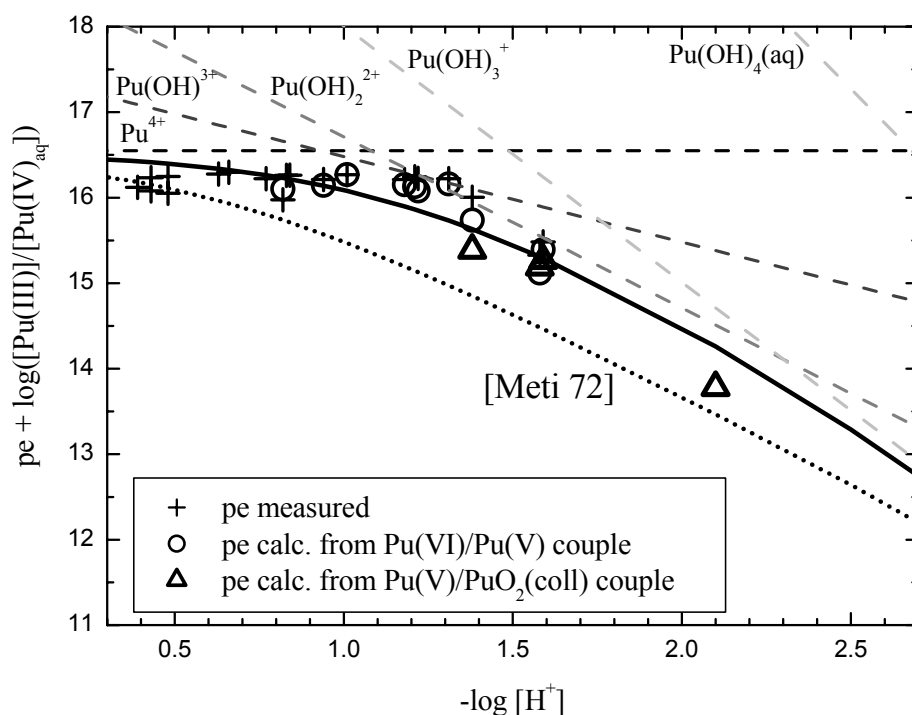


Fig. 6.13 The values of  $pe + \log[\text{Pu}^{3+}]/[\text{Pu(IV)}_{\text{aq}}]$  as a function of pH along with the measured  $pe$  (+), the calculated  $pe$  from the  $\text{PuO}_2^{2+}/\text{PuO}_2^+$  couple (O) and the  $\text{PuO}_2^+/\text{Pu(IV)}_{\text{coll}}$  couple ( $\Delta$ ).  $[\text{Pu}^{3+}]$  and  $[\text{Pu(IV)}_{\text{aq}}]$  are determined by spectroscopy. The dotted line represents the calculated  $-\log K' - \log(1 + \sum_{y=1}^4 \beta'_{1y} [\text{OH}^-]^y)$  with the formation constants of Metivier *et al.* ( $y = 1 - 4$ ) [Meti 72] and the solid lines the same relation with the corrected formation constants of hydrolysis species (see text).

The solid curve in Fig. 6.13 indicates the calculation of the right term of Eq. (6.11) with the corrected formation constants of mononuclear hydrolysis species. The first hydrolysis constant is lowered by 0.5, the second by 1.0 log units as compared to [Meti 72]. The experimental data do not allow independent determination of each formation constant. Thus, the formation constants are varied until the calculated curve is in good agreement with the experimental data. The present works are carried out at acidic conditions ( $0.1 > \text{pH} > 2.1$ ). Thus, only the first and second hydrolysis constants can be estimated (Table 6.2). The dashed lines indicate the calculations for each hydrolysis species with the corrected hydrolysis constants. The lack of data at higher pH prevents a precise determination of higher hydrolysis constants. The experiments have to be extended to higher pH.

Table 6.2 Corrected hydrolysis constants and corresponding formation constants of plutonium hydrolysis species using the measured redox potentials.

Medium/Species	$\log K'_{1y}$	$\log K^{\circ}_{1y}$	$\log \beta^{\circ}_{1y}$	Methods
0.5M HCl/NaCl, room temp./ Pu(OH) <sup>3+</sup>	-0.93	0.1	14.1	redox.
0.5M HCl/NaCl, room temp./ Pu(OH) <sub>2</sub> <sup>2+</sup>	-2.16	-0.4	27.6	redox.

As mentioned in Section 2.2.2, the only complete set of experimental data for the formation constants of all four mononuclear hydrolysis species ( $\log \beta_{1y}$ ,  $y = 1 - 4$ ) at trace Pu concentrations are those of [Meti 72]. However, there are several literature values of the first hydrolysis constant (Table 2.1) and the suggested value of  $\log \beta_{11} = 14.1$  in the present work compares reasonably well with the first hydrolysis constants measured by potentiometry [Rabi 51; Rabi 57] which are lower about 1 log unit than that of Metivier *et al.* (see Table 2.1).

## 7 Conclusion

In this study, the hydrolysis, solubility and colloid formation of tetravalent plutonium and redox equilibria between four different plutonium oxidation states are investigated using several complementary methods. These chemical properties of Pu(IV) are important for the performance assessment of nuclear waste disposals, in particular for the isolation and immobilization of radionuclides. However, the strong tendency of hydrolysis and subsequent colloid formation of Pu(IV) and moreover the redox instability of plutonium complicate the precise investigation of Pu. Thus, similar investigations with the redox stable and non-radioactive zirconium are also carried out for the purpose of comparison.

### Comparison of hydrolysis of Pu(IV) and Zr

On the basis of ionic radii and charge, the tendency of  $\text{Pu}^{4+}$  to undergo hydrolysis should exceed that of its predecessors in the actinide series ( $\text{Pu}^{4+} > \text{Np}^{4+} > \text{U}^{4+} > \text{Th}^{4+}$ ) and should be considerably smaller than  $\text{Zr}^{4+}$  or  $\text{Hf}^{4+}$  [Katz 86] due to their ionic radii in the order of  $\text{Zr}^{4+} (\approx \text{Hf}^{4+}) < \text{Pu}^{4+} < \text{Np}^{4+} < \text{U}^{4+} < \text{Th}^{4+}$ . However, the available experimental data on mononuclear hydrolysis of Zr(IV) and Pu(IV) indicate similar first hydrolysis constants of both elements.

The first and second hydrolysis constants of Pu(IV) determined by potentiometry in the present work (Table 6.2) are very similar to those of Zr(IV) (Table 2.2). The distributions of mononuclear hydrolysis species of Pu and Zr at  $I = 0.5 \text{ M}$  are compared in Fig. 7.1. The third and fourth hydrolysis constants of Pu(IV) could not be determined from experiments in the present work. The distribution of Pu(IV) hydrolysis species in Fig. 7.1 (a) at higher pH is calculated with the third hydrolysis constant lowered by 1.5 and the fourth by 2.0 log units as compared to the values by [Meti 72].

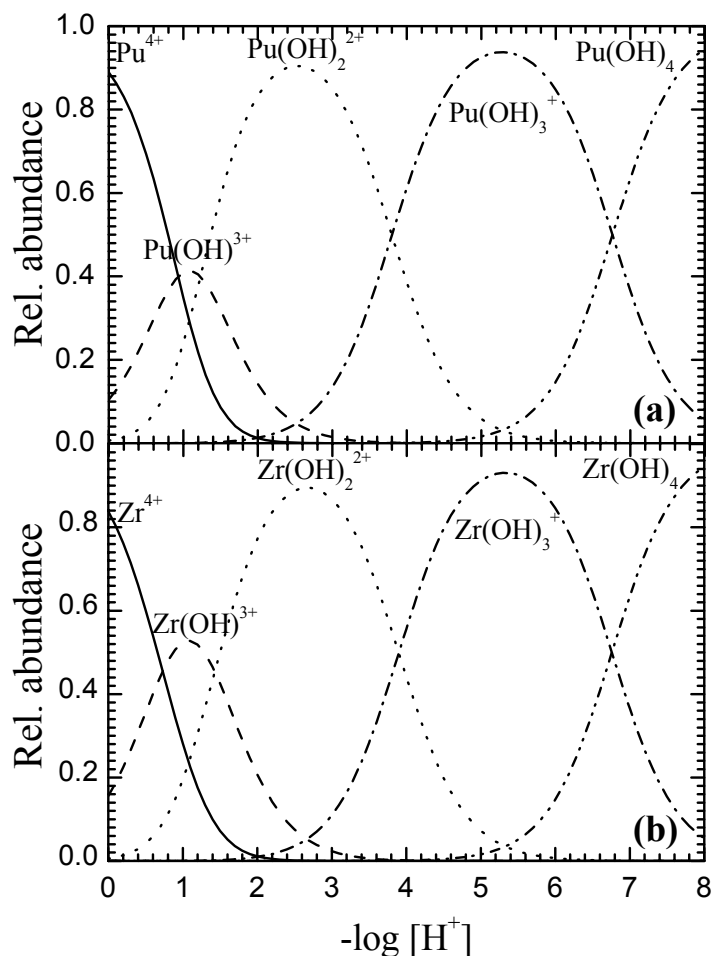


Fig. 7.1 (a) Pu at  $I = 0.5M$ , mononuclear hydrolysis species distribution calculated from the corrected formation constants (see Section 6.4). (b) Zr at  $I = 0.5 M$ ,  $\log \beta_{11}^{\circ}$ : [Baes 76; Ekbe 2001],  $\log \beta_{12}^{\circ} - \log \beta_{14}^{\circ}$ : estimated with  $d_{Zr-O} = 2.22$  (8-fold coordination in [Shan 76]) (Table 2.2 in Section 2.3)

### The solubility of zirconium and its polymer species

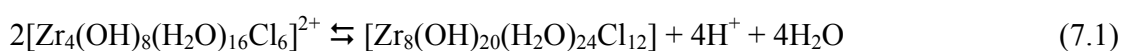
The solubility limiting phase of Zr(IV) in oversaturation experiments by LIBD is interpreted to be  $Zr(OH)_4(am)$  assuming that Zr(IV) exhibits a similar behavior to that of Th(IV) (Section 5.1). This interpretation is supported by the results of XAFS measurements (Section 5.2).

Highly concentrated solution of 10 mM contains particles of about 10 nm size as estimated by LIBD and with a strong Zr-Zr interaction and a single oxygen shell tentatively built up by tetrameric  $[Zr_4(OH)_8(H_2O)_{16}]^{8+}$  units as determined by EXAFS measurement. The XANES spectrum indicates also some crystalline feature of the particles. However, EXAFS measurements at high pH and low concentra-

tion (1 mM) indicate that the dominant species in these solutions does neither resemble the tetramers nor a simple  $ZrO_2$  structure<sup>7</sup> known from literature [Li 93]. It indicates that the dominant solution species strongly depends on Zr concentration and pH.

Besides these findings, there are conditions where the  $Zr^{4+}$  mononuclear species prevails as evident from the missing Zr-Zr interaction of a colloid-free sample at  $[Zr] = 1$  mM, pH 1 by EXAFS. Upon pH increase (pH 2.0 – 2.8), the formation of polynuclear species is observed by EXAFS while there are still no colloids detectable by LIBD. At pH close to 3, colloids are detected by LIBD and these colloids grow in size as pH increases. This means that, as the solubility limit is approached and before measurable colloids are present, polynuclear Zr species form.

In a review [Baes 76] on the hydrolysis constants of Zr, the authors conclude that the mononuclear species of Zr are dominant only at low Zr concentration ( $< 10^{-4}$  M) and at high Zr concentration, the polynuclear species form as a trimer,  $Zr_3(OH)_4^{8+}$  or  $Zr_3(OH)_5^{7+}$  or a tetramer  $Zr_4(OH)_8^{8+}$ . Recent studies [Sing 96; Ekbe 2004] indicate also the existence of the tetramer as dominant species at high Zr concentrations (4 - 50 mM). In addition, Singhal *et al.* [Sing 96] observed that the dominant tetrameric species grows to octameric species at increasing pH ( $[Zr] = 0.05$  M) by stacking two tetramers on top of each other:



and at higher pH, polymeric Zr species form even larger in size.

The presence of polynuclear species even at low concentration has important consequences for the interpretation of solubility data. The solubility curve for  $Zr(OH)_4(am)$  which is described by considering only mononuclear hydrolysis species is in good agreement with the experimental LIBD data (Fig. 5.6). Nevertheless, this solubility product ( $\log K_{sp}^\circ = -53.1 \pm 0.5$ ) may be considered to be only an operative value but the underlying model might not reflect the formation process of colloids. The polynuclear species are detected only at high Zr concentrations (1 mM) by XAFS even in samples at relatively low pH, but the polynuclear species are expected to predominate even at low Zr concentration at relatively high pH which is close to the solubility limit. With increasing pH, the solution approaches the solubility limit enhancing the polymerization of Zr(IV). However, experimental evidence of the polynuclear species at lower concentration is still missing.

The solubility data of Zr(IV) oxide (pH > 3) deviate from the calculated solubility curve of  $ZrO_2$  and approach the solubility data of  $Zr(OH)_4(am)$ . The similar phenomenon has been observed for the solubility data of thorium and uranium. In the case of thorium, this phenomenon is explained in conjunction with the

<sup>7</sup> the monoclinic, cubic, orthorhombic and tetragonal  $ZrO_2$  structure

hydrolysis of  $\text{Th}^{4+}$ . If the thorium hydrolysis species is dominant in solution, the  $\text{ThO}_2(\text{mcr})$  dissolves through an irreversible reaction to  $\text{Th}_x(\text{OH})_y^{4x-y}(\text{aq})$  being in equilibrium with  $\text{Th}(\text{OH})_4(\text{am})$  [Neck 2003]. However, there is an important difference from the cases of Zr and U. The hydrolysis of Zr and U starts at lower pH ( $< 1$ ) than thorium and nevertheless, the solubility of microcrystalline dioxide is measured until pH 2~3 similar to thorium.

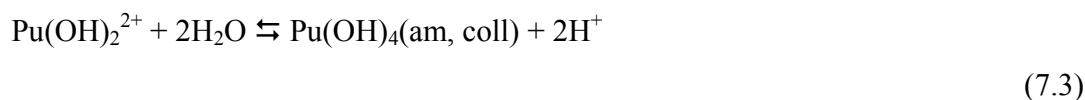
### The solubility of plutonium and its colloid structure

In the present work, the solubility of Pu is investigated at relatively high Pu concentrations ( $> 10^{-5}$  M) limited by the sensitivity of spectroscopy. The solubility product of Pu  $\log K_{\text{sp}}^{\circ}(\text{Pu(IV)}) -58.3 \pm 0.4$ , is many orders of magnitude lower than that of  $\text{Zr}(\text{OH})_4(\text{am})$ .

From the solubility data of  $\text{Pu}(\text{OH})_4(\text{am})$  (Fig. 6.5) and the distribution of Pu mononuclear hydrolysis species (Fig. 7.1 (a)), a model for the Pu(IV) colloid formation mechanism was suggested [Roth 2004]. As seen in Fig. 7.1 (a),  $\text{Pu}(\text{OH})_2^{2+}$  is the predominant mononuclear hydrolysis species in the range of pH 1 - 3. Hydrolysis is a very fast reaction:



and hence, during the preparation of the samples, the distribution of hydrolysis species adapts readily to the pH change. In the present experiments, the formation of the second hydrolysis species coincides with the solubility limit of  $\text{Pu}(\text{OH})_4(\text{am})$ . The solubility data for colloidal Pu(IV) in the present work decreases with pH with a slope of  $-2$  (see Fig. 6.5). This indicates that the data refer to the equilibrium between  $\text{Pu}(\text{OH})_4(\text{am})$  and  $\text{Pu}(\text{OH})_2^{2+}(\text{aq})$  according to



or



However, the species distribution obtained from the corrected hydrolysis constants (Fig. 7.1 (a)) shows that  $\text{Pu}(\text{OH})_2^{2+}$  is not the dominant species below pH 1.4. Bell *et al.* demonstrated that the rate of polymerization or colloid formation depends on the inverse square of the  $[\text{H}^+]$  [Bell 73a]. The concentrations of five components in solution,  $\text{Pu(III)}_{\text{aq}}$ ,  $\text{Pu(IV)}_{\text{aq}}$ ,  $\text{Pu(V)}_{\text{aq}}$ ,  $\text{Pu(VI)}_{\text{aq}}$ , and  $\text{Pu(IV)}_{\text{coll}}$ , were obtained by spectroscopy as a function of time like in the present work. The Pu concentrations were considerably above the solubility limit of Pu(IV) ( $[\text{Pu}] = \text{ca } 0.01 \text{ M}$  at pH 1 ~ pH 1.4) and the polymerization could be observed as a function of time. The concentration of Pu(IV) colloids continuously increased with time and the rate of

formation of Pu(IV) colloids was proportional to the first power of the Pu(IV) concentration and to the inverse square of the acidity. The authors demonstrated that the formation of Pu(IV) colloids followed



However, this kind of interpretation only gives information on the ratio between the stoichiometric coefficients of Pu(IV) and OH<sup>-</sup> and does not allow to distinguish between the mononuclear Pu(OH)<sub>2</sub><sup>2+</sup> and any polynuclear species of the same stoichiometry as actual reactant for colloid formation. The predominant Pu species is expected to be a polynuclear species in concentrated Pu solutions or near the solubility limit similar to the case of Zr. Thus, the formation of Pu(IV) colloids might be considered as a reaction between polynuclear species. Recent investigations by combining XAFS and LIBD demonstrated the formation of Pu(IV) colloids by stacking 8 – fold coordinated Pu units [Roth 2004]. In this work, the XAFS investigation was carried out at the relatively high Pu concentration of 1mM in the pH range of 0 – 1.75. The EXAFS results show that Pu polynuclear species dominate in solutions close to the solubility limit. Furthermore the EXAFS results indicate that the predominant species contain highly asymmetric oxygen coordination which indicates the presence of different Pu-O bond lengths from different coordinated oxygen atoms (-O, -OH, -OH<sub>2</sub>). The authors postulate Pu<sub>x</sub>O<sub>y</sub>(OH)<sub>4x-2y</sub>(H<sub>2</sub>O)<sub>z</sub> (0 ≤ y ≤ 2x) as colloid structure formed by stacking of mononuclear or polynuclear building blocks on top of each other.

According to the LIBD measurements, the Pu(IV) colloids in the present work seem to be very small.

### Redox reactions between plutonium oxidation states

The present investigation indicates that the redox reactions do not follow the disproportionation according to reaction (2.27) of Pu but rather two groups of reactions, Pu(IV)<sub>aq</sub> ⇌ Pu(III)<sub>aq</sub> and Pu(IV)<sub>coll</sub> ⇌ Pu(V)<sub>aq</sub> ⇌ Pu(VI)<sub>aq</sub> which show a dependency on pH, even though these redox reactions contain neither H<sup>+</sup> nor OH<sup>-</sup> as reactant or product. However, hydrolysis, polymerization and colloid formation of Pu(IV) are strongly coupled to the two groups of redox reactions and cause the pH dependence. With increasing pH, the Pu(IV) concentration decreases necessarily through either the colloid formation or reduction (Pu<sup>4+</sup> reacts to Pu<sup>3+</sup>). Under the present experimental conditions, the reduction of Pu(IV) is favored. The formed colloidal or polynuclear species might oxidize to Pu(V) and can dissolve to aquatic Pu(V) species which is in equilibrium with aquatic Pu(VI) species.

With increasing pH, the concentration of Pu(IV) decreases and the concentrations of Pu(V) and Pu(III) increase at steady state. Additionally, upon pH increase, Pu(IV) polynuclear species or colloids become more prominent. As a consequence, the total amount of Pu-oxo components (Pu(IV)(am, coll) + Pu(V) +



Pu(VI)) increases. Even if the pH is low like under the present experimental conditions ( $< \text{pH } 1.5$ ), only a low concentration of  $\text{Pu(IV)}_{\text{aq}}$  is stable in solution. This complicates the investigation of Pu(IV) solutions. Choppin summarized in a review [Chop 83b] that the lower oxidation states are favored at low pH values, whereas the higher oxidation states become more stable as the pH is increased. For example, Pu(III) and Pu(IV) are most prominent in acidic solutions ( $\text{pH} < 1$ ) in contact with air, whereas  $\text{PuO}_2^+$  is more stable at neutral pH under the same conditions.

The redox behavior of Pu in acidic condition depends also on the Pu concentration. At constant pH, a more concentrated solution is closer to the solubility limit of Pu(IV) and contains more Pu(IV) polynuclear species. Accordingly, polynuclear species are in turn oxidized to aquatic Pu(V) and Pu(VI) species. The redox behavior at pH 1.0 or pH 1.2 of series 1 and 5 are examples for this dependency.

### Future perspectives

EXAFS measurements on zirconium prove that polynuclear species are formed close to the solubility limit at millimolar concentrations. Recent technical advances at ANKA lowered the detection limit for Zr down to  $10^{-4}$  M, which allows to clarify the role of polymers at lower concentration and the colloid formation mechanism. For Pu, the EXAFS detection limits are even lower than for Zr and it will be a highly prior task in the near future to extend the study of [Roth 2004] stepwise to  $\geq 5 \cdot 10^{-5}$  M in order to better understand the formation of polynuclear species close to the solubility limit of Pu(IV).

In the present work at  $\text{pH} < 2$  starting with  $\text{Pu(IV)}_{\text{aq}}$ , the redox reactions of Pu show no dependence on the amount of dissolved oxygen in the samples. Instead, the distribution of oxidation states shows the excessive oxidant ( $\text{Pu(IV)}_{\text{aq}} \rightarrow \text{Pu(III)}_{\text{aq}}$ ) which would oxidize  $\text{Pu(IV)}_{\text{coll}}$  to  $\text{Pu(V)}_{\text{aq}}$  without any other oxidizing agents such as dissolved  $\text{O}_2$ . In contrary, in the solubility studies starting with  $\text{PuO}_2(\text{am})$  precipitates [Rai 84; Silv 89; Neck 2005] ( $\text{pH} > 4$ ),  $\text{PuO}_2(\text{am})$  precipitates oxidized and dissolved to  $\text{Pu(V)}_{\text{aq}}$  that may regard to the amount of oxygen present in the solution. The significance of the proposed reaction mechanism (Section 2.2.4) of  $\text{Pu(IV)}_{\text{coll}} \rightleftharpoons \text{Pu(V)}_{\text{aq}}$  is still under discussion and deserves further experimental investigations, especially at a broader pH range.

The hydrolysis constants of Pu(IV) are estimated by the measurement of redox potentials at low pH ( $< 2$ ). From these experiments, only the first and second hydrolysis constants are determined. According to the comparison between the first hydrolysis constants obtained by Metivier *et al.* [Meti 72] and Rabideau *et al.* [Rabi 51; Rabi 57], the present correction seems to be reasonable. However, for the precise determination

of the formation constants ( $\beta'_{1y}$ ,  $y = 2 - 4$ ), the experiments for redox potential measurements should be extended to higher pH, which requires low Pu concentrations. Hence, sensitive detection methods for speciation of Pu are needed. At high pH,  $[\text{Pu(IV)}_{\text{aq}}]$  may be too low to be detected by spectroscopy due to the low solubility of Pu(IV) even if  $[\text{Pu}]_{\text{tot}}$  is high.

Since the speciation of Pu oxidation states is a prerequisite for many investigations of plutonium, a general need for sensitive techniques becomes obvious. The spectroscopic method used in the present work is the most simple and precise method if the concentration of each oxidation state is sufficiently high. For Pu solutions at low concentration, several sensitive methods (e.g. LPAS, TLS and CE-ICP-MS see Chapter 3) are applied for the speciation of Pu. The detection limits of these methods are around  $10^{-7} \sim 10^{-8}$  M. Most recently, an even more sensitive method is applied for the speciation of Pu, which is CE coupled with RIMS (resonance ionisation mass spectrometry, detection limit  $\approx 10^6 \sim 10^7$  atoms). The CE-RIMS is successfully applied for the Pu speciation of about  $6 \cdot 10^9$  atoms of 500  $\mu\text{l}$  [Bürg 2005]. Using such sensitive methods, the investigation of Pu solution chemistry can be extended to the lower concentration and higher pH.

## 8 Appendix

### 8.1 Ionic strength corrections: Specific ion interaction theory (SIT)

Measurements to obtain thermodynamic data are often carried out under different ionic strength conditions. To compare these data, normally the experimental equilibrium data are extrapolated to a selected standard state. According to the definition given by IUPAC (International Union of Pure and Applied Chemistry) [Laff 82], the standard state for a solute  $i$  in a solution is a hypothetical solution, at the standard state pressure (1 bar), in which  $m_i = m^\circ = 1 \text{ mol}\cdot\text{kg}^{-1}$ , and in which the activity coefficient  $\gamma_i$  is unity. Here a method is described which was used in this study for the extrapolation of experimental equilibrium data to zero ionic strength [Lemi 2001].

Two alternative methods can be used to describe the ionic medium dependence of equilibrium constants:

- One method takes into account the individual characteristics of the ionic media by using a medium dependent expression for the activity coefficients of the species involved in the equilibrium reactions. The medium dependence is described by virial or ion interaction coefficients as used in the Pitzer Equations [Pitz 73a] and in the specific ion interaction theory (SIT).
- The other method uses an extended Debye-Hückel expression in which the activity coefficients of reactants and products depend only on the ionic charge and the ionic strength, but it accounts for the medium specific properties by introducing ion pairing between the medium ions and the species involved in the equilibrium reactions.

The SIT is applied for the calculation of activity coefficients. The simple SIT equation is preferred to the more elaborated Pitzer approach, because with the present knowledge and experimental data, it is not possible to evaluate the Pitzer parameters necessary to calculate activity coefficients for Pu(IV) hydrolysis species [Knop 99]. The two basic assumptions in the SIT are described below.

- Assumption 1: The activity coefficient  $\gamma_j$  of an ion  $j$  of charge  $z_j$  in the solution of ionic strength  $I$  is described by the follows equation

$$\log_{10} \gamma_j = -z_j^2 D + \sum_k \varepsilon(j, k, I) m_k \quad (8.1)$$

where  $D$  is the Debye-Hückel term

$$D = \frac{A \sqrt{I}}{1 + B a_j \sqrt{I}} \quad (8.2)$$

and  $I$  is the molal ionic strength

$$I = \frac{1}{2} \sum_i m_i z_i^2 \quad (8.3)$$

$A$  and  $B$  are constants, which are temperature and pressure dependent, and  $a_j$  is an ion size parameter (“distance of closest approach”) for the hydrated ion  $j$ . The Debye-Hückel limiting slope,  $A$ , has a value of  $(0.509 \pm 0.001) \text{ kg}^{1/2} \cdot \text{mol}^{1/2}$  at  $25^\circ\text{C}$  and 1 bar. The term  $B a_j$  in the denominator of the Debye-Hückel term has been assigned a value of  $B a_j = 1.5 \text{ kg}^{1/2} \cdot \text{mol}^{1/2}$  at  $25^\circ\text{C}$  and 1 bar, as proposed by Scatchard [Scat 76] and accepted by Ciavatta [Ciav 80]. This value has been found to minimize, for several species, the ionic strength dependence of  $\varepsilon(j, k, I)$  between  $I = 0.5$  and  $I = 3.5$  m. The ion interaction coefficients at  $25^\circ\text{C}$  listed in Table 8.1 have to be used with  $B a_j = 1.5 \text{ kg}^{1/2} \cdot \text{mol}^{1/2}$ .

The summation in Eq. 8.1 extends over all ions  $k$  present in solution. Their molality is denoted by  $m_k$ , and the specific ion interaction parameters  $\varepsilon(j, k, I)$ , in general depend only slightly on the ionic strength. The concentrations of the ions of the ionic medium are often very much larger than those of the reacting species. Hence, the ionic medium ions will make the main contribution to the value of  $\log \gamma_j$  for the reacting ions. This fact often makes it possible to simplify the summation,  $\sum_k \varepsilon(j, k, I) m_k$ , so that only ion interaction coefficients between the participating ionic species and the ionic medium ions are included.

- Assumption 2: The ion interaction coefficients  $\varepsilon(j, k, I)$  are zero for ions of the same charge sign and for uncharged species. The rationale behind this is that  $\varepsilon$  which describes specific short-range interactions must be small for ions of the same charge since they are usually far from one another due to electrostatic repulsion. This holds to a lesser extent also for uncharged species.

Table 8.1 The ion interaction coefficients at 25°C.

j	K	$\epsilon(j, k)$
H <sup>+</sup>	ClO <sub>4</sub> <sup>-</sup>	0.14 ± 0.02 <sup>1)</sup>
H <sup>+</sup>	Cl <sup>-</sup>	0.12 ± 0.01 <sup>1)</sup>
OH <sup>-</sup>	Na <sup>+</sup>	0.04 ± 0.01 <sup>1)</sup>
Pu <sup>4+</sup>	Cl <sup>-</sup>	0.4 ± 0.1 <sup>2)</sup>
Pu(OH) <sup>3+</sup>	Cl <sup>-</sup>	0.2 ± 0.1 <sup>2)</sup>
Pu(OH) <sub>2</sub> <sup>2+</sup>	Cl <sup>-</sup>	0.1 ± 0.1 <sup>2)</sup>
Pu(OH) <sub>3</sub> <sup>+</sup>	Cl <sup>-</sup>	0.05 ± 0.1 <sup>2)</sup>
Pu(OH) <sub>4</sub>	Cl <sup>-</sup>	0
NpO <sub>2</sub> <sup>+</sup>	Cl <sup>-</sup>	0.09 ± 0.05 <sup>3)</sup>
UO <sub>2</sub> <sup>2+</sup>	Cl <sup>-</sup>	0.21 ± 0.05 <sup>3)</sup>
Am <sup>3+</sup>	Cl <sup>-</sup>	0.23 ± 0.02 <sup>3)</sup>

1) from the NEA-TDB [Lemi 2001].

2) Estimated in [Knop 99] according to the analogies and systematic pointed out in the NEA-TDB [Lemi 2001].

3) The values are taken as an analog to Pu due to the lack of data for Pu from the NEA-TDB [Lemi 2001].

## 8.2 Tables of zirconium investigation

Table 8.2 Summary of coulometric titration (CT)-LIBD series examined in the present work (Fig. 5.6).

series	log [Zr]	pH at CT start	pH colloid formation onset
1	-2.91	1.03	2.95
2	-2.97	1.00	3.00
3	-3.25	1.33	3.20
4	-3.41	1.30	3.21
5	-3.94	1.48	3.37

6	-4.59	1.98	3.90
7	-4.99	1.89	3.93
8	-5.27	2.53	4.66
9	-6.06	3.04	5.56
10	-6.46 <sup>1)</sup>	1.94	6.75
11	-6.96 <sup>1)</sup>	4.01	7.23
12	-7.11 <sup>1)</sup>	4.53	8.04
13	-7.61 <sup>1)</sup>	4.94	8.86

- 1) The concentrations can not be directly determined by ICP-MS because of the interference of concentrated Na<sup>+</sup> ion (0.5M). The values are calculated from the ICP-MS results of the stock solutions with concentrations of ca. 1·10<sup>-4</sup> M for series 10 and 11 and ca. 3·10<sup>-6</sup> M for 12 and 13.

Table 8.3 Summary of samples examined by XAFS in this study (Fig. 4.1).

ID	sample description	Colloids present
<b>a</b>	concentrated 'micro-crystalline' log [Zr]=-1; pH 0.2	~ 10 nm
<b>b</b>	reference colloids	Yes
<b>c</b>	monoclinic ZrO <sub>2</sub>	-
<b>d</b>	log [Zr]=-2.97; pH 1.0	No
<b>e</b>	log [Zr]=-2.97; pH 2.0	No
<b>f</b>	log [Zr]=-2.97; pH 2.8	No
<b>g</b>	log [Zr]=-2.97; pH 3.0	Yes
<b>h</b>	log [Zr]=-2.97; pH 3.1	Yes
<b>i</b>	log [Zr]=-2.97; pH 3.3	Yes

Table 8.4 Data range and metric parameters extracted by least-squares fit analysis of Zr K EXAFS spectra shown in Fig. 5.9 and Fig. 5.10. Values in parentheses are statistical uncertainties, except where f is given; in this case, the parameter is held constant during the fit procedure. Values in italics and square brackets are from the XRD crystal structure reported in [Gual 96].

ID	fit range R- $\Delta$ ( $\text{\AA}$ )	shell	R ( $\text{\AA}$ )	N	$\sigma^2$ ( $\text{\AA}^2$ )	$\Delta E$ (eV)	R-factor
<b>a</b>	0.07 - 3.90	O	2.189(8)	8.8(9)	0.009(1)	1(1)	0.037
		Zr	3.59(2)	1.8(2)	0.005(f)	2(4)	
<b>b</b>	1.10 - 3.93	O	2.13(1)	7.2	0.011(1)	0(2)	0.033
		Zr	3.50(3)	4(2)	0.012(4)	5(4)	
<b>c</b>	0.86 - 3.19	O	2.16(2) <i>[2.168]</i>	8.4 (1.5) <i>[7]</i>	0.011(2)	-5(2)	0.018
		Zr	3.46(1) <i>[3.45]</i>	6.0(1.3) <i>[7]</i>	0.006(1)	-7(2)	
<b>d</b> pH 1.0	1.23 - 2.33	O	2.14(1)	3.2(5)	0.000(1) <sup>a</sup>	-2(2) <sup>a</sup>	0.007
		O	2.28(2)	3.4(4)	0.000(1) <sup>a</sup>	-2(2) <sup>a</sup>	
<b>e</b> pH 2.0	1.10 - 3.44	O	2.210(5)	8.8(9)	0.0053(6)	4.4(9)	0.013
		Zr	3.39(2)	2.2(9)	0.007(f)	8(4)	
<b>f</b> pH 2.8	0.86 - 3.44	O	2.201(5)	8.9(7)	0.0044(6)	3(1)	0.022
		Zr	3.43(2)	1.2(9)	0.004(3)	17(6)	
<b>g</b> pH 3.0	0.86 - 3.4	O	2.200(8)	11(1)	0.0065(9)	2(1)	0.034
		Zr	3.38(5)	1.0(4)	0.005(f)	11(10)	
<b>h</b> pH 3.1	0.61 - 3.44	O	2.200(6)	10.2(9)	0.0062(7)	-5(1)	0.021
		Zr	3.36(3)	3(2)	0.011(4)	-1(6)	
<b>i</b> pH 3.3	0.86 - 3.4	O	2.21(1)	10(1)	0.006(1)	4(2)	0.044
		Zr	3.42(7)	1(2)	0.006(8)	10(14)	

<sup>a</sup> Defined as a global parameter for both shells

### 8.3 Coulometric titration of the Pu(IV) solution

The starting solution for coulometric pH titration is prepared with a freshly electrolyzed Pu(IV) stock solution diluted by 0.5 M (H/Na)Cl solution at  $[\text{Pu}]_{\text{tot.}} = 1.01 \cdot 10^{-5}$  M and pH 1.3 in 40 ml volume (Fig. 8.1 (a)). The same experimental equipment for coulometric titration is used as for the Zr experiments (see Fig. 4.2). For the test of coulometric pH titration, a constant current 50  $\mu\text{A}$  is applied for about 15 hours, that is relatively small being able to reduce only about  $7 \cdot 10^{-4}$  M  $\text{H}^+$  concentration in 40 ml. However, after the application of the current, all Pu oxidation states are reduced to Pu(III) (Fig. 8.1 (b)). Due to the redox sensitivity of Pu, the coulometric pH titration can not be applied for Pu experiments.

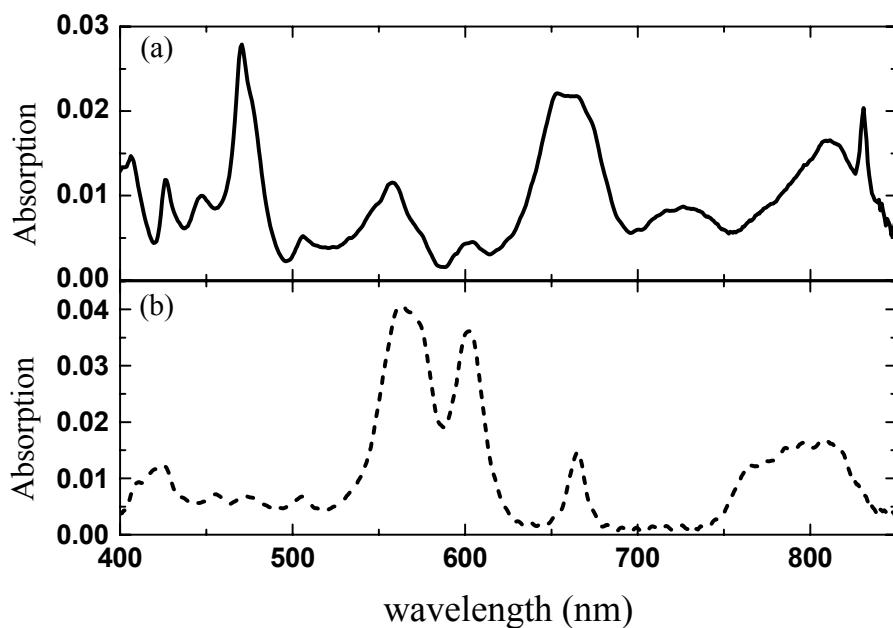


Fig. 8.1 The absorption spectra of Pu sample, 40ml  $[\text{Pu}]_{\text{tot.}} = 1.01 \cdot 10^{-5}$  M in home made quartz reactor (a) before coulometric pH titration at pH 1.3 (b) after the application of coulometric pH titration with a current of 0.05mA for about 15 hours, pH 1.3



#### 8.4 The absorption spectrum of Pu(IV) colloids

For more than several decades, the properties of the intrinsic Pu(IV) colloids have been studied in detail. The early works focused on the identification of the Pu(IV) colloids by their extinction spectrum (see Fig. 8.2), which differs from that of mononuclear Pu(IV) hydrolysis species (see Fig. 3.1). The extinction spectrum of colloids<sup>8</sup> shows the strong increase in UV region due to Rayleigh scattering and the characteristic absorption at 620 nm. The colloid absorption obeys Beer's law (3.1), allowing a direct quantification of the colloid concentration.

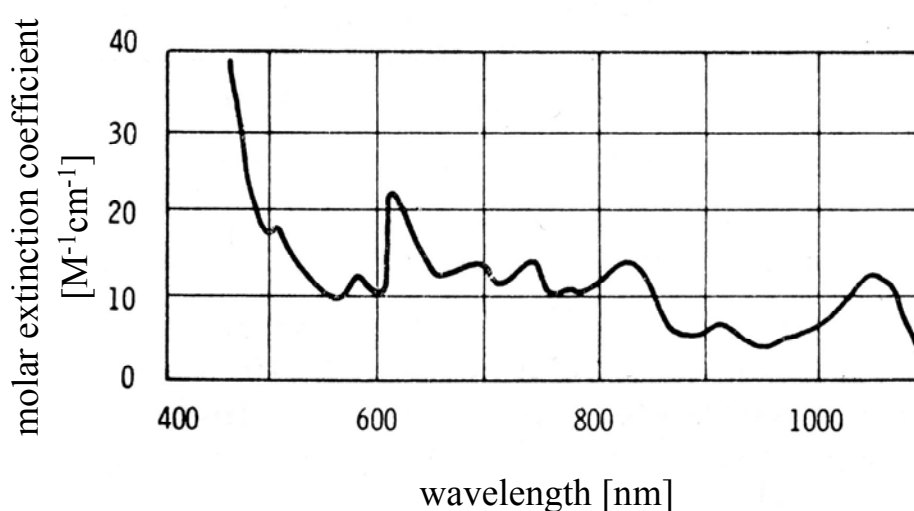


Fig. 8.2 The absorption spectrum of Pu(IV) colloids [Clev 79].

<sup>8</sup> extinction = sum of absorption and scattering

### 8.5 LIBD system for the Pu investigation

Fig. 8.3 shows the calibration curves with reference colloids of the laser system which is applied for Pu investigation in the control area. The BDP is plotted as a function of the laser pulse energy,  $E$  [mJ]. The threshold  $E_T$  [mJ] of the so called ‘s-curve’ increases with decreasing particle size (polystyrene reference colloids). The particle number densities are  $10^8$  particles/cm<sup>3</sup>. Comparing to Fig. 3.13, the calibration curves of the laser system used for the Zr investigation, the threshold energy  $E_T$  [mJ] for each particle size is slightly lower due to different focusing optics.

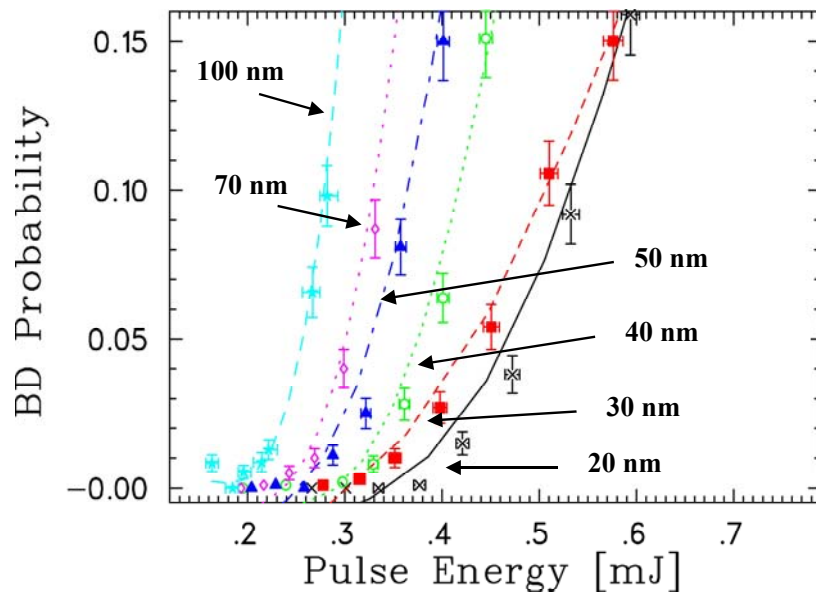


Fig. 8.3 The BDP is plotted as a function of the laser pulse energy,  $E$  [mJ]. The threshold  $E_T$  [mJ] of the so called ‘s-curve’ increases with decreasing particle size (polystyrene reference colloids). The particle number densities are  $1 \cdot 10^8$  particles/cm<sup>3</sup>.

## 8.6 Tables of Pu oxidation state distribution

Table 8.5 Concentrations, the distribution of the Pu oxidation states and the existence of colloids to be detectable using LIBD (Series 1 in Fig. 6.7 and Fig. 6.10).

pH	[Pu] <sub>tot</sub> [M]	time [d]	Pu(III) <sub>aq</sub> [%]	Pu(IV) <sub>aq</sub> [%]	Pu(V) <sub>aq</sub> [%]	Pu(VI) <sub>aq</sub> [%]	Pu(IV) <sub>coll</sub> [%]	coll	Pu(III)+Pu(IV)
0.48	1.7·10 <sup>-3</sup> M	stock sol.	4.96	94.20	2.79	0.78	-2.73	×	
	3.3·10 <sup>-4</sup> M	1	11.30	79.49	u.d.	0.97	8.24	×	90.79
		3	14.84	73.49	u.d.	2.22	9.45	×	88.33
		6	19.55	68.92	u.d.	3.77	7.75	×	88.47
		8	21.70	66.79	u.d.	4.76	6.76	×	88.49
		10	23.70	64.48	u.d.	5.92	6.53	×	88.18
		29	35.69	51.82	u.d.	8.45	4.05	×	87.51
		49	35.11	51.25	u.d.	7.87	5.77	×	86.36
114	38.88	54.07	u.d.	7.07	-0.03	×	92.95		
0.66	1.7·10 <sup>-3</sup> M	stock sol.	4.96	94.20	2.79	0.78	-2.73	×	
	3.4·10 <sup>-4</sup> M	1	13.50	70.67	u.d.	2.04	13.79	○	84.17
		3	25.03	58.22	u.d.	6.18	10.57	×	83.25
		6	34.37	48.03	u.d.	9.09	8.51	×	82.40
		8	36.70	45.22	u.d.	10.29	7.79	×	81.92
		10	38.33	40.99	u.d.	10.80	9.88	×	79.32
		29	45.00	35.63	u.d.	12.03	7.34	×	80.63
		49	43.29	36.32	u.d.	11.34	9.04	n.m.	79.61
114	46.45	39.87	u.d.	10.92	2.76	×	86.32		
0.83	4.9·10 <sup>-3</sup> M	stock sol.	9.43	85.02	2.92	2.61	u.d.	○	
	4.0·10 <sup>-4</sup> M	1	28.63	52.36	3.08	10.57	5.36	×	80.99
		2	39.61	38.38	5.09	14.21	2.70	n.m.	77.99
		6	48.56	26.11	4.81	16.12	4.39	×	74.67
		8	49.45	24.88	4.39	16.21	5.06	×	74.33
		14	47.03	27.64	5.37	16.10	3.87	×	74.67
		34	48.61	27.00	4.25	15.88	4.27	n.m.	75.61
		98	50.03	28.5	3.48	15.57	2.43	×	78.53
1.01	4.9·10 <sup>-3</sup> M	stock sol.	9.43	85.02	2.92	2.61	u.d.	○	
	3.9·10 <sup>-4</sup> M	1	50.31	23.58	6.79	16.96	2.36	×	73.89
		2	54.28	18.37	10.01	17.26	0.08	n.m.	72.65
		6	56.99	14.53	8.99	17.06	2.44	×	71.52
		8	57.08	14.68	9.55	16.95	1.74	×	71.76
		14	56.17	15.57	8.11	16.72	3.43	×	71.74
		34	57.23	16.21	7.73	17.05	1.78	n.m.	73.44
		98	58.54	17.42	6.98	16.83	0.23	×	75.96
1.21	3.5·10 <sup>-3</sup> M	stock sol.	1.03	89.91	4.22	0.21	4.63	×	
	3.3·10 <sup>-4</sup> M	1	51.52	18.55	10.16	16.97	2.81	×	70.07

		3	57.90	10.11	12.92	15.69	3.38	×	68.01
		9	57.64	10.21	14.86	15.54	1.75	n.m.	67.85
		15	58.48	8.78	11.75	15.37	5.61	×	67.26
		29	58.38	10.16	14.11	15.46	1.89	×	68.54
		88	61.39	9.37	14.87	14.62	-0.25	n.m.	70.76
		92	60.83	11.32	13.72	15.06	-0.93	n.m.	72.15
The pH 1.21 sample at 92 days acidified to pH 0.82									
0.82	3.3·10 <sup>-4</sup> M	92(0)	61.49	11.71	15.46	15.66	-4.32	n.m.	73.20
		93(1)	59.38	14.47	9.55	15.91	0.69	n.m.	73.85
		94(2)	57.30	18.50	6.28	16.30	1.62	n.m.	75.80
		107(15)	51.32	27.44	2.62	15.60	3.02	×	78.76
		128(36)	52.60	26.23	5.15	15.26	0.76	×	78.83
		191(99)	55.13	28.3	5.04	14.28	-2.75	×	83.43
		287(195)	55.11	28.81	5.14	14.21	-3.27	n.m.	83.92

[Pu]<sub>tot</sub> are measured by LSC

u.d. : under detection limit

[Pu(IV)<sub>coll</sub>] = [Pu]<sub>tot(LSC)</sub> - [Pu(III)<sub>aq</sub>] - [Pu(IV)<sub>aq</sub>] - [Pu(V)<sub>aq</sub>] - [Pu(VI)<sub>aq</sub>]

coll: ○ indicates that the sample has colloids which can be detected by LIBD

× indicates that the sample has no colloid which can be detected by LIBD

n.m. indicates "no measurement"

■ :the time of Eh measurements

Table 8.6 Concentrations, the distribution of the Pu oxidation states and the existence of colloids to be detectable using LIBD (Series 2 in Fig. 6.11).

pH	[Pu] <sub>tot</sub> [M]	time [d]	Pu(III) <sub>aq</sub> [%]	Pu(IV) <sub>aq</sub> [%]	Pu(V) <sub>aq</sub> [%]	Pu(VI) <sub>aq</sub> [%]	Pu(IV) <sub>coll</sub> [%]	coll	Pu(III)+Pu(IV)	
0.39	4.3·10 <sup>-3</sup> M	stock sol.	10.91	87.20	0.32	3.99		×		
		3.1·10 <sup>-4</sup> M	0	9.16	89.42	1.69	4.21	-4.47	○	
			3	18.59	77.90	u.d.	5.29	-1.78	n.m.	
			5	17.34	75.89	u.d.	6.15	0.62	○	
			26	33.91	58.22	3.26	9.69	-5.08	n.m.	
			31	36.47	54.54	u.d.	8.81	0.19	×	
			61	39.3	54.64	1.15	7.12	-2.18	n.m.	
0.43	1.2·10 <sup>-3</sup> M	stock sol.	5.72	88.90	5.14	0.19	0		n.m.	
		2.9·10 <sup>-4</sup> M	0	7.22	65.66	u.d.	0.12	27.00	○	72.88
			3	14.87	82.17	u.d.	1.72	1.24	○	97.04
			5	16.24	79.15	u.d.	3.15	0.46	n.m.	95.39
			7	20.22	76.70	u.d.	4.58	-1.50	n.m.	96.92
			10	23.06	71.67	u.d.	4.67	0.61	n.m.	94.73
			12	22.90	70.42	u.d.	5.27	1.42	○	93.32
			14	25.65	68.06	u.d.	5.63	0.67	n.m.	93.71
			19	26.25	66.48	u.d.	6.44	0.84	n.m.	92.73
			33	31.80	61.59	u.d.	7.81	-1.20	○	93.39
			47	33.32	58.55	u.d.	7.54	0.59	×	91.87
			75	35.00	56.35	u.d.	7.94	0.71	○	91.35
		101	35.87	55.8	u.d.	7.96	0.37	○	91.67	

0.77	4.3·10 <sup>-3</sup> M	stock sol.	8.04	91.20	0.29	3.07	-2.60	×	
	3.2·10 <sup>-4</sup> M	0	28.97	62.19	u.d.	3.62	5.21	○	91.16
		1	39.51	47.91	2.93	6.83	2.82	○	87.42
		4	53.24	28.30	u.d.	9.26	9.20	n.m.	81.54
		6	53.99	27.06	3.27	11.30	4.38	○	81.05
		27	64.76	22.19	13.50	8.18	-8.63	n.m.	86.95
		32	65.39	22.23	9.55	7.19	-4.36	○	87.62
		62	69.30	22.31	6.90	6.01	-4.54	○	91.61
0.94	4.3·10 <sup>-3</sup> M	stock sol.	8.04	91.20	0.29	3.07	-2.60	×	
	3.2·10 <sup>-4</sup> M	0	14.54	69.26	4.14	6.67	5.38	×	83.80
		1	41.00	35.06	7.89	15.67	0.38	n.m.	76.06
		4	55.51	16.93	u.d.	15.79	11.77	n.m.	72.44
		6	52.84	17.37	5.29	17.47	7.03	×	70.21
		27	58.02	16.00	10.38	15.71	-0.10	×	74.02
		32	57.98	16.48	9.30	15.45	0.80	×	74.46
		62	61.28	17.14	8.57	14.62	-1.61	×	78.42
1.18	4.3·10 <sup>-3</sup> M	stock sol.	3.75	97.05	u.d.	1.29	-2.09	×	
	3.2·10 <sup>-4</sup> M	0	32.63	40.38	9.13	14.44	3.41	○	73.01
		1	52.23	17.54	15.86	17.83	-3.48	○	69.77
		5	59.40	6.98	u.d.	13.53	20.09	n.m.	66.38
		7	55.89	8.66	9.14	15.39	10.92	○	64.55
		28	55.22	8.99	18.47	15.18	2.14	○	64.21
		33	57.03	9.22	15.32	15.62	2.81	○	66.25
		63	58.98	9.79	15.23	15.68	0.32	×	68.77

[Pu]<sub>tot</sub> are measured by LSC

u.d. : under detection limit

[Pu(IV)<sub>coll</sub>] = [Pu]<sub>tot(LSC)</sub> - [Pu(III)<sub>aq</sub>] - [Pu(IV)<sub>aq</sub>] - [Pu(V)<sub>aq</sub>] - [Pu(VI)<sub>aq</sub>]

coll: ○ indicates that the sample has colloids which can be detected by LIBD

× indicates that the sample has no colloid which can be detected by LIBD

n.m. indicates "no measurement"

■ :the time of Eh measurements

Table 8.7 Concentrations, the distribution of the Pu oxidation states and the existence of colloids to be detectable using LIBD (Series 3 in Fig. 6.3 (a))

pH	[Pu] <sub>tot</sub> [M]	Time [d]	Pu(III) <sub>aq</sub> [%]	Pu(IV) <sub>aq</sub> [%]	Pu(V) <sub>aq</sub> [%]	Pu(VI) <sub>aq</sub> [%]	Pu(IV) <sub>coll</sub> [%]	coll
0.3	8.2·10 <sup>-5</sup> M	0	22.72	66.92	u.d.	3.60	6.76	×
1.04	8.3·10 <sup>-5</sup> M	0	11.54	81.72	u.d.	4.09	2.65	×
1.13	8.1·10 <sup>-5</sup> M	0	9.61	77.62	u.d.	4.07	8.69	○
1.23	9.0·10 <sup>-5</sup> M	0	8.94	45.87	u.d.	4.48	40.71	○

[Pu]<sub>tot</sub> are measured by LSC

u.d. : under detection limit

[Pu(IV)<sub>coll</sub>] = [Pu]<sub>tot(LSC)</sub> - [Pu(III)<sub>aq</sub>] - [Pu(IV)<sub>aq</sub>] - [Pu(V)<sub>aq</sub>] - [Pu(VI)<sub>aq</sub>]

coll: ○ indicates that the sample has colloids which can be detected by LIBD

× indicates that the sample has no colloid which can be detected by LIBD

Table 8.8 Concentrations, the distribution of the Pu oxidation states and the existence of colloids to be detectable using LIBD (Series 4).

pH	[Pu] <sub>tot.</sub> [M]	time [d]	Pu(III) <sub>aq</sub> [%]	Pu(IV) <sub>aq</sub> [%]	Pu(V) <sub>aq</sub> [%]	Pu(VI) <sub>aq</sub> [%]	Pu(IV) <sub>coll</sub> [%]	coll	Pu(III)+Pu(IV)	
1.38	1.3·10 <sup>-3</sup> M	stock sol.	2.09	95.60	3.72	u.d.	-1.41	×		
		3.1·10 <sup>-4</sup> M	1	38.81	31.56	4.88	14.13	10.62	○	70.37
			2	48.31	21.58	7.56	16.62	5.85	○	69.89
			5	52.66	14.25	12.35	15.39	5.35	×	66.91
			8	53.78	11.63	14.61	14.51	5.48	n.m	65.41
			103	57.00	11.11	15.96	16.76	-0.84	n.m	68.11
1.58	1.3·10 <sup>-3</sup> M	stock sol.	2.09	95.60	3.72	u.d.	-1.41	×		
		2.9·10 <sup>-4</sup> M	1	47.31	16.25	11.06	15.02	10.36	×	63.56
			2	48.45	10.20	14.94	12.68	13.73	×	58.65
			5	50.41	8.40	19.25	10.96	10.99	×	58.81
			8	52.20	7.31	21.86	10.30	8.33	n.m	59.51
			103	40.13	15.68	20.55	9.29	14.34	n.m	55.81
1.59	3.5·10 <sup>-3</sup> M	stock sol.	1.03	89.91	4.22	0.21	4.63	×		
		3.2·10 <sup>-4</sup> M	1	41.52	21.73	8.07	15.54	13.15	×	63.25
			3	45.61	11.20	16.32	12.61	14.26	×	56.81
			4	49.42	13.48	16.78	14.26	6.06	×	62.90
			7	51.17	11.35	19.74	13.30	4.44	×	62.52
			10	51.75	9.80	21.37	12.13	4.94	n.m	61.55
105	47.08	9.30	21.43	8.83	13.36	n.m	56.38			

[Pu]<sub>tot.</sub> are measured by LSC

u.d. : under detection limit

[Pu(IV)<sub>coll</sub>] = [Pu]<sub>tot.(LSC)</sub> - [Pu(III)<sub>aq</sub>] - [Pu(IV)<sub>aq</sub>] - [Pu(V)<sub>aq</sub>] - [Pu(VI)<sub>aq</sub>]

coll: ○ indicates that the sample has colloids which can be detected by LIBD

×

n.m. indicates "no measurement"

■ :the time of Eh measurements

Table 8.9 Concentrations, the distribution of the Pu oxidation states and the existence of colloids to be detectable using LIBD (Series 5 in Fig. 6.3 (b) and Fig. 6.8).

pH	[Pu] <sub>tot.</sub> [M]	Time [d]	Pu(III) <sub>aq</sub> [%]	Pu(IV) <sub>aq</sub> [%]	Pu(V) <sub>aq</sub> [%]	Pu(VI) <sub>aq</sub> [%]	Pu(IV) <sub>coll</sub> [%]	coll
0.37	1.2·10 <sup>-5</sup> M	1	2.38	86.44	u.d.	0.06	11.11	○
0.65	1.2·10 <sup>-5</sup> M	1	22.23	54.64	u.d.	u.d.	23.13	○
0.70	1.2·10 <sup>-5</sup> M	1	6.97	72.85	u.d.	0.34	19.85	○
1.07	1.3·10 <sup>-5</sup> M	1	4.41	69.21	3.98	0.62	21.78	○
		4	8.98	62.76	5.32	1.13	21.81	
		5	13.07	59.45	2.50	1.07	23.91	

		8	17.24	50.24	2.48	1.09	28.94	
		11	19.45	47.32	3.24	1.24	28.75	
		29	25.12	40.79	0.75	1.83	31.51	
		68	32.44	30.71	2.07	3.12	31.66	
1.22	1.2·10 <sup>-5</sup> M	1	8.70	59.19	3.04	1.59	27.49	○
		2	14.31	54.80	2.59	1.75	26.55	
		5	18.94	46.83	1.36	1.83	31.04	
		8	22.60	43.25	3.59	1.83	28.73	
		26	30.81	34.96	2.66	2.11	29.46	
		65	38.37	21.46	4.11	2.69	33.36	
1.53	1.2·10 <sup>-5</sup> M	1	-	39.06	15.56	u.d.	45.38	○
		2	1.38	38.72	13.08	u.d.	46.83	
		5	1.00	36.15	13.33	u.d.	49.51	
		8	1.53	35.30	13.76	u.d.	49.41	
		26	2.39	34.96	13.08	u.d.	49.57	
		65	3.57	30.68	11.97	u.d.	53.78	
2.13	1.1·10 <sup>-5</sup> M	1	4.30	37.39	15.77	u.d.	42.55	○
		3	11.62	32.70	13.60	u.d.	42.07	
		6	19.19	28.02	15.77	u.d.	37.03	
		23	30.36	21.35	16.13	u.d.	32.16	
		64	20.54	18.47	20.63	u.d.	40.36	
		64	19	37	20	u.d.	24	

[Pu]<sub>tot.</sub> are measured by LSC

u.d. : under detection limit

$[Pu(IV)_{coll}] = [Pu]_{tot.(LSC)} - [Pu(III)_{aq}] - [Pu(IV)_{aq}] - [Pu(V)_{aq}] - [Pu(VI)_{aq}]$

coll: ○ indicates that the sample has colloids which can be detected by LIBD

× indicates that the sample has no colloid which can be detected by LIBD

■ :the time of CE measurements

## 8.7 List of abbreviations

AFM	:	atomic force microscopy
ANKA	:	Angströmquelle Karlsruhe
BDP	:	breakdown probability
CE	:	capillary electrophoresis
EOF	:	electroosmotic flow
EXAFS	:	extended X-ray absorption fine structure
FFF	:	field flow fractionation
FT	:	Fourier transform
FWHM	:	full width at half maximum height
ICP-MS	:	inductively coupled plasma mass spectrometry
IUPAC	:	international union of pure and applied chemistry
LCW	:	liquid core waveguide
LCW-DAS	:	LCW coupled with diode-array spectrometer

LIBD	: laser induced breakdown detection
LPAS	: laser induced photoacoustic spectroscopy
LSC	: liquid scintillation counter
PAS	: photoacoustic spectroscopy
PCS	: photon correlation spectroscopy
PDS	: photothermal deflection spectroscopy
PFA	: perflouroalkoxy
PSD	: particle size distribution
RIMS	: resonance ionization mass spectrometry
SEM	: scanning electron microscopy
SHE	: standard hydrogen electrode
SIT	: specific ion interaction theory
SPC	: single particle counter
TEM	: transmission electron microscopy
TLS	: thermal lensing spectroscopy
TTA	: thenoyl trifluoroacetone
UWXAFS	: university of Washington XAFS analysis program
WL	: white line
XAFS	: X-ray absorption fine structure
XANES	: X-ray absorption near-edge structure
XPS	: X-ray photoelectron spectroscopy
XRD	: X-ray diffraction

## 8.8 List of symbols

$A$	: absorption
$a_i$	: activity of elements $i$
$a_j$	: ion size parameter in Deby-Hückel term
$a_w$	: activity of water
$c$	: concentration [M]
$C$	: the parameter of colloid number density
$D$	: Deby-Hückel term
$d_{\text{An-OH}}$	: distance between the centers of actinide ion and $\text{OH}^-$ ligand ion
$D_i$	: particle diameter
$e$	: charge of an electron ( $1.602 \cdot 10^{-19}$ C)
$E$	: energy
$E_h$	: relative redox potential to the standard hydrogen electrode (SHE)
$E_h^\circ$	: standard redox potential to the standard hydrogen electrode (SHE)



${}^{\text{el}}E_{\text{An-OH}}$	: electrostatic interaction energy between the actinide ion and OH <sup>-</sup> ligand
$E_{\text{T}}$ [mJ]	: threshold energy in s-curve investigation
$F$	: Faraday constant (96487 C mol <sup>-1</sup> )
$f_{\text{H}_2}$	: fugacity of H <sub>2</sub>
$F_i(\mathbf{k})$	: backscattering amplitude from neighboring atom type $i$ in Section 3.3
$\Delta_f G_m^\circ$	: molar standard Gibbs energy for formation
$h$	: Planck's constant
$I$	: ionic strength
$\mathbf{k}$	: wave vector
$K'$	: equilibrium constant of any reaction in a given medium
$K'_{\text{IV}}$	: equilibrium constant of reaction (2.27) in a given medium
$K'_{\text{V}}$	: equilibrium constant of reaction (2.28) in a given medium
$K'_{\text{sp}}$	: solubility product in a given medium
$K'_{\text{xy}}$	: hydrolysis constant in a given medium
$K^\circ$	: equilibrium constant of any reaction at infinite dilution
$K^\circ_{\text{IV}}$	: equilibrium constant of reaction (2.27) at infinite dilution
$K^\circ_{\text{sp}}$	: solubility product at infinite dilution
$K^\circ_{\text{V}}$	: equilibrium constant of reaction (2.28) at infinite dilution
$K^\circ_{\text{xy}}$	: hydrolysis constant at infinite dilution
$l$	: beam pathlength [cm] in absorption spectroscopy
$L_{\text{d}}$	: capillary length between sample introduction and detection in CE system
$L_{\text{t}}$	: total capillary length in Section 3.2
$m_i$	: molal concentration
$n$	: mole number
$N^{(i)}$	: colloid number density of particle size $i$
$N_i$	: $i$ -th coordination number in Section 3.3
$\text{pe}$	: $-\log a_{\text{e}^-}$ defined in analogy with pH ( $= -\log a_{\text{H}^+}$ )
$\text{pH}$	: $\log [\text{H}^+]$
$P_{\text{H}_2}$	: partial pressure of H <sub>2</sub> gas
$P_{\text{O}_2}$	: partial pressure of O <sub>2</sub> gas
$\text{Pu(III)}_{\text{aq}}$	: trivalent plutonium aquatic species ( $= \text{Pu}^{3+}$ in present experimental condition)
$\text{Pu(IV)}_{\text{aq}}$	: tetravalent plutonium aquatic species (ion and its hydrolysis species in present experimental condition)
$\text{Pu(IV)}_{\text{coll}}$	: tetravalent plutonium colloid
$\text{Pu}^{4+}$	: tetravalent plutonium "free ion"
$\text{Pu(V)}_{\text{aq}}$	: pentavalent plutonium aquatic species ( $= \text{PuO}_2^+$ in present experimental condition)

$\text{Pu(VI)}_{\text{aq}}$	: hexavalent plutonium aquatic species (= $\text{PuO}_2^{2+}$ in present experimental condition)
$R$	: gas constant ( $8.314 \text{ Jmol}^{-1}\text{K}^{-1}$ )
$r_i$	: ionic radii of ion $i$
$R_i$	: distance between absorbing atom and atom in $i$ -th coordinated shell in Section 3.3
$S_0^2$	: amplitude reduction factor in Section 3.3
$T$	: temperature in degree Kelvin
$t_{1/2}$	: half life
$t_m$	: time interval between the beginning of the separation and the passage of an analyte zone through the point of detection (migration time)
$U [\text{V}]$	: separation potentials in Section 3.2
$V_{\text{eff}}$	: effective focal volume
$v_{\text{EOF}}$	: magnitude and direction of the EOF
$v_{\text{obs}}$	: observed velocity of migration
$Z_{\text{An}}$	: effective charge of the actinide ion
$Z_i$	: effective charge of ion $i$
$\beta'_{xy}$	: formation constant of hydrolysis species in a given medium
$\beta^\circ_{xy}$	: formation constant of hydrolysis species at infinite dilution
$\epsilon$	: molar extinction coefficient [ $\text{M}^{-1}\text{cm}^{-1}$ ]
$\epsilon_{\text{rel}}$	: dielectric constant, the ratio of the permittivity of a substance to that of vacuum
$\epsilon(j,k,l)$	: specific ion interaction parameter in SIT theory
$\Phi_i(k)$	: total phase shift experienced by photoelectron in Section 3.3
$\gamma_i$	: activity coefficient for species $i$
$\eta$	: dynamic viscosity of the electrolyte medium
$\lambda$	: wavelength [nm]
$\lambda_i$	: electron mean free path in Section 3.3
$\mu$	: X-ray absorption coefficient in Section 3.3
$\mu_{\text{EOF}}$	: mobility of electroosmotic flow
$\mu_{\text{ion}}$	: inherent ionic mobility of the ionic analyte
$\mu_{\text{obs}}$	: observed electrophoretic mobilities in Section 3.2
$\nu$	: frequency
$\sigma_i$	: Debye-Waller factor due to thermal vibration and static disorder in Section 3.3
$\zeta$	: zeta potential [V]

## 8.9 List of Figures

Fig. 1.1 The radiotoxicity inventory of one ton spent fuel in a pressurized water reactor.....	1
Fig. 2.1 Oxidation states of the light actinide elements and their electron configuration ( <i>f</i> electrons).....	6
Fig. 2.2 The Eh-pH correlation found in waters in the natural environment. ....	8
Fig. 2.3. The correlation of $\log \beta_{1y}$ , of actinide hydroxide complexes with ${}^{el}E_{An-OH}$ between the actinide ion and OH <sup>-</sup> ions.....	10
Fig. 2.4. Solubility products of An(OH) <sub>4</sub> (am) and AnO <sub>2</sub> (cr) as a function of the distance $d_{An-O}$ . ....	13
Fig. 2.5 Formal potentials at I = 0 for plutonium at 25°C, in units of V vs. SHE.....	16
Fig. 2.6 Solubility data of Pu(OH) <sub>4</sub> (am) or PuO <sub>2</sub> (cr) for acidic and basic media. ....	21
Fig. 2.7 Comparison between the formation constants for mononuclear hydrolysis species of Pu(IV) and zirconium.....	28
Fig. 2.8 The Solubility data of zirconium in acidic and neutral media from literature. ....	29
Fig. 3.1 The absorption spectra of four plutonium reference solutions.....	35
Fig. 3.2 The absorption spectra of Pu(IV) as a function of pH in the range from 0.5 to 1.2.....	37
Fig. 3.3 The spectrum of Pu(VI) <sub>aq</sub> in 0.5 M (H/Na)Cl. ....	38
Fig. 3.4 LCW coupled with the diode array spectrometer.....	39
Fig. 3.5 The absorption spectra of plutonium solution obtained with a 1 cm quartz cell and with the LCW-DAS.....	40
Fig. 3.6 The spectra of PuO <sub>2</sub> <sup>2+</sup> measured by Cary 5E and LCW-DAS .....	41
Fig. 3.7 The contributions to the directions and magnitude of the observed mobility $\mu_{obs}$ .....	42
Fig. 3.8 The set up of the homemade CE coupled with ICP-MS [Kucz 2003]. ....	44
Fig. 3.9 Schematic representation and resulting spectra of the absence and presence of a neighboring atom of EXAFS [Teo 86]. ....	46
Fig. 3.10 INE Beamline at the ANKA, Forschungszentrum Karlsruhe, Germany. ....	48
Fig. 3.11 The detection limit of LIBD in comparison to the conventional light scattering [Bund 2001a]. .	49
Fig. 3.12 LIBD, principle of operation [Walt 2003a].....	50
Fig. 3.13 The BDP is plotted as a function of E [mJ]. The dependence on particle size and concentration (polystyrene reference particles). ....	51
Fig. 3.14 The PSD of a three modal colloid sample prepared by mixing with polystyrene reference particles (a) s-curve and (b) PSD determined from the fit curve [Walt 2004]. ....	54
Fig. 3.15 Setup of the LIBD apparatus [Walt 2002]. ....	55
Fig. 3.16 The system set-up. of single particle counter (SPC) [Ross 2003]. ....	57
Fig. 4.1 The samples for Zr investigation.....	59
Fig. 4.2 Experimental setup of the coulometric pH titration combined with LIBD.....	61

Fig. 4.3 The set-up of electrolysis for the preparation of Pu(IV) stock solutions. ....	63
Fig. 4.4 The samples for Pu investigation. ....	65
Fig. 5.1 LIBD measurements of Zr stock solution and 0.5 M HCl and NaCl solution. ....	67
Fig. 5.2 LIBD measurements of titration series 2.....	68
Fig. 5.3 The BDP at the same energy, 1.5mJ as a function of pH.....	69
Fig. 5.4 PSD (number density as function of size) of titration series 2 ([Zr]= $1.07 \cdot 10^{-3}$ M).....	71
Fig. 5.5 The PSD from (a) LIBD measurement and (b) SPC measurement for series 10.....	72
Fig. 5.6 LIBD results for solubility of Zr(IV) and literature data .....	73
Fig. 5.7 The solubility of Zr(OH) <sub>4</sub> (am). The present results by LIBD (▲), the results from undersaturation by Sasaki <i>et al.</i> and from oversaturation by Altmaier <i>et al.</i> .....	76
Fig. 5.8 Normalized Zr K-XANES spectra of samples <b>a - i</b> . See Table 8.3 for sample descriptions. ....	77
Fig. 5.9 Zr K EXAFS and R-space fit results for reference samples ( <b>a</b> , <b>b</b> and <b>c</b> ).....	78
Fig. 5.10 Zr K EXAFS and R-space fit results for coulometric titration samples ( <b>d - i</b> ).....	79
Fig. 6.1 LIBD measurements of background solutions. ....	82
Fig. 6.2 LIBD measurements of Pu(IV) stock solutions .....	82
Fig. 6.3 Determination of the onset of colloid formation as function of pH.....	83
Fig. 6.4 The Pu(IV) colloid concentration (%) obtained from absorption spectra as a function of pH. ....	85
Fig. 6.5 The solubility of Pu(IV) hydrous oxide obtained in the present work and literature data.....	87
Fig. 6.6 The distribution of oxidation states versus time (days). [Pu] <sub>tot.</sub> is $3.3 \cdot 10^{-4}$ M at pH 0.48. ....	92
Fig. 6.7 The distribution of oxidation states versus time (days) for titration series 1.....	94
Fig. 6.8 The distribution of oxidation states versus time (days) for titration series 5. ....	96
Fig. 6.9 CE-ICP-MS measurement for sample [Pu] <sub>tot.</sub> = $1.2 \cdot 10^{-5}$ M at pH 2.13 after 60 days (series 5). ....	97
Fig. 6.10 The distribution of oxidation states for the acidified sample .....	98
Fig. 6.11 comparison between the oxidation state distributions under argon atmosphere (series 2) and in air (series 1).....	100
Fig. 6.12 Comparison between the measured $p_e$ and the calculated $p_e$ from the redox couples. ....	102
Fig. 6.13 The values of $p_e + \log[\text{Pu}^{3+}]/[\text{Pu(IV)}_{\text{aq.}}]$ as a function of pH .....	104
Fig. 7.1 The distribution of mononuclear hydrolysis species of Pu(IV) and Zr.....	107
Fig. 8.1 The absorption spectra of Pu sample before and after coulometric pH titration.....	118
Fig. 8.2 The absorption spectrum of Pu(IV) colloid [Clev 79]. ....	119
Fig. 8.3 The BDP is plotted as a function of the laser pulse energy (polystyrene reference colloids).....	120

## 8.10 List of Tables

Table 2.1 Pu(IV) hydrolysis constants at 20-25°C and the values converted to $I = 0$ .....	17
Table 2.2 Formation constants for mononuclear Zr(IV) hydroxide complexes .....	27
Table 3.1 The molar extinction coefficients for different oxidation states of plutonium.....	33
Table 3.2 The distributions of Pu(IV) hydrolysis species ( $I = 0.5$ M NaCl) at different pH estimated with the hydrolysis constants by Metivier <i>et al</i> [Meti 72]. .....	35
Table 3.3 The distribution of Pu oxidation states (%) at a steady state as a function of pH from the analysis of the absorption spectrum. ....	36
Table 3.4 The spectroscopic parameters of the predominant Pu(VI) <sub>aq</sub> species in NaCl [Rund 99]. ....	38
Table 4.1 Isotope distribution after the purification of Pu solution using $\alpha$ - and $\gamma$ -spectrometry. ....	62
Table 6.1 The concentration of Pu(IV) aquatic species and the Pu(IV) colloids. ....	87
Table 6.2 Corrected hydrolysis constants and corresponding formation constants of plutonium hydrolysis species using the measured redox potentials.....	105
Table 8.1 The ion interaction coefficients at 25°C.....	115
Table 8.2 Summary of coulometric titration (CT)-LIBD series examined in present work (Fig. 5.6). ....	115
Table 8.3 Summary of samples examined by XAFS in this study (Fig. 4.1). ....	116
Table 8.4 Data range and metric parameters extracted by least-squares fit analysis of Zr K EXAFS spectra shown in Fig. 5.8 and Fig. 5.9.....	117
Table 8.5 Concentrations, the distribution of the Pu oxidation states and the existence of colloids to be detectable using LIBD (Series 1 in Fig. 6.6 and Fig. 6.9).....	121
Table 8.6 Concentrations, the distribution of the Pu oxidation states and the existence of colloids to be detectable using LIBD (Series 2 in Fig. 6.10).....	122
Table 8.7 Concentrations, the distribution of the Pu oxidation states and the existence of colloids to be detectable using LIBD (Series 3 in Fig. 6.3 (a)) .....	123
Table 8.8 Concentrations, the distribution of the Pu oxidation states and the existence of colloids to be detectable using LIBD (Series 4). ....	124
Table 8.9 Concentrations, the distribution of the Pu oxidation states and the existence of colloids to be detectable using LIBD (Series 5 in Fig. 6.3 (b) and Fig. 6.7).....	124

## 9 References

- [Adai 87] Adair, J. H.; Denkwicz, R. P. and Arriagada, F., Precipitation and *in-situ* transformation in the hydrothermal synthesis of crystalline zirconium dioxide, *Cera. Trans.*, **1**, 135, 1987.
- [Aja 95] Aja, S. U.; Wood, S. A. and Williams-Jones, A. E., The aqueous geochemistry of Zr and the solubility of some Zr-bearing minerals, *appl. Geochem.*, **10**, 603, 1995.
- [Altm 2005] Altmaier, M.; Müller, R. and Neck, V., *unpublished results*, 2005.
- [Anku 96] Ankudinov, A. L.; Ravel, B.; Rehr, J. J. and Hrilić, J., Real-space multiple-scattering calculation and interpretation of X-ray-absorption near-edge structure, *Phys. Rev. B*, **58**, 7565, 1996.
- [Anku 97] Ankudinov, A. L. and Rehr, J. J., Relativistic calculations of spin-dependent X-ray-absorption spectra, *Phys. Rev. B*, **56**, 1712, 1997.
- [Avog 84] Avogadro, A. and Demarsily, G., The role of colloids in nuclear waste disposal, *MRS Proc.*, **26**, 495, 1984.
- [Baas 60] Baas Becking, L. G. M.; Kaplan, I. R. and Moore, D., Limits of the natural environment in terms of pH and oxidation-reduction potentials, *J. Geology*, **68**, 243, 1960.
- [Baes 76] Baes, C. F. and Mesmer, R. E. (1976). The hydrolysis of cations. New York, John Wiley and Sons.
- [Baum 62] Bauman, R. P. (1962). Absorption spectroscopy. New York, Wiley.
- [Behr 92b] Behrens, P., X-ray absorption spectroscopy in chemistry II. X-ray absorption near edge structure, *Tren. anal. chem.*, **11**(7), 237, 1992.
- [Bell 73a] Bell, J. T.; Costanzo, D. A. and Biggers, R. E., Plutonium polymerization. II. Kinetics of the plutonium, *J. Inorg. Nucl. Chem.*, **35**(2), 623, 1973.
- [Bili 66] Bilinski, H.; Branica, M. and Sillen, L. G., Precipitation and hydrolysis of metallic ions : II. Studies on the solubility of zirconium hydroxide in dilute solutions and in 1 M NaClO<sub>4</sub>, *Acta Chem. Scand.*, **20**, 853, 1966.
- [Bite 2003] Bitea, C.; Müller, R.; Neck, V.; Walther, C. and Kim, J. I., Study of the generation and stability of thorium(IV) colloids by LIBD combined with ultrafiltration, *Coll. Surf. A: Physicochem. Engin. Asp.*, **217**(1-3), 63, 2003.
- [Bite 2005] Bitea, C. (2005) Laser-induzierte Breakdown Detektion (LIBD): Quantifizierung der Kolloidbildung vierwertiger Actiniden und Homologen., Karlsruhe, Universität Karlsruhe.
- [Brew 53] Brewer, L., The Thermodynamic properties of the oxides and their vaporization processes, *Chem. Rev.*, **52**(1), 1, 1953.
- [Buff 95] Buffle, J. and Leppard, G. G., Characterization of aquatic colloids and macromolecules. 1. Structure and behavior of colloidal matter, *Environ. Sci. Technol.*, **29**(9), 2169, 1995.
- [Bund 2000] Bundschuh, T.; Knopp, R.; Müller, R.; Kim, J. I.; Neck, V. and Fanghänel, T., Application of LIBD to the determination of the solubility product of thorium(IV)-colloids, *Radiochim. Acta*, **88**(9-11), 625, 2000.

- [Bund 2001a] Bundschuh, T.; Hauser, W.; Kim, J. I.; Knopp, R. and F.J.Scherbaum, Determination of colloid size by two-dimensional optical detection of laser induced plasma, *Coll. Surf. A: Physicochem. Engin. Asp.*, **180**, 285, 2001.
- [Bund 2001b] Bundschuh, T.; Knopp, R. and Kim, J. I., Laser-induced breakdown detection (LIBD) of aquatic colloids with different laser systems, *Coll. Surf. A: Physicochem. Engin. Asp.*, **177**(1), 47, 2001.
- [Bürg 2005] Bürger, S. (2005) Spurenanalyse von Uran und Plutonium sowie Speziationsuntersuchungen an Plutonium mit massenspektrometrischen und kapillarelektrophoretischen Methoden., Mainz, Johannes Gutenberg-universität Mainz.
- [Capd 92] Capdevila, H.; Vitorge, P. and Giffaut, E., Stability of pentavalent plutonium - Spectrophotometric study of  $\text{PuO}_2^+$  and  $\text{Pu}^{4+}$  disproportionation in perchloric media, *Radiochim. Acta*, **58-9**, 45, 1992.
- [Capd 98] Capdevila, H. and Vitorge, P., Solubility product of  $\text{Pu}(\text{OH})_4(\text{am})$ , *Radiochim. Acta*, **82**, 11, 1998.
- [Cerv 75] Cervenán, M. R. and Isenor, N. R., Multiphoton ionization yield curves for Gaussian laser beams, *Optics. Comm.*, **13**(2), 175, 1975.
- [Cho 2005] Cho, H. R.; Walther, C.; Rothe, J.; Neck, V.; Denecke, M. A.; Dardenne, K. and Fanghänel, T., Combined LIBD and XAFS investigation of the formation and structure of Zr(IV) colloids, *Anal. Bioanal. Chem.*, 2005, available online.
- [Chop 83a] Choppin, G. R., Solution chemistry of the actinides, *Radiochim. Acta*, **32**, 43, 1983.
- [Chop 83b] Choppin, G. R., Plutonium chemistry, *ACS Symp. Ser.*, **216**, 214, 1983.
- [Chop 84] Choppin, G. R. and Rao, L. F., Complexation of pentavalent and hexavalent actinides by fluoride, *Radiochim. Acta*, **37**, 143, 1984.
- [Chop 94] Choppin, G. R. and Rizkalla, E. N., Solution chemistry of actinides and lanthanides, in Handbook on the physics and chemistry of rare earths, 559, North Holland, Amsterdam, 1994.
- [Chop 97] Choppin, G. R.; Bond, A. H. and Hromadka, P. M., Redox speciation of plutonium, *J. Radioanal. Nucl. Chem.*, **219**(2), 203, 1997.
- [Chop 2003] Choppin, G. R., Actinide speciation in the environment, *Radiochim. Acta*, **91**, 645, 2003.
- [Chyl 86] Chylek, P.; Jarzembski, M. A.; Chou, N. Y. and Pinnick, R. G., Effect of size and material of liquid spherical-particles on laser-induced breakdown, *Appl. Phys. Lett.*, **49**(21), 1475, 1986.
- [Ciav 80] Ciavatta, L., The specific interaction theory in evaluating ionic equilibria, *Annali di Chimica (Rome)*, **70**, 551, 1980.
- [Clev 68] Cleveland, J. M., Sulfamate complexes of plutonium(IV), *Inorg. Chem.*, **7**, 874, 1968.
- [Clev 79] Cleveland, J. M. (1979). The chemistry of plutonium. La Grange Park, IL, American Nuclear Society.
- [Coh 61] Cohen, D., Electrochemical studies of plutonium ions in perchloric acid solution, *J. Inorg. Nucl. Chem.*, **18**, 207, 1961.
- [Cölf 2000] Cölfen, H. and Antonietti, M., Field-flow fractionation techniques for polymer and colloid analysis, *Adv. Polym. Sci.*, **150**, 67, 2000.

- [Conn 51] Connick, R. E. and Reas, W. H., The hydrolysis and polymerization of zirconium in perchloric acid solution, *J. Am. Chem. Soc.*, **73**, 1171, 1951.
- [Conr 2004] Conradson, S. D.; Begg, B. D.; Clark, D. L.; den Auwer, C.; Ding, M.; Dorhout, P. K.; Espinosa-Faller, F. J.; Gordon, P. L.; Haire, R. G.; Hess, N. J., et al., Local and nanoscale structure and speciation in the  $\text{PuO}_{2+x-y}(\text{OH})_{2y}\text{zH}_2\text{O}$  system, *J. Am. Chem. Soc.*, **126**(41), 13443, 2004.
- [Cost 73] Costanzo, D. A.; Biggers, R. E. and Bell, J. T., Plutonium polymerization. I: A spectrophotometric study of the polymerization of plutonium(IV), *J. Inorg. Nucl. Chem.*, **35**(2), 609, 1973.
- [Davy 87] Davydov, Y. P. and Zabrodskii, V. N., Hydrolysis of zirconium(IV) with formation of mono- and polynuclear hydroxy complexes in solution, *Vestsi Akad. Navuk BSSR, Ser. Khim. Navuk*, **2**, 3, 1987.
- [Degu 95] Degueldre, C.; Bilewicz, A. and Alder, H. P., Behavior and removal of radionuclides generated in the cooling water of a proton accelerator, *Nucl. Sci. Engin.*, **120**, 65, 1995.
- [Degu 89] Degueldre, C.; Longworth, G.; Moulin, V. and Vilks, P., Grimsel colloid exercise, PSI report, no. 39, Paul Scherrer Institute, Villigen, Switzerland, 1989.
- [Degu 96a] Degueldre, C.; Schenker, E. and Nobbenhuis-Wedda, H., Investigation of the colloid characteristics in the water of boiling water reactors, *Water Chem. Nucl. Reactor Sys.*, **7**, 112, 1996.
- [Degu 2000] Degueldre, C.; Triay, I.; Kim, J. I.; Vilks, P.; Laaksoharju, M. and Miekeley, N., Groundwater colloid properties: a global approach, *Appl. Geochem.*, **15**, 1043, 2000.
- [Dene 2005] Denecke, M.; Rothe, J.; Dardenne, K.; Blank, H. and Hormes, J., The INE Beamline for actinide research at ANKA, *Phys. Scrip.*, **T115**, 1001, 2005.
- [Durr 70] Durrant, P. J. and Durrant, B. (1970). Introduction to advanced inorganic chemistry. London, Longman Grp. Ltd.
- [Ekbe 2001] Ekberg, C.; Brown, P.; Comarmond, J. and Albinsson, Y., On the hydrolysis of tetravalent metal ions, *Mat. Res. Soc. Symp. Proc.*, **663**, 1091, 2001.
- [Ekbe 2004] Ekberg, C. and Källvenius, G., Studies on the hydrolytic behavior of zirconium(IV), *J. Sol. Chem.*, **33**(1), 47, 2004.
- [Evan 2000] Evans, D. F. and Wennerström, H. (2000). The colloidal domain. New York, VCH.
- [Fang 83] Fang, H. L. and Swafford, R. L. (1983). Ultrasensitive laser spectroscopy. New York, Academic Press.
- [Farr 2004] Farr, J. D.; Schulze, R. K. and Neu, M. P., Surface chemistry of Pu oxides, *J. Nucl. Mat.*, **328**(2-3), 124, 2004.
- [Fay 88] Fay, M. J.; Proctor, A.; Hoffmann, D. P. and Hercules, D. M., Unraveling EXAFS spectroscopy, *Anal. Chem.*, **60**(21), 1225A, 1988.
- [Fuge 76] Fuger, J. and Oetting, F. L. (1976). The chemistry thermodynamics of actinide elements and compounds, part 2.: The actinide aqueous ions. Vienna, IAEA.
- [Fuji 2001] Fujiwara, K.; Yamana, H.; Fujii, T. and Moriyama, H., Solubility product of plutonium hydrous oxide, *J. Nucl. Fuel Cycle Environ.*, **7**, 17, 2001.



- [Fuji 2002] Fujiwara, K.; Yamana, H.; Fujii, T. and Moriyama, H., Solubility product of plutonium hydrous oxide and its ionic strength dependence, *Radiochim. Acta*, **90**(12), 857, 2002.
- [Fuji 2003] Fujiwara, K.; Yamana, H.; Fujii, T.; Moriyama, H., Determination of uranium(IV) hydrolysis constants and solubility product of  $\text{UO}_2 \cdot x\text{H}_2\text{O}$ , *Radiochim. Acta*, **91**(6), 345, 2003
- [Geis 2004] Geist, A.; Gompper, K.; Weigl, M. and Fanghänel, T., Reduzierung der Radiotoxizität abgebrannter Kernbrennstoffe durch Abtrennung und Transmutation von Actiniden : Partitioning, *Nachrichten-FZK*, S. 97, Feb. 2004.
- [Gren 97] Grenthe, I. and Puigdomenech, I. (1997). Modelling in aquatic chemistry. Paris, OECD/NEA.
- [Gual 96] Gualtieri, A.; Norby, P.; Hanson, J. and Hriljac, J., Rietveld refinement using synchrotron X-ray powder diffraction data collected in transmission geometry using an imaging-plate detector: Application to standard  $m\text{-ZrO}_2$ , *J. Appl. Crystallography*, **29**(6), 707, 1996.
- [Guil 2003] Guillaumont, R.; Fanghänel, T.; Fuger, J.; Grenthe, I.; Neck, V.; Palmer, D. A. and Rand, M. H. (2003). Update on the chemical thermodynamics of uranium, neptunium, plutonium, americium and technetium, Elsevier.
- [Hagf 2004] Hagfeldt, C.; Kessler, V. and Persson, I., Structure of the hydrated, hydrolyzed and solvated zirconium(IV) and hafnium(IV) ions in water and aprotic oxygen donor solvents. A crystallographic, EXAFS spectroscopic and large angle X-ray scattering study, *Dalton Trans.*, (14), 2142, 2004.
- [Hahn 98] Hahn, D. W., Laser-induced breakdown spectroscopy for sizing and elemental analysis of discrete aerosol particles, *App. Phys. Lett.*, **72**(23), 2960, 1998.
- [Hasc 2000a] Haschke, J. M.; Allen, T. H. and Morales, L. A., Reaction of plutonium dioxide with water : Formation and properties of  $\text{PuO}_{2+x}$ , *Science*, **287**, 285, 2000.
- [Hasc 2002b] Haschke, J. M. and Oversby, V. M., Plutonium chemistry: A synthesis of experimental data and a quantitative model for plutonium oxide solubility, *J. Nucl. Mater.*, **305**(2-3), 187, 2002.
- [Haus 98] Hauser, W. and Bundschuh, T. (1998). Verfahren zur Bestimmung der Größe von Partikeln in einer Lösung, Patent (Germany) DE, 19833339
- [Haus 99] Hauser, W. and Götz, R. (1999). Druckwellensensor, Patent (Germany) DE, 19602048C2
- [Haus 2002] Hauser, W.; Geckeis, H.; Kim, J. I. and Fierz, T., A mobile laser-induced breakdown detection system and its application for the in situ-monitoring of colloid migration, *Coll. Surf. A: Physicochem. Engin. Asp.*, **203**(1-3), 37, 2002.
- [Heck 2001] Hecker, S. S., The complex world of plutonium science, *MRS Bulletin*, **26**(9), 672, 2001.
- [Hoff 2002] Hoffman, D. C. (2002). Advances in plutonium chemistry, 1967-2000. La Grange park, Illinois, American Nuclear Society.
- [Humm 2002] Hummel, W.; Berner, U.; Curti, E.; Pearson, F. J. and Thoenen, T., Nagra/PSI chemical thermodynamic data base 01/01, *Radiochim. Acta*, **90**(9-11), 805, 2002.
- [Izum98] Izumida, S.; Onishi, K. and Saito, M., Estimation of laser-induced breakdown threshold of microparticles in water., *Jap. J. Appl. Phys. I*, **37**(4A), 2039, 1998.
- [Jack 81] Jackson, W. B.; Amer, N. M.; Boccara, A. C. and Fournier, D., Photothermal deflection spectroscopy and detection, *Appl. Opt.*, **20**, 1333, 1981.

- [Jand 93] Jandik, P. and Bonn, G. (1993). Capillary electrophoresis of small molecules and ions. New York, VCH.
- [Kash 49] Kasha, M., Reactions between plutonium ions in perchloric acid solution : Rate, mechanism, and equilibria, in the transuranium elements, 295, McGraw-Hill Inc., New York, 1949.
- [Katz 86] Katz, J. J.; Seaborg, G. T. and Morss, L. R. (1986). Chemistry of the actinide elements. London, Chapman and Hall.
- [Kell 71] Keller, C. (1971). The chemistry of the transuranium elements. Weinheim, Germany, Verlag Chemie.
- [Kers 99] Kersting, A. B.; Efurud, D. W.; Finnegan, D. L.; Rokop, D. J.; Smith, D. K. and Thompson, J. L., Migration of plutonium in ground water at the Nevada Test Site, *nature*, **397**, 56, 1999.
- [Kim 86] Kim, J. I., Chemical behaviour of transuranic elements in natural aquatic systems, in Handbook of the physics and chemistry of the actinides, ed. Freeman, A. J. and Keller, C., Ch 8. 413, Elsevier Science, Amsterdam, 1986.
- [Kim 89a] Kim, J. I. and Kanellakopoulos, B., Solubility products of plutonium(IV) oxide and hydroxide, *Radiochim. Acta*, **48**(3-4), 145, 1989.
- [Kim 89b] Kim, J. I.; Buckau, G.; Rommel, H. and Sohnius, B., Scientific basis for nuclear waste management XII, *Mater. Res. Soc. Symp. Proc.*, **127**, 849, 1989.
- [Kim90] Kim, J.-I.; Stumpe, R. and Klenze, R., Laser-induced photoacoustic spectroscopy for the speciation of transuranic elements in natural aquatic systems, in Chemical applications of nuclear probes, ed. Yoshihara, K., 131, Springer, Berlin, 1990.
- [Kim 91] Kim, J. I., Actinide colloid generation in groundwater, *Radiochim. Acta*, **52/53**, 71, 1991.
- [Kim 92] Kim, J. I.; Zeh, P. and Delakowitz, B., Chemical interactions of actinide ions with groundwater colloids in Gorleben aquifer systems, *Radiochim. Acta*, **58/59**, 147, 1992.
- [Kim 94] Kim, J. I., Actinide colloids in natural aquifer systems, *MRS Bulletin*, **XIX**(12), 47, 1994.
- [Kim 2000] Kim, J. I., Is the thermodynamic approach appropriate to describe natural dynamic systems? (Status and limitations), *Nucl. Engin. Des.*, **202**(2-3), 143, 2000.
- [Kita84] Kitamori, T.; Fujii, M.; Sawada, T. and Gohshi, Y., Frequency characteristics of photoacoustic signals generated in liquids, *J. Appl. Phys.*, **55**(11), 4005, 1984.
- [Kita 88] Kitamori, T.; Yokose, K.; Suzuki, K.; Sawada, T. and Goshi, Y., Laser breakdown acoustic effect of ultrafine particle in liquids and its application to particle counting, *Jap. J. Appl. Phys. 2.*, **27**(6), L983, 1988.
- [Kita 89] Kitamori, T.; Yokose, K.; Sakagami, M. and Sawada, T., Detection and counting of ultrafine particles in ultrapure water using laser breakdown acoustic method, *Jap. J. Appl. Phys.*, **28**(7), 1195, 1989.
- [Knop 99] Knopp, R.; Neck, V. and Kim, J. I., Solubility, hydrolysis and colloid formation of plutonium(IV), *Radiochim. Acta*, **86**, 101, 1999.
- [Koba 88] Kobashi, A.; Choppin, G. R. and Morse, J. W., A study of techniques for separating plutonium in different oxidation states, *Radiochim. Acta*, **43**, 211, 1988.
- [Köpf 79] Köpf, U. (1979). Laser in der Chemie. Frankfurt, Salle.

- [Kova 61] Kovalenko, P. N. and Bagdasarov, K. N., The solubility of zirconium hydroxide, *Russ. J. Inorg. Chem.*, **6**(3), 272, 1961.
- [Kral 97] Kralchevsky, P. A.; Danov, K. D. and Denkov, N. D., Chemical physics of colloid systems and interfaces, in Handbook of surface and colloid chemistry, ed. Birdi, K. S., 333, CRC Press, New York, 1997.
- [Krau 50] Kraus, K. A. and Nelson, F., Hydrolytic behavior of metal Ions.: I. The acid constants of uranium(IV) and plutonium(IV), *J. Am. Chem. Soc.*, **72**, 3901, 1950.
- [Kucz 2003] Kuczewski, B.; Marquardt, C. M.; Seibert, A.; Geckeis, H.; Kratz, J. V. and Trautmann, N., Separation of plutonium and neptunium species by capillary electrophoresis-inductively coupled plasma-mass spectrometry and application to natural groundwater samples, *Anal. Chem.*, **75**(24), 6769, 2003.
- [Laff 82] Laffitte, M., A report of IUPAC commission I.2 on thermodynamics: Notation for states and processes, significance of the word "standard" in chemical thermodynamics, and remarks on commonly tabulated forms of thermodynamic functions, *J. Chem. Thermodyn.*, **14**(9), 805, 1982.
- [Lars 65] Larsen, E. M. (1965). Transitional elements. New York, W. A. Benjamin Inc.
- [Lemi 2001] Lemire, R. J.; Fuger, J.; Mitsche, H.; Potter, P.; Rand, M. H.; Rydberg, J.; Spahiu, K.; Sullivan, J. C.; Ullman, W. J.; Vitorge, P., et al. (2001). Chemical thermodynamics of neptunium and plutonium, Elsevier.
- [Li 93] Li, P.; Chen, I. W. and Penner-Hahn, J. E., X-ray-absorption studies of zirconia polymorphs .1. Characteristic local structures, *Phys. Rev. B*, **48**(14), 10063, 1993.
- [Lier 86] Lierse, C. (1986). Chemisches Verhalten von Plutonium in natürlichen aquatischen Systemen : Hydrolyze, Carbonatkomplexierung und Redoxreaktionen., Technische Universität München.
- [Lloy 78] Lloyd, M. H. and Haire, R. G., The chemistry of plutonium in sol-gel processes, *Radiochim. Acta*, **25**(3-4), 139, 1978.
- [Macd 73] Macdermott, T. E., The structural chemistry of zirconium compounds, *Coord. Chem. Rev.*, **11**(1), 1, 1973.
- [Mak 68] Mak, T. C. W., Refinement of crystal structure of zirconyl chloride octahydrate, *Canad. J. Chem.*, **46**, 3491, 1968.
- [Mars 2001a] Marseguerra, M.; Patelli, E. and Zio, E., Groundwater contaminant transport in presence of colloids I. A stochastic nonlinear model and parameter identification, *Ann. Nucl. Ener.*, **28**(8), 777, 2001.
- [Mars 2001b] Marseguerra, M.; Patelli, E. and Zio, E., Groundwater contaminant transport in presence of colloids II: sensitivity and uncertainty analysis on literature case studies, *Ann. Nucl. Ener.*, **28**(18), 1799, 2001.
- [Mart 2003] Martin, P.; Grandjean, S.; Ripert, M.; Freyss, M.; Blanc, P. and Petit, T., Oxidation of plutonium dioxide: an X-ray absorption spectroscopy study, *J. Nucl. Mater.*, **320**(1-2), 138, 2003.
- [Meti 72] Metivier, H. and Guillaumont, R., Hydrolyse du plutonium tetravalent, *Radiochem. Radioanal. Lett.*, **10**, 27, 1972.

- [Mila 2003] Milas, S. M.; Ye, J. Y.; Norris, T. B.; Balogh, L. P.; Baker, J. R.; Hollman, K. W.; Emelianov, S. and O'Donnell, M., Acoustic detection of microbubble formation induced by enhanced optical breakdown of silver dendrimer nanocomposites, *Appl. Phys. Lett.*, **82**(6), 994, 2003.
- [Moon 89] Moon, H., Equilibrium ultrafiltration of hydrolyzed thorium(IV) solutions, *Bull. Kor. Chem. Soc.*, **10**(3), 270, 1989.
- [Muha 60] Muha, G. M. and Vaughan, P. A., Structure of the complex ion in aqueous solutions of zirconyl and hafnyl oxyhalides., *J. Chem. Phys.*, **33**(1), 194, 1960.
- [Neck 2000] Neck, V. and Kim, J. I., An electrostatic approach for the prediction of actinide complexation constants with inorganic ligands-application to carbonate complexes, *Radiochim. Acta*, **88**, 815, 2000.
- [Neck 2001a] Neck, V. and Kim, J. I., Solubility and hydrolysis of tetravalent actinides, *Radiochim. Acta*, **89**(1), 1, 2001.
- [Neck 2001b] Neck, V.; Kim, J. I.; Seidel, B. S.; Marquardt, C. M.; Dardenne, K.; Jensen, M. P. and Hauser, W., A spectroscopic study of the hydrolysis, colloid formation and solubility of Np(IV), *Radiochim. Acta*, **89**(7), 439, 2001.
- [Neck 2002] Neck, V.; Müller, R.; Bouby, M.; Altmaier, M.; Rothe, J.; Denecke, M. A. and Kim, J. I., Solubility of amorphous Th(IV) hydroxide - application of LIBD to determine the solubility product and EXAFS for aqueous speciation, *Radiochim. Acta*, **90**(9-11), 485, 2002.
- [Neck 2003] Neck, V.; Altmaier, M.; Müller, R.; Bauer, A.; Fanghänel, T. and Kim, J. I., Solubility of crystalline thorium dioxide, *Radiochim. Acta*, **91**(5), 253, 2003.
- [Neck 2005] Neck, V.; Altmaier, M. and Fanghänel, T., Solubility and redox reactions of plutonium(IV) hydrous oxide in the presence of oxygen, *Actinides 4. - 8. July*, 2005.
- [Nits 96] Nitsche, H. and Silva, R. J., Investigation of the carbonate complexation of Pu(IV) in aqueous solution, *Radiochim. Acta*, **72**(2), 65, 1996.
- [Nore 73] Noren, B., Hydrolysis of zirconium(4+) and hafnium(4+) ions, *Acta. Chem. Scand.*, **27**, 1369, 1973.
- [Nutt 93] Nuttall, H. E. and Long, R. L., Mobility of radioactive colloid particles in groundwater, *Radioactive Waste Management and the Nuclear Fuel Cycle*, **17**(3-4), 237, 1993.
- [Nyha 85] Nyhan, J. W.; Drennon, B. J.; Abeele, W. V.; Wheeler, M. L.; Purtymun, W. D.; Trujillo, G.; Herrera, W. J.; Booth, J. W., Distribution of plutonium and americium beneath a 33-year-old liquid waste disposal site, *J. Environ. Qual.*, **14**(4), 501, 1985.
- [Ohta 90] Ohtaka, O.; Yamanaka, T.; Kume, S.; Hara, N.; Asano, H. and Izumi, F., Structural analysis of orthorhombic ZrO<sub>2</sub> by high-resolution neutron powder diffraction, *Proc. Jap. Acad., Series. B*, **66**(10), 193, 1990.
- [Para 58] Paramonova, V. I. and Sergeev, Use of ion exchange to study of substances in solution.: V. Study of the process of complex formation between Zr and HNO<sub>3</sub>, A. N., *Zh. Neorg. Khim.*, **3**, 215, 1958.
- [Park 85] Parks, G. A. and Pohl, D. C., Hydrothermal solubility of uraninite., Report DOE/ER 12016-1, Stanford, 1985.

- [Pere 65] Perez-Bustamante, J. A., Solubility product of tetravalent plutonium hydroxide and study of the amphoteric character of hexavalent plutonium hydroxide, *Radiochim. Acta*, **4**(2), 67, 1965.
- [Pitz 73a] Pitzer, K., Thermodynamic properties of electrolytes. I. Theoretical basis and general equations, *J. Phys. Chem.*, **77**(2), 268, 1973.
- [Pouc 2001] Pouchon, M. A.; Curti, E.; Degueldre, C. and Tobler, L., The influence of carbonate complexes on the solubility of zirconia: new experimental data, *Prog. Nucl. Ener.*, **38**(3-4), 443, 2001.
- [Poul 95] Poulain, D. E. and Alexander, D. R., Influences on concentration measurements of liquid aerosols by laser-induced breakdown spectroscopy, *Appl. Spec.*, **49**(5), 569, 1995.
- [Pras 67] Prasad, R.; Beasley, M. L. and Milligan, W. O., Aging of hydrous thoria gels, *J. Elec. Microscopy*, **16**, 101, 1967.
- [Rabi 51] Rabideau, S. W. and Lemons, J. F., The potential of the Pu(III)-Pu(IV) couple and the equilibrium constants for some complex ions of Pu(IV), *J. Am. Chem. Soc.*, **73**, 2895, 1951.
- [Rabi 53] Rabideau, S. W., Equilibria and reaction rates in the disproportionation of Pu(IV), *J. Am. Chem. Soc.*, **75**(4), 798, 1953.
- [Rabi 57] Rabideau, S. W., The hydrolysis of plutonium(IV), *J. Am. Chem. Soc.*, **79**, 3675, 1957.
- [Rabi 60] Rabideau, S. and Kline, R. J., A spectrophotometric study of the hydrolysis of plutonium(IV), *J. Phys. Chem.*, **64**, 680, 1960.
- [Radz 89] Radziemski, L. J. and Cremers, D. A. (1989). Laser-induced plasmas and applications. Rochester, Marcel Dekker.
- [Rai 80] Rai, D.; Serne, R. J. and Moore, D. A., Solubility of plutonium compounds and their behavior in soils, *Soil Sci. Soc. Am. Journal*, **44**, 490, 1980.
- [Rai 81] Rai, D. and Swanson, J. L., Properties of plutonium(IV) polymer of environmental importance, *Nucl. Tech.*, **54**(1), 107, 1981.
- [Rai 82] Rai, D. and Ryan, J. L., Crystallinity and solubility of plutonium(IV) oxide and hydrous oxide in aged aqueous suspensions, *Radiochim. Acta*, **30**(4), 213, 1982.
- [Rai 84] Rai, D., Solubility products of Pu(IV) hydrous oxide and equilibrium constants of Pu(IV)/Pu(V), Pu(IV)/Pu(VI), and Pu(V)/Pu(VI) couples, *Radiochim. Acta*, **35**, 97, 1984.
- [Rai 87] Rai, D.; Swanson, J. L. and Ryan, J. L., Solubility of  $\text{NpO}_2 \cdot x\text{H}_2\text{O}(s)$  in the presence of Cu(I)/Cu(II) redox buffer, *Radiochim. Acta*, **42**, 35, 1987.
- [Rai 99] Rai, D.; Hess, N. J.; Felmy, A. R.; Moore, D. A.; Yui, M. and Vitorge, P., A thermodynamic model for the solubility of  $\text{PuO}_2(am)$  in the aqueous  $\text{K}^+ - \text{HCO}_3^- - \text{CO}_3^{2-} - \text{OH}^- - \text{H}_2\text{O}$  system, *Radiochim. Acta*, **86**(3-4), 89, 1999.
- [Rai 2000] Rai, D.; Moore, D. A.; Oakes, C. S. and Yui, M., Thermodynamic model for the solubility of thorium dioxide in the  $\text{Na}^+ - \text{Cl}^- - \text{OH}^- - \text{H}_2\text{O}$  system at 23°C and 90°C, *Radiochim. Acta*, **88**(5), 297, 2000.
- [Rai 2002] Rai, D.; Gorby, Y. A.; Fredrickson, J. K.; Moore, D. A. and Yui, M., Reductive dissolution of  $\text{PuO}_2(am)$ : The effect of Fe(II) and hydroquinone, *J. Sol. Chem.*, **31**(6), 433, 2002.
- [Rai 2003] Rai, D.; Yui, M.; Moore, D. A., Solubility and solubility product at 22°C of  $\text{UO}_2(c)$  precipitated from aqueous U(IV) solutions, *J. Sol. Chem.*, **32**(1), 1, 2003

- [Rams 88] Ramsay, D. A., The role of colloids in the release of radionuclides from nuclear waste, *Radiochim. Acta*, **44/45**, 165, 1988.
- [Ress 97] Ressler, T., WinXAS: A new software package not only for the analysis of energy-dispersive XAS data, *J. Phys. IV*, **7-C2**, 269, 1997.
- [Ross 2003] Rosse, P. and Loizeau, J. L., Use of single particle counters for the determination of the number and size distribution of colloids in natural surface waters, *Coll. Surf. A: Physicochem. Engin. Asp.*, **217**(1-3), 109, 2003.
- [Ross 61] Rossotti, F. J. C. and Rossotti, H. S. (1961). The determination of stability constants. New York, McGraw-Hill.
- [Roth 2004] Rothe, J.; Walther, C.; Denecke, M. A. and Fanghänel, T., XAFS and LIBD investigation of the formation and structure of colloidal Pu(IV) hydrolysis products, *Inorg. Chem.*, **43**(15), 4708, 2004.
- [Rund 99] Runde, W.; Reilly, S. D. and Neu, M. P., Spectroscopic investigation of the formation of  $\text{PuO}_2\text{Cl}^+$  and  $\text{PuO}_2\text{Cl}_2$  in NaCl solutions and application for natural brine solutions, *Geochem. Cosmochim. Acta*, **63**(19-20), 3443, 1999.
- [Sait 99] Saito, M.; Izumida, S.; Onishi, K. and Akazawa, J., Detection efficiency of microparticles in laser breakdown water analysis, *J. Appl. Phys.*, **85**(9), 6353, 1999.
- [Sasa 2005] Sasaki, T.; Kobayashi, T.; Takagi, I and Moriyama, H., *10th International Conference on Chemistry and Migration Behaviour of Actinides and Fission Products in the Geosphere* in Avignon, France 2005.
- [Saye 88] Sayers, D. E. and Bunker, B. A. (1988). X-ray absorption: Techniques of EXAFS, SEXAFS and XANES. New York, J. Wiley & Sons.
- [Scat 76] Scatchard, G. (1976). Equilibrium in solutions: Surface and colloid chemistry. Cambridge, Massachusetts, Harvard University Press.
- [Sche 96] Scherbaum, F. J.; Knopp, R. and Kim, J. I., Counting of particles in aqueous solutions by laser-induced photoacoustic breakdown detection, *Appl. Phys. B*, **63**, 299, 1996.
- [Schi 65] Schindler, P.; Althau, H.; Hofer, F. and Minder, W., Löslichkeitsprodukte von Metalloxiden und -hydroxiden., *Helvet. Chim. Acta*, **48**, 1204, 1965.
- [Seab 54] Seaborg, G. T. and Katz, J. J. (1954). The actinide elements. New York, McGraw-Hill.
- [Seab 49] Seaborg, G. T.; Katz, J. J. and Manning, W. M. (1949). The transuranium elements: research papers., New York, McGraw-Hill.
- [Shan 76] Shannon, R. D., Revised Effective Ionic Radii and Systematic Studies of Interatomic distances in halides and chalcogenides, *Acta Cryst.*, **32**, 751, 1976.
- [Silv 95] Silva, R. J. and Nitsche, H., Actinide environmental chemistry, *Radiochim. Acta*, **70/71**, 377, 1995.
- [Silv 89] Silver, G. L., The ratio Pu(V)/Pu(IV) in natural-water, *J. Radioanal. Nucl. Chem.-Lett.*, **137**(1), 75, 1989.
- [Sing 96] Singhal, A.; Toth, L. M.; Lin, J. S. and Affholter, K., Zirconium(IV) tetramer/octamer hydrolysis equilibrium in aqueous hydrochloric acid solution, *J. Am. Chem. Soc.*, **118**(46), 11529, 1996.

- [Sout 2002] Southon, P. D.; Bartlett, J. R.; Woolfrey, J. L. and Ben-Nissan, B., Formation and characterization of an aqueous zirconium hydroxide colloid, *Chem. Mater.*, **14**(10), 4313, 2002.
- [Ster 95] Stern, E. A.; Newville, M.; Ravel, B.; Yacoby, Y. and Kaskel, D., The UWXAFS analysis package: Philosophy and details, *Phys. B: Condensed Matter*, **208/209**, 117, 1995.
- [Stum 81] Stumm, W. and Morgan, J. J. (1981). Aquatic chemistry. New York, John Wiley and Sons.
- [Stum 84] Stumpe, R.; Kim, J. I.; Schrepp, W. and Walther, H., Speciation of actinide ions in aqueous solution by laser-induced photoacoustic spectroscopy, *Appl. Phys. B*, **34**, 203, 1984.
- [Tam 86] Tam, A. C., Applications of photoacoustic sensing techniques, *Rev. Mod. Phys.*, **58**, 381, 1986.
- [Tava 95] Tavares, M. F. M. and McGuffin, V. L., Theoretical model of electroosmotic flow for capillary zone electrophoresis, *Anal. Chem.*, **67**, 3687, 1995.
- [Teo 86] Teo, B. K. (1986). EXAFS: Basic principles and data analysis (Inorganic chemistry concepts), Springer-Verlag.
- [Teuf 62] Teufer, G., The crystal structure of tetragonal  $ZrO_2$ , *Acta Crystallo.*, **15**(11), 1187, 1962.
- [Thor 98] Thormann, W.; Zhang, C.-X.; Caslavská, J.; Gebauer, P. and Mosher, R. A., Modeling of the impact of ionic strength on the electroosmotic flow in capillary electrophoresis with uniform and discontinuous buffer systems, *Anal. Chem.*, **70**, 549, 1998.
- [Tonn 99] Tonner, B. P.; Droubay, T.; Denlinger, J.; Meyer-Ilse, W.; Warwick, T.; Rothe, J.; Kneedler, E.; Pecher, K.; Neelson, K. and Grundl, T., Soft X-ray spectroscopy and imaging of interfacial chemistry in environmental species, *Surf. Interface Anal.*, **27**, 247, 1999.
- [Torr 90] Torres, R. A.; Palmer, C. A.; Baisden, P. A.; Russo, R. E. and Silva, R. J., Comparison of photoacoustic spectroscopy, Conventional absorption spectroscopy, and potentiometry as probes of lanthanide speciation, *Anal. Chem.*, **62**(3), 298, 1990.
- [Toth 90] Toth, L. M.; Bell, J. T. and Friedman, H. A., The disproportionation of  $Pu^{4+}$  in nitric acid solutions, *Radiochim. Acta*, **49**, 193, 1990.
- [Tria 91] Triay, I. R.; Hobart, D. E.; Mitchell, A. J.; Newton, T. W.; Ott, M. A.; Palmer, P. D.; Rundberg, R. S. and Thompson, J. L., Size determinations of plutonium colloids using autocorrelation photon spectroscopy, *Radiochim. Acta*, **52-3**, 127, 1991.
- [Veyl 98] Veyland, A.; Dupont, L.; Pierrard, J. C.; Rimbault, J. and Aplincourt, M., Thermodynamic stability of zirconium(IV) complexes with hydroxy ions, *Euro. J. Inorg. Chem.*, (11), 1765, 1998.
- [Veyl 2000] Veyland, A.; Dupont, L.; Rimbault, J.; Pierrard, J. C. and Aplincourt, M., Aqueous chemistry of zirconium(IV) in carbonate media, *Helv. Chim. Acta*, **83**(2), 414, 2000.
- [Walt 2002] Walther, C.; Bitea, C.; Hauser, W.; Kim, J. I. and Scherbaum, F. J., Laser induced breakdown detection for the assessment of colloid mediated radionuclide migration, *Nucl. Instr. Meth. B*, **195**, 374, 2002.
- [Walt 2003a] Walther, C., Comparison of colloid investigations by single particle analytical techniques - a case study on thorium-oxyhydroxides, *Coll. Surf. A: Physicochem. Engin. Asp.*, **217**(1-3), 81, 2003.

- [Walt 2003b] Walther, C.; Bitea, C.; Yun, J. I.; Kim, J. I.; Fanghänel, T.; Marquardt, C. M.; Neck, V. and Seibert, A., Nanoscopic approaches to the aquatic plutonium chemistry, *Actinide Research Quarterly*, **11**, 12, 2003.
- [Walt 2004] Walther, C.; Cho, H. R. and Fanghänel, T., Measuring multimodal size distributions of aquatic colloids at trace concentrations, *Appl. Phys. Lett.*, **85**(26), 6329, 2004.
- [Wei 83] Wei, L.; Fujiwara, K. and Fuwa, K., Determination of phosphorus in natural waters by long-capillary-cell absorption spectrometry, *Anal. Chem.*, **55**(6), 951, 1983.
- [Wils 2005] Wilson, R. E.; Hu, Y.-J. and Nitsche, H., Detection and quantification of Pu(III, IV, V, and VI) using a 1.0-meter liquid core waveguide, *Radiochim. Acta*, **93**, 203, 2005.
- [Wint 2000] Winterer, M., Reverse Monte Carlo analysis of extended X-ray absorption fine structure spectra of monoclinic and amorphous zirconia, *J. Appl. Phys.*, **88**, 5635, 2000.
- [Yaji 95] Yajima, T.; Kawamura, Y. and Ueta, S., Uranium(IV) solubility and hydrolysis constants under reduced conditions, *Mat. Res. Soc. Symp. Proc.*, **353**, 1137, 1995.
- [Yuso 2004] Yusov, A. B.; Fedosseev, A. M. and Delegard, C. H., Hydrolysis of Np(IV) and Pu(IV) and their complexation by aqueous Si(OH)<sub>4</sub>, *Radiochim. Acta*, **92**(12), 869, 2004.
- [Ziel 56] Zielen, A. J. and Connick, R. E., The hydrolytic polymerization of zirconium in perchloric acid solutions, *J. Am. Chem. Soc.*, **78**(20), 5785, 1956.
- [Zyuz 2004] Zyuzin, D. A.; Moroz, E. M.; Ivanova, A. S.; Shmakov, A. N. and Kustova, G. N., Local Structure of amorphous and highly dispersed zirconium hydroxides and oxides, *Kinet. Catal.*, **45**(5), 739, 2004.



## ***Lebenslauf***

### ***Persönliche Daten***

*Name* Hye-Ryun Cho  
*Geburtsdatum* 13. März 1976  
*Geburtsort* Seoul, Korea(Süd)

### ***Schulbildung***

*1983~1989* Besuch der Grundschule,  
Hongik Elementary School in Seoul, Korea  
*1989~1992* Besuch der Mittelschule,  
Kumran Middle School in Seoul, Korea  
*1992~1995* Besuch der Oberschule,  
Daeil Foreign Language High School in Seoul, Korea  
*November 1994* Hochschulaufnahmeprüfung

### ***Studium***

*1995~1999* B. Sc. Department of Chemistry, Faculty of Science,  
Yonsei University, Korea  
*1999~2001* M. Sc. Department of Chemistry, Faculty of Science,  
Yonsei University, Korea

### ***Tätigkeit***

*seit Mai 2002* Wissenschaftlicher Mitarbeiter am Institut für Nukleare Ent-  
sorgung (INE) des Forschungszentrums Karlsruhe (FZK)  
*seit Mai 2002* Bearbeitung der Dissertation



Ich erkläre hiermit, dass ich die vorgelegte Dissertation selbst verfasst und mich keiner anderen als der von mir ausdrücklich bezeichneten Quellen und Hilfen bedient habe, ich erkläre hiermit, dass ich an keiner anderen Stelle ein Prüfungsverfahren beantragt bzw. die Dissertation in dieser oder anderer Form bereits anderweitig als Prüfungsarbeit verwendet oder einer anderen Fakultät als Dissertation vorgelegt habe.